A design function for Bitumen Stabilised Material performance based on laboratory and field evaluation

by

Carl Roos Bierman

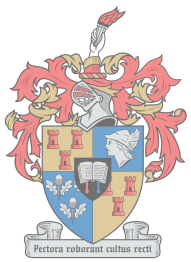

Thesis presented in fulfilment of the requirements for the degree of

Master of Engineering in Civil Engineering in the Faculty of Engineering

at Stellenbosch University

Supervisor: Prof. Kim Jonathan Jenkins

Co-supervisor: Mrs Chantal Rudman

March 2018

Declaration

By submitting this thesis electronically, I declare that the entirety of the work contained therein is my own, original work, that I am the sole author thereof (save to the extent explicitly otherwise stated), that reproduction and publication thereof by Stellenbosch University will not infringe any third party rights and that I have not previously in its entirety or in part submitted it for obtaining any qualification.

Date: March 2018

Summary

The use of stabilised granular materials for road pavements are ever increasing throughout South Africa. There are currently two commonly used methods for the stabilisation of granular materials in road construction. The first method is stabilisation with cement or lime to create a cemented layer with increased tensile strength. The second is stabilisation with bitumen and an active filler to create Bitumen Stabilised Material (BSM).

BSMs are constructed by stabilising granular material using either foamed bitumen or bitumen emulsion. Unlike asphalt where all the aggregate is coated with bitumen, the bitumen in a BSM is dispersed among the fine particles of the aggregate. When a BSM is compacted, the bitumen-rich fines are forced against each other resulting in localised bonds (spot welds). This produces a material with improved engineering properties. Although the material is treated with a binder, it fails in permanent deformation similar to a granular material.

The need for improved design methods for BSMs is driven by the increased use of this material by the industry. This study aims to produce a mechanistic-empirical design function for BSMs which relates the mechanical properties to in-field performance. This function can then be used to design BSMs based on material properties and stress conditions.

The new transfer function for BSMs has similar architecture to the function developed for waterbound macadam by Theyse et al. (2000). This function calculates the number of load repetitions the layer can sustain before a specified limit of permanent strain is reached. The function was altered to incorporate material properties that are specified for the design of BSMs. The factors influencing the new BSM transfer function are density, moisture susceptibility, deviator stress ratio and the permanent strain limit.

Data was gathered from fourteen pavement structures that formed part of a long-term pavement performance study. These pavements incorporate BSM base or subbase layers and were analysed at different stages of their design lives. The data obtained from these studies was used to calibrate the new transfer function for BSMs.

The calibrated transfer function was adjusted to predict the data at a range of reliabilities i.e. 95%, 90%, 80% and 50%. These reliabilities were based on the required reliability levels of the design categories.

The new transfer function was validated by investigating its ability to predict the life of a BSM that did not form part of the calibration process. The N7 highway near Cape Town was selected for the comparison as a substantial body of information was available to investigate the effect of the different factors on the transfer function.

FWD data was obtained from the N7 at different points in time. Back calculation of layer stiffnesses allowed insight into the resilient modulus development of the BSM. Cores were drilled from this pavement for triaxial testing. The triaxial tests provide insight into the shear properties of the base layer. The shear properties and stiffnesses obtained from the triaxial tests show that this base layer does not behave like a typical BSM. It was, however, still used for validation as it provides valuable information into the transfer function's sensitivity to these factors.

The new transfer function was compared to other design methods to validate its predictions. The function was found to produce less conservative results at lower stress ratios. The function showed significant sensitivity to the deviator stress ratio induced by loading.

In conclusion, the new transfer function for BSMs was calibrated to best describe the data from the fourteen long-term studies. The function was altered for design by adjusting it to different levels of reliability. Limits were recommended on the minimum and maximum values for the input variables to ensure a realistic result. The validation of the function yielded representative and realistic results.

Opsomming

Die gebruik van gestabiliseerde materiale in plaveisels word toenemend in Suid-Afika in werking gestel. Daar is tans twee metodes vir die stabilisering van granulêre materiale wat algemeen gebruik word in padkonstruksie. Die eerste metode is sement- of kalkstabilisering om 'n gesementeerde laag te skep met 'n verbeterde treksterkte. Die tweede metode is stabilisering deur middel van bitumen en 'n aktiewe vuller om 'n bitumen gestabiliseerde materiaal (Engels: Bitumen Stabilised Materials (BSMs)) te skep.

Bitumen Getabiliseerde Materiale word saamgestel deur granulfe materiale te stabiliseer deur óf skuimbitumen óf 'n bitumen-emulsie te gebruik. In teenstelling met asfalt waar al die aggregaat totaal met bitumen bedek is, word die bitumen in BSMs eweredig versprei tussen die fyn deeltjies van die aggregaat. Wanneer BSMs gekompakteer word, word die bitumenryke fynfraksies teen mekaar vas gedwing, wat manifesteer in gelokaliseerde lasverbindings. Dit lewer 'n materiaal met verhoogde en verbeterde ingenieurskenmerke. Alhoewel die materiaal met 'n bindmiddel behandel word, faal dit op soortgelyke wyse as 'n korrelmateriaal in permanente deformasie.

Die behoefte aan verbeterde ontwerpmetodes vir BSMs word gedryf deur die toenemende gebruik van dié materiaal in die padboubedryf. Hierdie studie het ten doel om 'n meganies-empiriese ontwerpfunksie daar te stel wat die meganiese eienskappe in verhouding sal stel tot waargeneemde werksverrigting. Die funksie kan dan gebruik word om BSMs te ontwerp gebaseer op materaaleienskappe en spanningstoestande.

Die nuwe oordragsfunksie vir BSMs is gebaseer op die funksie wat ontwikkel is vir "waterbound macadam" deur Theyse et al. (2000). Hierdie funksie bereken die aantal lasherhalings wat die laag kan dra voordat 'n gespesifiseerde limiet van permanente vervorming bereik word. Die funksie is ontwikkel om materiaaleienskappe in te sluit wat gespesifiseer is vir die ontwerp van BSMs. Die faktore wat die nuwe BSM oordragfunksie benvloed is digtheid, sensitiwiteit vir vog, afwykingspanningverhouding en die permanente vervorming limiet.

Data is versamel uit veertien plaveisels wat deel gevorm het van 'n langtermyn plaveisel gedrag studie. Hierdie plaveisels gebruik BSM basis- of sub-basislae en is ontleed in verskillende stadiums van die pad se ontwerpleeftyd. Die inligting wat verkry is uit hierdie studies is gebruik om die nuwe oordragsfunksie vir BSMs te kalibreer.

Die gekalibreerde oordragsfunksie is verstel om die inligtingsdata oor 'n reeks van betroubaarheidsvlakke te voorspel. Hierdie betroubaarheidsvlakke is gebaseer op die vereiste vlakke van betroubaarheid van die ontwerpkategorie. Die oordragfunksie is daarom gekalibreer tot betroubaarheidsvlakke van 95%, 90%, 80% en 50%.

Die geldigheid van die nuwe oordragsfunksie is bepaal deur die funksie se vermoë om die lewensduur van 'n BSM laag, wat nie vir kalibrering gebruik is nie, te voorspel. Die N7-snelweg naby Kaapstad is gekies vir die vergelykende studie, omdat dit 'n groot hoeveelheid inligting kon verskaf om die effek van die verskillkende faktore op die funksie te ondersoek.

FWD data is op verskillende tydstippe vanaf die N7 verkry. Terugberekening van laagstyfhede het insig verskaf rakende die styfheidsontwikkeling van BSMs. Kerne is uit die oppervlakke geboor vir drie-assige toetsing. Die drie-assige toetse het insig verskaf rakende die skuif eienskappe van die basislaag. Die skuif eienskappe en laagstyfhede wat verkry is uit die drie-assige toetse het gewys dat hierdie basislaag nie reageer soos 'n tipiese BSM nie. Dit is nogtans gebruik om geldigheid te bepaal, omdat dit waardevolle inligting verskaf het met betrekking tot die oordragsfunksie se sensitiweit vir hierdie faktore.

Die nuut ontwikkelde oordragsfunksie is getoets teen ander ontwerpmetodes om die funksie se voorspellings te valideer. Daar is bevind dat die funksie minder konserwatiewe resultate lewer by lae stresverhoudings. Die funksie het beduidende gevoeligheid getoon vir lading-geinduseerde afwykingspanningverhouding.

Laastens is die nuwe oordragsfunksie gekalibreer om die data te verkry van die veertien langtermynstudies ten beste te beskryf. Die funksie is aangepas vir ontwerp doeleindes deur dit aan te pas by verskillende vlakke van betroubaarheid. Limiete is aanbeveel vir die minimum en maksimum waardes van inleesdata om 'n realistiese resultaat te verseker. Die funksie is geldig bevind, en daar is getoon dat dit op voorspelbare en verteenwoordigende wyse reageer op die die veranderinge in die materiaal.

Acknowledgements

I would like to express my gratitude to the following people who provided assistance in numerous ways during this study:

- Professor Kim Jenkins - Stellenbosch University
- Mrs. Chantal Rudman - Stellenbosch University
- Ir. Lambert Houben - Delft University of Technology
- Mr. Glynn Llewellyn - Hatch Africa
- Mrs. Ronel Bierman - Moederlief
- Ms. Michelle du Toit - My goose
- Mr. Carl Roos Bierman - My liewe vader
- Roadmac Surfacing Cape
- Mr. Collin and Mr. Gavin - Stellenbosch University

Contents

List of Figures

List of Tables

Chapter 1

Introduction

1.1 Stabilised materials

Ever increasing economic pressure as well as environmental awareness drives the development of more effective technologies for road construction and rehabilitation. This has led to an increased interest in pavement rehabilitation using in situ stabilisation with bitumen. Stabilisation with bitumen provides environmental benefits such as low temperature construction and the use of existing material in the pavement structure.

Bitumen stabilised materials (BSMs) have been used worldwide over the past 30 years mainly as a base layer in pavement structures. The majority of these projects required rehabilitation that included recycling of the material in the existing base layer. Despite the relative success of these pavement rehabilitation projects, a lack of understanding of the nature and failure mechanism of BSMs remains.

Bitumen stabilisation is typically used in the rehabilitation or construction of base layers. Granular materials can be stabilised using either foamed bitumen or a bitumen emulsion to create a BSM. The materials that is produced by either method will yield similar performance and no distinction is made during the design or analysis of a pavement structure. Bitumen treated base layers are typically granular or RAP materials treated with small amounts of bitumen, i.e. less than 3%. A small amount of active filler, typically 1%, is used in the mix to improve the bitumen adhesion to the aggregate.

When a material is stabilised with bitumen, the bitumen is dispersed selectively amongst the finer particles of the aggregate. When a foam BSM is compacted during construction, the bitumen rich fines are forced against neighbouring aggregate particles creating localised bonds. This results in a non-continuously bound material that differs from hot mix asphalt (HMA) or cement stabilised materials. The stabilisation of granular materials significantly increases cohesion while having a

negligible effect on the angle of friction. When constructed, a BSM behaves like an unbound granular material with increased cohesion. This is well understood, but predictions of the long-term stiffness behaviour and development of permanent deformation has not been developed to the same degree (Collings and Jenkins, 2011).

1.2 BSM design

The non-continuous binding behaviour of BSMs is explained in the Technical Guideline (TG2 2009). However, there still remains confusion concerning the behaviour of BSMs, specifically with regards to the mode of failure. BSMs fail by means of permanent deformation, similar to granular materials. Therefore, the critical parameter in the design of BSMs is permanent deformation and not fatigue cracking.

Pavement design aims to protect the subgrade against imposed traffic loading by providing structural layers that distribute the load. There are currently three accepted structural design methods for BSMs (Wirtgen Group, 2012):

1. The empirical AASHTO design using the Structural Number (SN) method that relates the material properties to a layer coefficient, which is then multiplied with the layer thickness. The number for each layer is then added to obtain a structural number for the pavement structure. This is a simple method based on the performance of existing pavement structures.

2. The pavement number (PN) design method was developed as part of TG2 (2009) guidelines for BSM designs. This is a knowledge-based approach similar to the structural number method with certain advantages. The PN method introduces effective long-term stiffness (ELTS) values for certain material types which are used to determine an intelligent structural number relating to structural capacity.

3. The mechanistic-empirical deviator stress ratio design method is recommended for pavements with design traffic loading up to and greater than 30 million equivalent standard axles (MESA) . This method relates the rate of permanent deformation to the deviator stress ratio to obtain the number of standard axles the pavement can sustain before reaching the failure criteria. This method requires a resilient modulus value for the BSM, which is estimated using triaxial testing and pavement monitoring. The preferred approach for this method is to limit the DSR in order to increase the life of the pavement.

When examining these three methods it is apparent that long-term stiffness has not been fully utilised in current BSM design. The prediction of long-term stiffness has also not been fully developed for BSMs.

1.3 Problem statement

The design methods of continuously bound materials, such as hot mix asphalt (HMA), are well developed and understood. In first world countries like the USA, the design methods were developed to limit the fatigue and deformation of thick asphalt layers. For economic reasons, third world countries like South Africa focus on the design of granular layers. The design of granular layers aim to limit permanent deformation whilst accommodating the design traffic.

BSMs can be classified somewhere between these two materials as they are only partly bound, providing improved cohesion and some tensile strength, but in general performing more like granular materials. The current design methods for BSMs do not include a mechanistic-empirical transfer function which relates the material properties in conjunction with stresses and strains, to the pavement life. The deviator stress ratio (DSR) method was designed to fill this gap, but the model is not yet fully developed. To improve design, it is therefore necessary to further expand this method by producing a transfer function to relate the material performance properties to the life of a pavement structure incorporating a BSM layer.

1.4 Objectives

The aim of this study is to develop, calibrate and validate a BSM transfer function that incorporates variables such as the material properties, performance properties as well as the stresses and strains in the material. In order to achieve this goal, long-term data from different pavement structures is required. The objectives of this study are:

1. To define the failure mechanism of a BSM as this would be an important factor to determine the life of a BSM layer. The properties that influence the failure mechanism should also be defined.

2. To determine the long term stiffness of a BSM in order to understand the behaviour of the material and to obtain a representative resilient modulus over a long period of time.

3. To produce a new mechanistic-empirical transfer function for BSMs that uses material properties as well as stress conditions to determine the design life of a BSM.

4. To calibrate the function for different levels of reliability to comply with the current design requirements.

5. To validate this function and understand its reaction to the factors that influences it.

6. To bridge the gap between understanding the performance behaviour of BSMs and implementing it in the design function. This function should be calibrated and validated using various test sections. Comparisons between actual performance and the outcomes of the new transfer function and the other design functions will provide valuable insight into the reliability of this function.

1.5 Limitations

The limitations of this study are as follows:

1. The calibration of the transfer functions is dependent on data from different pavement structures incorporating BSMs. The number of pavement structures with significant long term pavement performance data is limited.

2. The detailed information that was available from long term pavement studies is limited. Shear properties are expensive to determine and require specialised equipment. Therefore, it was not available for a large number of pavement studies used for calibration.

3. The development of permanent strain in the base layer is difficult to evaluate separately and a number of assumptions were made to estimate the accumulated strain.

1.6 Layout

This report is divided into six chapters. Chapter 1 provides the background about BSMs and the motivation for this study. The objectives and limitations are also provided in this Chapter.

Chapter 2 contains literature reviews for this study. The development and history of BSMs are discussed. The behaviour and performance of BSMs, specifically long term performance, were investigated. The findings and conclusions of relevant previous studies can be found in this chapter.

Chapter 3 describes the procedures followed in this study for the analysis of available data as well as the test procedures followed. The test plans and the research overview are covered in Chapter 3. The origin, development and the processes followed for calibration and validation of the new transfer function are covered in this chapter.

Chapter 4 contains the results obtained from calculations and analyses performed during this study. The chapter also focusses on the results from the calibration of the new transfer function and its adjustments to for design purposes.

Chapter 5 covers the validation of the transfer function. The function's ability to predict data was investigated and compared to other design methods. The transfer function's sensitivity to different variables was investigated.

Chapter 5 discusses the conclusions that were drawn from the findings. Recommendations are given for further studies and improvements that can be made to the net transfer function.

Chapter 2

Literature Study

Stabilisation with bitumen emulsion and foamed bitumen are both methods of reducing the viscosity of bitumen in order to allow mixing with cold, moist materials. BSMs improve the strength, durability and flexibility of the granular parent material. Bitumen stabilisation also increases the parent material's resistance to moisture damage. The behaviour of BSMs is similar to that of granular materials. However, bitumen stabilisation increases the cohesion with little effect on the friction angle. The type of material that is produced with either bitumen emulsion or foam bitumen is similar. Therefore, a common approach has been developed for both types of stabilisation (Asphalt Academy, 2009). This chapter covers background information about bitumen stabilised materials, including the performance and the behaviour of the material. The production, characteristics and uses of these two materials are discussed.

2.1 Stabilisation with bitumen emulsions

Bitumen emulsion comprises bitumen emulsified in water. Bitumen is dispersed in the water in the form of an oil-in-water type emulsion. The bitumen is held in suspension by an emulsifying agent. The bitumen emulsion can then be mixed with cold moist aggregate to produce a layer that may be subjected to traffic within hours after construction.

2.1.1 Brief history of bitumen emulsions

Bitumen emulsions were first developed at the beginning of the 20th century for sealing applications and to prevent dust caused by increasing traffic. The use of bitumen emulsions for road construction was only introduced in the 1920s when Hugh Mackay, an English chemist, developed and filed a patent on anionic bitumen emulsion. The trade mark was labelled "Cold Spray", but was later changed to "Cold Asphalt" and abbreviated to "COLAS". The use of this technology in road works increased rapidly and within four years, five countries had manufacturing plants. By 1926 the combined annual production of these five countries was estimated at 150 000 tons (Mulusa, 2009).

The company named COLAS established the first bitumen emulsion manufacturing plant in Bellville, South Africa in 1928 . The fuel crisis in the 1970's provided incentive for a reduction in energy consumption, boosting the use of bitumen emulsion in the stabilisation of mineral aggregate.

2.1.2 Description of bitumen emulsion

An emulsion describes a dispersion of small droplets of one liquid in another. The liquids should be immiscible, where one is in the dispersed phase and the other in the continuous phase. In the case of bitumen emulsions the two liquids are bitumen and water, with water usually in the continuous phase and bitumen dispersed (droplets of 0.001 mm to 0.01 mm) (Mulusa, 2009).

The bitumen is held in suspension by an emulsifying agent, which determines the charge of the emulsion droplets. The bitumen droplets can either be positively (cationic) or negatively (anionic) charged. Anionic emulsions are produced using negatively charged emulsifiers, like fatty acids, while in the case of cationic emulsions positively charged emulsifiers such as amines are used. When the bitumen emulsion is mixed with aggregate, the charge of the bitumen droplets causes attraction forces to the aggregate particles. The charged bitumen droplets are attracted to the smaller fractions of the aggregate due to the surface area and charge concentration features. The moisture and type of aggregate used in the mix are important factors for the dispersion of the bitumen and for preventing the emulsion from breaking (separation of the bitumen from the water) prematurely (Asphalt Academy, 2009).

Once the emulsion has been mixed with the aggregate, the bitumen emulsion should break in order to perform as a binder. The emulsion acts as a lubricant and should therefore only break after the material has been fully compacted. The stabilised material has a speckled appearance due to the bitumen droplets favouring the finer particles.

2.1.3 Production of bitumen emulsions

Emulsions are produced by applying energy to a mixture of two immiscible liquids. This can be done by means of shaking, stirring, homogenising or spray processes. The amount of energy that is required can be significantly reduced by the addition of an emulsifier. Figure 2.1 illustrates the emulsion production process. The type of emulsifier added affects the size as well as the charge of the bitumen droplets. Emulsion is not formed spontaneously. It is therefore unstable and will tend to revert back to its original state over time.

In order to prevent the emulsion from reverting back to the stable phase, surface active substances (surfactants) are added. Surfactants increase the kinetic energy of emulsions to allow the emulsion to be stored over time without changing back to the stable state (Mulusa, 2009).

Three distinct grades of bitumen emulsion are used for road construction and rehabilitation (Asphalt Institute, 2008):

1. Quick set or pray grade: The quick setting grades are used for slurry seals and micro-surfacing applications. Low amounts of emulsifiers are used to ensure fast curing times.
2. Medium set or premix grade: The premix grade emulsions are designed for mixing with granular materials. The emulsion does not break upon contact with the aggregate and can therefore coat a wide variety of graded aggregates.
3. Slow set or stable grade: Stable grade emulsions are designed for mixing stability. These are used to ensure good workability with dense-graded aggregates with a high fines content.

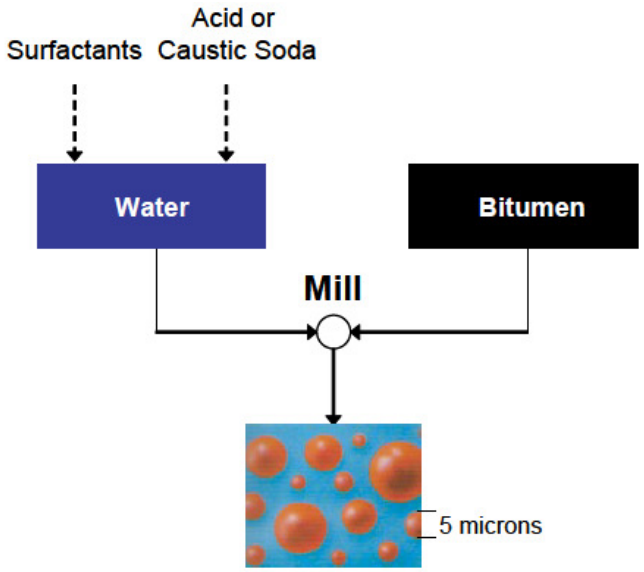

Figure 2.1: Illustration of emulsion production (Asphalt Academy, 2009)

Bitumen emulsions used for stabilising road construction materials are usually produced with the use of a coloid mill as shown in the schematic diagram in Figure 2.2. The colloid mill applies energy to the mix of hot bitumen and water by passing it through a small gap between the disc or cone and the stator (case of the mill). Both the rotating and stationary parts may be grooved to ensure turbulent flow through the gap.

Bitumen emulsion can be produced by two types of plants: A batch or an in-line (continuous) process plant. The batch plant process involves a minimum of two steps, the first of which is the preparation of the water phase, where water, emulsifier and other chemicals are measured and mixed in a tank. In the second phase, the emulsion production process, the bitumen and the water mixture is dosed to the colloid mill. The production of bitumen emulsion is thoroughly discussed in the ScanRoad document (1983).

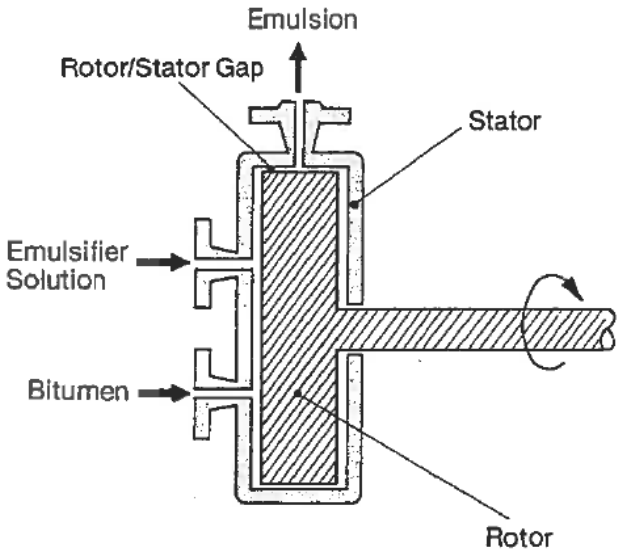

Figure 2.2: Schematic of colloid mill for bitumen emulsion production (ScanRoad, 1983)

The in-line plant process involves a number of material flows, allowing for manual process control. The water heating and all material dosages are done continuously using pumps for each material. The quality of the emulsion produced from this process depends on the accuracy of metering the different components. Semi-automatic control is possible, which increases accuracy and reduces the chance of human error.

The in-line plant process has the advantage of being a closed system with no open tanks and mixing tank, as some of the chemicals can be hazardous or corrosive. Care should be taken with such a system as the water phase should have enough time to react with the added chemicals before the water phase meets the bitumen (Mulusa, 2009).

2.1.4 Breaking of bitumen emulsion

In order to achieve the desired effect, bitumen emulsion must revert back to a continuous bitumen film. This process, known as breaking, is the separation of bitumen from water and the coalescence

of bitumen droplets to form a continuous film of bitumen on the aggregate. The remaining water is deposited into the mix. The time from mixing to the separation is referred to as the breaking time of the emulsion. Once the breaking process has been completed, curing begins. Water is removed from the system, mainly through evaporation, and an increase in stiffness and tensile strength occurs in the pavement layer.

2.2 Stabilising with foamed bitumen

Foam is essentially a substance that is formed by gas bubbles trapped in a solid or a liquid. Foamed bitumen is produced by adding a small amount of water to hot bitumen, which results in spontaneous foaming. The physical properties of the bitumen are temporarily altered when the water that is injected makes contact with the hot bitumen. The water turns into vapour which is trapped in small bitumen bubbles.

2.2.1 Foamed bitumen production

This foaming process occurs in an expansion chamber that was developed by Mobil in the 1960s and is still commonly used (Asphalt Academy, 2009). Expansion chambers are small, thick-walled tubes about 50 mm in depth and diameter. Water and hot bitumen is injected into this chamber at high pressures to produce foam. The foaming process in the expansion chamber is illustrated in Figure 2.3.

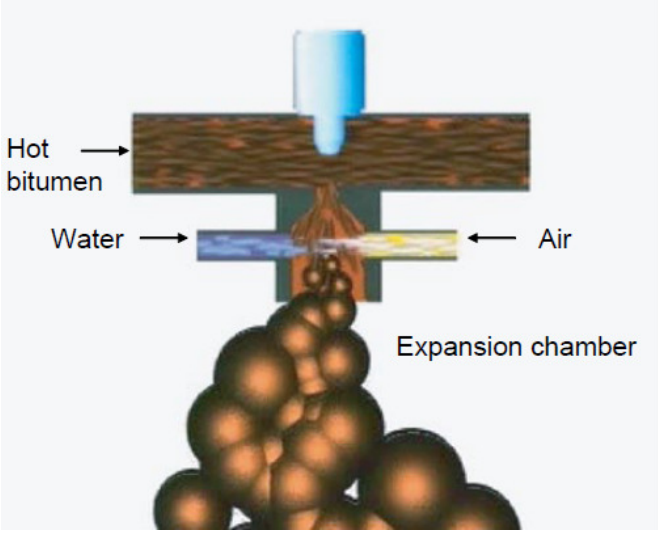

Figure 2.3: Production of foamed bitumen in an expansion chamber (Asphalt Academy, 2009)

To produce a BSM-foam, bitumen is foamed on site and mixed into the aggregate while still in its foamed state. Foamed bitumen bubbles take less than a minute to collapse. During mixing the bitumen bubbles burst, resulting in very small bitumen particles (bitumen splinters) that disperse throughout the aggregate. The bitumen particles adhere to the finer parts of the aggregate to form a mastic. A greater expansion of the foam leads to a better distribution of the bitumen in the aggregate. Moisture content in the aggregate before mixing plays an important role in the dispersion of bitumen. When the BSM is then compacted, the bitumen particles in the mastic press against the larger aggregate particles. This leads to localised, non-continuous bonds referred to as spot welds (Wirtgen Group, 2012).

Mathaniya (2010) investigated the governing processes during the formation of bonds in BSMs. Figure 2.4 illustrates the step by step formation of bonds for both emulsion and foam BSMs. The differences in bond formation, during mixing and compaction, between foam and emulsion BSMs are highlighted in this figure.

2.2.2 Characterisation of foamed bitumen

There are two main properties that characterise foamed bitumen namely expansion ratio and half life. Expansion ratio is a measure of the viscosity of the foam and determines how well it can disperse throughout a mix. The expansion rate is measured as the factor of the increase in volume. Half-life is the measure of stability of the foam, providing an indication of the rate of collapse of the foam. Half-life is measured as the time for the foam to collapse to half of its maximum volume (Mulusa, 2009). These two foam properties are influenced by a number of factors, four of which are described below (Wirtgen Group, 2012).

2.2.2.1 Water addition

Water injected into the expansion chamber is one of the dominant factors influencing the foam properties. If more water is injected, the size of the bubbles is increased leading to a higher expansion ratio. However, the increase in the size of the bubbles leads to a decrease in the film thickness of the bitumen bubbles. This leads to a decrease in the half-life of the foam. Therefore, a balance needs to be achieved to optimise both the expansion ratio and the half-life.

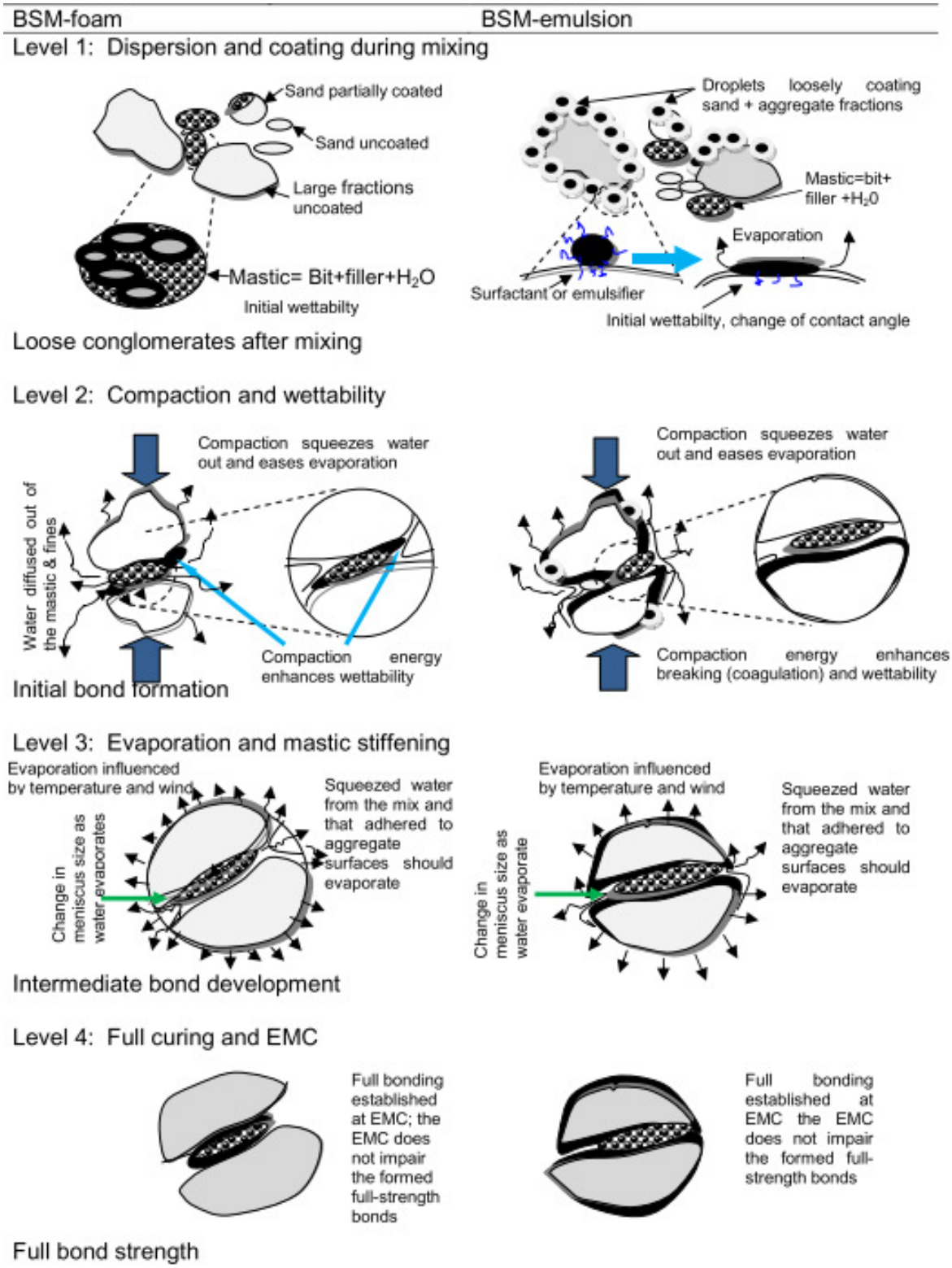

Figure 2.4: Governing process for bonding formation is both foam and emulsion BSMs (Mathaniya, 2010)

2.2.2.2 Bitumen type

Bitumens with penetration values between 80 and 100 are typically used for BSM-foam, although harder grade bitumen has been used with success in the past. However, harder bitumen should generally be avoided as it leads to poor quality foam resulting to poorer dispersion of bitumen in the aggregate. The penetration value alone does not dictate the foam quality of a bitumen, but the composition of a bitumen also has an influence on the foaming ability. Therefore, the foaming ability of each bitumen batch needs to be tested before it is used.

2.2.2.3 Temperature

When the temperature of bitumen is increased, its viscosity is decreased leading to an increase in the size of bitumen bubbles when foaming. To achieve a satisfactory expansion the temperature of the bitumen needs to be high enough (160°C to 180°C), as the change of state of the water draws heat from the bitumen.

2.2.2.4 Additives

The foaming properties of bitumen can be positively influenced by foamants or negatively influenced by the addition of anti-foaming agents. Foamants are only required when bitumen has been treated with anti-foaming agents during the refining process.

2.3 Behaviour of BSMs

The BSM produced when using foam bitumen or bitumen emulsion is similar and a common approach to the materials can be used. There are, however, differences in the materials that can be used in each method to obtain a good quality BSM. BSMs do not act as a continuously bound material, but like a granular material with increased cohesion. Because the material is not continuously bound, the failure mechanism is not fatigue cracking, but rather permanent deformation.

2.3.1 BSM produced using either foam or emulsion

The type of material produced when stabilising with either foam bitumen or bitumen emulsion is similar. There are several similarities to the end product to motivate a similar approach. Some of the similarities are noted below (Wirtgen Group, 2012).

1. Both methods create an improved granular layer, improving the cohesion of the material without altering the friction angle.
2. Emulsifying and foaming reduce the viscosity of bitumen to enable it to mix with aggregate at lower temperatures.
3. A BSM constructed with either method fails by means of permanent deformation.
4. The BSM is not a continuously bound material like hot mix asphalt.

While the end product of stabilisation with foam or emulsion is similar, the materials and mixing conditions differ. Some of the main differences between the bitumen treatment are listed below (Wirtgen Group, 2012).

1. The aggregate types differ: foam bitumen can be used on a wider range of aggregate available to produce a good BSM.
2. The temperature of bitumen before mixing is lower for bitumen emulsion (20°C to 70°C) than foam (160°C to 180°C).
3. Aggregate temperature during mixing should be greater than 10°C for emulsion and greater than 15°C for foam bitumen.

2.3.2 BSM behaviour overview

Bitumen stabilised materials behave similar to unbound granular materials, but the stabilised material is less sensitive to moisture and has improved cohesive strength. BSMs are different in

appearance to hot mix asphalt in that it does not appear black. This is due to the bitumen that is dispersed amongst the finer particles, not coating the larger aggregate. The material would be slightly darker than the parent material after it has been stabilised.

Usually, a small amount of active filler (cement or hydrated lime) is added to the mix along with the foam bitumen or bitumen emulsion. The active filler improves the retained strength under saturated conditions and assists in dispersing the bitumen within the mix. When bitumen emulsion is used, the active filler assists to extract the water from the emulsion causing the emulsion to break. When using foam bitumen, active filler acts as a catalyst in dispersing the bitumen particles (Asphalt Academy, 2009).

According to the TG2, it can be assumed that no distinction can be made between BSM-foam and BSM-emulsion. The TG2 based this assumption on numerous observations of in service pavement structures. The main features and the assumed behaviour of both BSM-foam and BSM-emulsion are (Asphalt Academy, 2009):

1. BSMs show a significant increase in cohesion compared to the parent material, whereas the angle of friction remains similar to the parent material. This was shown (Bredenhann and Jenkins, 2015) by performing a number of triaxial tests on G2 material and BSM as shown in Figure 2.5.

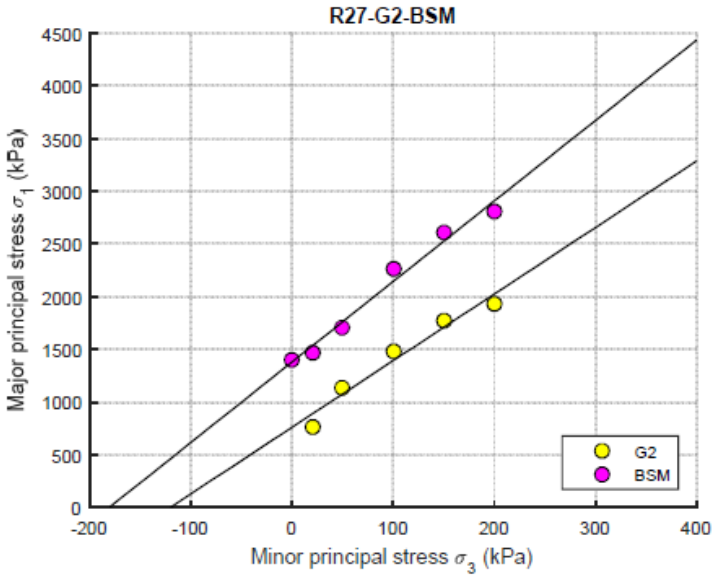

Figure 2.5: Mohr-Coulomb model for G2 and BSM (Bredenhann and Jenkins, 2015)

2. BSMs acquire flexural stiffness from the combined effect of the bitumen droplets in the mix. Individual bitumen particles are not linked and coarse particles are not coated. The BSM retains much of the granular characteristics of the parent material. Therefore, a BSM is stress dependent and is not prone to conventional fatigue or thermal cracking.

3. BSMs perform well when the cohesive strength has been optimized through proper mix design, and retains enough flexibility to activate friction resistance when loaded.

4. The bitumen is dispersed only among the finer particles of aggregate, encapsulating and immobilising these particles. This reduces the moisture sensitivity of the materials and improves the durability.

5. The stiffness of a BSM layer is dependent on several factors, similar to granular materials. The stiffness of a BSM is higher than that of granular materials due to the higher cohesive strength. The factors influencing the stiffness of a BSM are listed below.

    - The stiffness of the parent material
    - The density of the material, achieved through compaction
    - The amount of binder and active filler as well as their dispersion throughout the mix
    - The rainfall and temperature of the local environment
    - The support provided for the layer

6. The failure mode for BSMs is permanent deformation.

7. The behaviour and stiffness of a BSM depend on the quantities of bitumen and active filler used in the material. When excessive cement is used the material acts more like a cement treated material, causing the addition of bitumen to be of little effect. Therefore, cement content exceeding 1% is not recommended and the ratio of bitumen to active filler should be greater than 1.

For a BSM to perform optimally it is important that the pavement is designed well and the mix is in balance. There are two ways in which the optimum shear strength of a BSM can be compromised, both of which result from too much active filler. The first way is to use too much active filler in the mix. This will result in the BSM not performing as a flexible material, but as a brittle material. The cohesive strength will be significantly increased, but will be reduced once cracking occurs.

The second way is the use of poorly graded or non-durable parent material, reducing the frictional resistance of the material. Adding additional active filler to the mix would result in a fine-grained, brittle material highly susceptible to crushing and fatigue failure.

It is clear that BSMs are different to asphalt and cement stabilised materials in terms of behaviour and performance. BSMs should in particular not be confused with cold asphalt mixes manufactured using cut-back bitumen (Asphalt Academy, 2009).

2.3.3 Advantages of BSMs

The primary benefits of bitumen stabilised materials are listed below (Asphalt Academy, 2009).

1. The treatment with bitumen leads to an increase in strength of the materials. This material can replace high quality base material (like asphalt) resulting in a reduction in cost.
2. The bitumen, encapsulating the finer particles, leads to reduced moisture susceptibility and improved durability.
3. Lower quality aggregate can be used successfully. When using emulsions, materials with a low fines content can be used.
4. The failure mode of BSMs (permanent deformation), indicates that future rehabilitation would require less effort than materials that fail due to cracking.
5. The performance of a BSM is not temperature sensitive.

Additionally, several benefits arise when rehabilitating existing pavement structures using in situ recycling. A number of these benefits are listed below (Asphalt Academy, 2009).

Table 2.1: Advantages of stabilisation using either foam or emulsion

BSM - Emulsion	BSM - Foam
Materials with a low fines content can be used in the mix.	Mixes can be produced in bulk and stockpiled, to be compacted at a later stage.
May be subjected to traffic within a few hours after construction.	Materials with relatively high moisture content can be treated with foam.
	May be subjected to traffic immediately after compaction.

1. The environmental impact is significantly reduced in terms of conservation of natural aggregate, reduction in transport and material wastage. Where a BSM layer is substituted for an asphalt base layer, a significant amount of energy is saved for the heating of the material.

2. BSMs are not overly sensitive. Small variations in the amount of bitumen added and the untreated materials do not significantly change the end product. This allows for the variation that results from the recycling process to be tolerated.

3. Traffic delays and disruptions are minimized by being able to work in half widths and opening soon after completion.

4. Pavements showing a wide range of distress and failure can be effectively rehabilitated.

Constructing a BMS layer with either BSM foam or BSM emulsion each has its own set of advantages. The advantages of using either are summarised in Table 2.1.

2.3.4 Disadvantages of BSMs

The application of BSMs can provide some challenges, under certain conditions. Using bitumen adds significant cost to a project due to the price of bitumen and active filler, as well as the cost of transportation. In cases where good quality granular materials are readily available at a reasonable cost and the design traffic is moderate, stabilisation is not economically feasible. The behaviour of BSMs is different to conventional construction materials and is often not well understood. It is therefore important that the necessary knowledge and expertise are acquired before designing or constructing BSMs (Asphalt Academy, 2009). In addition, control of the quality and variability of the material to be recycled is imperative, in order to provide a reliable product.

When using emulsion a number of limitations arise. Some of these limitations are listed below.

1. A high moisture content of the in-situ materials can increase the total fluids content when the emulsion has been added. The total fluids content can be increased beyond the zero-voids line limit when compacted. When this occurs the material cannot be properly compacted and cannot achieve the desired performance.

2. The bitumen emulsion used must be stable enough to tolerate the pressure from the pump and spraying processes without breaking.

3. The proper formulation of the bitumen emulsion is very important. If the emulsion is not appropriately formulated, it may break prematurely, preventing mixing and clogging the chambers of the recycler. The other extreme is that the emulsion might not break for an extended period of time, thereby running the risk of premature permanent deformation..

The use of foam for stabilisation has specific limitations as listed below.

1. Foamed bitumen requires materials with a sufficient amount of fine material to facilitate the dispersed bitumen particles. When materials with insufficient fines are used, bitumen lumps are formed.

2. The equipment needed to produce foamed bitumen is very specialised. It is important to use well engineered equipment to prevent failures and delays on site.

3. Water and bitumen are incompatible liquids, meaning that they are never both in the liquid state. Water vaporises above 100 °C and the typical bitumen used for foam does not flow below this temperature. If the foam system is not properly designed, system blockages will appear, resulting in delays in construction.

The limitations of stabilisation using either emulsion of foamed is summarised in Table 2.2.

Table 2.2: Limitations of stabilisation using either foam or emulsion

BSM - Emulsion	BSM - Foam
Stabilising materials with high moisture contents can hinder compaction.	Foamed bitumen requires sufficient fine particles in the parent material to avoid poor mixes (forming lumps of bitumen).
Bitumen emulsion should be sufficiently stable to tolerate pump and spray bar pressures.	Foaming equipment that was not engineered properly may lead to an inconsistent and non uniform supply of bitumen.
Poorly formulated bitumen emulsion may result in premature breaking or not breaking for months or years.	Due to the incompatibility of water and hot bitumen, these materials should not come into contact before foaming. This requires a well designed and high quality system.

2.4 Performance behaviour of BSMs

By determining various properties of a BSM, using for example triaxial tests, the short term performance of the materials can be predicted. These tests give an indication of how the materials will behave after constructed. The important properties that should be determined include the shear behaviour, resilient modulus and the permanent deformation.

2.4.1 Shear behaviour

The shear behaviour of a BSM is similar to that of the parent material but with specific differences. Bitumen stabilisation changes the shear properties by significantly increasing the cohesion (c) while a small reduction occurs in the angle of friction (ϕ). These shear properties can be determined with the use of monotonic triaxial testing. The stress-strain relationship of the materials can then be determined as shown in Figure 2.7 (A).

The elastic modulus (E) is shown as the slope of the stress-strain relationship. Monotonic triaxial testing requires various comparable specimens to be tested to failure at different confinement pressures (σ_3). The principle stress at failure ($\sigma_{1,f}$) is the total stress applied to the specimen by the loading thereof. Cylindrical specimens with a diameter of 150 mm and a height of 300 mm are routinely used for the testing of a BSM.

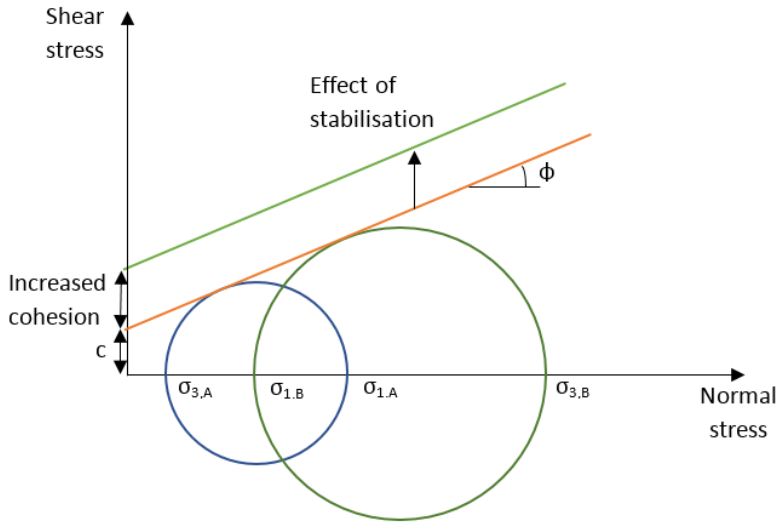

Figure 2.6: Mohr-Coloumb methods showing the effect of bitumen stabilisation on the failure envelope

The results from the monotonic triaxial testing can then be used to determine the shear parameters using the Mohr-Coloumb model. The failure condition is represented by a straight line enveloping the Mohr circles. Figure 2.6 shows a typical example of two monotonic triaxial test results. The first Circle (A) is at a lower confining pressure than the larger circle (B) resulting in a lower applied stress at failure. A tangent line was drawn to the circles and the cohesion and friction angles were determined. The increase in cohesion with slight difference to the angle of friction is also shown in this figure.

The increase of cohesion, with a small change in the friction angle, shifts the failure envelope of the materials. This shift allows for a much higher applied stress before the materials fails (Jenkins et al., 2002).

2.4.2 Retained cohesion

The moisture susceptibility of a BSM can be determined and expressed as the retained cohesion using triaxial testing. BSMs are much less susceptible to water than granular materials and have a higher retained cohesion.

The retained cohesion is a ratio of soaked principle stress to unsoaked, determined using monotonic triaxial tests at a confining pressure of 100 kPa. The determination of retained cohesion is shown in Equation 2.1. In order to soak a compacted and cured triaxial specimen, it should be submerged under water for 24 hours at 25°C.

$$RetainedCohesion = RetC = \frac{\sigma_{1,100,S} - 100}{\sigma_{1,100,U/S} - 100} \times 100 \tag{2.1}$$

Where:

$\sigma_{1,100,S}$ = Applied principle stress at failure for the soaked specimen at $\sigma_3 = 100kPa$

$\sigma_{1,100,U/S}$ = Applied principle stress at failure for unsoaked specimen at $\sigma_3 = 100kPa$

2.4.3 Resilient modulus

The load spreading ability of granular or stabilised layers is a function of the stiffness of the materials. The stiffness or resilient modulus (M_r) of a material describes the response of the material to dynamic loading. Resilient modulus determines the layers load spreading ability and is therefore an important property to consider. The stiffness is not a constant value, but is dependant on the applied and confining stress. Stiffness, expressed as E, indicates the response of the materials to a single load. Figure 2.7 (A) illustrates the stress strain relationship of materials loaded to failure.

The slope of the relationship is the stiffness of the material (E). The long term stiffness response of BSMs is discussed in more detail in Section 2.6.

Granular materials subjected to repeated loading, within the elastic limit, experience permanent and recoverable strain. The loading and recovering cycle of typical granular materials are shown in Figure 2.7 (B). The slope given by the resilient strain after a number of load repetitions is the resilient modulus. To obtain the resilient modulus, granular materials are subjected to repeated loading and the response measured. This simulates the response of in-field materials as pavement structures are subject to repeated loading.

To determine the resilient modulus of a material, a short duration dynamic loading triaxial test is used (Van Niekerk, 2002). This test measures the response of a specimen to different levels of loading at a range of confining pressures. Typically the same confining pressures are used as for the monotonic testing (Mulusa, 2009).

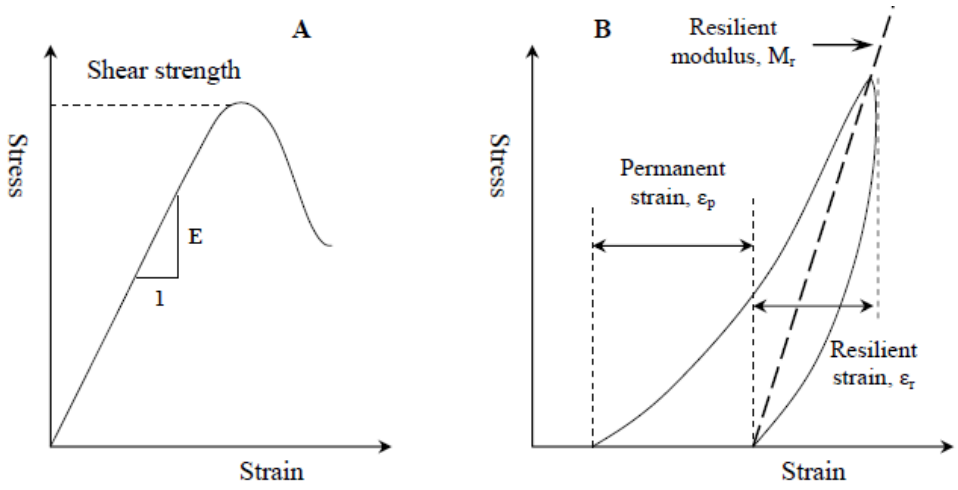

Figure 2.7: (A) Monotonic loading of granular materials to failure. (B) Stress-strain relationship for loading within the elastic limit (Bredenhann and Jenkins, 2015)

During this test relatively low stresses are applied to a specimen creating low strains. This is done to ensure the elastic range of the materials are not exceeded. The loading level can be described by the ratio between the applied deviator stress and the deviator stress at failure according to Equation (2.2). Figure 2.8 shows the Mohr circles indicating the applied load and the failure load at a specific confining pressure. The principal stress at failure is determined with Equation (2.3). It is also assumed that within the elastic range, the stress history does not effect the material.

$$DSR = \frac{\sigma_{d,applied}}{\sigma_{d,failure}} \tag{2.2}$$

$$\sigma_{1,f} = \frac{(1 + \sin(\phi)\sigma_3 + 2.c.\cos(\phi)}{(1 - sin(\phi))} \tag{2.3}$$

Similar to coarse grained granular materials, BSMs are stress dependent. This implies that the stiffness of the layer increases with an increase in stresses.

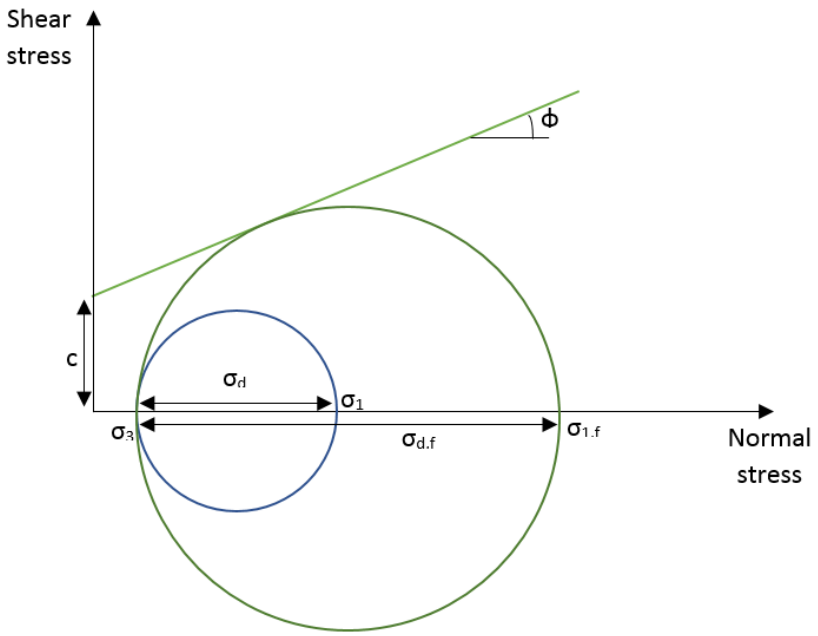

Figure 2.8: Illustration of deviator stress ratio

The value of M_r can be related to θ for granular materials, as the response of these materials depends on the load situation. In this case θ is defined as the sum of the principle stresses ($\theta = \sigma_1 + \sigma_2 + \sigma_3 = \sigma_1 + 2\sigma_3$).

Van Niekerk (2002) investigated different ways to model the stress dependent behaviour of granular materials, the first of which was a simple model shown in Equation 2.4. During the lab testing 3 phenomena were observed (Van Niekerk, 2002):

1. The value of M_r increases with increasing confining stress (σ_3). This is always observed for granular materials and is well understood. An increase in normal stress mobilizes friction between the grains, increasing strength and stiffness.

2. At a particular σ_3 level, the values of M_r are at first increased, before decreasing (stress softening) with an increased loading. It was observed by Huurman and van Niekerk (1995) particularly for sands, that at a certain σ_3 level the M_r values at first remain constant before decreasing with an increase of applied load closer to failure. At a certain point the deviator stress becomes excessive and the materials lose stiffness. This is shown for different confining pressures in Figure 2.9.

3. Much higher M_r values were obtained under mild loading when compared to specimens under severe loading. This is shown in Figure 2.9, where much lower M_r values were obtained from severe loading (12 (II)) than for mild loading (12 (I)). This was explained by the development of bonds between grains as a result of cementation and carbonization. The bonds were strong enough to endure the mild loading, but could not endure the severe loading, breaking the bonds that have formed.

These observations were used to compare different models to describe the stress dependency of granular materials. Van Niekerk (2002) stated that the model should be capable of relating M_r to the confining stress and deviator stress. The model should be able to discriminate between stiffening at low stress levels and softening at relatively high stress levels.

The models considered for bitumen stabilised materials are discussed in this section. The first and most simple model, as given in Equation 2.4, reflects a linear increase of M_r with an increase in confining pressure (stiffening). As the confining pressure increases, the friction between particles increases, resulting in an increase in strength and stiffness. The linear increase in M_r is shown in Figure 2.10.

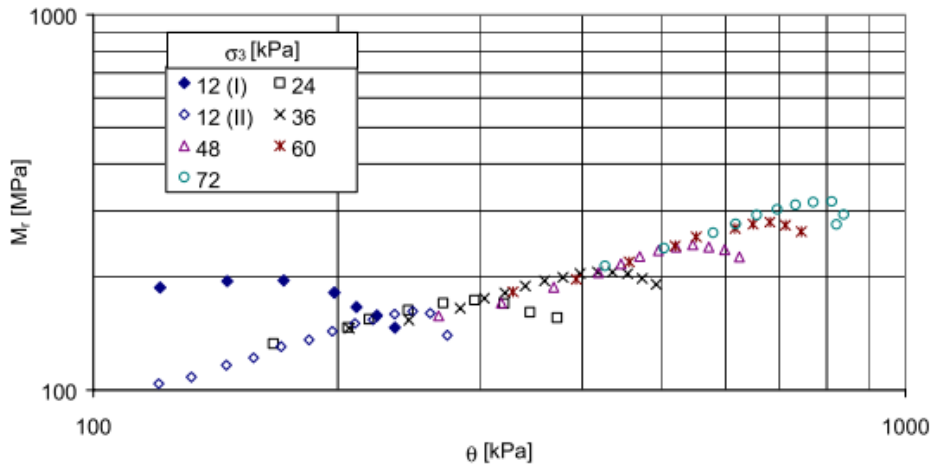

Figure 2.9: Stress stiffening followed by stress softening of granular materials (Van Niekerk, 2002)

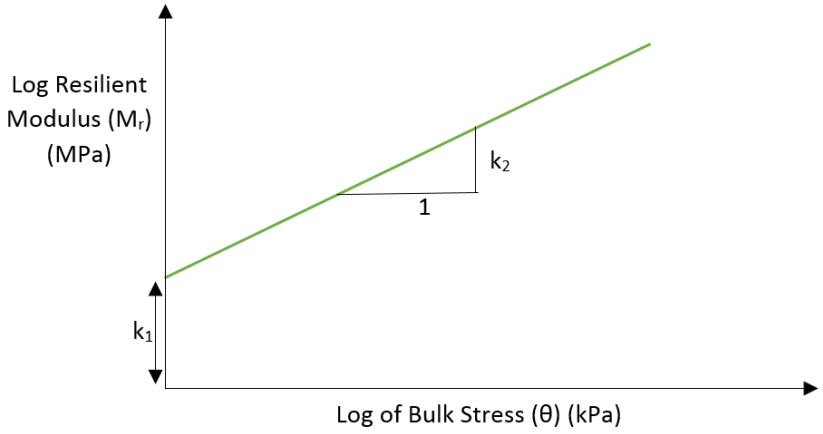

Figure 2.10: Mr-θ model of resilient modulus

This model is physically incorrect as it can not discriminate between the influence that confining pressure and deviator stress individually have on M_r. This model predicts the same M_r values for materials with a low confinement and high applied stress as for materials with high confinement and low applied stress.

$$M_r = k_1.\theta^{k_2} \tag{2.4}$$

Where:

M_r = Resilient Modulus (MPa)

k_1, k_2, k_3, k_4, = model coefficients

θ = Bulk stress = $\sigma_1 + \sigma_2 + \sigma_3$ (kPa)

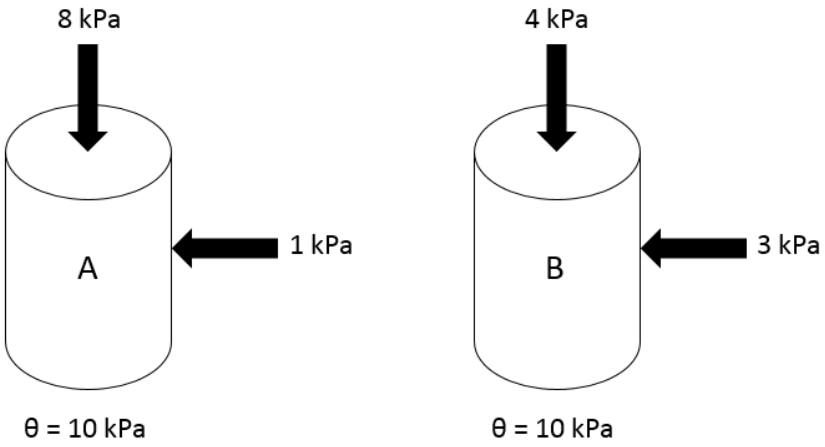

Figure 2.11: Calculation of θ

The inability of θ and this model to discriminate between confining stress and applied stress is illustrated in Figure 2.11. The figure shows that, when using this model, materials with very low confining pressure can have the same M_r as materials with high confining pressure if a higher load is applied.

Despite these drawbacks, it was found that this model very accurately predicted M_r under mild stress conditions (Van Niekerk, 2002). For severe stress conditions the model was less accurate, but still within acceptable limits.

The second model investigated by Van Niekerk was the $M_r - \sigma_3 - \sigma_d$ model as shown in Equation 2.5. This universal material model was introduced by Uzan and Witzack (1992) and is physically more correct than the $M_r - \theta$ model. This is due to the model differentiating the effects of σ_3 and σ on M_r. This model is only capable of describing either an increase or decrease of M_r with increasing σ_d values. It is not capable of describing an initial increase and the subsequent decrease of M_r (Van Niekerk, 2002).

$$M_r = k_1.(\sigma_3)^{k_2}.(\sigma_d)^{k_3} \tag{2.5}$$

Where:

σ_d = Deviator stress (kPa)

The third model was developed by Van Niekerk and is an alternative formulation of the $M_r - \sigma_3 - \sigma_d$ model. This parabolic model is given in Equation 2.6. The parabolic part of the model allows it to describe both the initial increase and the subsequent decrease of M_r with an increasing applied stress. This model describes both the effect of confinement (σ_3) and the effect of the deviator stress as a ratio to the deviator stress at failure.

$$M_r = k_1.(\sigma_3)^{k_2}.\left(1 - k_3.\left(\frac{\sigma_d}{\sigma_{d,f}}\right)^2 + k_4.\left(\frac{\sigma_d}{\sigma_{d,f}}\right)\right) \tag{2.6}$$

Where:

$\sigma_{d,f}$ = Deviator stress at failure (kPa)

The final method described by Van Niekerk is known as the $M_r - \theta - \sigma_d/\sigma_{d,f}$ model and is shown in Equation 2.7. This model was derived from the $M_r - \theta$ model and therefore shows the same drawback. The model fits the data globally, but is physically not correct. The first term ($k_1.\theta^{k_2}$)

describes the increase of M_r with increasing confinement or applied stress, but cannot discriminate between the influence that the stress invariants σ_3 and $\sigma_{d,f}$ individually have on the resilient modulus. The second term
$1 - k_3(\sigma_d/\sigma_{d,f})^{k4}$ describes the decrease of M_r as the material approaches failure. The model is therefore able to describe the initial increase of M_r as well as the subsequent decrease.

$$M_r = k_1.(\sigma_3)^{k_2}.\left(1 - k_4.\left(\frac{\sigma_d}{\sigma_{d,f}}\right)^{k_5}\right) \tag{2.7}$$

2.5 Permanent deformation

Permanent deformation (rutting) is the accumulation of shear deformation caused by repeated loading. Permanent deformation in BSM base layers and underlying granular layers can contribute to low serviceability and shorten the life of the structure. Accumulation of rutting is dependent on a number of factors including the material's shear properties and effective compaction (Wirtgen Group, 2012).

Table 2.3: Permanent deformation mechanism in granular materials (Dawson and Kolisoja, 2006)

Deformation	Description	Illustration
Mode 0	Permanent deformation caused by compaction of non-saturated meterial. Typically normal compaction prior to trafficking is sufficient to prevent further compaction under trafficking. This mode is self-stabilizing, apearing as a narrow depression.	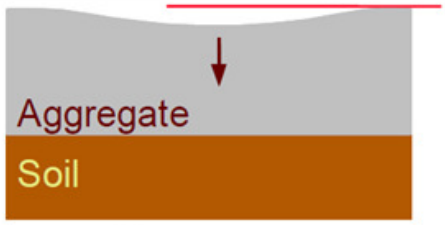
Mode 1	In weaker granular materials, local shear close to the wheel may occur giving rise to heace immediately adjacenet to the wheel path. This form of permanent deformation is mostly due to inadequate shear strength of the material close to the surface.	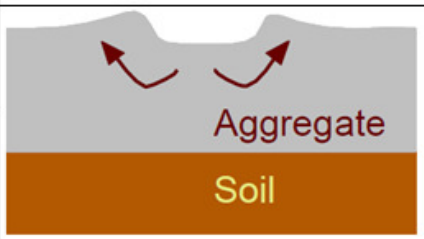
Mode 3	With a good quality aggregate, the pavement as a whole may deform without thining of the granular layer. The subgrade deforms, causing a broad rut with a slight heave away from the wheel path at the surface.	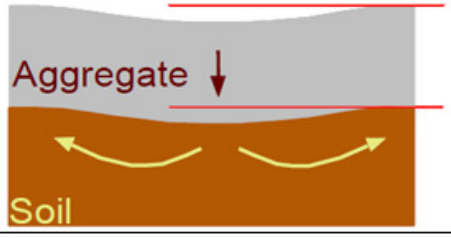

Other factors influencing the susceptibility to permanent deformation include the number of load cycles, moisture content, stress history and grading (Werkmeister, 2003). Permanent deformation

is the main failure mode for granular materials and in turn for BSMs. The design of granular materials and BSMs is aimed at reducing the development of weak points and to limit the amount of permanent deformation. Shear properties, specifically the calculation of DSR, was explained in Section 2.4.1.

Failure due to permanent deformation can be defined as the vertical displacement of the surface of the road beyond a specific value, typically 10 mm or 20 mm. Pavement structures undergo different types of permanent deformation depending on the nature of the damage and the materials in the structure. Dawson and Kolisoja (2006) described three types of permanent deformation mechanisms that occur in granular materials, which is also applicable for BSMs. These three types of permanent deformation are summarized in Table 2.3.

From the illustrations in Table 2.3 it is clear that permanent deformation can influence different components of the pavement structure. There is another, more complex, pattern of permanent deformation which occurs due to a combination of these deformation mechanisms. The mechanism illustrated in Mode 0 can, for example, occur in the base or subbase or both.

The measurement of permanent deformation in pavement structures is rather simple, but the prediction thereof is much more complex. Lekarp et al. (2000) proposed that the prediction of permanent deformation should not only be dependent on material properties, but also on the environmental conditions and load spreading ability over the life of the pavement. Factors that influence permanent deformation in BSMs are discussed in Section 2.5.1 to Section 2.5.8.

2.5.1 Effect of grading

The relative density and resistance to permanent deformation are, to a great extent, dependent on the grading of the material (Werkmeister, 2003). The influence that grading has on permanent deformation is in turn influenced by the degree of compaction of that material. Van Niekerk (2002) noted that if the grading of materials is changed in such a way that the relative density increases, the resistance to permanent deformation will rise. Therefore the influence of grading on permanent deformation is influenced by the compaction effort during construction.

Materials with the same particle distribution and the same fines content, experience an increase in stiffness with an increase of particle size. As the size of the particles increase, the contact surface between particles decreases causing a reduction in total deformation and a higher stiffness (Kancherla, 2004). Kolisoja (1998) showed that materials with a very high amount of fines (0.074 mm $>$ 15%) or very low amount of fines, experience a large increase in deformation. This was

explained by making the assumption that the fines fraction does not fit into the pore spaces created by the larger particles. This prevents full contact of the larger particles, reducing the stiffness and resistance to permanent deformation. Van Niekerk (2002) concluded that a balanced grading performs much better in terms of permanent deformation resistance than a uniform grading.

The filler fraction and the fine sand fraction have a significant effect on the dispersion of foamed bitumen or the breaking of bitumen emulsion. Materials that do not have a sufficient amount of fines will not mix well with foamed bitumen. However, bitumen emulsion can be used with materials with less fines and still produce a good quality mix. Figure 2.12 shows the general grading requirements for BSMs indicated in terms of zones of most suitable aggregate composition. The difference between the grading zones of BSM emulsion and BSM foam are very small and the difference cannot be shown on the figure.

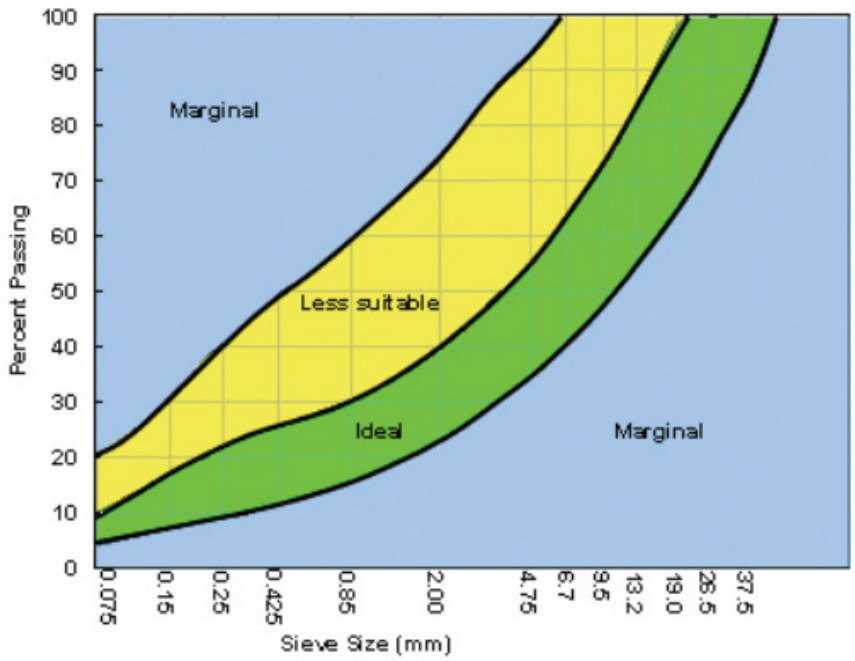

Figure 2.12: Grading of parent aggregate for BSM mixes (Asphalt Academy, 2009)

The amount of fines in a granular materials increase over time as aggregates break and segregate during construction and due to repeated loading (Kotze, 2014). Hicks and Monismith (1971) found that the stiffness modulus decreases with an increase in the amount of fines in partially broken aggregate, while the opposite was found in fully broken down aggregates. The effect of the amount of fines on permanent deformation resistance was investigated by Barksdale (1972) and Thom and Brown (1988). They concluded that deformation resistance in granular materials is reduced as the amount of fines increases.

2.5.2 Effect of physical properties of aggregate particles

The physical properties of aggregate particles, like grain shape and surface roughness, are some of the least observed parameters that affect permanent deformation (Werkmeister, 2003).

The grain shape of coarse-grained aggregates is significantly influenced by the mineralogical composition of these particles. The crushing technique used to produce crushed materials influences its grain shape. Two general groups can be distinguished with regards to grain shape; the first group consist of natural sands and gravels, the second group is composed of crushed materials (Werkmeister, 2003).

Particle contact in the first group is between two smooth surfaces, while in the second group (i.e. crushed aggregates) the particle edges can be very sharp. The difference between the rounded grains and the sharp edges has a significant effect in long term and permanent deformation behaviour. Crushed materials tend to have more grain abrasion, especially at high stress levels (Werkmeister, 2003).

The effect of macro and micro roughness of aggregate particles on deformation behaviour has been investigated by numerous researchers. Werkmeister (2003) states that the surface friction at the contact point of particles can be assumed to affect the resilient deformation behaviour, especially when external load reaches the value that causes particles to slide.

2.5.3 Effect of density

The methods used to determine a reference density for a specific material in a laboratory have evolved over the years. The reference density of the material can be used to determine the level of compaction achieved in the field. In 1933 Ralph Proctor introduced the Proctor Test, where the materials compacted in 3 layers, using a standard hammer, in a standard 100 mm diameter steel mould. The highest density achieved, after testing at various moisture contents, is calculated as a dry density and is known as the "maximum dry density" (MDD), while that moisture content is known as "optimum moisture content" (OMC)(SAPEM, 2014).

The Proctor Test is still used in dam earthworks construction, but has been superseded by a similar type of test in the road building industry. The compaction effort has been increased and is applied to the materials in five layers in a 150 mm mould. OMC and MDD are determined in the same manor as for the Proctor Test. This density obtained from this test is known as the "Mod" or Modified AASHTO density (SAPEM, 2014).

The resistance to permanent deformation of unbound granular materials under repeated loading can be improved by increasing the density of the material ((Werkmeister, 2003), (Van Niekerk, 2002), (Barksdale, 1972). (Barksdale, 1972) studied the influence of density on deformation behaviour of granular materials. He found an increase in permanent axial strain, in the order of 185%, when the material was compacted at 95% instead of 100% of normal Proctor density (Figure 2.13). Van Niekerk (2002) also found that higher axial stresses are necessary to achieve the same amount of axial deformation in samples compacted to 103% compared to 97% of Proctor density.

The resistance to permanent deformation due to repeated loading can be highly improved by increasing the density of the materials. Therefore the same stress path leads to a smaller permanent strain value for a specimen with a high density compared to one with a low density (Werkmeister, 2003).

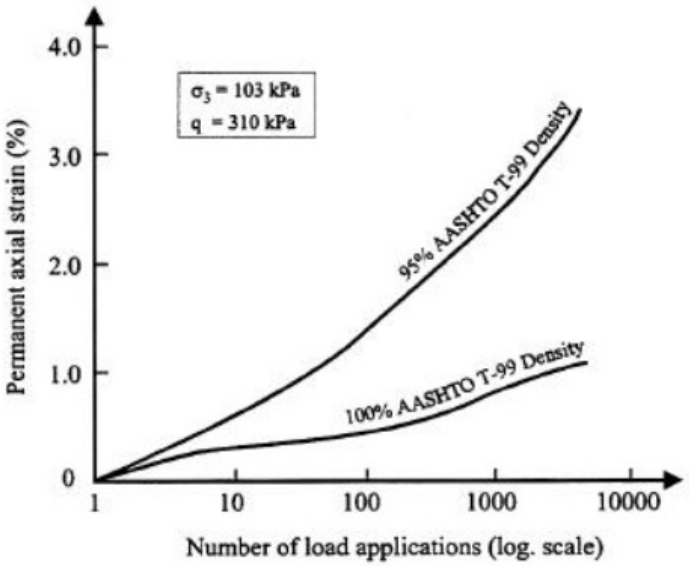

Figure 2.13: Effect of density on permanent axial strain (Barksdale, 1972)

The durability and performance of a BSM mix depend on its level of compaction. Compaction improved particle contact, reduces void contents and also improved binder adhesion to the aggregate in the mix (Jenkins, 2000*b*). During mixing of BSMs, foam bubbles disperse and emulsion droplets break and favourable coat the filler fraction and partly coat the coarse fraction. At this stage the mineral aggregates are in a conglomerate state which means the interaction between binder and aggregate is incomplete. Therefore, through compaction the following advantages may occur (Dal Ben, 2014):

1. Cohesion and adhesion of mastic and mineral aggregates are improved;
2. Compression of bitumen between larger fractions;
3. Moisture is squeezed out of the mineral aggregates and mastic;
4. Mineral aggregate packing is enhanced.

2.5.4 Effect of moisture content

The water film on the surface of granular particles influences the shear resistance of the materials. Moisture damage significantly contributes to the deterioration of pavement materials. This holds true for asphalt, BSMs or granular materials. In practice unbound granular materials always contain some water. A moderate moisture content improves the strength and the stress and strain behaviour of granular materials (Werkmeister, 2003).

If the moisture content is increased, reaching saturation, positive pore-water pressure develops under repeated load application. This excess pore-water pressure reduces the effective stress, resulting in diminishing permanent deformation resistance of the materials (Lekarp et al., 2000). Figure 2.14 shows results of a repeated tri-axial test of two specimen. One of the specimens was allowed to drain, while the moisture content was held constant in the other. The undrained specimen showed much more deformation at the same number of load repetitions.

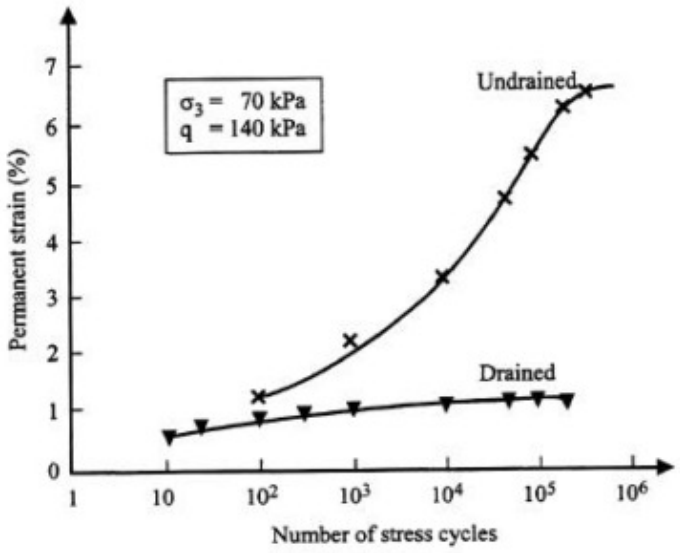

Figure 2.14: Influence of drainage on permanent deformation development (Dawson, 1990)

Research has shown that the effect of moisture content also depends on the type of analysis used. Hicks and Monismith (1971) explained that a decrease in stiffness is shown if the analysis is based on total stress. It was also noted that when tests were based on effective stress, the stiffness modulus remained constant. Dawson (1990) investigated a wide variety of well graded unbound granular materials and found that the stiffness of the materials increases with an increase of moisture content, only if the moisture content remains less than the optimum moisture content. When the limit is exceeded, the materials gets saturated and excess pore water pressure develop, leading to reduction of stiffness.

(Mathaniya, 2010) tested a number of BSM mixes at equilibrium moisture content and after MIST conditioning. The dry samples showed significantly less permanent strain accumulation over load repetitions when compared to the MIST conditioned samples.

2.5.5 Effect of number of load repetitions

A number of researchers have found that permanent deformation in unbound granular materials constantly increases with an increase in the number of load repetitions. Morgan (1966) reported that permanent deformation increases until the end of 2 000 000 load repetitions. Barksdale (1972) investigated permanent deformation to 100 000 load repetitions in sandstone and biotite granite gneiss materials. A linear logarithmic relationship was found between the cumulative permanent strain and the number of load repetitions. He also found that the increase in permanent deformation accumulation in materials subjected to small deviator stresses, decreases with number of load repetitions. However, the rate of permanent deformation accumulation increases, when the deviator stress exceeds a certain point.

(Kolisoja, 1998) found that test specimens stabilised after 90 000 load repetitions. Additional load repetitions were performed and showed a progressive linear relationship as permanent deformation accumulated (Figure 2.15). This figure clearly shows that there is a direct relationship between the amount of load repetitions and the deviator stress ratio.

Van den Berg (2014) performed repeated loading tests with up to 500 000 load repetitions. The importance of the application of a large amount of load repetitions compared to a limited amount was investigated by Kotze (2014). Van den Berg (2014) tested materials by applying 50 000 load repetitions to predict the deformation at 500 000 repetitions. The same models were used to predict the permanent deformation at 1 000 000 load repetitions. Table 2.4 shows the deviations that were observed from the long and short tests.

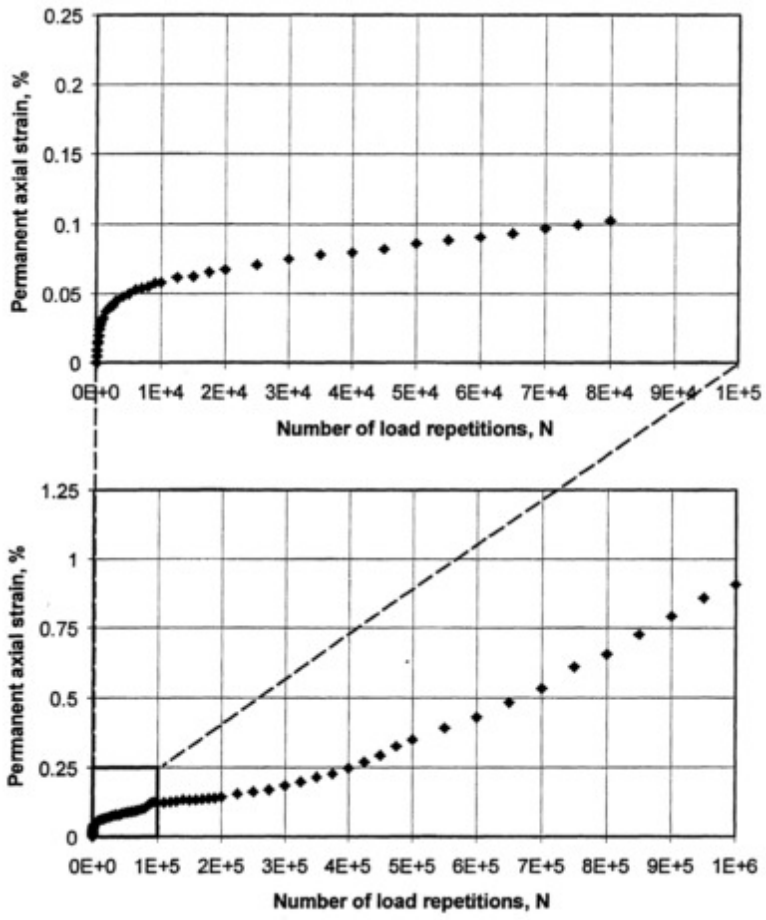

Figure 2.15: An example of the effect of the number of load repetitions on permanent strain (Kolisoja, 1998)

Van den Berg (2014) found that the short version of the test underestimated the permanent deformation at 1 000 000 load repetitions. He concluded that that the shorter version of the test was applicable when the objective of the test was to compare the long term performance of different mixes. If the objective of a study was to obtain information about a single mix, the longer form of the test would yield more reliable results.

The influence that the amount of load repetitions has on permanent deformation depends on the applied stress ratio. Van den Berg (2014) performed tests and modelled the permanent deformation behaviour at different stress ratios as shown in Figure 2.16. The tests were performed on a 14% natural filler mix. At relatively low stress ratios ($\sigma_d/\sigma_{d,f} = 35\%$) the rate of permanent deformation accumulation after 50 000 load repetitions became so low as to be negligible. When the stress ratio was increased ($\sigma_d/\sigma_{d,f} = 45\%$), the rate of permanent deformation accumulation only reached a plateau after 100 000 cycles. At a stress ratio of $\sigma_d/\sigma_{d,f} = 55\%$, permanent deformation

accumulated rapidly over the first 20 000 cycles, after which it increased at a constant rate up to 500 000 cycles.

Table 2.4: Comparison of Permanent Deformation Model Applications (Van den Berg, 2014)

% Fines	Estimated $\sigma_d/\sigma_{d,f}$ ratio	Actual $\sigma_d/\sigma_{d,f}$ ratio	ε_p at N=5x10^5 (%)		Deviation	Actual Applied Load Repetitions
			N = 50k Test	N = 500k Test		
F = 6%	35%	31%	0.707%	0.389%	182%	501400
	45%	40%	1.412%	0.843%	168%	501400
	55%	49%	3.699%	3.265%	113%	79000
F = 10%	35%	35%	1.390%	0.944%	147%	501400
	45%	45%	2.584%	1.796%	144%	358600
	55%	55%	4.257%	4.257%	100%	33400
F = 14% natural	35%	36%	1.330%	0.873%	152%	501400
	45%	46%	2.895%	2.033%	142%	501400
	55%	56%	3.571%	3.498%	102%	501400
F = 14% 50-50	35%	36%	0.665%	0.477%	139%	501400
	45%	46%	1.364%	1.053%	130%	501400
	55%	57%	3.175%	2.285%	139%	501400

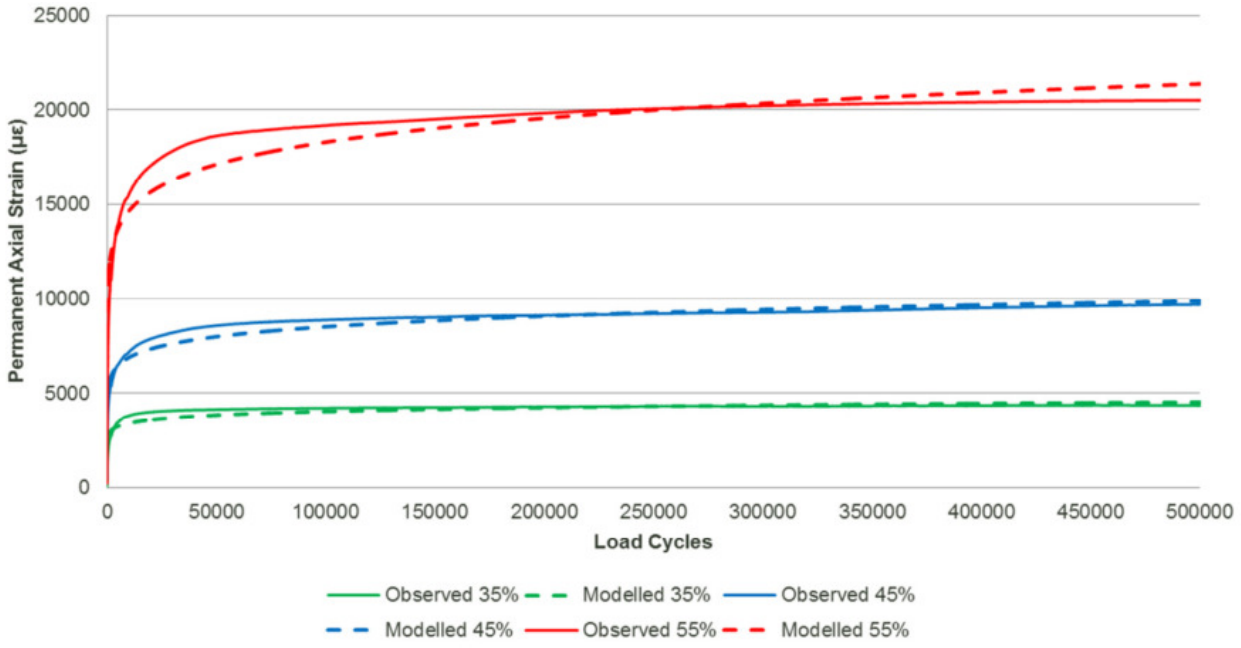

Figure 2.16: Observed and modelled permanent deformation behaviour of 14% natural filler mix (Van den Berg, 2014)

2.5.6 Effect of applied stress

The magnitude of permanent deformations that develop in granular materials strongly depends on the stress level, increasing with rising deviator stress and decreasing confining stress (Werkmeister, 2003). Morgan (1966) investigated the impact of deviator stress and confining stress on cumulative permanent deformations. A direct dependency between the cumulative strains, number of load cycles and deviator stress was found at a particular confining pressure. By maintaining a constant deviator stress level, Morgan (1966) also ascertained that the permanent axial strains were inversely proportional to the confining stress.

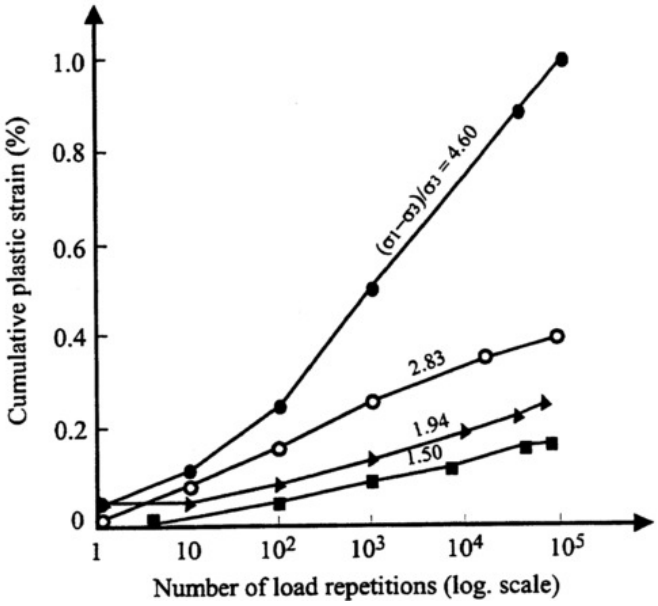

Figure 2.17: Influence of stress ratio on permanent deformation in a Granite Gneiss-material (Barksdale, 1972)

Barksdale (1972) conducted tri-axial tests on unbound granular materials at constant confining stress levels up to 100 000 load repetitions. He concluded that permanent deformation is highly dependent on applied load and increased when confining pressure decreased and deviator stress levels increased (Figure 2.17).

Lashine et al. (1971) tested partially saturated crushed limestone in drained conditions to show that permanent axial strain increases until reaching a constant value at a specific stress ratio. (Boyce, 1976) found that permanent deformation reaches a constant value if the deviator stress applied to the sample is rather low. When a higher deviator stress is applied, the material will continue to deform. Pappin (1979) confirmed these findings and suggested that axial deformation should

be a function of deviator stress ratio. Werkmeister (2003) tested sandy gravels and found that permanent deformation reached a balance at low deviator stress ratios and increased at high ratios.

Werkmeister (2003) highlighted the importance of the shakedown theory when investigating permanent deformation. The shakedown theory predicts an increase in permanent deformation of a pavement structure if the applied stress ratio exceeds a certain limit, known as the shakedown limit. If the applied stress ratio remains lower than the shakedown limit, permanent deformation in the material will reach a constant value after a certain number of load repetitions. Once this point has been reached, mostly plastic deformations occur in the material.

Figure 2.18 illustrates these findings and describes permanent deformation in terms of applied stress. The figure highlights four categories of material response under repeated loading (Werkmeister, 2003):

0. **Purely elastic**: if the applied repeated stress is sufficiently small no element of the material reaches the yield condition. All deformations are fully recovered under this loading and the response is purely elastic.

1. **Elastic shakedown**: occurs when the applied stress ratio is slightly less than required for plastic shakedown. In this case the material response is plastic for a finite number of load repetitions; however, the ultimate response is purely plastic. The material is said to have "shaken down". The maximum stress level at which this condition is possible is referred to as the "elastic shakedown limit".

2. **Plastic shakedown**: occurs when the applied repeated load is slightly less than that required to produce collapse after the accumulation of permanent strain. The materials show a long term steady state, i.e. no further accumulation of permanent strain is shown and each response is hysteretic (lagging behind the applied stress). This indicates that the material absorbs a certain amount of energy during each load application. When a purely resilient response has been obtained it is again referred to as "shaken down". The maximum stress limit at which this is possible is referred to as the "permanent shakedown limit".

3. **Incremental collapse**: also referred to as ratcheting, occurs when the applied load is relatively large. The applied stress causes the material to exceed the yield limit. This causes permanent strains to accumulate rapidly and the material failing in a relatively short time.

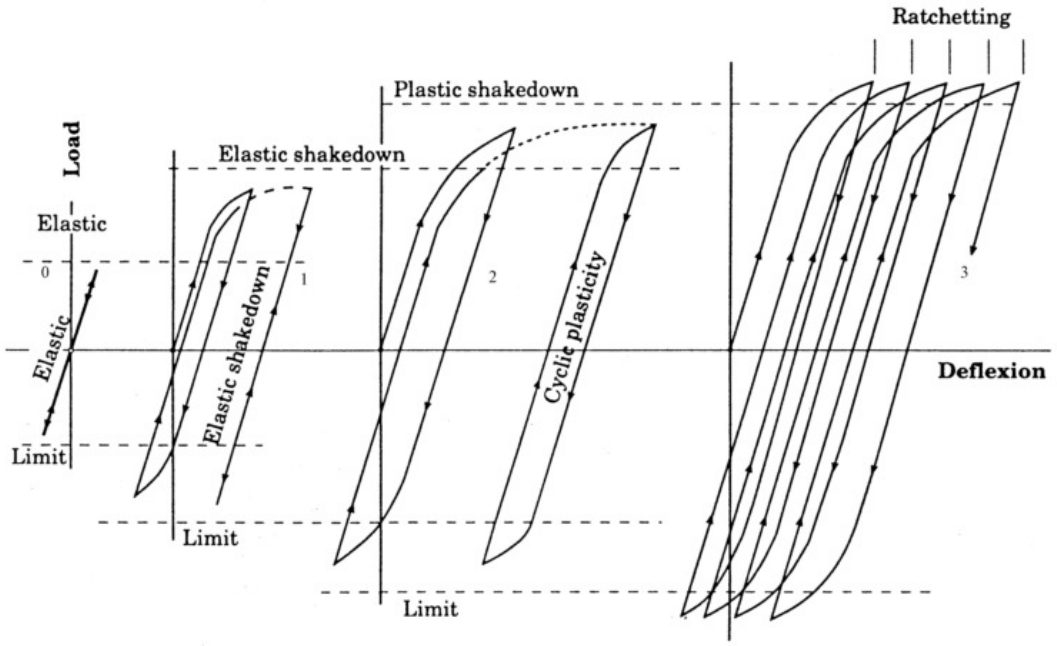

Figure 2.18: Elastic/permanent strain behaviour under repeated cyclic pressure and tensile load (Werkmeister, 2003)

2.5.7 Effect of stress history

Permanent deformation behaviour of unbound granular materials is directly linked to the stress history of the material. Brown and Hyde (1975) studied the impact of stress history on permanent deformation of granular materials. They found that a higher level of stress leads to larger permanent deformations as shown in Figure 2.19. It was also found that a slow increase in stress causes less permanent deformation, when compared to applying high stress immediately.

The effect of stress history on permanent deformation has been recognized, but limited research has been carried out to study this effect. When using the current permanent deformation laboratory tests, the effect of stress history is normally eliminated as a new specimen is used for each stress path applied (Werkmeister, 2003).

2.5.8 Effect of lateral pressure

The stiffness modulus of granular materials increases with an increase of lateral pressure (Lekarp et al., 2000). Allen and Thompson (1974) compared the stiffness of values obtained from tests performed at a constant confining pressure with tests performed at variable confining pressures. It was found that the stiffness modulus of material tested at a constant confining pressure was higher than at variable confining pressures. They also found that tests performed at a constant

confining pressure showed more lateral deformation and that permanent deformation decreases with a increase in confining pressure.

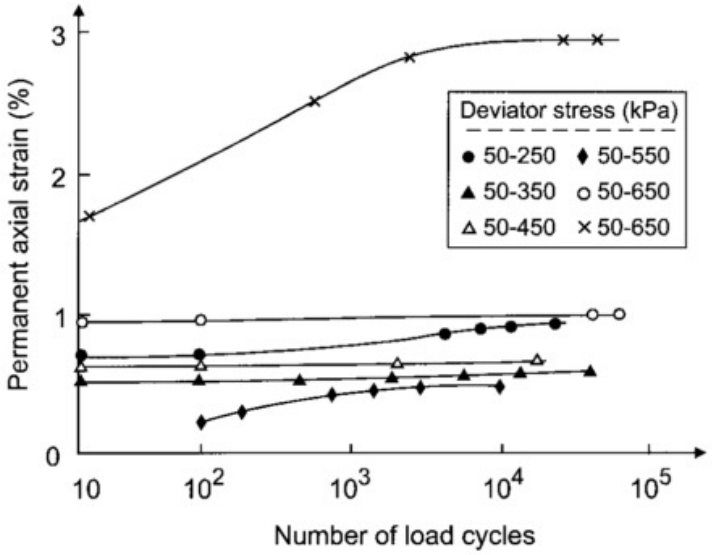

Figure 2.19: Effect of stress history on permanent strain (Brown and Hyde, 1975)

2.5.9 Effect of active filler

The types of filler used with BSMs are cement, lime, rock flour, fly ash and slagment. The term active filler is used for fillers that chemically alter the mix properties. Active fillers include cement, lime and fly ash and excludes the natural fillers such as rock flour.

Active fillers are incorporated in BSMs for a number of reasons (Asphalt Academy, 2009):

1. Improved adhesion of bitumen to the parent aggregate.
2. Improved dispersion of bitumen in the mix.
3. Reduces the plasticity of the natural materials.
4. Increases the rate of strength gain and stiffness of BSMs.
5. Acceleration of the curing process.

The application rate of cement as an active filler should be limited to a maximum 1% of the dry aggregate. When hydrated lime is used as an active filler, this rage might be increased to 1.5% of the dry aggregate (Asphalt Academy, 2009). These limits are set in place limit the loss of flexibility that occurs with an increased stiffness.

Ebels (2008) found that the addition of cement resulted in a reduction of the angle of internal friction. However, this reduction was compensated for by the more significant increase in cohesion and the overall increase of the shear strength.

Mathaniya (2010) investigated the moisture resistance of BSMs. It was found that BSMs with no addition of active filler fail at a low number of load repetitions compared to BSMs with additional active filler. (Long et al., 2004) also found that cement has a greater effect on the reduction of moisture sensitivity than foamed bitumen.

2.5.10 Laboratory tests for permanent deformation

The permanent deformation (ϵ_p) behaviour of a BSM is determined using the triaxial test by means of repeated loading for a fixed deviator stress ratio. After a number of load repetitions at a certain stress level, permanent deformation can be calculated using Equation 2.8.

$$\epsilon_p = \frac{\Delta H}{H_0} * 100\% \tag{2.8}$$

Where:

ϵ_p = Permanent deformation as a percentage of specimen height.

ΔH = Change in height of the specimen.

H_0 = Original height of the specimen.

Van Niekerk (2002) performed a number of permanent deformation tests on granular base materials at a constant confinement (σ_3 = 12 kPa) and increasing levels of applied stress. The results of these test showed that an increase in DSR has a large effect on the accumulation of permanent deformation. Figure 2.20 shows the permanent strain accumulation against number of repeated loads for different stress ratios.

A large increase in permanent deformation due to an increase in stress ratio can be observed. This gives an indication that stress ratio is a critical design parameter for granular materials and in turn BSMs. The stress ratios are calculated as illustrated in Figure 2.8 using Equation 2.2.

Ebels (2008) investigated the permanent deformation behaviour of BSMs. Figure 2.21 shows the permanent deformation behaviour of a BSM with active filler. This figure shows a significant reduction in life (number of load repetitions to reach 10% permanent strain) with an increase in stress ratio. Dal Ben (2014) found similar results for BSM foam mixes.

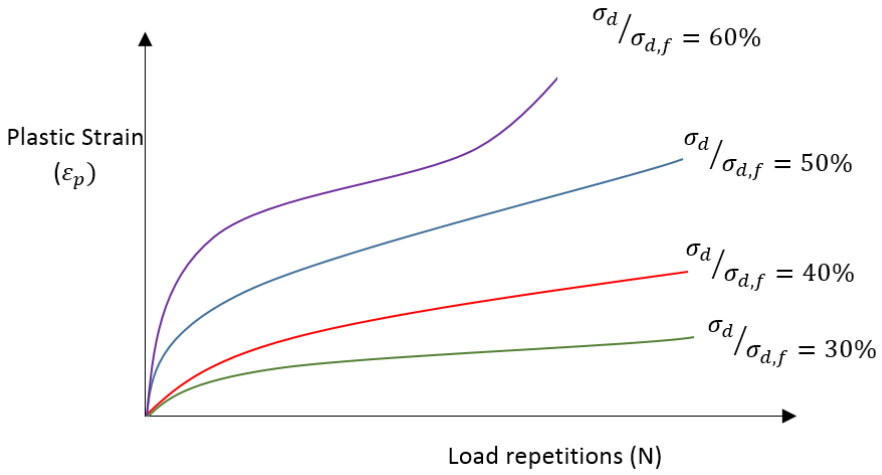

Figure 2.20: Plastic strain accumulation

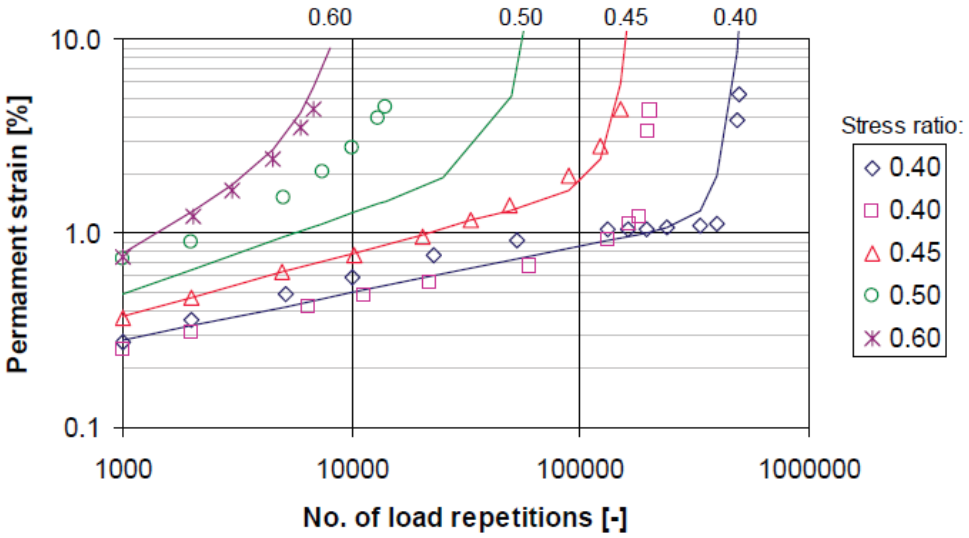

Figure 2.21: Permanent strain model fits (Ebels, 2008)

Permanent deformation is the critical failure mechanism for BSM and it is therefore important to measure the resistance to permanent deformation of the given material. From Figure 2.20 and Figure 2.21 it is clear that the DSR has a significant effect on the amount of plastic strain that accumulates. Therefore, when designing a BSM, the DSR should be kept as low as possible to ensure the best long term performance of the layer.

2.6 Long term performance behaviour of BSMs

The development of stiffness over long periods of time is important to the understanding of BSM performance under traffic loading as it defines the load spreading ability of the BSM over the life of the pavement. Collings and Jenkins (2011) investigated three heavily trafficked pavements, each

with less than 3% residual binder and less than 1.2% cement. These were good representations of typical BSMs produced in South Africa and the majority of BSMs used globally (Collings and Jenkins, 2011). These three studies are discussed in Sections 2.6.1 to 2.6.3.

Lynch and Jenkins (2013) supplemented these three studies with research into the long term pavement performance of in-service BSM base layers with a recent test section on the R35 rural road in South Africa. This study included variables of base type (granular, cemented and BSM), mix compositions, layer thickness and traffic. This study is discussed in Section 2.6.4

2.6.1 Athens-Corinth highway in Greece

The pavement section of the major 6-lane highway between Athens and Corinth in Greece was analysed in order to study the relationship between BSM stiffness and time lapsed. The pavement was rehabilitated in 2002 using in-place recycling with 2.3% foamed bitumen and 1% cement. The National Technical University of Athens (NTUA) carried out FWD measurements initially as part of the rehabilitation investigation. Subsequent measurements were taken 1 month, 6 months and then at yearly intervals until 4 years after construction (Loizos and Papavasiliou, 2007).

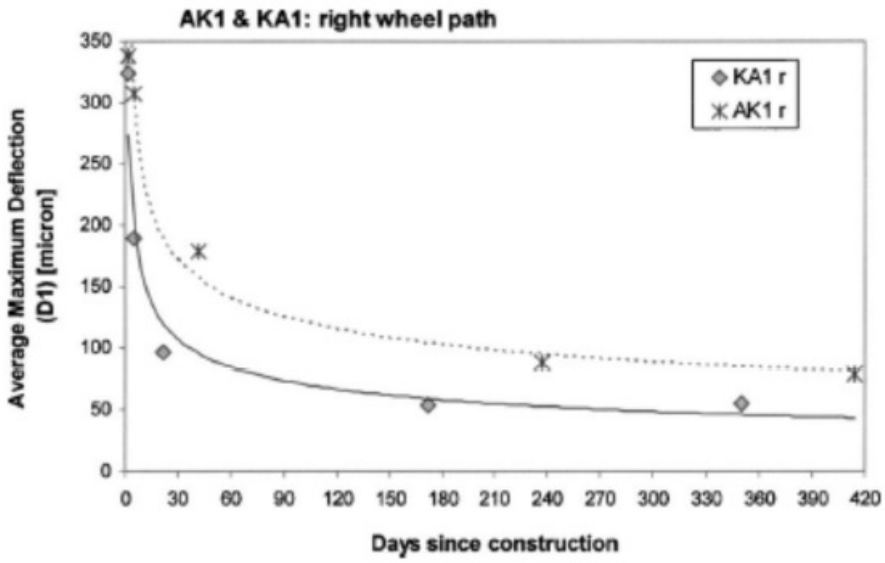

Figure 2.22: Change in maximum deflection over time (Loizos and Papavasiliou, 2007)

The reduction in the maximum deflection measured at these times for the slow lane is given in Figure 2.22. The BSM-foam and HMA were the only new layers in the pavement structure, therefore stiffening of the structure could only have emanated from the BSM layer.

The FWD data was further analysed using deflection bowl back calculation to determine the relationship between the stiffness modulus and the time elapsed. This relationship is shown in Figure 2.23. The stiffness values of the BSM were unrealistically high, but the trend of increasing stiffness over time is clear.

During the investigation period the pavement was subjected to around 60 000 vehicles per day. Around 20% of these vehicles were loaded to the legal axle limit of 130 kN. One of the important features shown by this study was the asymptotic relationship between back calculated stiffness with time, as the material continued to gain stiffness.

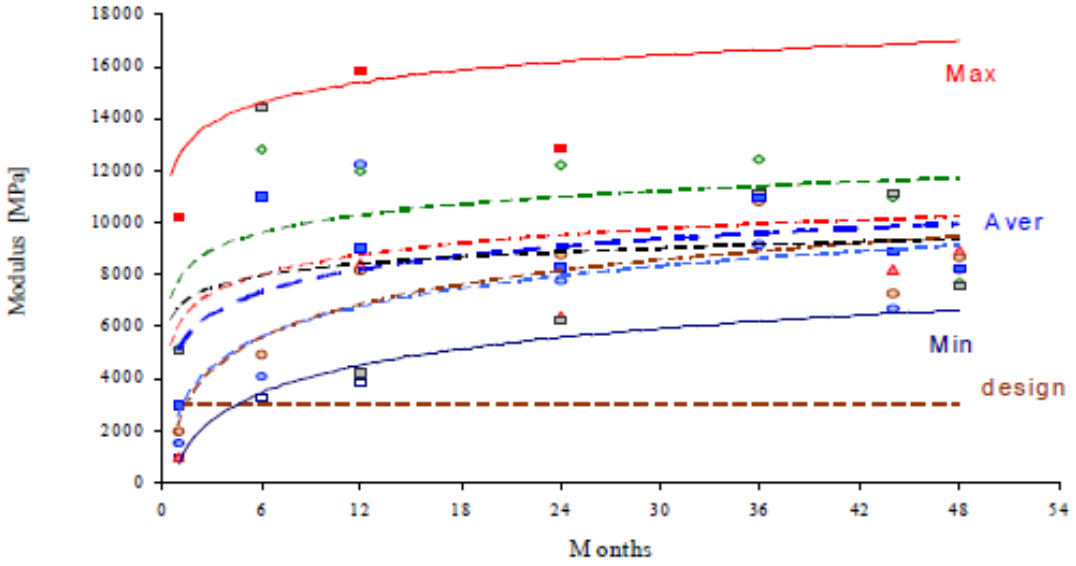

Figure 2.23: Change in effective modulus of BSM-foam over time (Loizos and Papavasiliou, 2007)

2.6.2 Jingshen highway in China

Another analysis of long term pavement behaviour, specifically BSMs, was carried out on the Jingshen Highway in China. The pavement was rehabilitated in 2005 where 200 mm of asphalt was milled and stockpiled. The cement stabilised crushed stone subbase was then recycled in situ to a depth of 200 mm adding 2.3% foamed bitumen and 1% cement. A 150 mm layer of reclaimed asphalt (RA) treated in plant with 2% foamed bitumen and 1% cement was paved as the new base layer.

The base layer was overlain with 50 mm HMA surfacing before opening to traffic. Deflections were measured using a Benkelman Beam by the Research Institute of Highways up to one year after construction. The measured deflections are shown in Figure 2.24 (Collings and Jenkins, 2011).

Figure 2.24 shows a significant reduction in the maximum and average deflection. The deflection reduction indicating an increase in the stiffiness modulus of the BSM. This reduction in deflections is almost asymptotic, indication the majority of the change occurring during the first month after construction and reducing with time. This pavement was exposed to extreme traffic during the whole year after construction. In spite of the extreme traffic, the BSM layer continued to increase in stiffness (Collings and Jenkins, 2011).

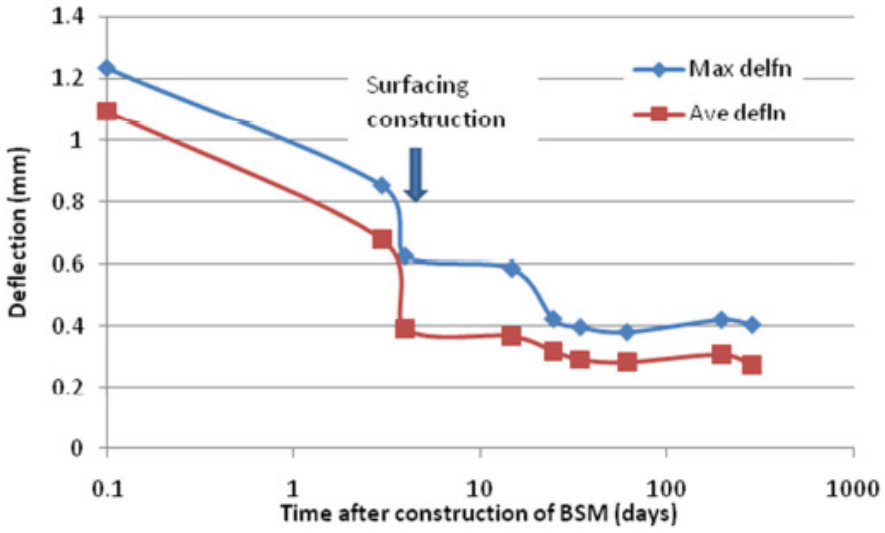

Figure 2.24: Jingshen Highway, deflections with time after construction (Collings and Jenkins, 2011)

2.6.3 National Route 7 Section 1 near Cape Town

A section of the N7 highway near Cape Town was rehabilitated with BSM-foam (2.3% bitumen and 1% cement) on the Southbound Carriageway in 2002. The Northbound Carriageway of the same section was rehabilitated in 2007 with BSM emulsion (2% residual bitumen and 1% cement). The construction of both carriageways involved in situ recycling to a depth of 250 mm. Physical moisture measurements were taken of the BSM emulsion in the laboratory, supplemented by moisture button monitoring in the layer (Moloto, 2010).

Additionally, Portable Seismic Pavement Analyser (PSPA) measurements were taken at different points in time in order to evaluate the modulus of the base over time. Figure 2.25 and Figure 2.26 show the development of moisture content and stiffness modulus over time. The Mr values indicated in these figures are unrealistic for BSMs. These high Mr values may be due to a high cement content in the mix. However, from these figures it can be observed that the modulus is

inversely proportional to the moisture content in the BSM emulsion layer. This process is known as curing (Collings and Jenkins, 2011).

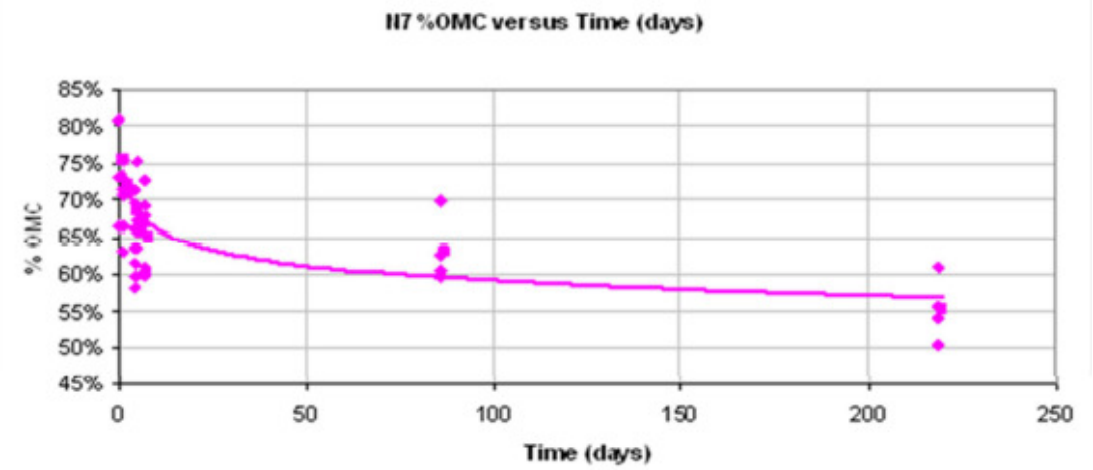

Figure 2.25: Moisture content in BSM emulsion base from oven drying (Moloto, 2010)

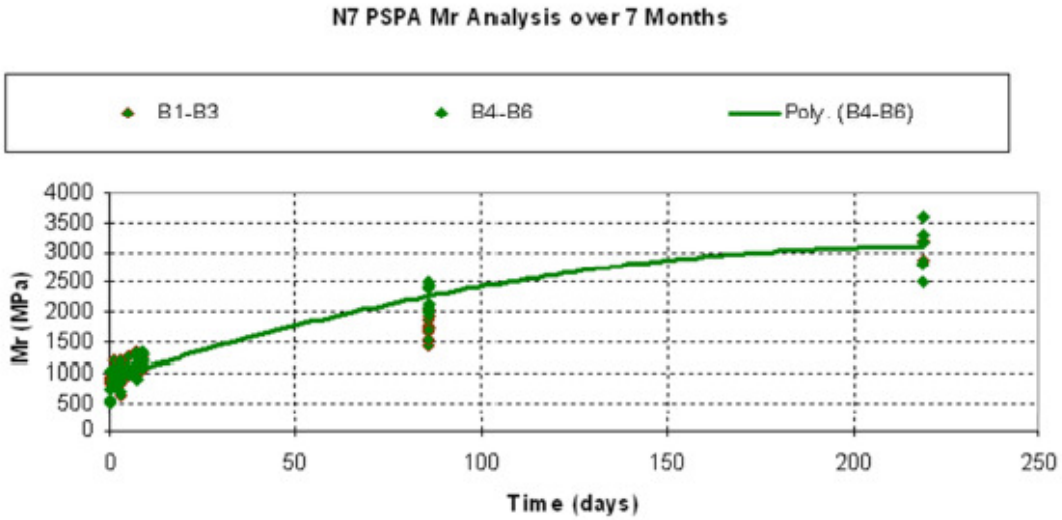

Figure 2.26: Modulus of BSM emulsion base measured with PSPA (Moloto, 2010)

These three examples focused on the first year after construction, each demonstrating an increase in effective stiffness of the BSM base layers. These results were consistent with trends found in the laboratory during curing of BSMs. From these findings the following insights were obtained (Collings and Jenkins, 2011):

1. The effects of curing and moisture reduction in BSMs exposed to traffic, dominate the behaviour of the materials for about one year after construction.

2. It is probable that the stiffness of BSMs exposed to traffic can stabilise and reduce after several years of service. This reduction is likely to be a result of rupturing of the bitumen spot welds due to excessive shear stresses caused by heavy vehicles or elevated moisture contents, rather than fatigue failure.

3. The increase in stiffness, of the BSM layers in these studies, with accumulated traffic are counter to the trend for continuously bound materials. Continuously bound materials are prone to fatigue degradation, reducing the stiffness with accumulated traffic. Such a trend would appear to confirm that non-continuously bound BSMs are not prone to fatigue degradation.

2.6.4 R35 experimental section Mpumalanga

As part of the revision of the South African Mechanistic Design Method, the South African National Roads Agency (SANRAL) constructed a 4.5 km long experimental section to investigate the long term performance of stabilised materials. This section included both purely cemented and bitumen stabilised materials (Lynch and Jenkins, 2013). For the purpose of this study, focus was placed on the foamed bitumen stabilised materials in this section.

Construction of the experimental section took place during 2012 on the R35, north of Bethal, Mpumalanga, South Africa. In situ recycling was used for the stabilisation during this project. The foamed bitumen mixtures used either 1% or 2% cement content together with 2.4% residual bitumen. The layer thicknesses of the BSM foam was either 175 mm or 200 mm. The region was classified as a moist sub-humid climate according to the modified Thornwaite Moisture index.

FWD measurements were carried out at 5 metre intervals over a 360 day period from the completion of each section. The method to obtain FWD data is discussed in Section 3.3 with the FWD setup depicted in Figure 3.12.

The results of the FWD analysis were back calculated to obtain stiffness values for the BSM layers. Figure 2.27 exhibits the trend in average back calculated stiffness of the 175 mm BSM foam layer with 1% cement for the Southbound section.

Events that may have influenced the results are indicated on the figure along with important rainfall data. This figure shows the important factors which had an effect on the stiffness on the layer. Most significant is the reduced stiffness from opening to traffic (90 days) to 180 days. The blue markers show that at 180 days the area was receiving very heavy rainfall, which effected the stiffness values.

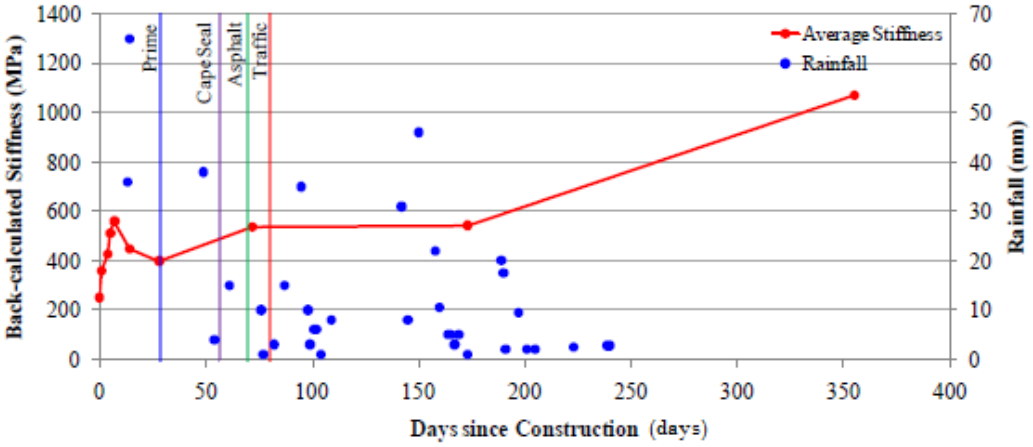

Figure 2.27: Average back Calculated stiffness trend - 175 mm BSM foam 1% cement, Southbound (Lynch and Jenkins, 2013)

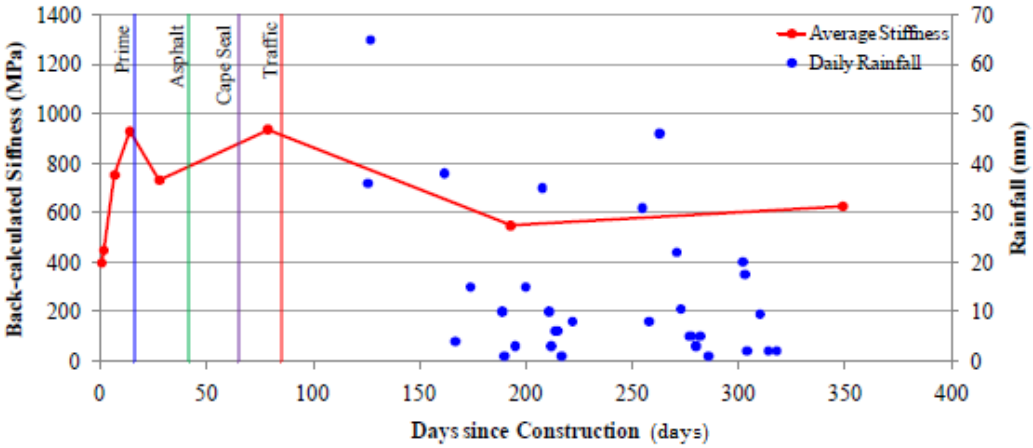

Figure 2.28: Average back calculated stiffness trend - 200 mm BSM foam 1% cement, Northbound (Lynch and Jenkins, 2013)

Figure 2.28 shows this information for the 200 mm BSM layer with 1% cement for the Northbound section. This section was constructed about 3 months before the Southbound. This is clear when investigating the rainfall data. This figure shows that after the heavy rainfall, the average stiffness increased throughout testing.

A conceptual stiffness model for BSMs during the service life was proposed by (Ebels, 2008) as shown in Figure 2.29. This model indicates an initial increase in stiffness due to curing and possible increase in density caused by traffic. After the initial curing phase, the stiffness of the materials decrease due to repeated traffic loading. This model describes the steady increase in

stiffness throughout the first year after construction. However, further studies should be done to determine the behaviour over longer periods of time.

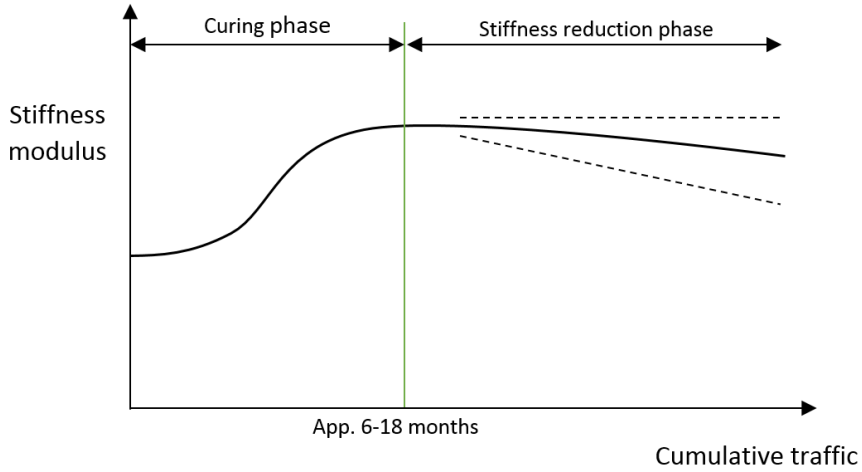

Figure 2.29: Conceptual long term stiffness of BSMs (Ebels et al., 2005)

2.7 BSM durability

Mixture design is a key factor in the long-term performance of bitumen stabilised materials in pavement structures. For hot mix asphalt, durability is measured as the binder's resistance to striping, ageing and degredation of modifiers in the binder, assuming that the parent aggregate in the mix is adequately durable (Hunter et al., 2015). The durability of BSM is based on material durability as well as mixture durability. Moisture damage is considered to be the main factor influencing durability, but the durability of the parent aggregate and bitumen also play a significant role (Jenkins, 2000*a*).

Moisture transport mechanisms together with environmental conditions, coupled with repeated loading, have been found to influence moisture damage mechanisms of BSMs (Mathaniya, 2010). Therefore, a test is required to induce moisture conditioning into test samples before mechanical testing. The moisture induction simulation test (MIST) is used to simulate realistic pulsing of water pressure into the mix matrix to determine the adhesion and cohesion deterioration of a mix.

2.7.1 Influence of compaction

Compaction method as well as degree of compaction plays a significant role in the durability of both laboratory and field constructed BSMs. During the mixing process dispersed bitumen particles

favourably coat the fine fraction and only partly coat the coarse fraction of the aggregate (Dal Ben, 2014). At this stage the mineral aggregate has not completed the binder-aggregate interaction. Compaction allows the following advantages to occur (Dal Ben, 2014):

1. Adhesion and cohesion of mastic and mineral aggregates are improved.
2. Bitumen or mastic between large fractions is compressed.
3. Moisture is squeezed out of the mineral aggregate and mastic to the surface.
4. Packing of mineral aggregates is enhanced.

2.7.2 Influence of curing

Curing of BSMs is the main influential process for bond development between bitumen and aggregate particle interfaces. Therefore, curing plays a vital role in the development of durability properties. Failure manifestation in BSM mixes may occur at an early age of the service life due to insufficient curing (Serfass et al., 2008). Dal Ben (2014) found that high water pressures, water expulsion and evaporation all effect curing of BSMs.

2.7.3 Moisture damage

Moisture damage is one of the main contributors to premature deterioration of asphalt, BSMs or granular materials. Deterioration is the process of degradation of the mechanical properties of materials due to infiltration of excess moisture into the microstructure (Dal Ben, 2014).
A damage mechanism is defined as a process that leads to change in the internal or external conditions of a system producing a new state or condition. When a system reaches a state where its original integrity has been reduced, the process is considered to be a damage mechanism. The moisture damage mechanism consists of the following two steps (Dal Ben, 2014):

1. Moisture transport: Process by which moisture or vapour infiltrates the material and reaches the binder and aggregate interface.
2. System response: The change in the material's microstructure properties leading to a loss of engineering properties.

Moisture transportation is influenced by the following material and mixture properties in BSMs:

1. Binder in BSMs does not completely cover larger aggregate particles.
2. Binder content in BSMs is lower than HMA, which may interconnect the voids in the mix.

3. The mineral aggregate is moist at the time of mixing, reducing adhesion.

4. The air void content is much higher in a BSM than in HMA.

These mechanisms have two different effects on the materials. High amounts of air voids with low connectivity allow development of pore pressure in a saturated flow condition. This process can cause mechanical failure due to erosion under repeated loading. Excessive moisture in the mix can diffuse through the mastic and displace binder from the aggregate, resulting in poor bond strength at the interface. BSM mixes are generally characterised by large localised voids with few interconnected voids. Therefore, pore pressure is characteristic of the moisture damage mechanisms in BSMs (Dal Ben, 2014).

2.8 Design methods

The basic principle of pavement design is to protect the pavement subgrade against stresses imposed by traffic. This is achieved by providing structural layers on the subgrade that distribute the imposed loads. The subgrade and structural layer should function as a unit in a balanced system in order to achieve the desired design structural capacity. The basic principle of pavement balance requires that there should be a gradual decrease in stiffness from the top to the bottom of the pavement layers. If the stiffness of the structural layers is far greater than that of the subgrade the pavement would not be in balance (Asphalt Academy, 2009).

The TG2 recommends using the PN method for pavements that carry between 1 and 30 million equivalent standard axles (MESA). This includes Category A (95% reliability) and Category B (90% reliability) roads. The structural design methods of BSMs do not differentiate between BSMs produced with bitumen emulsion and BSMs produced with foamed bitumen.

2.8.1 Pavement number design method

The pavement number design method (PN) uses a knowledge-based approach for structural design of pavements incorporating a BSM. The PN method is applicable for Category A and B roads with design traffic loads between 1 and 30 MESA. The PN is based on the Structural Number concept from the original AASHTO methods with some improvements. The method is applicable to pavement materials commonly used in South Africa. In order to produce an appropriate pavement design solution, the PN method uses well-established principles of pavement behaviour and performance.

If certain situations apply to the desired pavement the PN method should not be used (Asphalt Academy, 2009):

1. If the design traffic is greater than 30 MESA the PN method is not adequate and a more in-depth analysis should be used.

2. When the materials below the surface or between stabilised layers consists of thin, weak layers the PN calculations will not apply. This is due to the zones of high slip and shear that develop due to these weak lenses.

3. The PN method should not be used when very poor subgrade conditions are present. If the CBR of the subgrade materials is less than 3% at a depth of 600 mm the PN method should not be used.

The PN method contains a number of rules of thumb. These rules reflect well-established principles of the behaviour and performance of pavement structures. The most important rules of thumb relating to the pavement system in general for the PN method when working with BSMs are as follows:

1. The structural capacity of the pavement is a function of the long term load spreading ability of the layers as well as the relative quality of the subgrade.

2. The subgrade is the key determinant in the overall pavement deflection and therefore the relative quality and stiffness of the subgrade is the departure point for design.

3. For pavements which incorporate thin surfacing layers, the base layer is the critical component. Experience can guide the confidence in material types to serve as base layers.

The rules relating to specific pavement layers are as follows (Asphalt Academy, 2009):

1. The load spreading potential of a layer is the product of its thickness and its effective long term stiffness. Effective long term stiffness (ELTS) is an indicator of the average long term in situ stiffness of the materials. The ELTS is not a value that can be determined by means of laboratory or field tests and does not represent the stiffness at any specific time.

   The ELTS of the layer depends on the material type and class, as well as the placement within the pavement strucute.

2. Fine grained subgrade materials act in a stress softening manner, implying that this material will soften with decrease in cover thickness. The ELTS of the subgrade materials is mainly determined by the material quality, the climatic conditions and the cover depth.

3. The modular ratio is the ratio of a layer's stiffness relative to the stiffness of the layer below it. The modular ratio accounts for the stress dependent behaviour of granular and bitumen stabilised materials.

4. Coarse grained unbound materials act in a stress stiffening manner. The ELTS of these materials are determined by the material quality and the stiffness of the supporting layers. The stiffness of the materials will increase with better support, by means of the modular ratio, up to a maximum stiffness determined by the material quality.

The calculation of the PN is fully explained in the TG2. The PN calculation follows certain main steps as summarized below:

1. Check if the design method is applicable to the situation in terms of traffic loads and subgrade quality.

2. Determine the layer thicknesses and material properties for each layer as well as the design equivalent material class.

3. Layers with similar properties should be combined to obtain a 5 layer system (including the subgrade).

4. Determine the basic stiffness of the subgrade and adjust it for the cover depth and climatic conditions.

5. Determine the modular ratio and maximum allowed stiffness for each of the layers above the subgrade.

6. Determine the base confidence factor (BCF).

7. Calculate the layer contribution using the ELTS and layer thickness for each layer.

8. Determine the PN by adding the contributions of each of the individual layers.

The PN design method has a number of shortcomings (Asphalt Academy, 2009):

1. This design method was calibrated using a knowledge base which was limited to pavements that had accommodated less than 30 MESA.

2. The method is not applicable if the pavement has weak lenses of material existing below the surface.

3. Weak subgrade layers, CBR less than 3%, were not used during the calibration of this method. It is therefore not applicable if this situation arises.

4. The method is known to be conservative, therefore, the pavement may be over designed. This may result in uneconomical pavement design.

5. This method does not incorporate stress conditions in the pavement design.

2.8.2 Catalogue design for low traffic roads

The PN design method is only valid for Category A and B roads that carry between 1 and 30 MESA. For low traffic loads with less than 1 MESA the TG2 prescribes a catalogue design. This catalogue is only applicable for Category B, C and D roads. This method is applicable for new constructions and can be used as a guideline for the rehabilitation of existing roads. The design catalogue from the TG2 is shown in Figure A.1 in Appendix A.

2.8.3 Deviator stress ratio design method

Pavements structures with a design traffic load larger than 30 MESA require a more in-depth analysis than the PN method provides. The deviator stress ratio design method is prescribed for the design of these pavement structures (Wirtgen Group, 2012). The DSR method is based on the premise that the rate of permanent deformation in a BSM layer is a function of the applied deviator stress relative to the deviator stress at failure of the materials. The DSR is calculated as shown in Equation 2.2.

To be able to perform a mechanistic-empirical analysis of the pavement structure, a resilient modulus is required for the BSM layer. Wirtgen Group (2012) prescribes ranges of resilient moduli for BSM layers based on triaxial testing and pavement monitoring. The preferred approach for advanced design is to select a deviator stress ratio limit depending on the required reliability and design traffic of the road. Figure 2.20 shows how the increase in DSR decreases the life of the pavement. For roads with a design reliability of 95% a DSR limit of 35% is recommended for a 10 mm maximum deformation. A DSR limit of 40% is recommended for arterials with a design reliability of 80 - 90%.

These limits are however not cast in stone. The DSR in a material can vary significantly based on the moisture conditions or the degree of compaction. These limits were set for optimal moisture conditions and do not account for moisture damage during testing or in-field conditions. The limits for the DSR are lower for coarse grained materials than for finer grained (sandy) materials.

2.8.4 New design requirements

The three design methods show a number of shortcomings for the design of BSMs. It is clear that an improved design method is necessary which incorporates material properties and stress conditions in the material. Therefore, this study aims to produce a new mechanistic-empirical transfer function for BSMs. This function uses material properties and stress conditions to predict permanent deformation development caused by traffic loading in a BSM.

2.9 Synthesis

BSMs behave differently to other types of material as it utilizes a binder but is not continuously bound. The understanding of this behaviour has been developed over the past 20 years. Although there still remains some confusion, it is well understood that BSMs fail due to permanent deformation and not due to fatigue. However, there is a need to developed to create a mechanistic-empirical design method. This study aims to further analyse the long term performance of BSMs in order to better understand and design BSMs.

Chapter 3

Research Methodology

3.1 Research overview

This chapter focusses on the research design and methodology followed in this study. The main objective of this study was to develop a mechanistic-empirical design function for bitumen stabilised materials. The first phase of this study focuses obtaining data from different pavement structures incorporating BSMs. The second phase uses this data to develop and validate a new transfer function. Figure 3.1 and Figure 3.2 shows the layout of this chapter for the two phases.

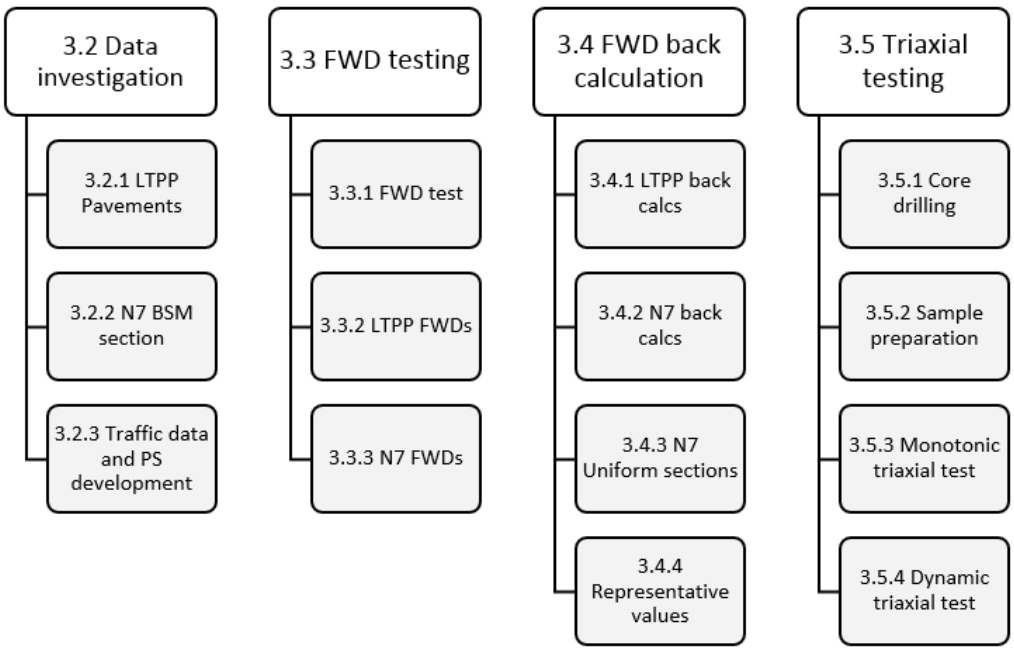

Figure 3.1: Phase 1: Data acquisition and analysis

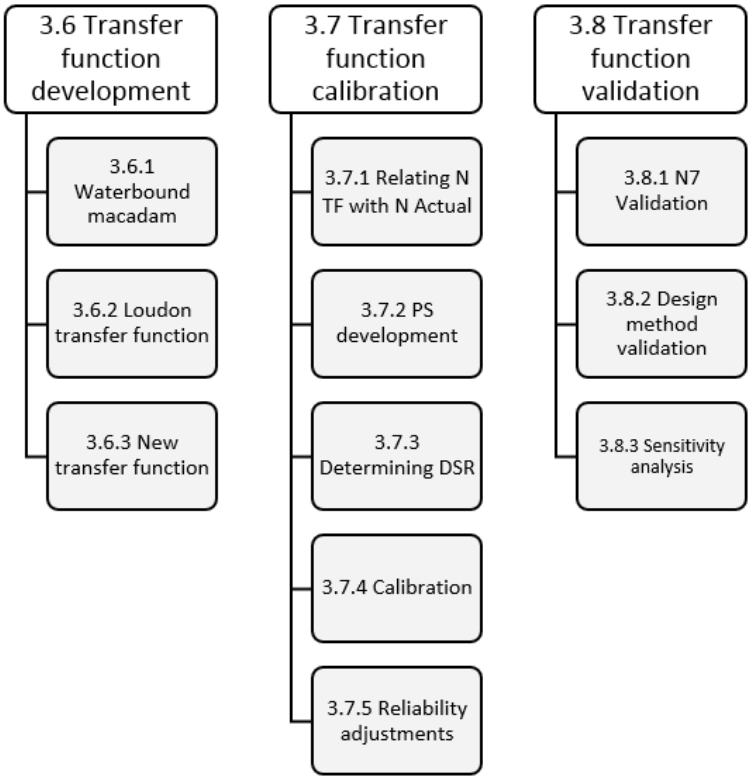

Figure 3.2: Phase 2: Development, calibration and validation of transfer function

3.1.1 Phase 1: Data acquisition

The first phase focuses on obtaining material properties, structural properties and traffic data for various pavement structures incorporating BSMs. A number of long term pavement performance (LTPP) studies performed by SANRAL were identified and analysed as discussed in Section 3.2. A section of the N7 highway, with a BSM base layer, was thoroughly investigated over a number of years.

Traffic counts were used to estimate the amount of standard axles these pavements had accommodates at different points in time. These values were related to rutting measurement for the same points in time.

FWD test results were analysed for the N7 as well as the LTPP pavements. The FWD test results were back calculated to obtain representative resilient modulus values for the different layers in the pavement structures at various stages of their design life. The methods used to analyse the FWD test results and to perform back calculations are discussed in Sections 3.3 and 3.4.

Further investigations were performed on the N7 highway as part of this study. Core samples were taken from the N7, in order to obtain shear properties of an in-field BSM layer after fifteen

years of service. These cores were prepared for testing at Stellenbosch University and tested using monotonic and dynamic triaxial testing.

At the end of the first phase of this study values representing the resilient modulus, cohesion, friction angle and the retained cohesion of in-field BSM layers were obtained.

3.1.2 Phase 2: Transfer function development

The second phase of this study focuses on the development of a transfer function for BSMs. The origin of the transfer function, calibration and the methods used to calibrate it are discussed in this chapter. The new BSM design function is a function of 4 variables; Retained cohesion, deviator stress ratio, density and plastic strain as the controlling factors.

Phase 1 of this study aims to obtain representative values for these input parameters for different pavement pavement structures at various stages of their design life. Figure 3.3 illustrates the factors influencing the function and the source of the information used to calibrate the function. Most of the data was obtained from as built data and field investigations. Where data was unavailable, conservative estimates were made based other available information.

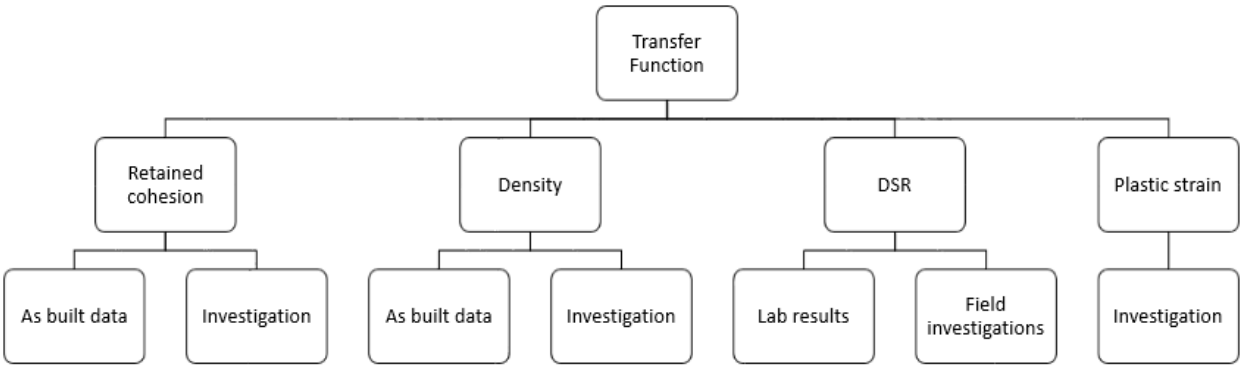

Figure 3.3: Transfer function parameters with information sources

To obtain the deviator stress ratio (DSR) was more complicated than the other parameters. Deviator stress ratio is dependant on a number of factors; layer stiffness, shear properties, pavement structure and the applied load. The information required to obtain a representative DSR was obtained from field investigations, lab testing and design criteria. In many cases the information required to calculate the DSR was not available or only available to a limited extent. In these cases conservative assumptions were made to obtain a realistic DSR within the BSM. The information required and the sources of this information is illustrated in Figure 3.4.

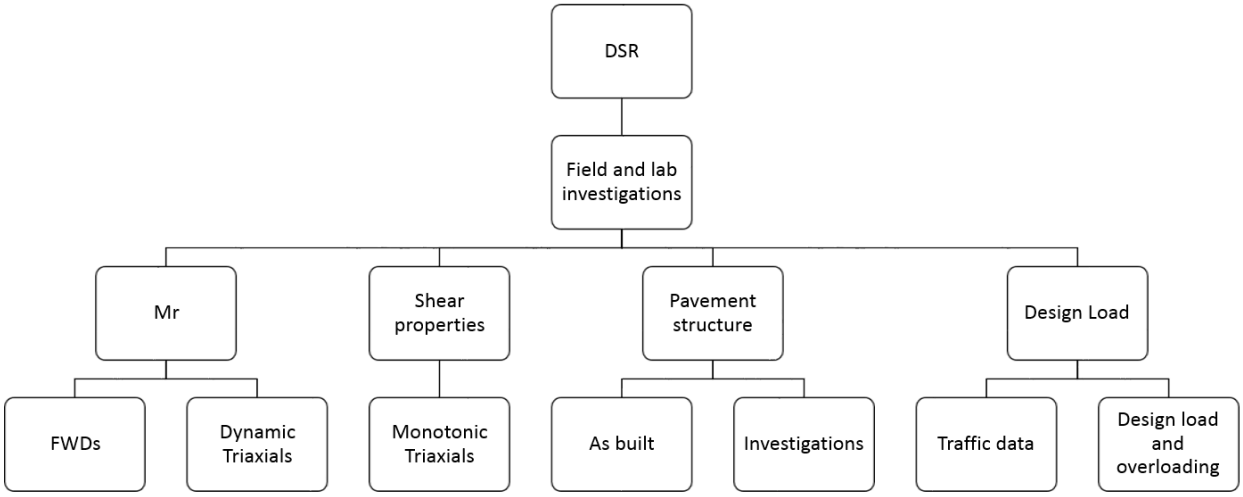

Figure 3.4: Determination of deviator stress ratio

Traffic data was obtained for each pavement at each stage, allowing a comparison between life prediction obtained from the transfer function and from actual traffic. Figure 3.5 provides a broad overview of the process followed to obtain comparable life values for each pavement at a specific stage of its design life. Data was gathered for a number of pavements at a range of stages in their design life. This data was processed using the new transfer function to determine a remaining life value at each stage (N).

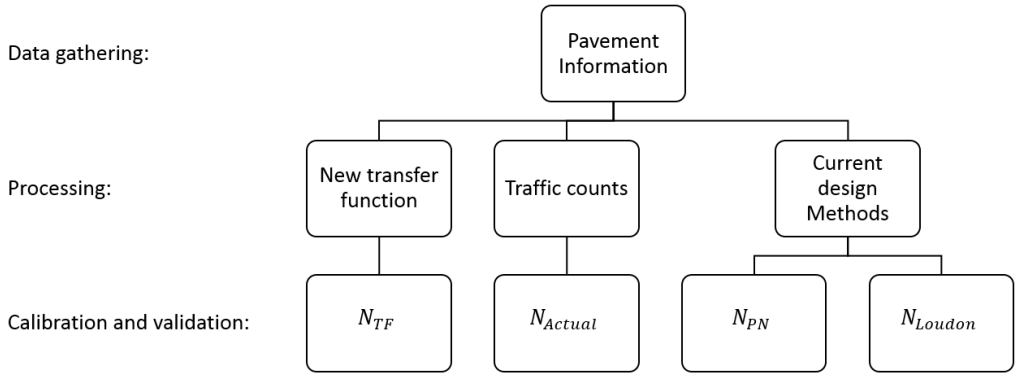

Figure 3.5: Process of obtaining life of a pavement structure

The data obtained from the new BSM transfer function was compared to that of actual traffic data in order to calibrate the function as discussed in Section 3.7. The values obtained from the new transfer function were also compared to that of other design methods to validate the function as discussed in Section 3.8. Finally, sensitivity analyses were done on different factors influencing the new BSM transfer function as per Section 3.8.3.

3.2 Data investigation

In order to effectively model the deformation of BSMs, data concerning the properties and subsequent long term performance of pavement structures incorporating BSMs was gathered and analysed. To get an overall representation of the properties and performance of BSMs, the results of fourteen long-term pavement performance (LTPP) studies were gathered and analysed. This section discusses the data obtained for these pavements, while the rest of chapter discusses the analysis and further processing of the information obtained.

A section of the N7 highway near Cape Town, incorporating a BSM layer was investigated and analysed. Information was available for this pavement at various stages in its design life. This information was investigated at various points in time, amounting to a large amount of information. This section was selected for detailed investigated as part of this study.

3.2.1 LTPP pavements

Long term pavement performance data was gathered for fourteen pavement structures incorporating BSMs. These pavements were part of a Long Term Pavement Performance study performed by SANRAL. Each of these pavements either had a BSM1 or BSM2 base layer with a minimum thickness of 100 mm. The data available for these pavements included densities, moisture contents, layer thicknesses, material types and classes as well as traffic data.

The data also included FWD and rut depth measurements at different stages in their design life. The pavement's name, layer thicknesses, material class as well as a description of the materials are summarized in Table 3.1 and 3.2. The layer thicknesses shown in these tables were used for the back calculation and determination of stress ratios and is discussed in Section 3.4.

The information used during the analysis of these pavements are discussed in detail in Long and Jooste (2007). This information was analysed and used in the calibration of the new BSM transfer function. The FWD data for these pavements is discussed in Section 3.3. Traffic data and the plastic strain development is discussed in Section 3.2.3. Where the data was not sufficient, assumptions were made for these pavements based on the performance and conditions of these pavements. The cohesion (c), friction angle(ϕ) and retained cohesion (RetC) values were generally not available, therefore realistic and representative assumptions were made. Reasonable and conservative values were assumed for each pavement, based on the minimum design values specified in the TG2. A summary of the data obtained and the assumptions made for each of these pavements is discussed in Appendix B for each of the pavement structures.

Table 3.1: LTPP assumed pavement structures (1)

Road	Layer	Layer Thickness (mm)	Material Class	PMS Description
MR 27	1	50	DS	Double Seal and 40 mm Continously graded asphalt
	2	100	BSM 1	BSM 1 base (emulsion, 1% bitumen)
	3	100	C3	Cement stabilised subbase
	4	150	G7	Laterite selected layer
	5	-	G9	In-situ sand
MR 504 (A)	1	20	SS	Single seal
	2	175	BSM 1	BSM1 base (1.7% foamed bitumen)
	3	150	G7	Weathered granite subbase
	4	-	G10	Subgrade of in situ weathered granite
MR 504 (B)	1	30	AC	Asphalt
	2	175	BSM 2	BSM 2 base (3.5% foamed bitumen, 1% lime)
	3	150	G7	Weathered granite subbase
	4	-	G10	Subgrade of in situ weathered granite
N1 - 1	1	80	AC	Asphalt
	2	100	BSM 1	BSM 1 base (emulsion, 1% bitumen)
	3	100	C3	Cement stabilised subbase
	4	150	G5	Selected layer
	5	-	G8	Subgrade
N1 - 13	1	10	SS	Seal (bitumen rubber)
	2	30	AC	Asphalt (includes old seal)
	3	150	BSM 2	BSM 2 base (emulsion, 1% cem, 0.7% bitumen)
	4	100	BSM 2	BSM 2 subbase (emulsion, 0.6% bitumen)
	5	300	G6	G6 selected layer
	6	-	G7	
N1 - 14	1	10	SS	Seal (bitumen rubber)
	2	30	AC	Asphalt (includes old seal)
	3	150	BSM 1	BSM 1 base (emulsion, 1% cement, 0.7% bitumen)
	4	100	G4	Subbase
	5	300	G6	Selected layer
	6	-	G7	Subgrade
N2 - 16	1	40	AC	Asphalt gap-graded
	2	140	BSM 2	BSM 2 base (emulsion, 1% bitumen)
	3	130	C4	C4 subbase
	4	300	G7	Selected layer
	5	-	G9	Subgrade
N2 - 20	1	30	AC	HMA + seal
	2	180	BSM 1	BSM 1 base (emulsion, 1.5% bitumen, 1.75% cement)
	3	270	G6	Decomposed dolerite subbase
	4	150	G7	Selected layer
	5	-	G10	Subgrade
N4 - 1	1	30	AC	Asphalt
	2	170	BSM 1	BSM 1 base (emulsion, 1% bitumen, 1% cement)
	3	130	C4	Cement stabilised subbase
	4	300	G6	Selected layer
	5	-	G7	Subgrade

Table 3.2: LTPP assumed pavement structures (2)

Road	Layer	Layer Thickness (mm)	Material Class	PMS Description
N4 - 5X	1	30	AC	Asphalt
	2	150	BSM 1	BSM 1 base (emulsion, 0.4% bitumen, 1% cement)
	3	150	C3	C3 cement stabilised subbase
	4	150	G7	G7 laterite selected layer
	5	-	G9	G9 In-situ sand
N11 - 8	1	20	AC	UTFC
	2	280	BSM 2	BSM 2 base (1.5% foamed bitumen, 1% cement)
	3	250	G6	Subbase
	4	-	G8	Subgrade
N12 - 19(3)	1	55	AC	Asphalt
	2	120	BSM 1	BSM 1 base (1% bitumen, emulsion)
	3	120	C3	Cemented subbase
	4	80	C3	Cemented selected subgrade
	5	-	G6	Subgrade
N12 - 19(4)	1	55	AC	Asphalt
	2	135	BSM 1	BSM 1 base (1% bitumen, emulsion)
	3	130	C3	C3 cement stabilised subbase
	4	220	G5	G5 selected layer
	5	-	G6	Subgrade
P243 - 1	1	25	AC	AC and single seal
	2	250	BSM 2	BSM 2 (1.8% foamed bitumen, 2% cement)
	3	150	G8	Subbase
	4	-	G9	Subgrade

Other information regarding these pavement structures include information regarding the climatic conditions, visual inspections and ride quality. The climatic conditions could prove to be valuable when considering the moisture conditions in these pavements. Ride quality was not taken into account during this study, but the visual inspection data was used during the analysis.

3.2.2 N7 BSM section

A section of the N7 highway near Cape Town was rehabilitated in different phases implementing bitumen stabilised base materials. The geographical location of the test section is shown on the map in Figure 3.6. The climate in this region is classified as 'moderate' according to the TRH4's macro climatic regions. The Weiner N-value of this region lies between 2 and 5, indicating the region has a moist sub-humid climate.

The slow lanes of both the North and Southbound carriageways between km 5.8 and 18 were rehabilitated using bitumen stabilised base layers. The first phase of this rehabilitation was done in 2002 using in situ foam stabilisation. The second phase was rehabilitated in 2007 implementing

bitumen emulsion stabilisation. The section treated with bitumen emulsion is further discussed in Section 3.2.2.2.

The pavement structures before the rehabilitation were similar for both North and Southbound carriageways. Only a few variations in base layer thickness were observed in the as built data. The old pavement structure consisted of a double seal on a 200 mm G2 granular base layer. The base layer's thickness reduced to 150 mm in certain sections. A 150 mm G3 crushed stone granular layer was used for the subbase and the subgrade consisted of a G8 sand. The structure of the pavement before rehabilitation is illustrated in Figure 3.7 for the Northbound carriageway and in Figure 3.8 for the Southbound carriageway.

Figure 3.9 and Figure 3.10 illustrates the carriageways, chainages and the year of rehabilitation for the emulsion and foam stabilised sections. The BSM foam section is further discussed in Section 3.2.2.1. The information regarding the layer thicknesses and material classifications is based on the as built data.

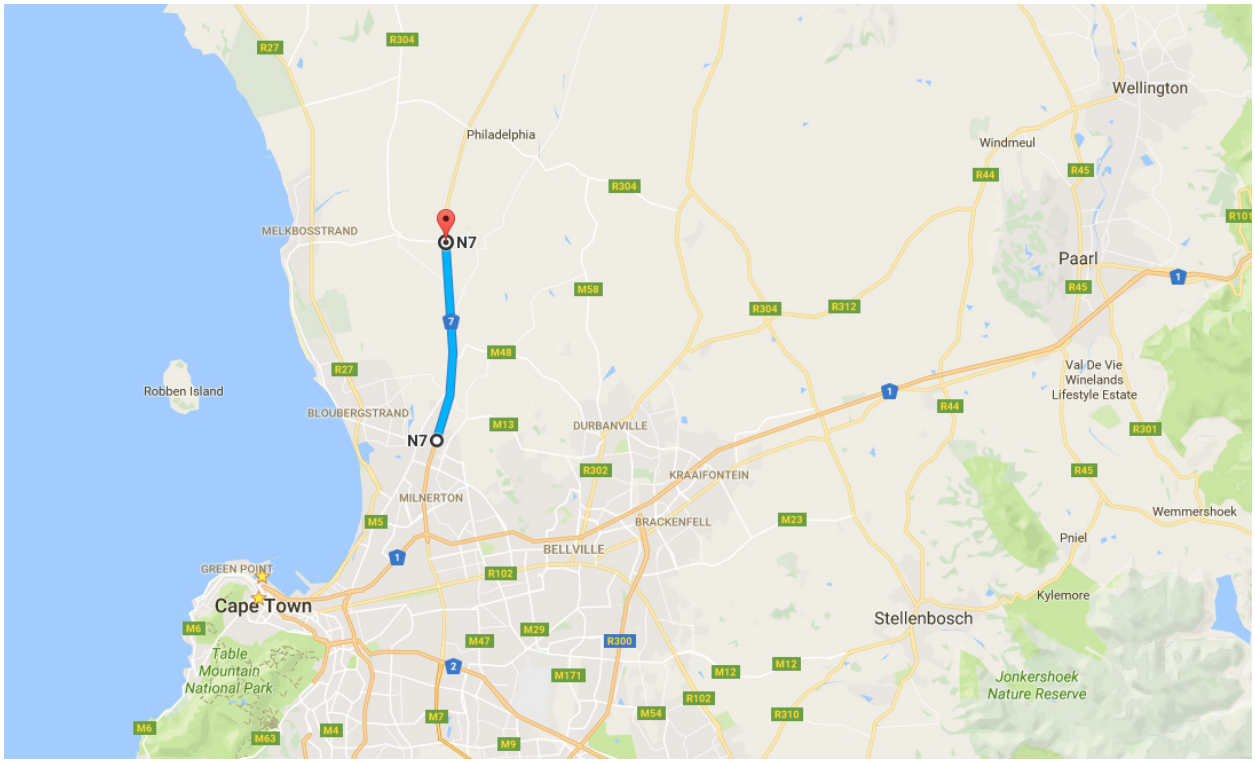

Figure 3.6: Geographical location of the BSM test section on the N7

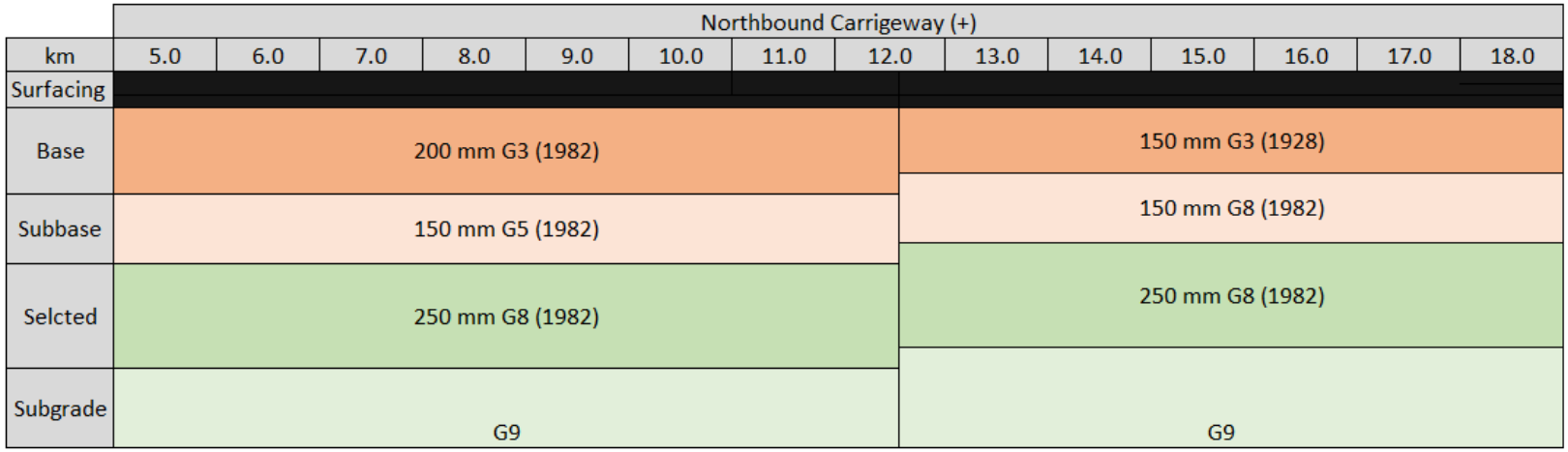

Figure 3.7: N7 Northbound pavement structure before rehabilitation (as built data)

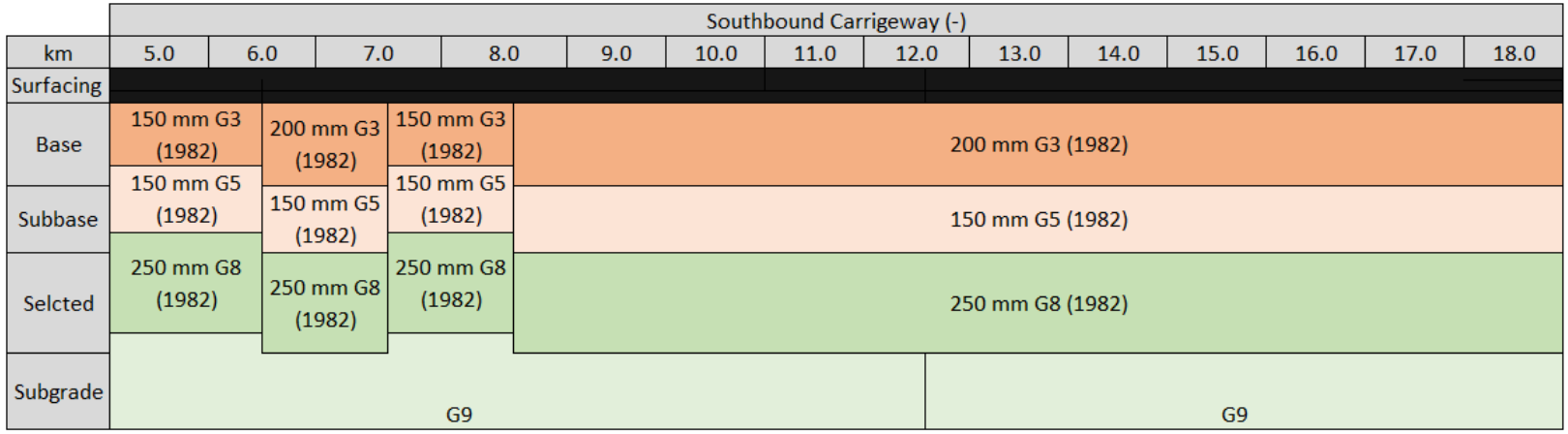

Figure 3.8: N7 Southbound pavement structure before rehabilitation (as built data)

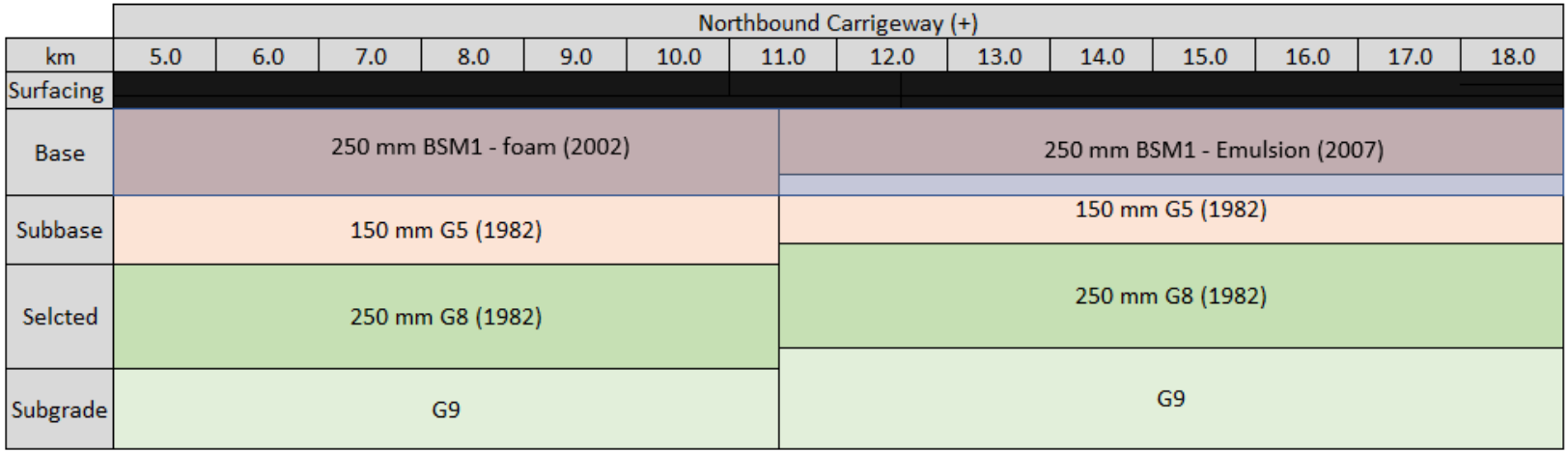

Figure 3.9: N7 Northbound pavement structure after rehabilitation (as built data)

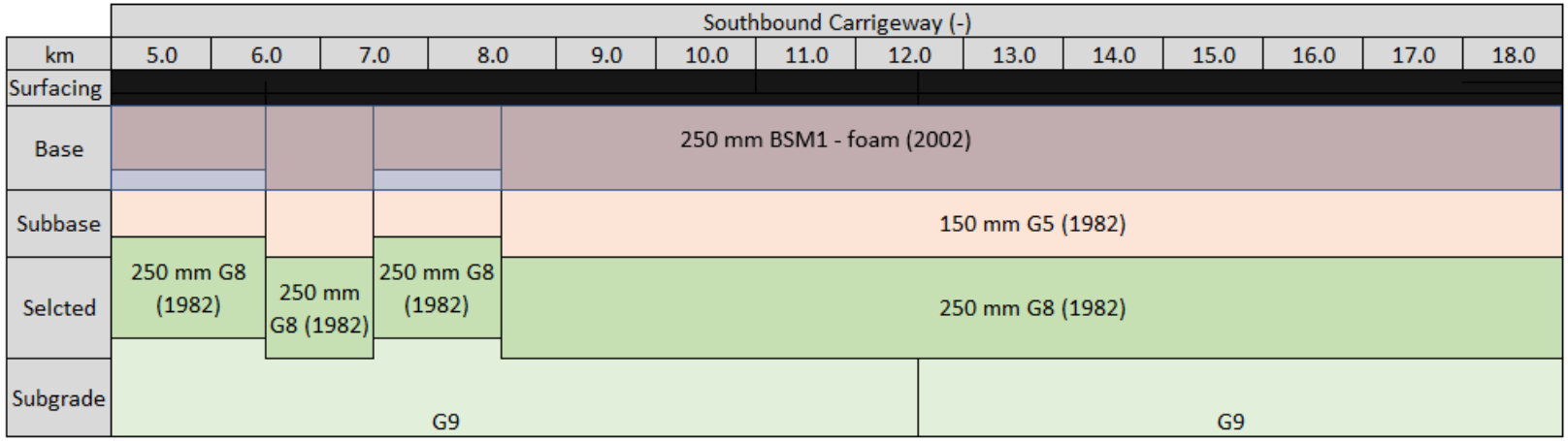

Figure 3.10: N7 Southbound pavement structure after rehabilitation (as built data)

3.2.2.1 N7 Foam stabilisation (2002)

Specific sections of the N7 was rehabilitated in 2002 using in situ foam stabilisation. The Southbound carriageway of the N7 between km 5.8 and km 18.0, as well as the Northbound carriageway between km 5.8 and 11.6, was rehabilitated implementing a foamed bitumen base layer. Figures 3.10 and Figure 3.9 illustrate the carriageways and chainages stabilised with foamed bitumen.

The designed rehabilitated pavement structure consisted of a 250 mm G8 sand selected layer on the G9 quality subgrade. Between 50 and 100 mm G5 material, constructed in 1982, remained as the subbase. The base layer was designed as a 250 mm BSM foam layer. The surfacing consisted of a 35 mm asphalt layer with an additional 18 mm Novachip surfacing layer. The designed pavement structure for the Southbound carriageway is similar to the foam section of the Northbound carriageway. The designed structure of the rehabilitated pavement is illustrated in Figure 3.10 and 3.9.

FWD tests were performed on the old structure in 1994 and 2000, while FWD tests on the BSM foam structure was performed in 2004, 2010 and 2016. This allows for the comparison of BSM layer stiffness at three different points in time. It may also provide valuable insight into the response of the pavement before and after rehabilitation. The FWD tests performed over a period of twelve years are useful for this study as they provide data on the long term stiffness development of BSMs. The FWD tests performed on this section is discussed in Section 3.3.3. The back calculation of the FWD test results are discussed in Section 3.4.

3.2.2.2 N7 Emulsion stabilisation (2007)

The slow lane of the Northbound carriageway between km 11.6 and km 18 was rehabilitated in 2007. This section was constructed with a bitumen emulsion stabilised base layer. The pavement structure of this section is illustrated in Figure 3.9. Similar to the foam section, the designed pavement had a 250 mm G8 sand selected subgrade on the G9 subgrade. The emulsion section only incorporated 50 mm of the old G5 subbase that was constructed in 1982. The base layer was designed as a 250 mm emulsion BSM. The surfacing of this section consisted of 35 mm asphalt with a 9.5 mm friction layer.

FWD tests were performed on the initial pavement structure in 1994, 2000 and in 2004. The results of FWD tests for the emulsion treated base layer were available for 2010 and 2016. These results may provide insight into the long term performance of bitumen emulsion treated base layers.

The resilient modulus development of this section can also be compared to that of the BSM foam section. FWD test results before and after rehabilitation could also be investigated for this section.

3.2.3 Traffic data and permanent deformation mesurement

Traffic data was gathered for the LTPP roads as well as the N7 highway. The past traffic these pavements accommodated was determined at various points in time. The rut depth measurements at various points in time was related to traffic data. By comparing the traffic data with deformation measurements, accumulation of permanent deformation in these pavements could be determined.

3.2.3.1 LTTP Traffic data and deflection measurements

Traffic counts and economic growth rates were used to obtain an estimation of the amount of standard axles that each of the LTPP pavements has accommodated. Although this provides only an estimation, it is referred to the actual traffic (N_{actual}) in this study. Details about the traffic counts for each of the LTPP pavements can be found in Appendix B. These traffic counts were obtained from Long and Jooste (2007). Table 3.3 provide a summary of the amount of standard axles that each pavement had accommodated at specific points in time. Traffic in this Table and further in this study is measured in million equivalent standard axles (MESA). A standard axle was defined as an axle with an 80 kN load. It was assumed that the pavements had accommodated zero traffic at the time of opening.

Rut depth measurements were taken at various stages of each of these pavements' design life. Traffic data, from similar points in time, were related to the rutting depth measured for each individual pavement. In the case where the pavements were rehabilitated or resurfaced, rutting was determined cumulatively. This research focuses on the deformation of the BSM layers, therefore, levelling the pavement with a seal or asphalt overlay did not have an effect on the deformation that has accumulated in the base layer. Figure 3.11 illustrates the assumed accumulation of rutting if the measurements decreased over time.

The use of rutting to define deformation in the BSM layer is further discussed in Section 3.6. Table 3.3 provides a summary of the average rut depth measurements with the amount of traffic for each of the LTPP pavements.

Table 3.3: LTPP Traffic data and rut measurements

Road	Year	Actual Traffic (MESA)	Rutting (mm)
MR 27 SB	1988	0	0.0
	2002	2.6	4.2
	2006	4.2	7.4
	2008	5	8.6
MR 27 NB	1988	0	0.0
	2002	2.6	5.7
	2006	4.2	7.9
	2008	5	9.8
MR 504 (A) NB	1995	0	0.0
	1998	0.25	5.0
	2006	1.25	10.0
	2008	1.6	12.9
MR 504 (A) SB	1995	0	0.0
	1998	0.25	6.0
	2006	1.25	11.0
	2008	1.6	14.2
MR 504 (B) NB	1995	0	0.0
	1998	0.25	6.0
	2006	1.25	11.0
	2008	1.6	14.2
MR 504 (B) SB	1995	0	0.0
	1998	0.25	5.0
	2006	1.25	10.0
	2008	1.6	12.9
N1 - 1 SB	1984	0	0.0
	1995	3.9	8.0
	2006	13.8	18.0
	2008	17	22.5
N1 - 1 NB	1984	0	0.0
	1995	3.9	6.0
	2006	13.8	16.0
	2008	17	19.9
N1 - 13 SB	1980	0	0.0
	1991	3.2	10.0
	1997	6	16.0
	2006	12	21.0
	2008	14	26.4
N1 - 13 NB	1980	0	0.0
	1991	3.2	10.0
	1997	6	16.0
	2006	12	21.0
	2008	14	26.4

Road	Year	Actual Traffic (MESA)	Rutting (mm)
N1 - 14	1980	0	0.0
	1991	3.2	6.0
	1997	6	12.0
	2006	12	16.0
	2008	14	20.0
N2 - 16	1980	0	0.0
	1990	0.6	4.0
	2005	2.7	16.4
	2006	2.9	21.6
	2006	3.4	23.2
N2 - 20 EB	2000	0	0.0
	2006	1.6	6.0
	2008	2.4	8.0
N2 - 20 WB	2000	0	0.0
	2006	1.6	6.0
	2008	2.4	8.0
N4 - 1 EB	1997	0	0.0
	2006	4.2	5.0
	2008	5.6	6.7
N4 - 1 WB	1997	0	0.0
	2006	4.2	5.0
	2008	5.6	6.7
N4 - 5X	1996	0	0.0
	2006	5.1	10.0
	2008	6.7	13.1
N11 - 8	2004	0	0.0
	2006	0.4	5.0
	2008	1.1	13.7
N12 - 19(3)	1974	0	0.0
	1991	5.5	6.0
	2000	11	10.0
	2006	16	12.0
	2008	18	14.4
N12 - 19(4)	1974	0	0.0
	1991	5.5	3.0
	2000	11	9.0
	2006	16	12.0
	2008	18	13.8
P243 - 1	2000	0	0.0
	2006	0.34	5.0
	2008	0.48	7.1

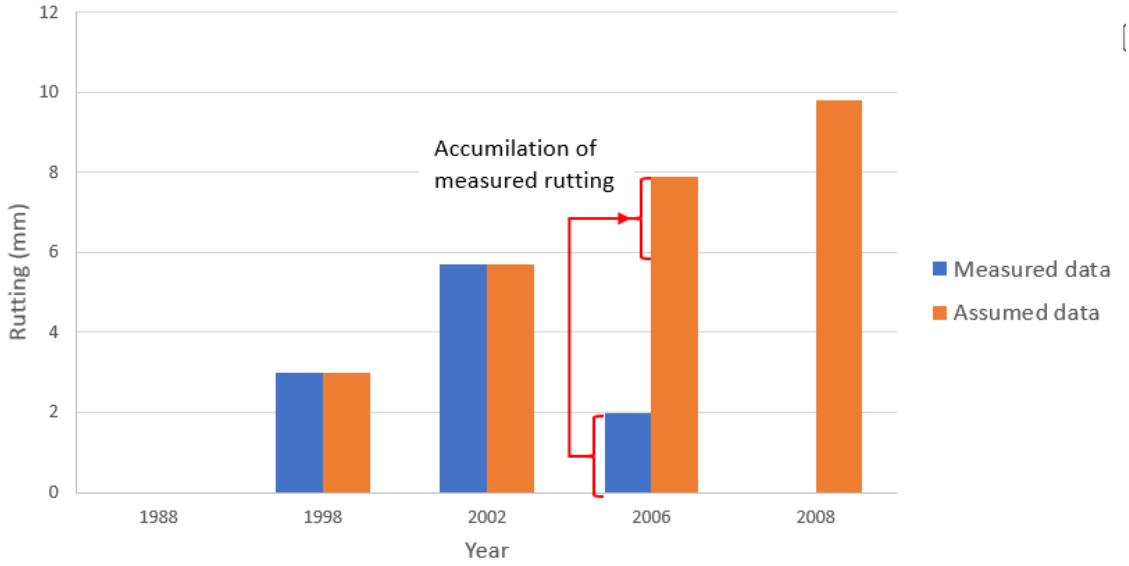

Figure 3.11: Accumulated rutting as for MR 27 NB

3.2.3.2 N7 traffic data and deflection measurements

Traffic count data was obtained for the N7 highway at a number of stations over its length. Data was available for fourteen counting stations based on data obtained form the Roads Network Information System (RNIS) with an additional nine stations available from Syntell. The data from the RNIS was based on twelve hour counts, while the Syntell data was obtained from seven day counts. Therefore, the Syntell data was used to estimate the cumulative traffic on the N7 for this study.

Table 3.4: N7 traffic loading assumptions

Description	Assumption
ADT growth rate	Varies (from 2002 to 20016)
ADTT growth rate	Varies (from 2002 to 20016)
E80s per heavy growth rate (p.a.)	1.5%
Final year 2017 E80s per heavy vehicle	2.20
Base yaer (2002 / 2007) E80s per heavy vehicle	1.80

Table 3.4 shows the assumptions made regarding growth rates and standard axles per heavy vehicle. The number of standard axles per heavy vehicle at the base year (2002 or 2007) was assumed as 1.8 and increased to a maximum of 2.2 by 2017 at a growth rate of 1.5%. The average daily

traffic (ADT) and average daily heavy traffic (ADTT) growth rates varied between the different stations. The growth rate used for each station was based on the data obtained from RNIS data. The station number, location, ADTT, growth rate and cumulative traffic for 2017 is summarized in Table 3.5. The cumulative traffic estimates the total number of standard axles the pavement has accommodated in either 50 (2002 - 2017) or 10 years (2007 - 2017).

Uniform sections were identified for the N7 based on the FWD results. The FWD results and uniform section allocation is discussed in Section 4.2.2 and 4.2.3 respectively. The traffic count station in these sections were used to estimate the cumulative traffic for each section at various points in time. Traffic data was assigned to each section based on the nearest counting station. In cases where the uniform section was between two stations or contained two counting stations, the average of the two stations was used.

Table 3.5: N7 cumulative traffic 2017

Station	Chainage (km)	ADTT	Growth rate (%)	Cumulative traffic (MESA)
North bound				
881	1.0	2256	1.67	25.45
1208	3.1	1478	3.82	19.93
281	4.9	1088	4.74	15.84
111330	10.0	1344	2.43	16.14
111331	12.1	1288	2.01	9.45
111332	12.9	894	3.5	7.13
111333	13.4	932	3.23	7.33
315	15.0	856	3.77	6.94
1464	17.5	812	2.23	6.04
South bound				
881	1.0	1903	1.67	21.47
1208	3.1	1604	3.82	21.63
281	4.9	1077	4.74	15.68
111330	10.0	1480	2.43	17.77
111331	12.1	1284	2.01	14.89
111332	12.9	841	3.5	11.04
111333	13.4	915	3.23	11.74
315	15.0	808	3.77	10.84
1464	17.5	844	2.23	9.97

The average rut depth for each uniform section was also determined from the available data. Deformation measurements were related to the traffic data as shown in Table M.2 and M.3 for

the Southbound carriageway and in Table M.1 for the Northbound carriageway in Appendix M. Deformation measurements showed a much higher deformation before the 2002 count than in 2002. It was therefore assumed that the deformation measurements taken in 2002 were after rehabilitation of the foam sections. The measurements in 2002 were assumed to be a result of the first year's traffic.

Average deformation measurements were used for each stage of each uniform section. In certain cases the average measured deformation decreased over time. The allocation of cumulative traffic to each of the uniform sections is shown in Table N.1 for the three uniform sections on the Northbound carriageway. Table N.2 and Table N.3 in Appendix N show the allocation for the eight uniform section on the Southbound carriageway.

The accumulation of deformation of the BSM layer cannot be negative, as this would suggest that the pavement was expanding. The reduction in average deformation may be due to a wider rut forming, additional settling of the materials or patching that occurred. Therefore, the rut measurements were added cumulatively if the rut depth decreased over time. Adjustments were made to ensure that the accumulation of permanent deformation reflected the actual accumulation of deformation in the base layer.

The traffic data and deformation measurements calculated in this section was further analysed to calculate the deformation in the BSM. This analysis and results thereof is discussed in Section 5.1.

3.3 Falling Weight Deflectometer

3.3.1 FWD testing

The purpose of FWD testing is to measure the response of a pavement structure by imitating the dynamic loading induced by a heavy vehicle. The FWD apparatus loads the pavement structure with a falling weight onto rubber buffers. The buffers are situated on a loading plate with a diameter of 300 mm. A photograph of FWD loading plates and measuring geophones is shown in Figure 3.12. The loading plate is placed directly on the pavement surface. The weight is dropped 3 times at each test location and the response of the third drop recorded (Lynch, 2013).

During FWD testing the following parameters are measured:

1. Peak load and loading rate applied to the pavement structure
2. Deflections measured at each geophone

3. Air temperature

4. The surface temperature of the pavement

The load applied to the pavement surface is controlled by the mass of the falling weight as well as the height from which it is dropped. This load is measured as it should replicate the load applied to the pavement structure by a heavy vehicle vehicle. The load is typically representative of one wheel of a standard axle passing over it. In South Africa a standard axle is an 80 kN axle, and therefore the peak load of a FWD drop simulating a standard axle should be 40 kN.

Figure 3.12: FWD load plate and geophones (Lynch, 2013)

The loading plate of the FWD has a diameter of 300 mm, resulting in a calculated pressure of 566 kPa at peak loading. The actual peak stress varies slightly due to surface properties of the pavement, the load not being exactly 40 kN and random variability (Lynch, 2013). The rate of loading is controlled by rubber buffers positioned between the load plate and the falling weight.

The deflection of the pavement surface during application of the load is measured using geophones. These geophones are spaced at intervals from the centre of the loading plate as illustrated in Figure 3.13 (units in mm). The measurements at the different geophones are indicated as D_{xxx}, where 'D' indicates deflection (in mm) and 'xxx' the distance from the centre of the loading plate (in mm).

By measuring the deflection bowl caused by the loading, with the magnitude and geometry of the stress applied to the pavement surface known, the stiffnesses of the pavement layers can be determined through the method of back-calculation. The method of back calculation is discussed in Section 3.4.

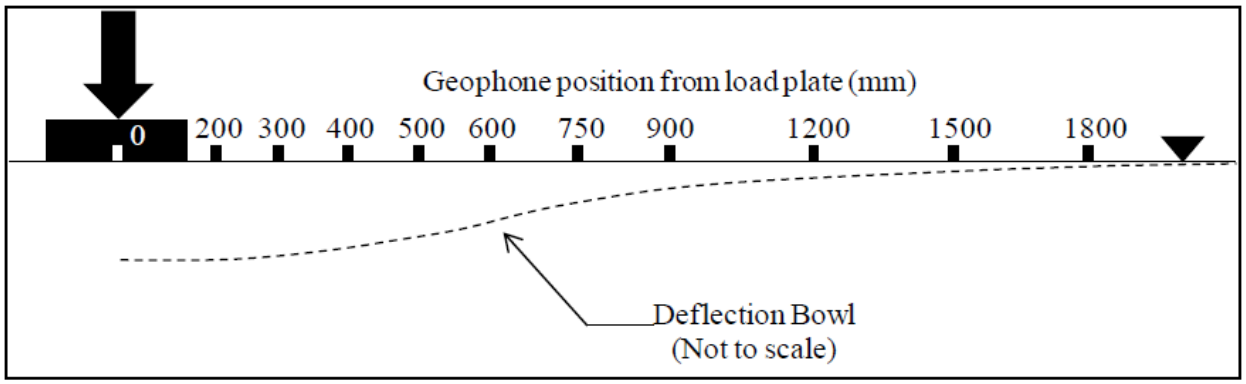

Figure 3.13: Illustration of FWD geophone positions from the centre of the loading plate (Lynch, 2013)

Other, more fundamental, parameters were used to indicate the structural condition of the pavement layers include:

1. The maximum deflection (D_0 or D_{max}) was measured as the maximum deflection at the point of loading. This parameter provides an indication of the overall condition of the pavement structure.

2. The Base Layer Index (BLI) was calculated from the deflection bowl measurements as shown in Equation 3.1. The BLI provides valuable information about the condition of the surfacing and base layers.

$$BLI = D_0 - D_{300} \tag{3.1}$$

3. The Middle Layer Index (MLI) was calculated from the deflection bowl measurements as shown in Equation 3.2. The MLI index provides an indication of the condition of the subbase and the upper selected subgrade.

$$MLI = D_{300} - D_{600} \tag{3.2}$$

4. The Lower Layer Index (LLI) was calculated from the defection bowl measurements as shown in Equation 3.3. The LLI gives an indication of the condition of the lower selected subgrade

and the subgrade.

$$LLI = D_{600} - D_{900} \tag{3.3}$$

Air and surface temperature are usually measured at the time of testing for each station where a FWD test is carried out. The temperature measurements are used when tests are carried out on bituminous materials like asphalt or surface seals. The properties of bituminous materials, specifically resilient modulus, are significantly affected by temperature and loading rate (Lynch, 2013).

3.3.2 LTPP FWDs

FWD tests were performed on the LTPP sections at different points in time. A large amount of FWD test data was available for these pavements, therefore, only a summary of the results is included in this study. The FWD test results available for each of the LTPP pavements is discussed in Appendix B.

The FWD data was analysed to obtain the layer indices as well as the development of these layer indices over time. The LTPP FWD tests were performed using a 40 kN loading plate with a diameter of 300 mm. In some cases the pressure applied by the loading plate was measured and used during back calculations. Where the pressure of the loading was not measured it was assumed to be 566 kPa. The results of the LTPP FWD tests are discussed in Section 4.2.1.

3.3.3 N7 FWDs

FWD tests were performed on the BSM section of the N7 highway in 1994, 2000, 2004, 2010 and 2016 in order to monitor the long term pavement performance of bitumen stabilised materials. FWD tests were performed every 200 meters in the slow lanes of the North and Southbound carriageways. A timeline of the FWD testing and rehabilitation is shown in Figure 3.14.

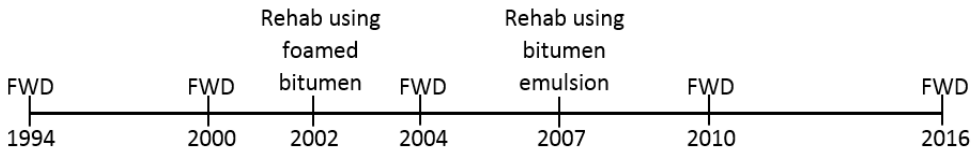

Figure 3.14: Timeline of N7 testing and rehabilitation

The FWD tests performed on the N7 used an applied load of 40 kN on a loading plate with a diameter of 300 mm. The pressure beneath the loading plate was calculated as 566 kPa. The air

and surface temperatures were measured at each test location at the time of testing. The FWD tests performed in 1994, 2000, 2004 and 2010 made use of 7 geophones to measure the pavement deflection, while the tests performed in 2016 made use of 9 geophones. Rut measurements, ride quality, visual inspection and texture analyses were made along with the FWD measurements.

The results of the N7 FWD tests were analysed and used to divide the road into uniform sections. The division of uniform sections is discussed in Section 3.4.3. The results of the FWD back calculations are discussed in Section 4.3.2.

The FWD test results from different years were used to thoroughly analyse the bitumen stabilised sections of the N7 between Cape Town and Melkbosstrand (5.8 - 18 km). The main focus was to determine the effective long term stiffness (and performance) of the bitumen stabilised base layers in pavement structures over a given number of years and to determine the trend in resilient modulus development of this layer over time.

Limitations in the N7 investigation were present due to FWD data only being available for certain years. The Western Cape's road network is only investigated every 4 to 6 years with FWD tests, resulting in considerable time intervals between test results. The result of this is a less accurate determination of the trends in resilient modulus of the pavement structure and specifically the BSM layer.

In order to make an accurate determination of the time lapse between construction and the onset of BSM resilient modulus increase, annual FWD data from 2002 to 2017 would have to be analysed. This is not possible as aforementioned annual data is not available. The foamed section of the N7 was constructed in 2002 with FWD tests being performed in 2004, 2010 and 2016. The FWD results from 1994 and 2000 were also analysed and interpreted to compare the average stiffnesses before and after rehabilitation.

3.4 Back calculation of FWD results

The process of back-calculation allows the estimation of layer stiffnesses by measuring the response of the pavement to loading. This process aims to assign stiffness values to the layers of the pavement which reflect the response measured with the FWD. Back-calculation can be done by hand or by software such as Rubicon and Back-GAMES. All back calculations performed during this study were done using the Rubicon toolbox software. The process of back-calculation is described in this Section.

Information required to perform back-calculations include:

1. FWD deflection measurements
2. Weight of the falling load
3. Pavement structure (layer thicknesses)
4. Poisson's ratio of pavement materials

With these parameters known, a seed layer stiffness value is required as a reference point for the resilient modulus calculations. The deflection measurement and stress applied to the pavement form part of the input template used by Rubicon. An example of a completed FWD import template is shown in Figure C.1 in Appendix C. This template was populated using the deflection measurements gathered from FWD testing. Layer thicknesses were imported into Rubicon using thickness import template. An example of this template is shown in C.2 in Appendix C.

Rubicon uses Multi Layer Linear Elastic (MLLE) theory to model the deflection of the pavement structure due to the FWD load. The layer stiffnesses are varied within the model until the modelled deflections fit the measured deflections. The deflections are adjusted to fall within the acceptable 10 micron tolerance.

All resilient modulus values obtained from Rubicon were checked and adjusted to ensure that the results were reasonable and tenable. Focus was placed on the resilient modulus results of the BSM layer for the purpose of this study. The measured deflections, calculated deflection and the layer stiffnesses were modelled on a deflection bowl as shown in Figure 3.15. This Figure also shows shows the back calculation results for km 7.8 on the N7 Southbound carriageway in 2010. The red line on the deflection bowl in Figure 3.15 indicates the calculated deflection bowl, while the blue dots indicate the measured deflections. Layer thickness, resilient modulus and Poisson's ratio are also shown on this figure.

The back calculation of the FWD data provides valuable insight into the resilient modulus of the different layers in the pavement structures. However, The resilient modulus values obtained from back calculation should not be taken as a certainty. The back calculated results were assessed to determine whether they were reasonable. These values should be used with other tests and performance indicators to get a good representation of the actual pavement response. The layer stiffnesses obtained from back calculation can be compared to laboratory test results, for example dynamic triaxial testing. Dynamic-triaxial testing is discussed in Section 3.5.4.

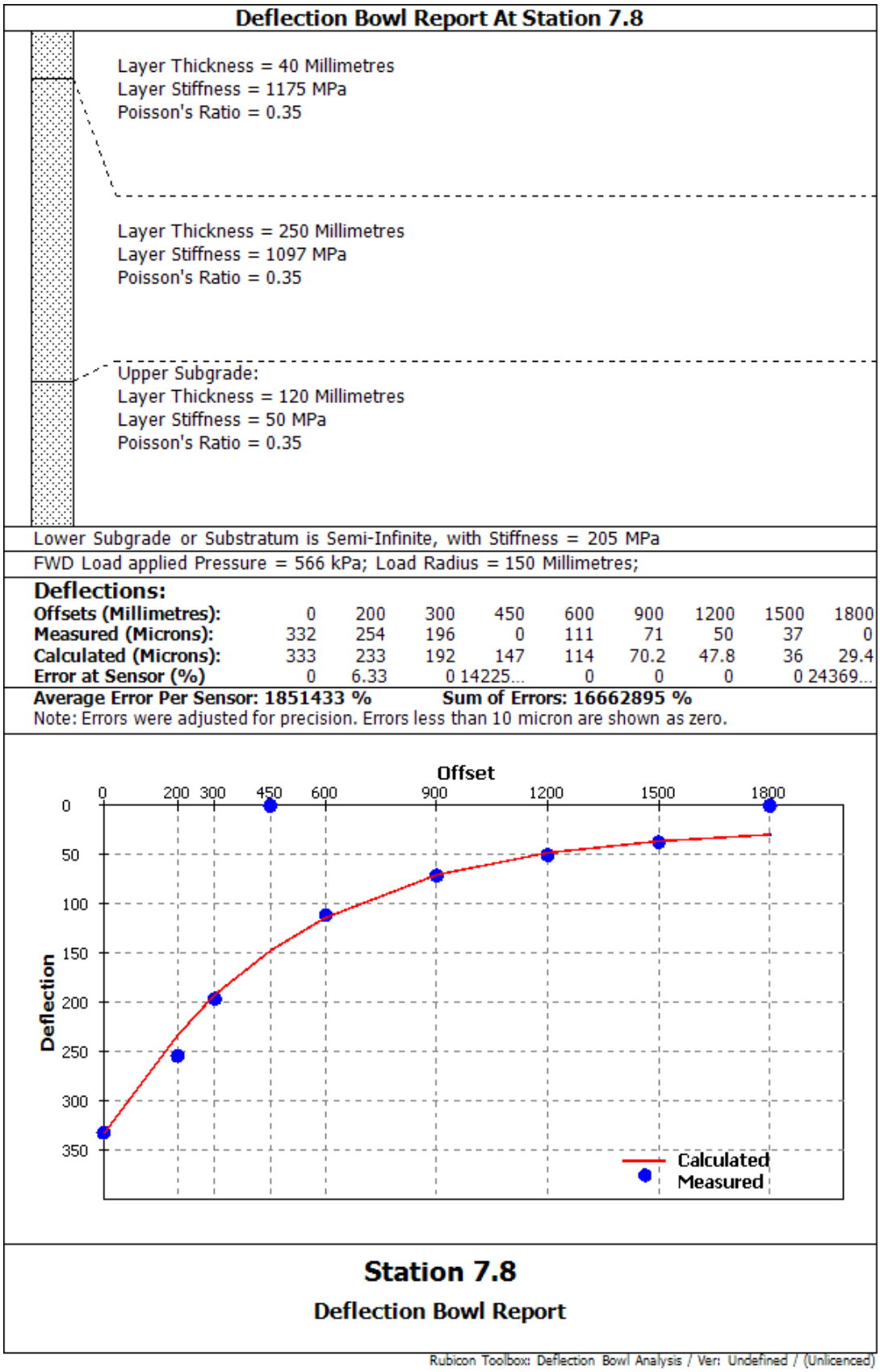

Figure 3.15: Back calculated deflection bowl for 2010 at 7.8 km Southbound

3.4.1 LTPP back calculations

Deflection bowls were analysed for all the available FWD data for the LTPP pavement structures. The deflection bowls for each of these stations can be found electronically on the attached CD. The layer thicknesses used during back calculation for each of these pavements is shown in Table 3.1 and 3.2 on pages 60 and 61.

Similar to the N7 back calculations, Rubicon was used to analyse the deflection bowls. Measured deflections were plotted against the calculated deflections and adjustments were made to the difference between the two was less than 10 micron. Where the resilient modulus values were unrealistic, adjustments were made to fit the profile of the deflection rather than the absolute values. The results of the LTPP back calculations are discussed in Section 4.3.1.

3.4.2 N7 back calculations

Deflection bowls were analysed for each station of the N7 from 5.8 km to 18 km in both directions for 1994, 2000, 2004, 2010 and 2016. The deflection bowls of all stations used in this study can be found electronically on the attached CD. The pavement structures used for back calculation of the N7 data is illustrated in Figures 3.7 to Figure 3.10 in Section 3.2.2 on pages 63 and 63.

Rubicon was used to plot the calculated deflection against the measured deflections for each testing site. Adjustments were made to the resilient modulus of each of the layers to ensure that the difference between measured and calculated deflections was less than 10 micron. In some cases this was not reasonable as the resilient modulus of the materials would be unrealistic. In these instances the profile of the calculated line was adjusted to meet that of the measured values.

The values measured 200 mm away from the centre of loading were not deemed critical as local effects close to the edge of the loading plate can give variable results. In addition, the radius of the loading plate being 150 mm, only 50 mm away from the geophone, may result in unreliable results. The results obtained from the back calculation of FWD tests performed on the N7 are discussed in Section 4.3.2.

3.4.3 N7 Uniform sections

The BSM sections analysed for the N7 highway consisted of 13 km in each direction. This amounted in a large amount of variable data. The N7 North and Southbound sections were divided into uniform sections as discussed in this section. The large amount of data was then sorted and values were determined for different degrees of reliability.

The BSM section of the N7 was divided into a number of uniform sections with similar responses. This was done to obtain more accurate representative Mr values for each of the sections. Firstly three distinct sections were identified based on the direction and base type:

1. Southbound between 5.8 and 18.0 km. This section was rehabilitated in 2002 using foamed bitumen.

2. Northbound between 5.8 and 11.4 km. This section was also rehabilitated in 2002 using foamed bitumen. This section was not incorporated as part of the Southbound section as it was constructed at a different point in time with a different construction method. Additionally this section, leading in the opposite direction, was subject to dissimilar traffic and axle loads.

3. Northbound between 11.6 and 18 km. This section was rehabilitated in 2007 using bitumen emulsion for the stabilised base layer.

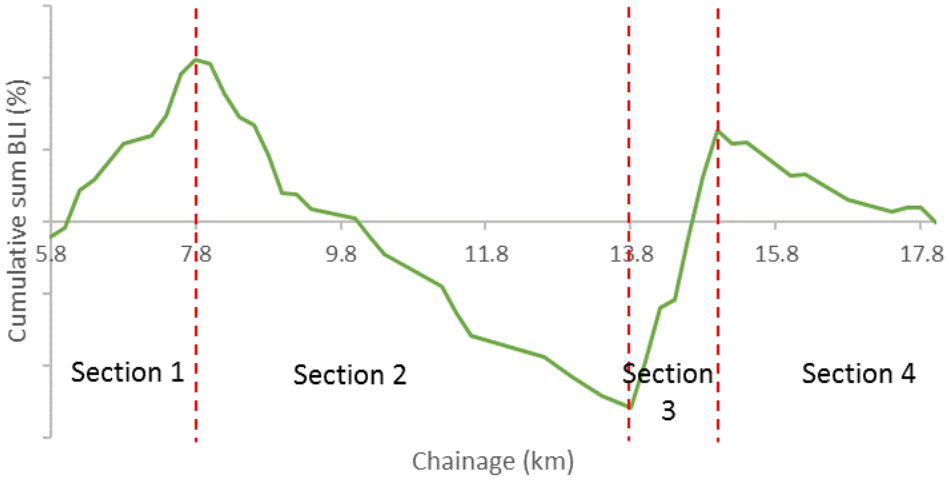

Figure 3.16: Example of uniform sections identified using the cumulative sum method based on BLI

Each of the three sections identified above was analysed using the cumulative sum method to identify uniform sections. The cumulative sum method is a sequential analysis technique that can be used to monitor change in a data set. The uniform sections were analysed based on the cumulative sum analysis of layer resilient modulus (Mr) and the three layer indices (BLI, MLI, LLI). Focus was placed on the resilient modulus of the base layer as this is the main area of investigation for this study. It is expected that points in a uniform section, identified from this analysis, would have little variance in resilient modulus and BLI results.

The cumulative sum method uses Equation 3.4 to calculate the cumulative sum value, for example BLI data, over the length of the road. The cumulative sum values can then be plotted relative to their location. A uniform section can then be identified identified between inflection lines as illustrated in Figure 3.16. The different sections of the N7 were investigated using the cumulative sum method. The result analysis and division into subsections are discussed in Section 4.2.3.

$$S_i = x_i - x + S_{i-1} \tag{3.4}$$

Where:

S_i = Cumulative sum of deviations of mean BLI values

x_i = BLI at point i

x = Mean BLI

S_{i-1} = Cumulative sum of previous point

3.4.4 Representative values

The resilient modulus data obtained from the back calculations was analysed to obtain resilient modulus values that represent the BSM layer at different points in its design life. The large amount of FWD and back calculated resilient modulus values complicate the interpretation of the data. Therefore, resilient modulus values were identified for each of the uniform sections at different levels of reliability and different ages in the service life.

The statistical method of percentiles was used to obtain resilient modulus values for different reliabilities of the materials for the N7 data. The 90th and 75th percentile values represent the base layers with higher resilient modulus values, where the 25th and 10th percentile values represent areas with a low resilient modulus. The 50th percentile was used as an indication of the average resilient modulus. Similarly the different percentile values were determined for the layer indices.

It is important to take note that the FWD data used in the back calculation was obtained from the actual test and not from a statistical point. A statistical point can be obtained by taking the percentile of each of the individual FWD measurements. For example the 95th percentile value for the deflection at 300 mm (D_{300}). This approach may cause problems and yield unrealistic results as a fictional point would be analysed with possibly unrepresentative relationships between measurements.

3.5 Triaxial testing

To further investigate the long term performance of BSMs, cores were drilled from the N7 BSM sections between June and October 2017. These samples were prepared for testing and were tested using the Material Test System (MTS 810, Model 318.10) at Stellenbosch University's pavement department. The tests include monotonic triaxial tests as well as dynamic triaxial tests. The use of these tests allowed for the accurate determination of cohesion, friction angle and resilient modulus of the materials. The preparation of test samples and the tests procedures used in this study are discussed in this section. All results from triaxial testing are discussed in Chapter 4.

Due to the high cost of specialised equipment and traffic accommodation, only a limited amount of cores could be obtained. The cores were obtained from different locations on the pavement. During drilling a number of cores broke and was not testable. Table 3.6 shows the test plan for monotonic triaxial testing on cores obtained from the N7. Cores were drilled from the outer wheel path (OWP) as well as between the wheel paths (BWP).

Table 3.6: Monotonic tests assigned to cores obtained from the N7

Direction	Chainage	Core Date	BSM	Condition	Testable Cores
SB	10.5	31/08/2017	Foam	Failed (Patching and rutting)	3 OWP 3 BWP
SB	16		Foam	Good	3 OWP
NB	9.2	06/07/2017	Foam	Good	4 OWP
NB	10	10-07-2017	Foam	Moderate	4 OWP
NB	11	11-07-2017	Foam	Failed (patch)	3 OWP 3 BWP
NB	12	12-07-2017	Emulsion	Good	4 OWP 3 BWP
NB	14.4	13-07-2017	Emulsion	Moderate	3 OWP
NB	16	14-07-2017	Emulsion	Moderate	3 OWP

3.5.1 Core drilling

Core samples were drilled from the N7 BSM sections between June and October 2017. Cores were drilled from the outer wheel path or between the wheel path at different locations on this section. These cores were drilled using the Eibenstock EBM 182/3 drill mounted on an Eibenstock BST 182 V drill stand. The cores were drilled with a 152 x 450 mm diamond core barrel. The drill configuration is shown in Figure 3.17.

Figure 3.17: Core drill rig

Figure 3.18: Operation of core drill

The drill rig was fastened to the pavement surface using M16 anchor sleeves drilled into the asphalt layer as indicated in Figure 3.17. The sleeves were put in place using an 8 mm pin. An anchor bolt was then screwed into this sleeve and the drill stand held in place by a washer and an anchor nut. To ensure that the drill-bit did not move, the drill operator stood on the base plate while drilling each core. The drill operation can be seen in Figure 3.18.

Figure 3.19: BSM foam core before preparation

A combination of wet and dry drilling was used to drill through the asphalt and BSM base. Wet drilling was used to drill through the asphalt layer, usually 50 - 70 mm from the surface. Wet drilling uses a small hand pump to pump water through the core barrel. This is necessary as fine materials build up in the system, which then forces the drill to a halt.

Due to BSMs sensitivity to water, dry drilling was used for all BSM cores. While drilling through the asphalt, with a constant supply of water, fine material was flushed from the drill environment.

When drilling without water, through the BSM layer, the drill bit got stuck in the hole and the core got stuck in the core barrel. To overcome this problem a compressor was used to supply a constant air flow through the drill bit when drilling through the BSM layer. This solution ensured that the core could be drilled without damaging the sample with water. No overheating was observed while drilling through BSMs without pumping water through the system. However, drilling without water does wear down drill bits much faster and produces a dust cloud.

Once the cores were removed from the pavement, they were labelled and sealed in plastic bags. The samples were transported back to Stellenbosch University for preparation and testing. Figure 3.19 shows a core obtained from a foam stabilised section, while Figure 3.20 shows a core from an emulsion stabilised section. The string in these figures indicate the different layers in the pavement structure. The core shows that the pavement consists of a granular subbase, BSM base (roughly 250 mm), an asphalt layer and a thin surfacing layer.

Figure 3.20: BSM emulsion core before preparation

3.5.2 Sample preparation

Most of the BSM cores obtained from the N7 consisted of the BSM, asphalt and granular materials (see Figure 3.20). To accurately test the properties of the BSM, the material was isolated before testing. The asphalt and surfacing layers were sawed off using a diamond blade saw shown in Figure 3.21. No water was used for sawing as not to induce any moisture damage to the material. By sawing off the asphalt layer, the BSM core had a flat surface, which is required for the triaxial loading plate.

The bottom of the cores were also sawn off to create a surface as flat as possible. The interface between the BSM layer and the granular layer below it would not produce a smooth, flat finish when sawed. Once the bottom was sawn off, the area was filled with a plaster of Paris mixture to create a flat surface for testing. The loading surface is very important as it ensures that the load

is equally applied over the whole sample. Figure 3.22 shows the bottom of a BSM core before and after applying the plaster of Paris mix. This created a flat loading area suitable for triaxial testing.

Figure 3.21: Sawing of BSM core

Figure 3.22: BSM core before and after surface was flattening with plaster of Paris

3.5.2.1 Rubber membrane production

Rubber membranes were used to isolate the cores from the high surrounding pressures. This ensures that confining pressure is evenly distributed over the sample. Membranes were made using rubber latex in liquid form dried on the turning cylinder. Three layers of latex was required to produce

one membrane. Thrice the latex was applied and dried before a membrane was ready to use. The apparatus used to make these membranes is shown in Figure 3.23. The membranes were open on both sides with an internal diameter of 150 mm and a length of 400 mm.

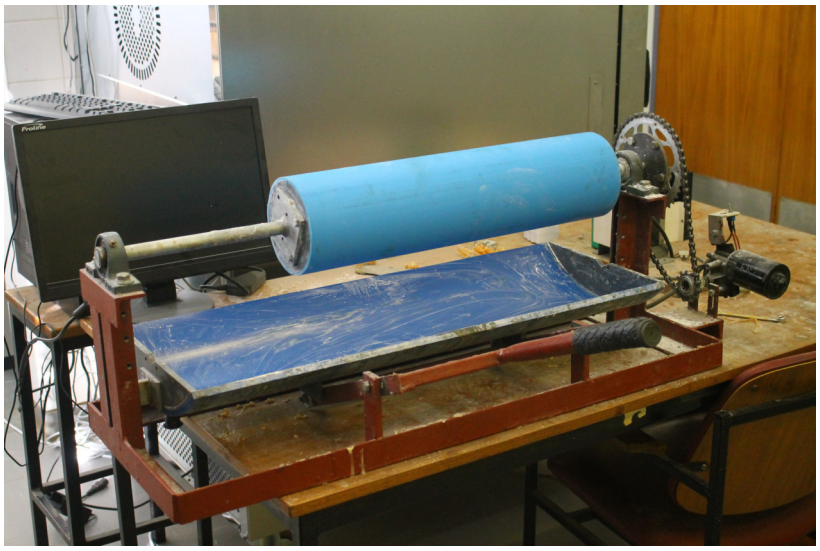

Figure 3.23: Rotating cylinder for latex membrane production

.

3.5.2.2 Monotonic test setup

The MTS at the University of Stellenbosch was used to test the BSM cores drilled from the N7. These tests were carried out using the same apparatus, methods and standards as Van den Berg (2014) and Kotze (2014). The MTS system applies air pressure to test the specimen at a range of confining pressures.

Cores were weighed on an electronic scale and the height and diameter of each sample was measured. The loading rate of monotonic tests is discusses in Section 3.5.3. Before each test it was ensured that the testing equipment was clean and fully functional.

A cylindrical membrane enlarger was used to stretch the rubber membranes (see Figure 3.24) over the core sample. It is important to inspect the membrane for any holes or tears as test results can be influenced if air is forced into a sample. A small rubber pipe was connected to the cylindrical unit, which was used to remove air between the membrane and the unit. This allowed the membrane to be placed over a core sample with ease and without damaging the sample or the membrane. The core sample was then placed on the base plate of the MTS.

Figure 3.24: Cylinder with hose for latex membrane fitting

Once in place, the rubber membrane was folded over the sides of the base and loading plates. A rubber O-ring was used to ensure an airtight seal between the loading and base plates. Additional membranes and O-rings were placed on the base and loading plates to ensure an airtight seal. The sample was positioned in the centre of the base plate and the centre of the loading plate directly beneath the loading pin of the MTS. The sample configuration is shown in Figure 3.25.

Before the dynamic triaxial tests were conducted, linear variable differential transformers LVDTs were placed directly on the sample to accurately measure the axial displacement in the sample. Dynamic triaxial tests are discussed in Section 3.5.4.

The LVDT's plastic collar clips were fixed to the specimen around the rubber membrane on the specimen. This collar serves as a holding ring for the LVDTs. A similar collar, serving as a base for the LVDTs, was fitted on the specimen. The cores were not 300 mm in height, therefore, the collars were placed to ensure 100 mm gap between them in the middle of the samples.

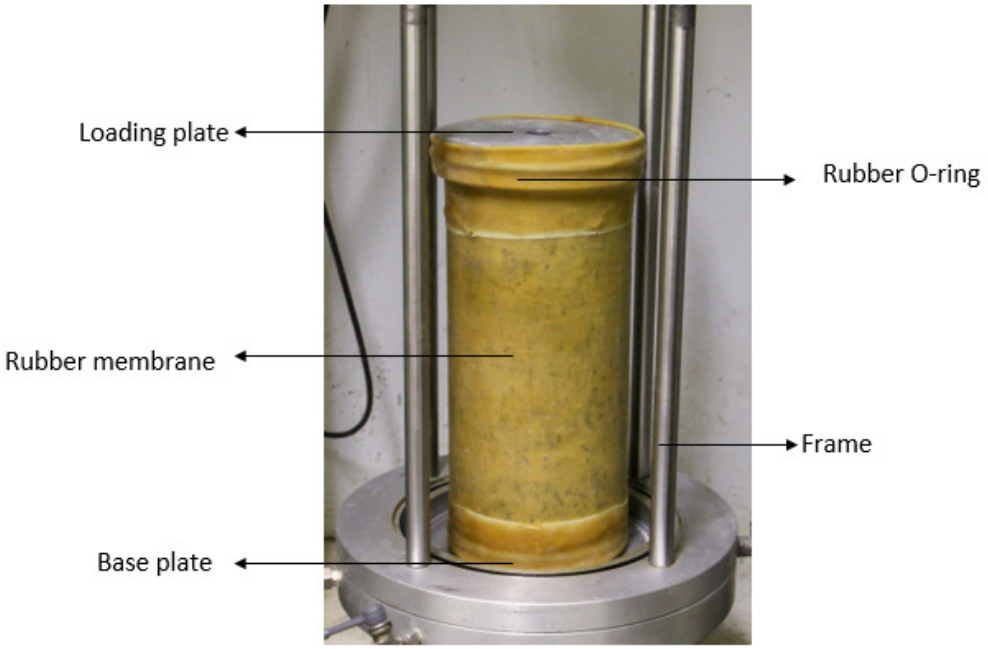

Figure 3.25: Core sample prepared for triaxial testing

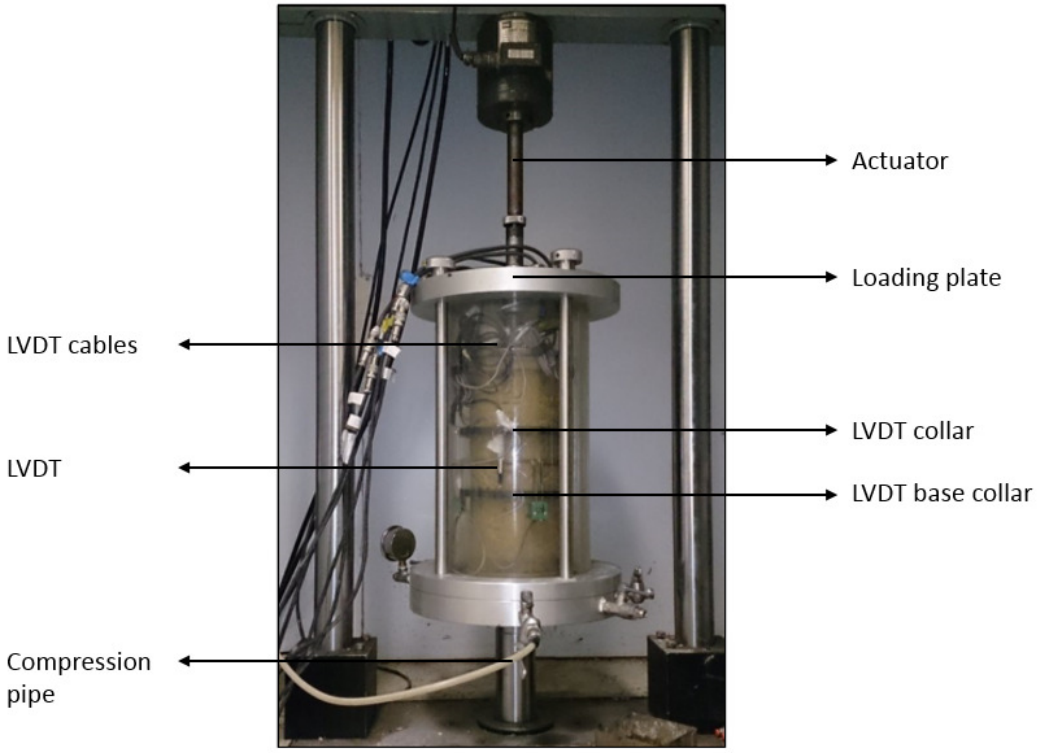

Figure 3.26: Core sample prepared for dynamic triaxial testing with LVDTs (Van den Berg, 2014)

The LVDTs were then attached between these two fittings. The cylindrical perspex unit was placed over the sample (this is required to maintain the desired air pressure for testing). Cables connecting

the LVDTs were connected before attaching and fastening the loading unit on the perspex cylinder. The LVDTs were tested before each run to ensure they were in working order. The set-up was checked before every test to ensure it was airtight.

The actuator of the triaxial machine was lowered by hand to the point of contact with the loading unit. The alignment of the loading rod, loading unit and sample was checked before connecting the air pressure pipe. The fully set-up dynamic triaxial test is shown in Figure 3.26.

3.5.3 Monotonic triaxial test

Monotonic triaxial tests were performed on BSM core samples taken from the N7 to obtain its shear parameters after 15 and 10 years of service. The location on the road and testing plan for these tests are discussed in Section 3.1. The samples were all drilled using the same method and kept in plastic bags until testing as described in Section 3.5.1. Samples were prepared as per Section 3.5.2 and kept at $25°C$ for at least four hours before testing.

The test set-up, specified in Section 3.5.2.2, was used for monotonic tests , with the only difference being that the LVDTs were not used during these tests. Once the test had been prepared the pressure inside the cylindrical unit was adjusted to obtain the desired confining pressure. The sample was then subjected to an applied stress (σ_1), which was applied at a constant rate of displacement of $3mm/min$ until the material failed. Material was assumed to fail once the applied force had reached a maximum and was reduced to 80% of that value. This process was repeated for all monotonic tests performed in this study. Samples were tested at four possible confining pressures: $0kPa$, $50kPa$, $100kPa$, $150kPa$. The monotonic test plan, indicating the confining pressures, is shown in Table 3.7. Due to the limited number of BSM cores, not all pressures were tested at all locations.

The results from the monotonic tests were analysed using the Mohr-Coulomb principals. Principal stresses were analysed on a shear-normal stress graph. Mohr circles were drawn on these points and connected with a tangent line representing the failure line of the material. This line describes the shear parameters; the cohesion (c) is described by the point at which the line crosses the vertical axis, while the friction angle (ϕ) is the slope of the line. Figure 3.27 shows how a typical Mohr-Coulomb graph is put together.

Table 3.7: Monotonic triaxial test plan at specific confining pressures for N7 cores

Direction	Chainage	Material	Position	Confining pressure (kPa)
SB	10.5	Foam	OWP	0 50 150
			BWP	0 50 100 150
SB	16	Foam	OWP	0 50 150
NB	9.2	Foam	OWP	0 50 100 150
NB	10	Foam	OWP	0 50 100 150
NB	11	Foam	OWP	0 50 150
			BWP	0 100 150
NB	12	Emulsion	OWP	0 50 100 150
			BWP	0 100 150
NB	14.4	Emulsion	OWP	0 50 100 150
NB	16	Emulsion	OWP	0 50 150

A number of calculations were done for each of the monotonic triaxial tests carried out:

1. The force that causes failure of the test sample was determined for each tests. This force is defined as the maximum applied force during the test. This force was converted into stress as per Equation 3.5.

$$\sigma_{a,f} = \sigma_{d,f} = (P_{a,f}/A) * 10^{-3} \tag{3.5}$$

Where:

$\sigma_{a,f}$ = Stress causing failure to occur (kPa).

($P_{a,f}$ = Force causing failure to occur (N).

A = Area of the cylindrical core (m^2).

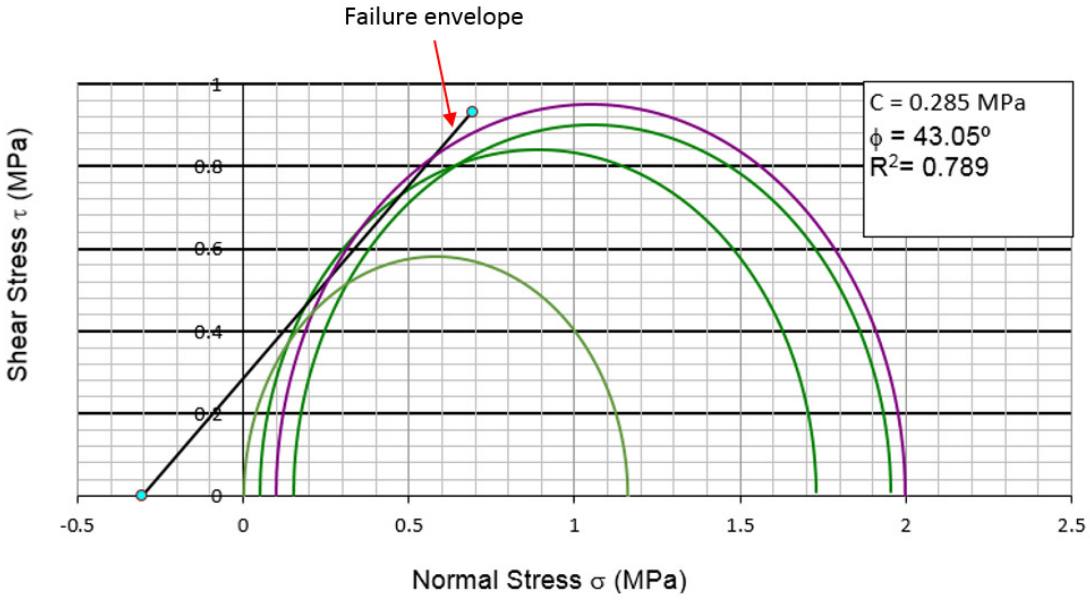

Figure 3.27: Example of a Mohr-Coulomb graph

2. The principal stress at failure was calculated for each sample as per Equation 3.6.

$$\sigma_{1,f} = \sigma_{a,f} + \sigma_3 \tag{3.6}$$

Where:

$\sigma_{1,f}$ = Principal stress at failure (kPa) σ_3 = Confining pressure inside the pressure vessel (kPa)

3. The relationship between σ_1, f and the confining pressure is described by the relationship in Equation 3.7, (SANRAL, 2011). The values for A and B were determined by performing a linear regression analysis on the combinations of $\sigma_{1,f}$ and σ_3 obtained from test results.

$$\sigma_{1,f} = A * \sigma_3 + B \tag{3.7}$$

Where:

$$A = (1 + sin(\phi))/(1 - sin(\phi)) \tag{3.8}$$

$$B = (2 * C * cos(\phi))/(1 - sin(\phi)) \tag{3.9}$$

4. The values for c (kPa) and ϕ (°) were obtained by rewriting Equation 3.8 and 3.9 into the following forms (SANRAL, 2011):

$$\phi = \sin^{-1}((A - 1)/(A + 1) \tag{3.10}$$

$$c = B * (1 - sin(\phi))/(2 * cos(\phi)) \tag{3.11}$$

3.5.4 Dynamic triaxial test

The resilient modulus (Mr) testing was performed on the BSM cores to determine the resilient modulus of the material at a range of confining stress conditions. The resilient modulus describes the load spreading ability of a material. By determining the resilient modulus of the material at different stages of its design life, the long term effective resilient modulus can be investigated.

The resilient modulus of a material is determined by measuring the deformation in the material at different confining pressures. The values obtained from these tests can also be compared to the back calculated stiffnesses from the FWD analysis. The specimen was set up for this test as described in Section 3.5.2.2. The set-up for the dynamic test differs from the monotonic test as LVDT measurements were used. LVDTs measure the vertical displacement of the material. These displacements are usually very small and therefore require very sensitive measuring apparatus.

The resilient modulus is determined by applying a repeated axial load, increasing every 100 load cycles up to a deviator stress ratio of 55%. As the number of samples were limited, some of the samples were utilised in more than one test. Therefore, maximum DSR applied during dynamic triaxial testing was limited to 55%.

The force required to achieve a specific stress ratio was calculated for each testing point from the monotonic tests. The loading sequence was repeated at different confining pressures. This allowed the stress dependant resilient response to be described over a range of stress conditions.

The loads applied to the specimen used a haversine shaped load pulse (loading and returning to the original position). Loads were applied over 0.1 seconds with a 0.9 second rest period thus applying a cycle rate of 10 Hz and a loading rate of 1 Hz. The applied axial stress used in this test was determined as 15%, 25% and 35% of the deviator stress at failure.

Four samples obtained from the N7 highway were tested with the dynamic triaxial test. These tests were compared to resilient modulus values obtained from deflection measurements. The results of the dynamic triaxial testing are discussed in Section 4.4.2.

3.6 Transfer function origin and development

The development and evolution of a mechanistic-empirical design function for BSMs are discussed in this section. The failure mechanism for BSMs, permanent deformation (or rutting), is similar to that of granular materials as was determined in Chapter 2. The starting point for the BSM transfer function to was to identify a transfer function that would describe the granular materials used in road construction. The transfer function for waterbound macadam was selected as a starting point in developing a transfer function for BSMs. This function calculates the bearing capacity in terms of the number of standard axle load repetitions that can be sustained before a certain level of plastic strain is induced in the layer. The development of the transfer function for waterbound macadam is discussed in Section 3.6.1.

Loudon International experimented with this transfer function, using the shear properties of BSMs and their extensive experience with the materials. The architecture of the waterbound macadam transfer function was used and coefficients were altered to better describe the unique properties of BSMs. This produced the preliminary transfer function for BSMs. The alterations included the replacement of the parameter for saturation (S) in the transfer function with retained cohesion (RetC). As the "Loudon Transfer Function" has not been published, limited information is available regarding the calibration of this function. The heuristic approach followed and the alterations made to obtain the "Loudon Transfer Function' are discussed in Section 3.6.2. It is important to note that this function has not been published or calibrated and should not be used for design.

This research project aims to further adjust the "Loudon Transfer function" and to calibrate this design function based on the long-term performance of pavements incorporating BSMs. A number of pavement structures that incorporated BSM layers were identified and analysed to obtain the input values for the transfer function at different stages in their design life. The number of standard axles obtained from the transfer function was compared to actual traffic data for the specific pavements.

The approach followed to calibrate the transfer function is discussed in Section 3.7.

The function was verified using other design methods which is discussed in Section 3.8. Comparisons were made between the new transfer function, the "Loudon Transfer Function", the PN design method and actual traffic data. This approach ensures that the new transfer function would provide reasonable results. The transfer function was also calibrated to describe the life of a certain pavement given the level of reliability required for the design as per Section 3.7.5.

3.6.1 Waterbound Macadam

BSMs are similar to granular materials in that they fail in permanent deformation rather than cracking like cement stabilised materials. The transfer function for BSMs is therefore principally based on that of waterbound macadam. Equation 3.12 shows the formula for calculating the life, in terms of number of axle load repetitions (N), that the layer can sustain before a certain level of plastic strain is reached (Theyse et al., 2000). This model was based on triaxial and heavy vehicle simulator (HVS) test data for waterbound macadam material with crusher sand and natural sand filler.

$$\log N = 1.891 + 0.075RD - 0.009S + 0.028PS - 1.643SR \tag{3.12}$$

Where:
N = Number of standard axles that the layer can sustain before reaching the specified plastic strain limit
RD = Relative Density (%)
S = Saturation (%)
PS = Plastic strain limit as a percentage of the layer thickness (%)
SR = Stress ratio as given in Equation 3.13

The stress ratio used in this equation is a function of the load intensity, the shear properties of the materials as well as the overall pavement structure. The stress ratio for waterbound macadam can be calculated as per Equation 3.13.

$$SR = \frac{(\sigma_1^a - \sigma_3)}{\sigma_3 \left[\left(\tan^2(45 + \frac{\phi}{2}) - 1\right)\right] + 2C \tan\left(45 + \frac{\phi}{2}\right)} \tag{3.13}$$

Where:

σ_1^a = Applied major principal stress (kPa)

σ_3 = Minor principal stress acting in the middle of the granular layer (kPa)

C = Cohesion

ϕ = Angle of internal friction, calculated using Equation 3.14.

Theyse et al. (2000) obtained a model for the angle of friction of waterbound macadam material as shown in Equation 3.14. This model describes the angle of friction as a function of relative density and saturation of the material. Relative density is expressed as a percentage of the apparent density, while saturation is expressed as a percentage of inter-particle voids (88% and 25% for example).

$$\phi = -26.38 + 1.021RD - 0.171S \tag{3.14}$$

3.6.2 Modified waterbound macadam transfer function (Loudon International)

Loudon International adjusted the waterbound macadam transfer function to better describe the performance of BSMs. The 'Loudon Transfer Function' was developed as a heuristic design tool based on known performance of pavement structures on five continents incorporating BSMs. Numerous BSM projects were taken into consideration before a function based on in-service performance was developed (Loudon International 2016, personal communication, August). The 'Loudon Transfer Function' is shown in Equation 3.15. This function has not been published and minimal information regarding the calibration and verification thereof is available.

$$\log N = 1.55 + 0.1(RD) + 0.05(RetC) + 0.1(PS) - 22.333(SR) \tag{3.15}$$

Where:

N = Number of axle repetitions to reach a rut depth of $PS\times$ layer thickness of BSM

RD = Relative Density (%)

$RetC$ = Retained cohesion (%)

SR = Stress Ratio

PS = Plastic strain or Permanent Deformation in BSM as % of BSM layer thickness (%)

3.6.3 New BSM transfer function

This research aims to further adjust the "Loudon Transfer Function" to better describe BSM behaviour. Adjustments were made to develop a preliminary design function for BSMs. The major adjustments made to this function were to replace the term for RD with Mod AASHTO density, saturation with retained cohesion (RetC) and to increase the significance of deviator stress ratio within the function. The terms which describe the influence of density and moisture resistance were incorporated into a single term, the effect of which is described by a single constant. The preliminary new transfer function is given in Equation 3.16.

$$\log N = A - B(DSR)^3 + C(P_{mod}.RetC) + D(PS) \tag{3.16}$$

Where:

N = Number of axle repetitions to accumulate deformation in the BSM layer of $PS\times$ layer thickness of the BSM

DSR = Deviator Stress Ratio (-)

P_{mod} = BSM density expressed as a percentage of 100% Mod.AASHTO density (%)

$RetC$ = Retained Cohesion (%)

PS = Permanent Deformation allowable before failure in the BSM as % of BSM layer thickness (%)

The letters A, B, C and D in Equation 3.16 represent constants used to calibrate the transfer function. Seed values for each of the constants were estimated at the start of this study and calibrated using laboratory and field results. The initial values for the 4 constants are:

A = 1

B = 60

C = 0.001

D = 0.1

The first adjustment made to the "Loudon Transfer Function" was to replace the term for relative density with density as a percentage of Mod AASHTO density. The compaction achieved during construction plays a vital role in all aspects of material behaviour.

The next significant adjustment to the waterbound macadam transfer function was the replacement of the term for saturation (S) with retained cohesion (RetC). As a result of bitumen treatment, BSMs have superior moisture resistance and are able to retain a greater percentage of cohesion when compared to granular materials. Monotonic triaxial testing on BSM samples that were conditioned

with moisture exposure using the Moisture Induced Sensitivity Test (MIST), provide the means to a more reliable measure of the moisture susceptibility of the material. Therefore, the material's moisture susceptibility, rather than the degree of saturation, was used in the transfer function.

In Equation 3.12 the term defining the influence of saturation has a negative symbol. Therefore, an increase in saturation of the material reduces the number of axles obtained from the transfer function. This is reasonable as an increase in moisture reduces the shear properties and consequently the life of the material.

In Equation 3.16 the term defining the influence of retained cohesion (which replaces the term for saturation), has a positive symbol. This indicates that an increase in retained cohesion increases the number of axles the material can sustain before failure. This is also reasonable as an increase in moisture resistance reduces the degree of damage to a material when exposed to moisture under repeated loading. The increase in the number of axles the material can sustain before failure, as a result of the increase in retained cohesion, as per the new design function, is shown in Figure 3.28.

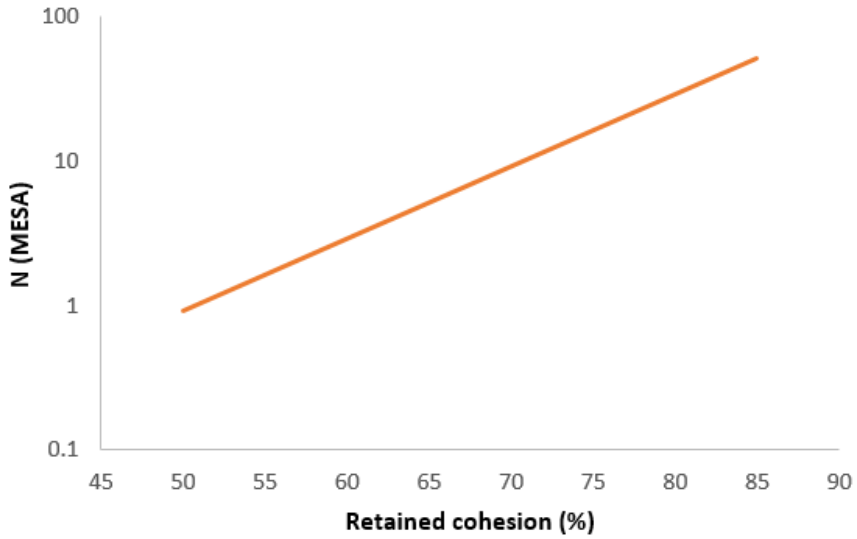

Figure 3.28: Increase in number of standard axles the material can sustain with an increase in retained cohesion according to the new design function

The new transfer function increases the significance of the deviator stress ratio on the life of the pavement. The term describing the effect of DSR has a negative symbol, indicating that an increase in DSR would shorten the life of the pavement.

The most significant adjustment to the preliminary transfer function was to subject DSR to the

power 3. The significance of this power and the investigation of its value are discussed in Section 3.7. The deviator stress ratio, measured at 25% of the BSM layer thickness from the top of the BSM layer, is dependent on a number of factors:

1. The load applied to the pavement: an increase in load increases the DSR. The transfer function was developed for a standard axle load of 80 kN. The effect of overloading was investigated as per Section 5.3.

2. The shear properties of the BSM: an increase in either cohesion or friction angle increases the failure envelope. For each corresponding confining stress, the larger failure envelope increases the failure stress and in turn reduces the DSR for a specific load.

3. The resilient modulus of the material controls the load spreading ability thereof. An increase in resilient modulus of a single layer attracts more stress to that layer, while offering better support to the layers above.

4. The overall pavement structure, the support under the BSM layer as well as the materials covering the BSM all have a large influence on the DSR in the BSM. Improved support for the BSM layer increases the confinement of this material under loading, reducing the DSR. The cover on the BSM layer determines the stress experienced by the BSM layer under loading. An increase in the cover depth and resilient modulus of the cover reduces the stress in the BSM and in turn the DSR.

3.7 Calibration of the new transfer function

The methods used to calibrate the new BSM transfer function are discussed in this section. The purpose of the calibration is to find values for the constants A, B, C, D, E in Equation 3.16 to best fit the prediction obtained from the function to actual traffic data. In order to calibrate the design function for a specific pavement the transfer function predictions should be compared the actual traffic the pavement has accommodated. This is not possible without the required information at various stages of the pavement's life. The LTPP pavements were used for calibration of the function, while the N7 was used to validate the calibrated function.

The transfer function can be calibrated to perfectly describe a specific case if the information is sufficient. However, this will not be useful as it will only describe the life of a specific BSM on a local scale, limiting the relevance for design. By investigating a number of pavement structures, with data available at multiple points in time, the transfer function can be calibrated to describe the life of BSMs on a more extensive scale.

The new BSM transfer function describes the number of standard axles a pavement can sustain before a certain amount of permanent strain has accumulated in the BSM layer. Therefore the requirements for calibration are number of axles and permanent deformation. The transfer function was calibrated with the maximum allowable permanent strain in the BSM layer fixed to 10% of the layer thickness. The number of standard axles was determined by traffic counts and is referred to as N_{actual}, while the permanent deformation was determined as a percentage of rut depth measured in field. Relating the values obtained from the transfer function to actual traffic is discussed in Section 3.7.1. Determining the permanent strain of the in field pavements is discussed in Section 3.7.2.

Input values for the transfer function were determined for each pavement used during the calibration. The values for retained cohesion, density and permanent strain were determined by investigating as built data, field investigations, field tests and laboratory investigation. Determining of the deviator stress ratio was a more complex procedure. The information required for the calculation of DSR is discussed in Section 3.7.3.

The required data was gathered for the fourteen LTPP pavement structures. Once the data was gathered and analysed, the transfer function could be calibrated to fit a number of pavements over a range of conditions. The transfer function was calibrated using linear regression analyses as discussed in Section 3.7.4.

3.7.1 Relating the transfer function to actual traffic

The transfer function relates the additional number of standard axles with the remaining amount of permanent strain in the BSM layer. The remaining amount of permanent strain in the layer is a limiting value set in by design criteria. This enables the designer to specify the amount of permanent deformation that may occur before the BSM is deemed to have failed. Note that this is not an absolute value, but an estimation.

In the field permanent strain accumulates with traffic loading as illustrated in Figure 3.29. This is what is expected as repeated loading of a granular materials causes permanent deformation in the layer.

The transfer function uses the allowable or remaining permanent deformation as an input value to determine the number of load repetitions the material can sustain before reaching the deformation limit. The traffic value obtained from the transfer function therefore decreases as permanent strain is accumulated. When the actual PS is used as input for the transfer function, the opposite trend

is observed as illustrated in Figure 3.30.

These figures illustrate that in order to compare N_{TF} ($N_{TransferFunction}$) with N_{Actual} the PS input value should not be input as the current level of PS, but rather the remaining amount of PS. This requires a limit of PS to be set in place, which was set to 10% of the layer thickness for this study and the calibration of the transfer function. Therefore, N_{Actual} at a certain PS should be compared to N_{TF} at $10 - PS$ as illustrated in Figure 3.31.

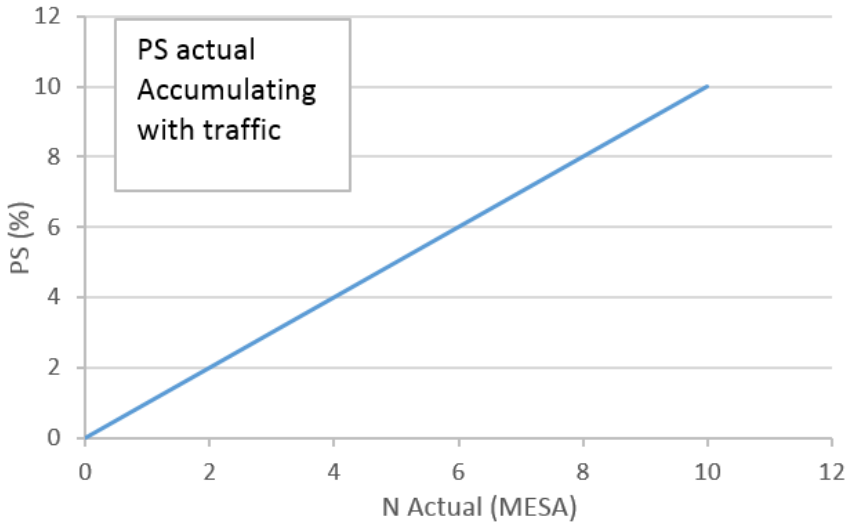

Figure 3.29: Permanent strain development with repeated loading

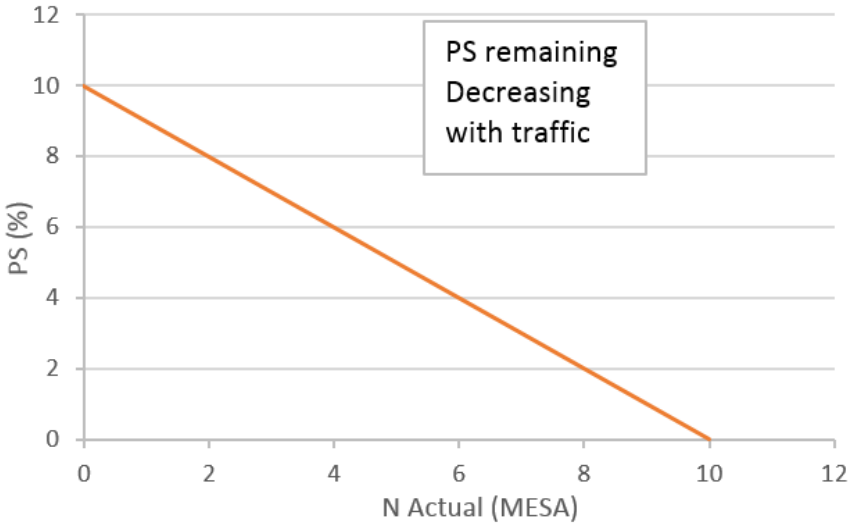

Figure 3.30: Decrease in N_{TF} with increase in PS

Comparison using this method requires at least 2 points of data obtained from field data for each

pavement. The first point (at the start of a pavement's life) would have an accumulated PS of 0% and a remaining PS of 10%. The second point would have accumulated for example 3% of PS and the remaining PS would be 7%. The number of standard axles the pavement accommodated during this time can be compared to values calculated with the new transfer function, to evaluate the difference. This provides a means of calibrating both the absolute values and the slope of results the transfer function yields with varying PS.

Figure 3.31 illustrates N_{TF} in a comparable format to N_{Actual}. By comparing the values obtained from the transfer function to the actual traffic in this manner, the transfer function can be calibrated. The process of calibration aims to reduce the difference in absolute values as well the difference in slope between N_{TF} and N_{Actual}. Prediction of the actual PS slope with the transfer function for the global set of data was deemed more important than predicting accurate results for single values.

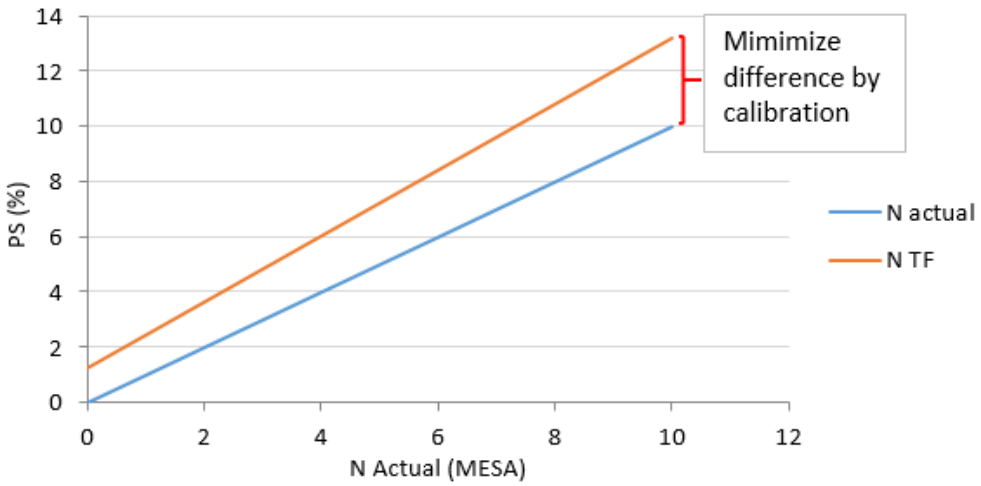

Figure 3.31: N_{TF} and N_{Actual} in comparable format

3.7.2 PS development with repeated loading

The new BSM transfer function uses permanent strain as the limiting factor when determining the life of a BSM. During the analysis of the pavements used to calibrate the transfer function, rutting measurements were taken at different points in time. The rutting measurements reflect the permanent deformation of the pavement structure as a whole. A percentage of the total permanent deformation was used to obtain the permanent deformation within the BSM base layers. Each pavement was assigned a value which indicates the portion of total deformation attributed to the BSM layer. This percentage was based on a number of factors:

1. A larger amount of deformation was attributed to the BSM layer for pavements which included thicker BSM layers. The same amount of deformation in the BSM layer (percentage wise) will have a larger effect on the total deformation if the layer is 300 mm thick instead of 100 mm.

2. Thick asphalt layers reduced the amount assigned to the base layer as some of the deformation may occur in the asphalt layer.

3. The supporting layer under the BSM significantly influences the deformation assigned to the BSM layer. Permanent deformation in pavements with weak support layer may be due to insufficient strength of the subbase or subgrade. Therefore, weak support resulted in smaller amounts of deformation attributed to the BSM layer.

4. Strong support layer, for example a C3 or C4 subbase, results in a better performing BSM layer. Due to the low deformation of the layer below the BSM base layer, the amount of deformation attributed to the BSM was increased.

For example, the MR 27 utilised a 100 mm thick BSM layer supported by a cement stabilised subbase. The relative thickness of the thin BSM layer reduced the rutting assigned to the layer. The cement stabilised layer would not deform significantly and therefore would not contribute to the overall deformation. The 50 mm asphalt layer may also show some deformation. The granular subgrade may also contribute to the total deformation, but the significant cover depth may reduce its contribution. The permanent deformation assigned to the BSM layer was determined to be 55% of the total deformation.

The plastic strain allocation calculations for the BSM layers of each of the LTPP pavement structures are summarised in Table I.1. These calculations are further discussed in Appendix I. A summary of the BSM deformation allocation is shown in Table 3.8.

The accumulated permanent strain in the BSM layers of the LTPP pavements varies for each pavement. This poses a challenge for the calibration of the transfer function. Pavements that showed little deformation would reflect the early life permanent deformation behaviour, while pavements that showed more significant deformation would reflect the long term permanent deformation behaviour. This would only allow the rates of permanent deformation accumulation for different pavements to be compared and not the absolute values.

To overcome these challenges, the PS limit for all BSMs in these pavements was selected as 10% of the layer thickness. This allowed load repetition comparisons between pavements over similar range

of PS values. In order to obtain values for the actual traffic at higher strain levels, the Huurman model for permanent strain development was implemented for each pavement. The Huurman model for PS development was used to determine the number of load repetitions at each of these PS levels up to the final level of 10%. The Huurman model for PS prediction is shown in Equation 3.17 (Huurman, 1997).

Table 3.8: BSM deformation allocation for LTPP pavements

Road	BSM thickness (mm)	BSM PS allocation (%)
MR27	100	55
MR504(A)	175	55
MR504(B)	175	55
N1-1	100	55
N1-13	150	50
N1-13 SB	100	35
N1-14	150	55
N2-16	140	70
N2-20	180	55
N4-1	170	70
N4-5X	150	65
N11-8	280	70
N12-19(3)	100	55
N12-19(4)	135	60
P243-1	250	70

$$\epsilon_p = A.\left(\frac{N}{1000}\right)^B \tag{3.17}$$

Where:

N = Number of load repetitions

ϵ_p =Plastic strain accumulated (%)

A, B = Regression parameters

The subject of this equation was exchanged to obtain an equation for load repetitions based on the level of permanent strain. This function is shown in Equation 3.18.

$$N = 1000.\left(\frac{\epsilon_p}{A}\right)^{\frac{1}{B}} \tag{3.18}$$

The regression parameters A and B were determined for each pavement based on the known traffic and deformation values. The equation was then used to determine values for N_{Actual} for the extrapolated PS values up to the limit of 10% of the layer thickness. The Huurman model was preferred for the extrapolation of the data as is predicts a logarithmic increase in plastic strain rather than a linear increase.

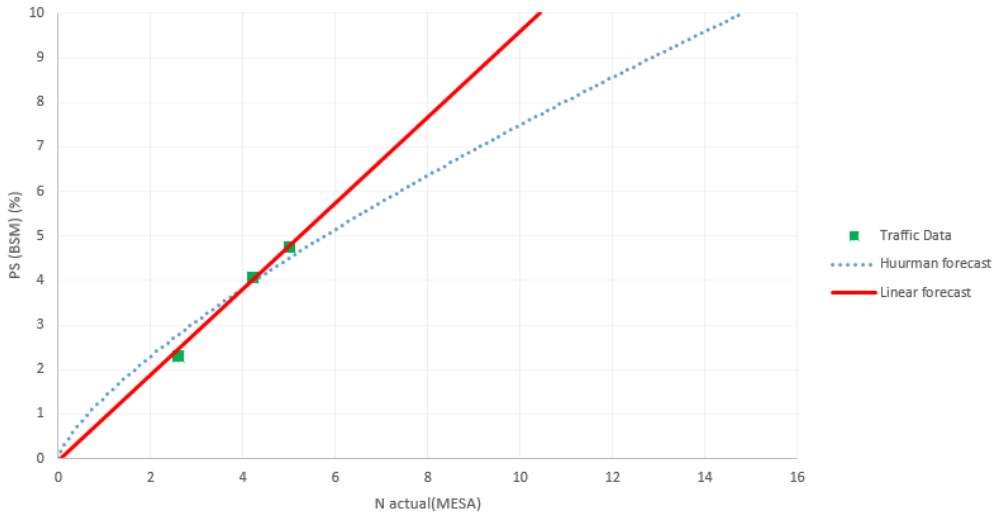

Figure 3.32: Traffic data extrapolation using linear forecasting and the Huurman model

With the available data it is possible to extrapolate the traffic using linear regression. However, the logarithmic shape of the permanent deformation trajectory is similar to that of repeated load triaxial tests performed in the laboratory. Section 2.5.5 discusses the accumulation of permanent deformation which highlights the logarithmic accumulation.

Figure 3.32 shows the extrapolation of load repetitions using linear forecasting and the Huurman model. From this figure it is clear that the Huurman model better describes the accumulation of permanent deformation in the long term than a linear forecast. It was assumed that these pavements remained in the stable state for the duration of their lives. Although this may not be accurate, it is a conservative assumption to make. The extrapolated traffic and PS values are discussed in Section 4.5.1.

The form of the new transfer function only describes the stable behaviour of BSMs. To model unstable behaviour with the function would require significant adjustments to the transfer function. Additional terms in the function would be required and would produce a complex equation. This study only aims to calibrate a transfer function for stable behaviour. Therefore, the transfer function was calibrated to fit the stable form of the Huurman model.

3.7.3 Determining DSR

The deviator stress ratio was has a large influence on the performance of granular materials and in turn BSMs. This ratio is dependant on a number of factors; layer stiffnesses, pavement structure, cohesion, friction angle as well as the load applied to the pavement. DSR is defined in Equation 3.19.

$$DSR = \frac{\sigma_1 - \sigma_3}{\sigma_{1,f} - \sigma_3} \tag{3.19}$$

Where:

σ_1 = Principle stress due to loading
σ_3 = Confining pressure
$\sigma_{1,f}$ = Principle stress at failure

The deviator stress ratio was determined using the linear elastic tools in Rubicon Toolbox. The structure of each pavement was defined in the software. Information required included:

1. Number of layers
2. Layer thickness (mm)
3. Resilient modulus (Mr) (MPa)
4. BSM: Cohesion (kPa)
5. Friction angle (°)

Once the pavement structures were modelled, the pavements were analysed using Rubicon's Standard Axle Analysis V2. In order to calculate the stress conditions, the software requires the load that that the pavement would be subjected to. The transfer function was calibrated for a 80 kN standard axle load with dual wheels spaced at 350 mm apart exuding a pressure of 750 kPa. Further investigation was also done on the effect on the DSR due to overloading.

Each pavement was analysed using this software according to different failure criteria based on the type of material. These values were checked to ensure that the results were reasonable. The software was set up to determine the maximum DSR of 3 locations in the BSM; 25%, 50% and 75% of the layer thickness from the top of the BSM. The critical shear stress ratio was identified and used during further analysis. An example of this analysis is shown in Figure 3.33. The results of the DSR calculations is given in Section 4.5.2.

Note that the analysis in Figure 3.33 determined the life of the BSM using the "Loudon Transfer Function". These values were not used during calibration. The results from the Loudon transfer function was analysed during the validation of the the new transfer function in Section 3.8 as a test of reasonableness.

3.7.4 Calibration with regression

With all the information available the transfer function can be calibrated to fit the actual traffic data. The calibration of the transfer function was done based on the LTPP data. The objective of the calibration is to find values for the constants A,B,C and D in the new transfer function which results in the closest approximation of the actual traffic data.

By plotting the actual traffic data against the corresponding transfer function prediction a graphical indication of the transfer function's ability to describe actual data can be obtained. An illustration of such a graph is shown in Figure 3.34. The transfer function's ability to predict the trends of actual traffic is deemed good when the slope of this line converges to one.

The relative accuracy of this function can be investigating the R^2 which describes the trendline through the data. A higher value for R^2 indicates a better accuracy in traffic estimation. Another indication of accuracy would be the residual sum of squares. The interception point of this line was mostly not taken into account during the calibration procedure.

In order to find the optimum values for the constants in this function, the excel solver function was used. Excel solver was used with the Evolutionary solving method to change the values of the 4 constants. The objective was set to find the minimum residual sum of squares, indicating the best accuracy of prediction. Constraints were set in place to keep the prediction slope as close to 1 as possible, indicating a good estimation of the trends of in field conditions. The results of this process is discussed in Section 4.5.

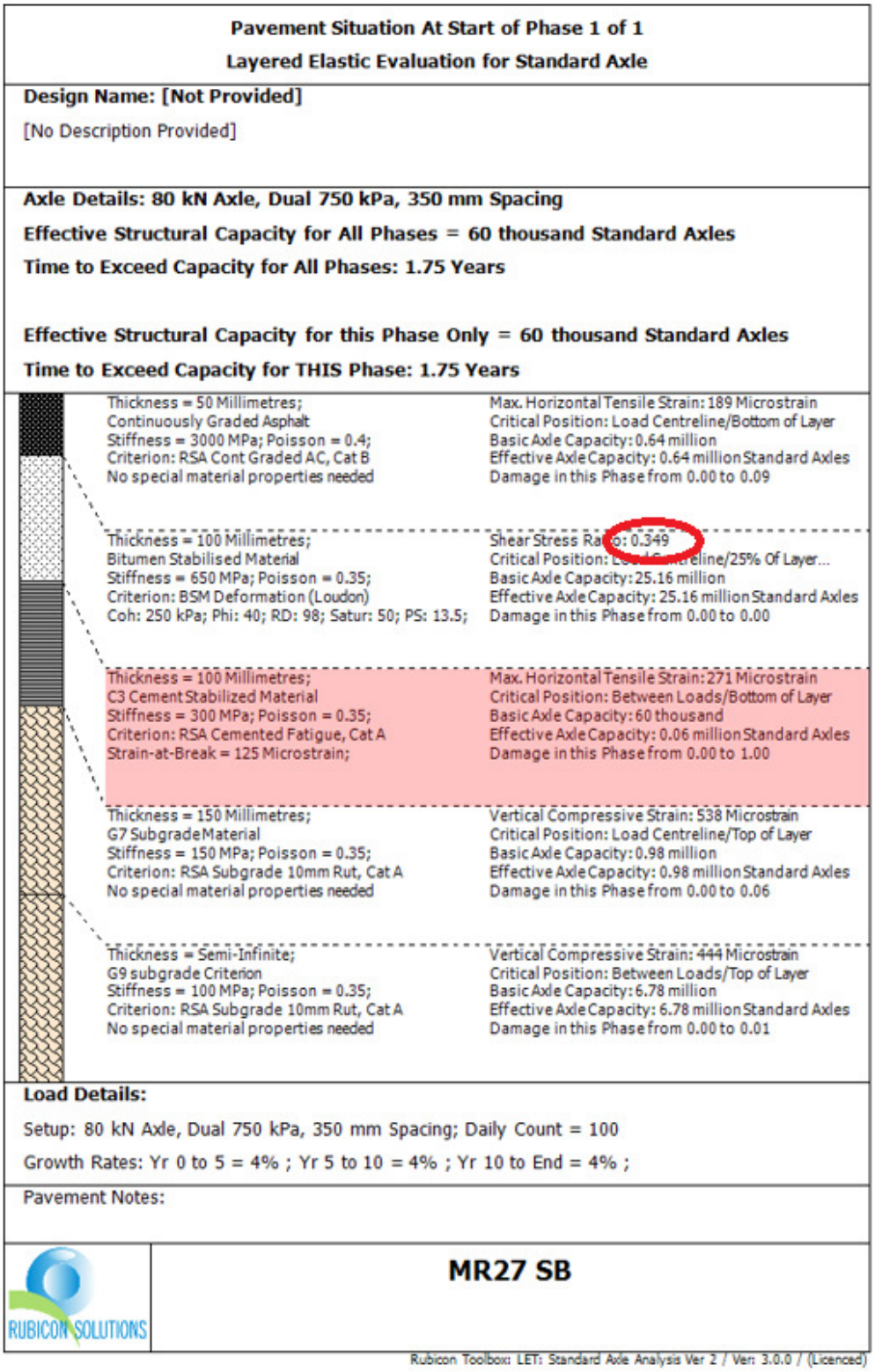

Figure 3.33: Example of DSR determination using Rubicon software

3.7.5 Reliability adjustments

The transfer function calibrated with the method stipulated in Section 3.7 aims to find the most accurate and best fitting transfer function for the data available. This method of calibration does

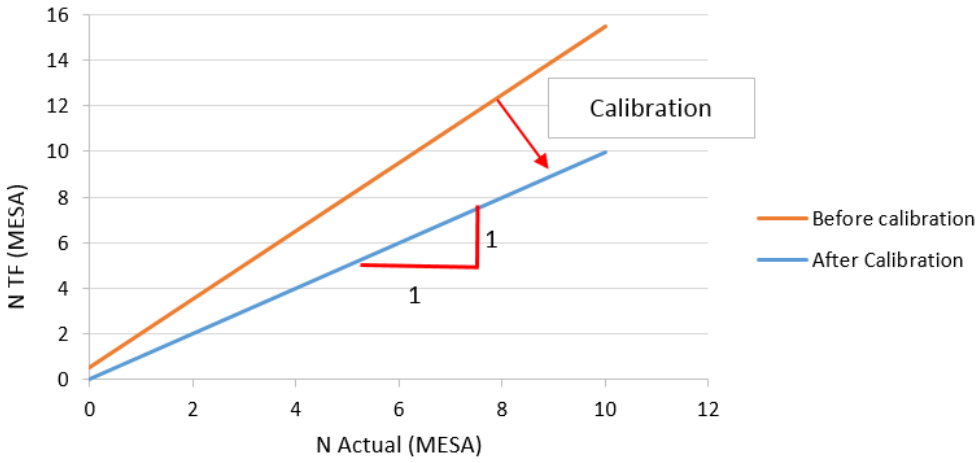

Figure 3.34: Calibration of N_{TF} to describe N_{Actual}

not take any safety factors or adjustments into account. The reliability of the transfer function would therefore not be adequate for design purposes, as it would be providing a 50% probability of failure. For this reason the transfer function was adjusted to describe the data at a number of levels of reliability. The adjustments made to the function were only made to the constant A, producing an easy to use function with only one constant to change for different levels of reliability. By only adjusting the constant A (in other words not changing the slope of the function), the relative influence of the four variables in the function were not altered.

The current design methods used in South Africa specify four levels of reliability based on the category of the road. The four categories are defined as category A (95% reliability), category B (90% reliability), category C (80% reliability) and category D (50% reliability). Category D roads are usually low volume roads and it is usually not economically viable to use BSMs for these roads. Calibration of the new transfer function at these levels of reliability is discussed in 4.6.

3.8 Transfer function validation

The new transfer function for BSMs was calibrated to predict the actual data observed during the LTPP studies. Once the function was calibrated and adjusted for certain levels of reliability, the function was deemed to be validated.

The function was validated by investigating the function's ability to predict the permanent strain development in a BSM layer that was not used during calibration of the function. For this reason the function was not calibrated using the N7 data, but rather validated using this data. Validation using the N7 data is discussed in Section 3.8.1. The new transfer function was also compared to

other design methods as part of the validation process as discussed in Section 3.8.2.

3.8.1 N7 Validation

The BSM section of the N7 highway near Cape Town was used to validate the new BSM transfer function. This section makes use of both BSM foam and BSM emulsion over a distance of 26 km. Results obtained from this road were not used during the calibration of the transfer function and is thus a good control to determine the accuracy of the new transfer function. The results of the validation of the new transfer function with the N7 data are given in Section 5.1.

The validation of the transfer function followed a similar method to that of calibration with the LTPP data. The main difference being that the constants were not calibrated to fit this data. The N7 was divided into uniform section, each with its own traffic counts, rut depth measurements, layer stiffnesses and layer thicknesses.

The traffic and rutting data from the N7 highway was related and extrapolated to reach a 10 mm rut depth. The same process was followed as discussed in Section 3.7.2 for the LTPP data. The layer stiffnesses assigned to each of the N7 uniform sections was obtained from the back calculation results. Layer thicknesses were obtained from test pits, dug over the length of the road between June and October 2017. The applied standard axle load was also assumed to be 80 kN, but investigation was done to determine the effect of overloading.

The testing of cores drilled from the N7 highway provided valuable insight to the shear properties of the material. Cohesion and friction angle values were judiciously assigned to each uniform section based on the test results from cores obtained from that section. The assignment of values is explained in Section 4.4.

The extensive investigation performed on the N7 provides valuable insight to the actual performance of the road. The estimations obtained from the transfer function was compared to actual observations and test results on this road. With this information available, the effect of local conditions on the transfer function could be investigated.

3.8.2 Validation with other design methods

The calibrated transfer function was also investigated using the existing design method. A number of example pavements were randomly selected and analysed using the PN design method, the "Loudon Transfer Function" and the new BSM transfer function. This process allows a comparison

of the results obtained and an investigation into the most influential properties. Validation with the other design methods is further discused in Section 5.2

3.8.3 Sensitivity analysis

The new transfer function uses four variables to determine the life of a BSM:

1. Density (Pmod)
2. Moisture susceptibility (RetC)
3. Deviator stress ratio (DSR)
4. Permanent strain to failure (PS)

Calibration of the transfer function assigned constants to each of these variables, describing their significance on the life of the pavement. Their significance was investigated to ensure that a realistic relationship was obtained. The transfer function's sensitivity to a change in one of the variables was investigated for each of the variables individually.

As DSR is the crucial parameter in the function, the other variables were investigated over a range of DSR values. The life of a BSM for a range of densities, RetC values and PS values was investigated. The results of the sensitivity analysis is discussed in Section 5.3

3.9 Summary

Chapter 3 is summarized as follows:

1. The research overview discussed the overall structure of this study. The significance of processes from pavement investigations to validation of the transfer function is discussed in this section.
2. Data was gathered from fourteen long term pavement performance studies. This data included FWD results, rutting measurements and traffic counts.
3. Data was gathered from the N7 highway, with focus placed on FWD data and permanent deformation measurements. Traffic data was also gathered at different stations on the road.
4. The stiffness back calculation process for the LTPP pavements and the N7 was discussed in this chapter.

5. Cores were drilled from the N7 and prepared for monotonic and dynamic triaxial testing. The processes followed during the drilling of cores, preparation of samples and test procedures were discussed in this chapter.

6. The origin and development of the new transfer function was discussed in this chapter. Changes made to the Waterbound Macadam transfer function was highlighted. The significant change to DSR was also discussed in detail.

7. The processes used to calibrate the new transfer function was thoroughly discussed in this chapter. The function was calibrated to best describe the observed data and adjusted to meet the design reliability requirements.

8. The function was validated using the data obtained from the N7. The new transfer function's sensitivity to the different variables was investigated.

Chapter 4

Results and discussion

4.1 Chapter overview

This chapter presents and discusses the results obtained from lab and field tests. Analysis of data obtained from other studies also forms part of this chapter. These results were part of the first phase of this study, the layout of which is illustrated in Figure 4.1.

The calibration of the transfer function, forming part of the second phase of this study, is also covered in this chapter. Figure 4.2 illustrates the layout of the second phase of this study covered in this chapter.

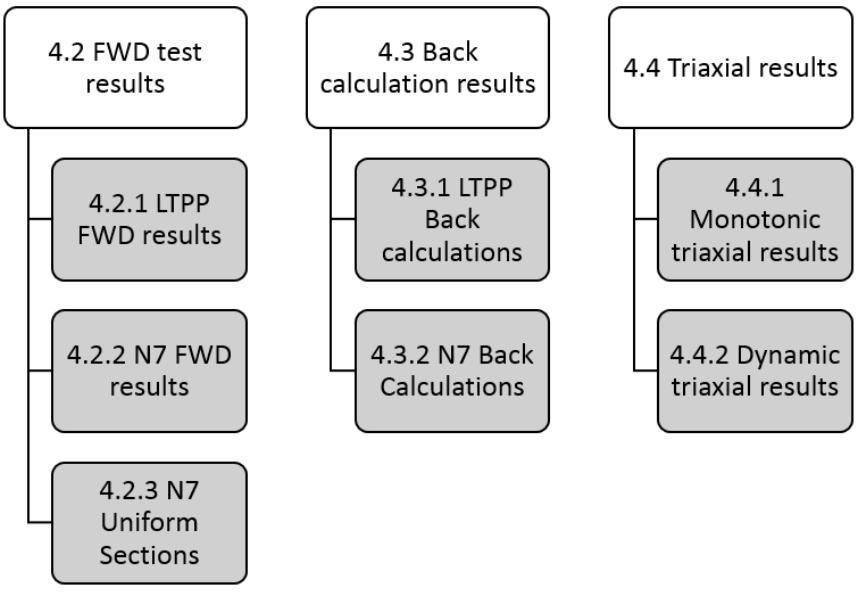

Figure 4.1: Chapter 4: Phase 1 layout

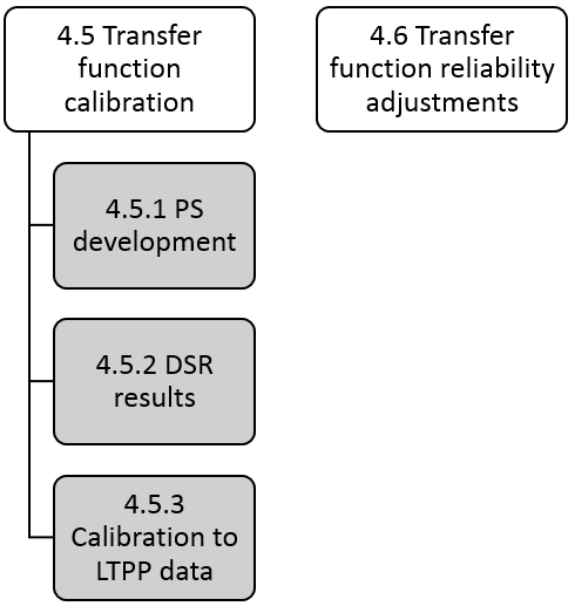

Figure 4.2: Chapter 4: Phase 2 layout

4.2 FWD test results

FWD tests were performed on a number of pavement structures which incorporated bitumen stabilised materials. FWD test results were gathered and analysed for the N7 highway as well as the LTPP pavements. These tests were performed at various stages of the design life of the pavements and in turn on the BSM. These test results provide valuable insight into the long-term performance of the materials. It is also a good indication of the condition of materials in the pavement structure at various points in time.

This section focuses on the analysis and interpretation of these FWD results. Important parameters obtained from the FWD tests, like BLI, MLI, LLI and maximum deflection, were investigated and used to divide the N7 into uniform sections. Focus was placed on the maximum deflection and the deflection at 300 mm as this provides an indication of the response of the base layer in the pavement structure. Back calculation of the FWD test results was performed to obtain material stiffnesses. These results are discussed in Section 4.3.

4.2.1 LTPP FWD results

FWD tests were performed on the LTPP pavements at various points in their design lives. The FWD data available for each of these 14 pavements is briefly summarized in Appendix B. The

information and test results were obtained from Long and Jooste (2007). The layer indices were calculated using the formulas stipulated in Section 3.3.

A large amount of FWD data was available for the LTPP pavements. This study uses only a portion of the available information for the calibration of a new transfer function for BSMs. The transfer function was initially calibrated to best fit the overall performance of BSMs. Therefore, averages were used as representative values to describe the response and characteristics of each of the LTPP pavements.

The data from each LTPP pavement was analysed to determine an average for d_{max}, BLI, MLI and LLI for each direction and year. Table 4.1 provides a summary of the maximum deflection and the three layer indices (BLI, MLI, LLI) obtained from FWD testing. Only the LTPP pavements with sufficient data available to obtain representative results are discussed in this section.

The average maximum deflection measurements for each pavement are shown graphically in Figure 4.3 and Figure 4.4. The average BLI for each of these pavements is shown in Figure 4.5 and Figure 4.6. The MLI and LLI are shown with the BLI and D_{max} for each of the LTPP pavements individually is shown in Figure F.1 to Figure F.10 in Appendix F.

Table 4.1 shows the average maximum deflection measurement and the average of each of the three layer indices for each of the LTPP pavements with sufficient deflection data. The averages were calculated per testing period, for example 1998 and 2002 for the MR 27. In the cases where the pavement implemented a BSM layer in two directions, averages were calculated separately for the two directions. This is shown for the MR 27 where the indices were calculated for the Northbound (NB) and Southbound (SB) carriageways at two points in time (1998 and 2002). The separation of direction was done as the traffic loads and volumes can vary for the two carriageways. The separation of data based on the time of testing was done as this allows for an indication of the change in the pavement's response and overall condition.

Figures 4.3 and 4.4 graphically represent the values for D_{max}, while Figures 4.5 and 4.6 show the values for the BLI. The red horizontal lines on these figures indicate the behaviour state ranges defined in SAPEM (2014) for granular base pavements. The overall pavement response was considered very stiff if the D_{max} values were below 300 μm, stiff between 300 μm and 500 μm, flexible between 500 and 750 μm and very flexible above 750 μm.

Figure 4.3 shows that the MR 27 and the N1-1 have a very stiff overall response. This can be

attributed to these pavements all incorporating a cement stabilised subbase. This stiff supporting layer reduces the deflection observed during FWD testing. The other pavements in this figure implement either granular or a BSM 2 subbase, therefore, a higher deflection measurement is expected. The N1-14 is described as very flexible when considering the maximum deflection. The LLI for this pavement is much higher when compared to the other pavements indicating a weak subgrade layer, explaining the high maximum deflections measured on this pavement.

Table 4.1: Summary of layer indices for the LTPP pavements

Road	Year	Direction	d_{max} (µm)	BLI (µm)	MLI (µm)	LLI (µm)
MR 27	1998	NB	308.0	170.7	78.5	26.0
MR 27	2002	NB	226.8	106.8	61.3	25.0
MR 27	1998	SB	270.0	138.2	72.0	28.2
MR 27	2002	SB	317.0	151.5	91.2	32.7
MR 504 (A)	1997	SB	404.1	194.5	101.2	43.5
MR 504 (B)	1997	SB	602.6	383.7	129.6	37.5
N1-1	1998	SB	299.7	117.4	79.7	43.7
N1-13	1999	SB	631.2	301.3	206.1	68.0
N1-13	2006	SB	653.7	330.2	202.7	68.0
N1-13	2006	NB	621.6	324.1	183.8	62.7
N1-14	1999	SB	815.5	417.1	256.1	83.4
N1-14	2006	SB	812.4	414.5	252.8	83.4
N2-16	2006	NB	323.9	146.2	89.2	41.1
N2-20	2001	WB	512.8	184.4	149.0	80.5
N2-20	2005	WB	338.6	102.5	94.1	55.0
N4-1	1999	WB	272.0	123.2	96.0	15.6
N4-1	2005	WB	291.5	132.1	74.1	31.8
N4-1	1999	EB	279.3	115.4	107.2	18.2
N4-1	2005	EB	326.1	146.7	90.2	35.9
N4-5X	2000	EB	348.2	178.3	86.6	28.7
N4-5X	2002	EB	317.6	150.5	74.9	33.1
N4-5X	2004	EB	318.9	160.0	80.3	28.2
N11-8	2005	NB	543.7	241.9	157.0	69.7

Figure 4.4 shows that the N2-16, N4-1 and N4-5X have an overall very stiff response. These pavements also implement cement stabilised subbase layers, supporting the low deflection measurements. The deflection measurements taken on the N2-20 in 2001 indicated a flexible layer, making use of a granular subbase layer. However, deflection measurements taken in 2005 showed a significant decrease in maximum deflection and in turn resilient modulus. This may be due to residual compaction or settlement of the subgrade, providing better support to the upper layers over time. This conclusion is supported by the significant reduction in the LLI observed for this pavement.

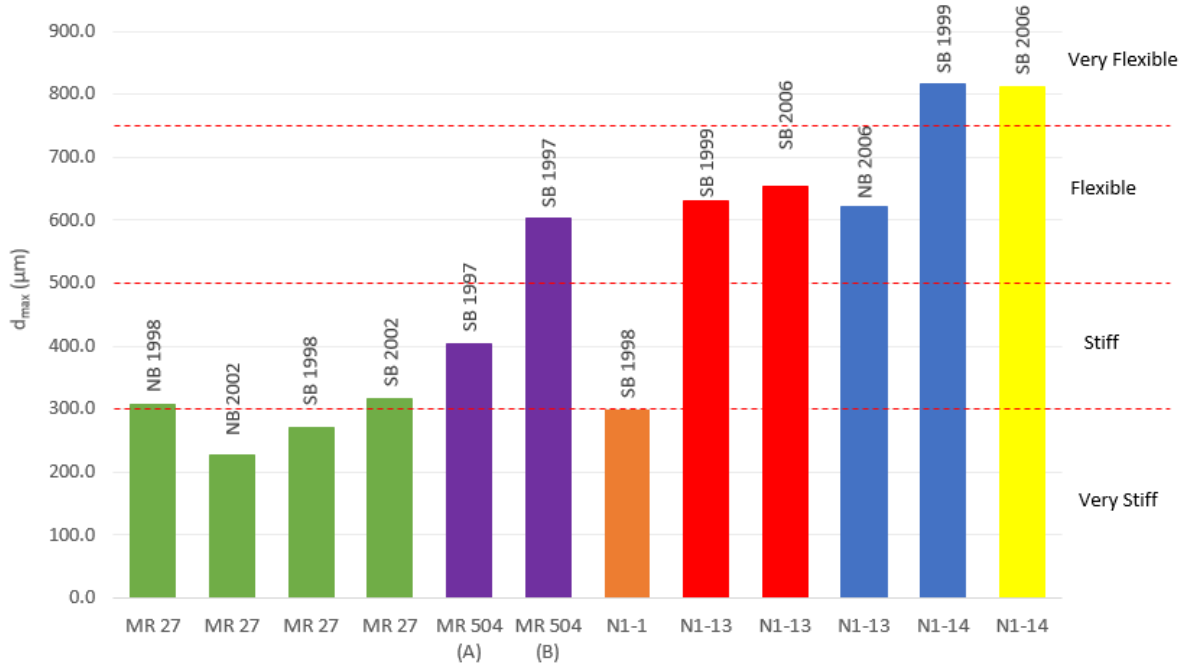

Figure 4.3: Average maximum deflection measurements for LTTP pavements

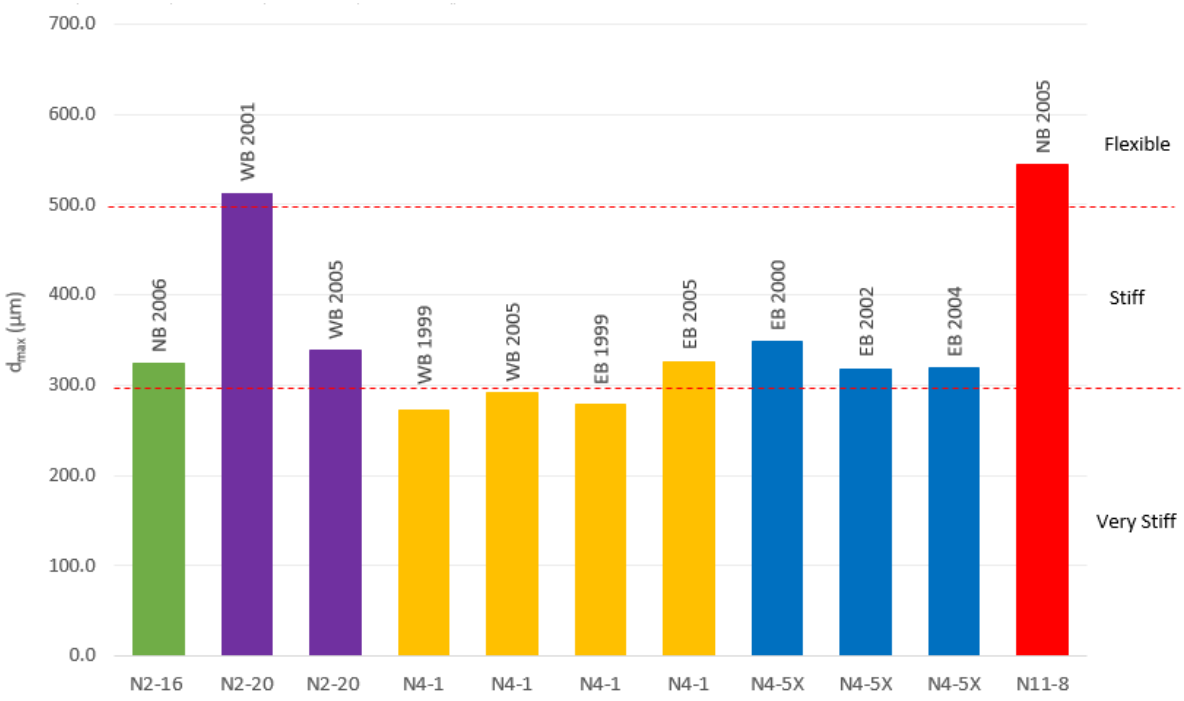

Figure 4.4: Average maximum deflection measurements for LTTP pavements (continued)

The pavement temperature and moisture conditions can have a significant effect on its response to loading. Therefore, the time of year the FWD tests were performed may have an influence on the the results. Limited information was available regarding the time of year and pavement temperature during FWD testing. Due to the limited information, the time of year and pavement

temperatures were not investigated in this study.

The response of the BSM base layer was considered very stiff when the BLI values were below 80 μm, stiff between 80 μm and 250 μm, flexible between 250 and 500 μm and very flexible above 500 μm. Figure 4.5 shows that the MR 27 and N1-1 have stiff to very stiff base layers. The stiff response may be due to the stiff support provided by the cemented subbase. However, care should be taken when analysing these results as the BLI describes the response of the top 300 mm of the pavement structure. The top 300 mm of these pavements include the surfacing and a part of the cemented subbase. The other pavements shown in these figures showed reasonable responses when considering the granular support layers in these pavements.

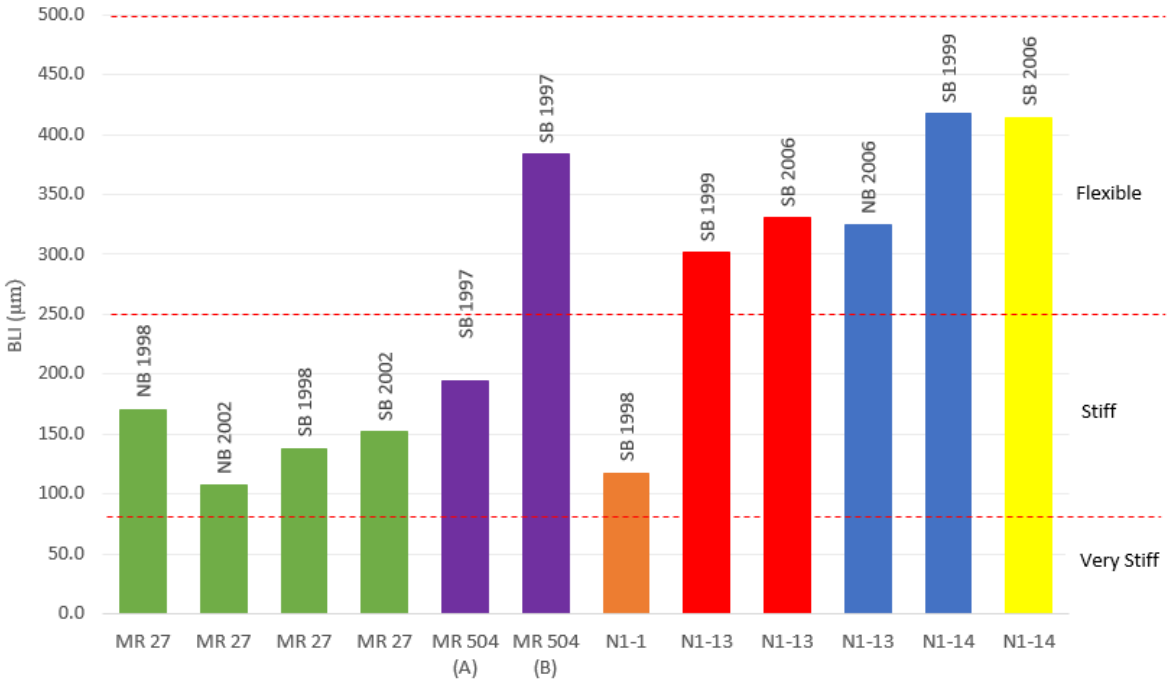

Figure 4.5: Average BLI for LTTP pavements

Figure 4.6 indicates that the base layers of the N2-16, N4-1 and N4-5X have a very stiff response. Similar to the MR 27 and N1-1, the response of the cement stabilised subbase and asphalt may influence the BLI. The BLI of the N2-20 shows the same resilient modulus increasing trend that was observed for the maximum deflection of this pavement.

The results obtained from the FWD testing of the LTPP pavements were considered reasonable and a realistic representation of the condition of these pavements. The FWD was further analysed through the process of back calculation, the results of which are discussed in Section 4.3.1.

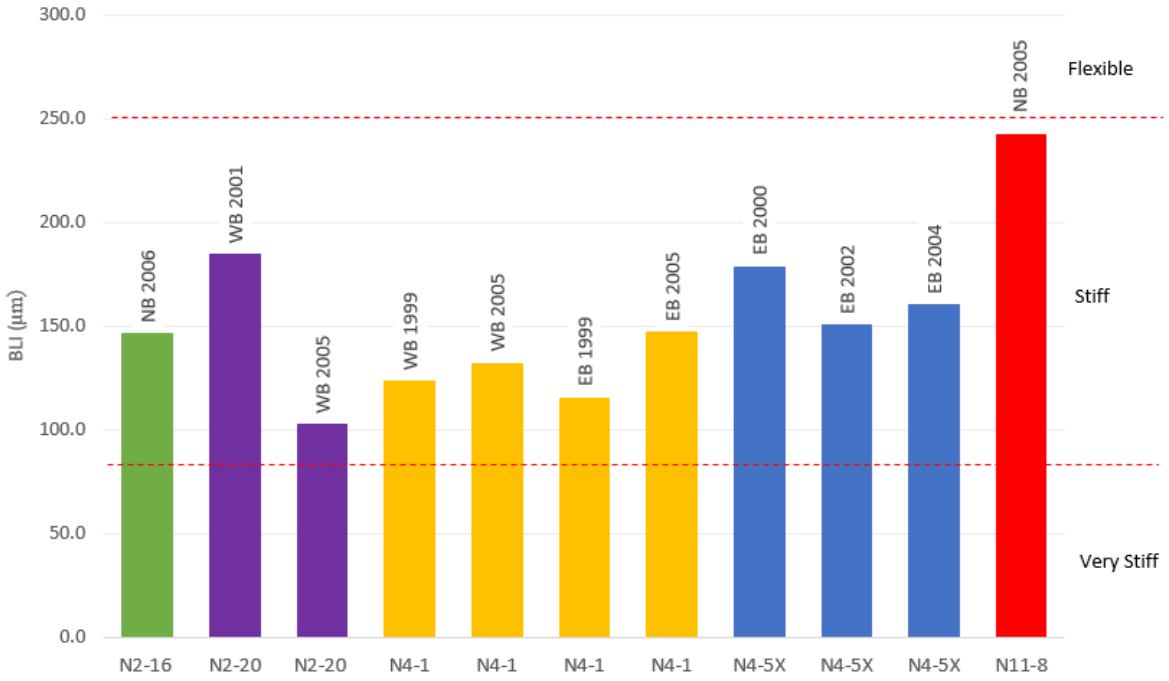

Figure 4.6: Average BLI for LTTP pavements (continued)

4.2.2 N7 FWD results

FWD tests were performed on the N7 Highway near Cape Town in 1994, 2000, 2004, 2010 and 2016. The test were performed on the BSM slow lanes at 200 m intervals. The layout of the sections incorporating BSMs is discussed in Section 3.3. Two construction phases were identified for this section of the N7. The first phase was constructed in 2002 and included a foam stabilised BSM layer, while the second was constructed in 2007 with a bitumen emulsion stabilised base layer.

The FWD test results for all of the above mentioned test years can be found on the attached CD. From the first analysis three distinct sections were identified (as illustrated on page 64:

1. Southbound, BSM foam from km 5.8 to km 18.0, constructed in 2002.
2. Northbound, BSM foam from km 5.8 to km 11.6, constructed in 2002.
3. Northbound, BSM emulsion from km 11.6 to km 18.0, constructed in 2007.

4.2.2.1 Evaluation of d_{max}

The maximum deflection (dmax) and the three layer indices (BLI, MLI and LLI) were obtained for each point of testing. Due to the large number of data points in the sets, the data was processed to obtain representative values at specific levels of reliability. The reliability levels were chosen as 10%, 25%, 50%, 75% and 90%.

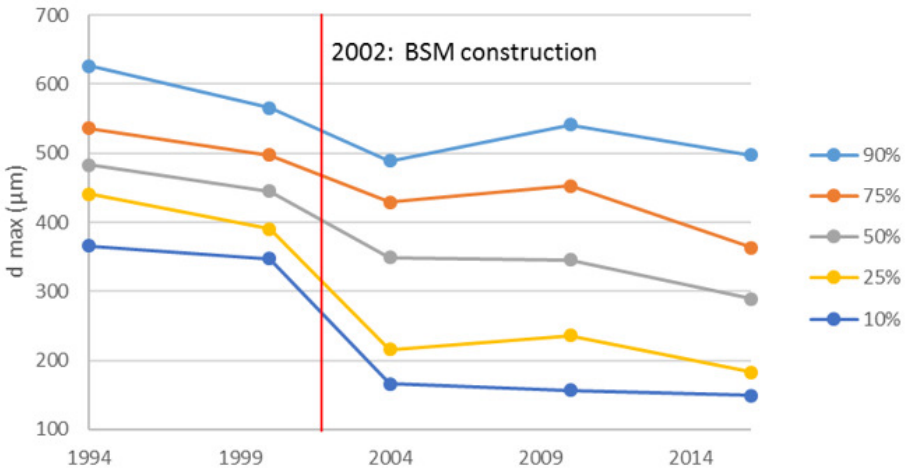

Figure 4.7: Maximum deflection development for different levels of reliability for the N7 Southbound foam section

Figure 4.8: Maximum deflection development for different levels of reliability for the N7 Northbound foam section

The maximum deflection development over the BSM's years of service is presented for the Southbound section in Figure 4.7, for the Northbound foam section in Figure 4.8 and for the Northbound emulsion section in Figure 4.9. Higher deflection values in these graphs indicate weaker pavement structures. The 90% values are therefore representative of the weakest pavement structures, while the 10% values represent the structures with the strongest pavement structures.

The date of rehabilitation is indicated by a red line on each of the three figures. It can be observed from these figures that the maximum deflection of the foam stabilised sections decreased significantly after construction in 2002. The reduction in maximum deflection is a good indication

of the overall condition of the road. Therefore, the structural condition of the road was improved after construction of the BSM base layer.

Figure 4.7 shows that the maximum deflection after construction gradually decreased from measurements taken in 2004 to 2016. This may be due to residual compaction of the pavement layers caused by long-term exposure to traffic. Figure 4.8 shows a sharp increase in maximum deflection between 2004 and 2010, indicating a reduction in the overall pavement condition. The deflections values declined between 2010 to 2016 indicating a stable layer with consolidation occurring.

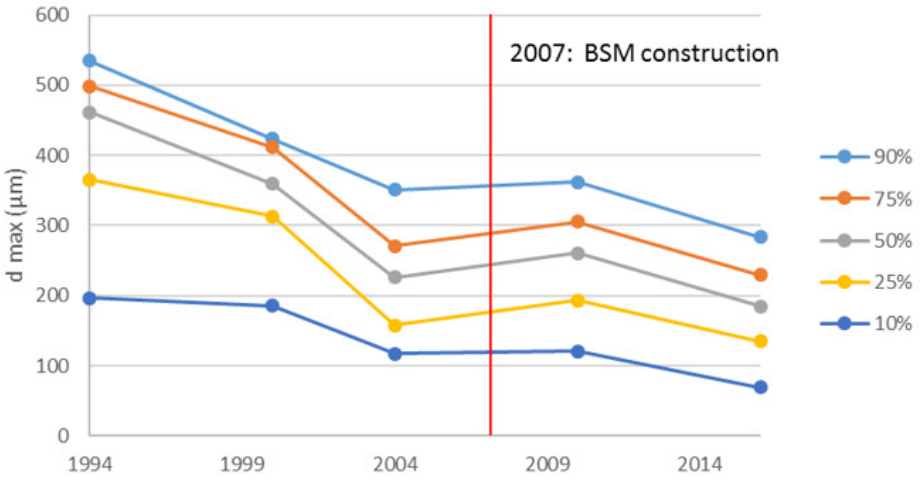

Figure 4.9: Maximum deflection development for different levels of reliability for the N7 Northbound emulsion section

The maximum deflections on the emulsion section before and after construction (in 2007) do not show such a significant difference. The overall deflections remain similar to that of the pavement structure in 2004. However, the deflections measured in 2016 were considerably lower than those measured in 2010. This may indicate that the base layer gained resilient modulus over time, which may be a result of the curing process. It also indicates that residual compaction has occurred due to exposure to traffic.

4.2.2.2 Layer indices

Using the same methods as in the previous section, the development of the base layer index over time, at different levels of reliability, was analysed for the three identified sections. The BLI development for the Southbound foam section is shown in Figure 4.10, for the Northbound foam section in Figure 4.11, and for the Northbound emulsion section in Figure 4.12. The BLI gives an indication of the condition of the base layer, in this case the BSM layer. The results for the MLI

and LLI give an indication of the condition of the subbase and subgrade of the pavement structure. The results for the MLI and LLI for these pavement structures are shown in Figure D.1 and Figure D.6 in Appendix D.

The BLI of the Southbound foam section, shown in Figure 4.10, shows a reduction in BLI between 1994 and 2000. This was before rehabilitation and indicates that the deflection in this layer reduced over a period of time. This may be due to consolidation of the base layer over time. A large reduction in BLI can be observed between 2000 and 2004. This indicates that the quality of the base layer was significantly improved by rehabilitation. A gradual decrease in BLI followed after construction of the base layer due to consolidation of the layer.

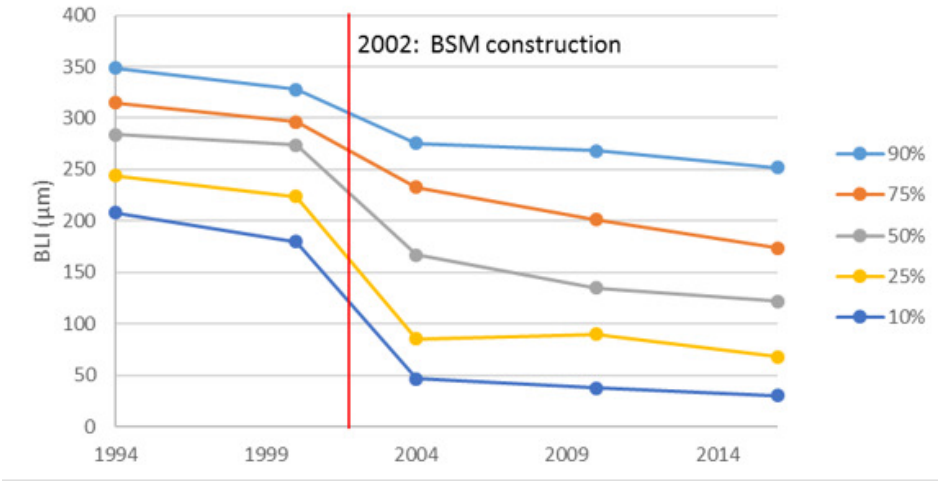

Figure 4.10: BLI development for different levels of reliability for the N7 Southbound foam section

The BLI of the foamed BSM on the Northbound section, shown in Figure 4.11, can be compared directly to that of the Southbound foam as they were constructed at the same time with the same structure. The same reduction in BLI before rehabilitation was found for the Northbound foamed section, indicating consolidation of the base layer over time.

The magnitude of the BLI was comparable to that of the Southbound section, but showed less variability in 2000. A clear reduction in BLI was observed after construction, indicating a significant increase in the condition of the layer. The BLI results for this section were smaller and showed less variability than the Southbound foam section in 2004 and 2010. However, the BLI gradually increased and by 2016 was comparable in magnitude and variability to the Southbound section.

The FWD measurements from 2004 to 2010 were taken in the 10th month of the year. This would

typically indicate moderate temperatures as October falls in Spring. The measurements taken in 2016 were taken during the winter. This may explain the decreased deflection measurements as in lower temperatures, the pavement would have a stiffer response.

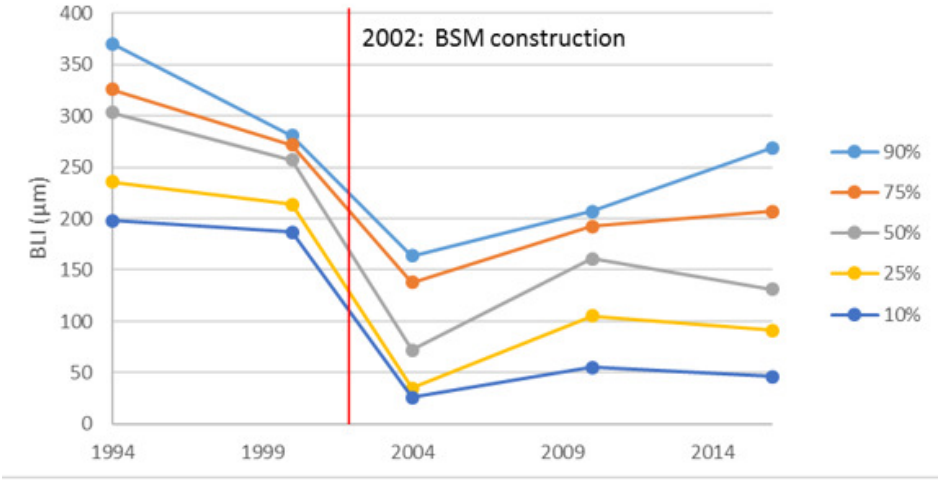

Figure 4.11: BLI development for different levels of reliability for the N7 Northbound foam section

The BLI analysis for the Northbound emulsion section, Figure 4.12, also shows a decrease of BLI up to the time of rehabilitation. A significant decrease can be observed from 1999 to 2004. After rehabilitation i.e. implementing BSM emulsion in 2007, the BLI results were slightly higher than before. This may be due to the breaking up of the old base layer and the re-compaction thereof.

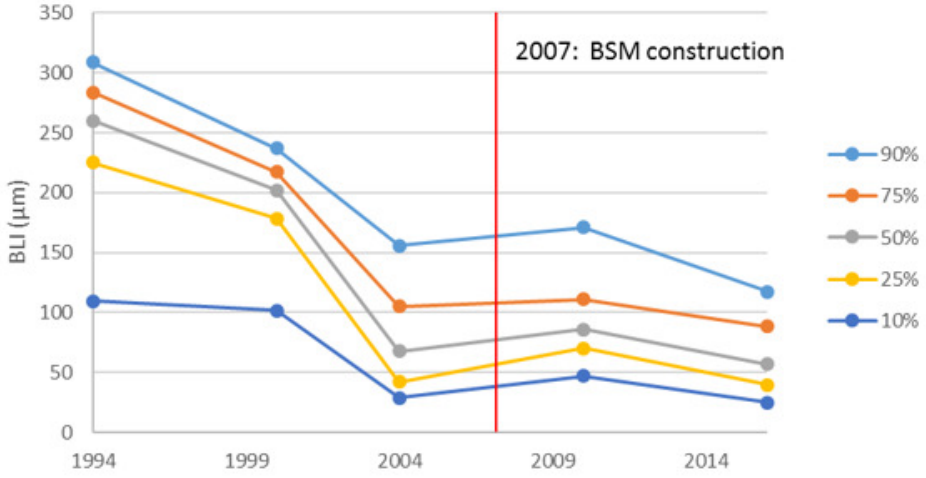

Figure 4.12: BLI development for different levels of reliability for the N7 Northbound Emulsion section

The compaction levels achieved during rehabilitation could be less than those of the old base layer, as it had been exposed to traffic for a significant period of time. The BLI increased after rehabilitation of the base layer and increased after 2010, indicating settlement and curing of the BSM. The low values of the BLI results of this section indicate a stiff material. This section also shows low levels of variability compared to the two foam sections.

The results obtained from the BLI analysis of these three pavement structure provide a good understanding of the overall condition of the base layer. The MLI and LLI of each of these sections can be analysed to gain a better understanding of the overall condition of the pavement. To better define the base layer, back calculations were done on the FWD results as discussed in Section 4.3. The maximum deflection results in 2016 were used to divide the road into uniform sections as discussed in Section 4.2.3.

4.2.3 N7 Uniform sections based on FWD results

FWD results obtained from the N7 highway were used to divide the road into uniform sections. The cumulative sum method was used as described in Section 3.4.3. The most recent FWD results, taken in 2016, were used to determine the uniform sections. Only the maximum deflection measurements and the base layer index were used during the division into uniform sections.

Figure 4.13 shows the results of the cumulative sum method for the N7 Southbound carriageway. The figure shows a similar trend for both the maximum deflection and the BLI. This is an indication that the overall pavement performance is extensively reliant on the condition of the base layer. The lines in this figure indicate a high level of variability even within some uniform sections, which may be a result of the age of the pavement.

The Southbound carriageway was divided into eight uniform sections based on the maximum deflection measurements and the BLI. The red lines in Figure 4.13 indicate the uniform sections identified for this study. These uniform sections still show a large amount of variation, but was significantly less than the section as a whole. Table 4.2 summarizes the uniform section locations, the length of these sections and an overall condition of these sections.

Figure 4.15 illustrates the maximum deflections for the uniform sections over the length of the road. The figure shows the average, 90th percentile and 10th percentile maximum deflection for each uniform section individually. The 90th percentile represents the weakest pavements with the lowest resilient modulus, while the 10th percentile represents the pavements with the highest resilient modulus values. The difference between the 90th and 10th percentile values gives an

indication of the variance in each of the sections. Note that uniform sections 3 to 5 are relatively short sections, indicating that they represent local situations.

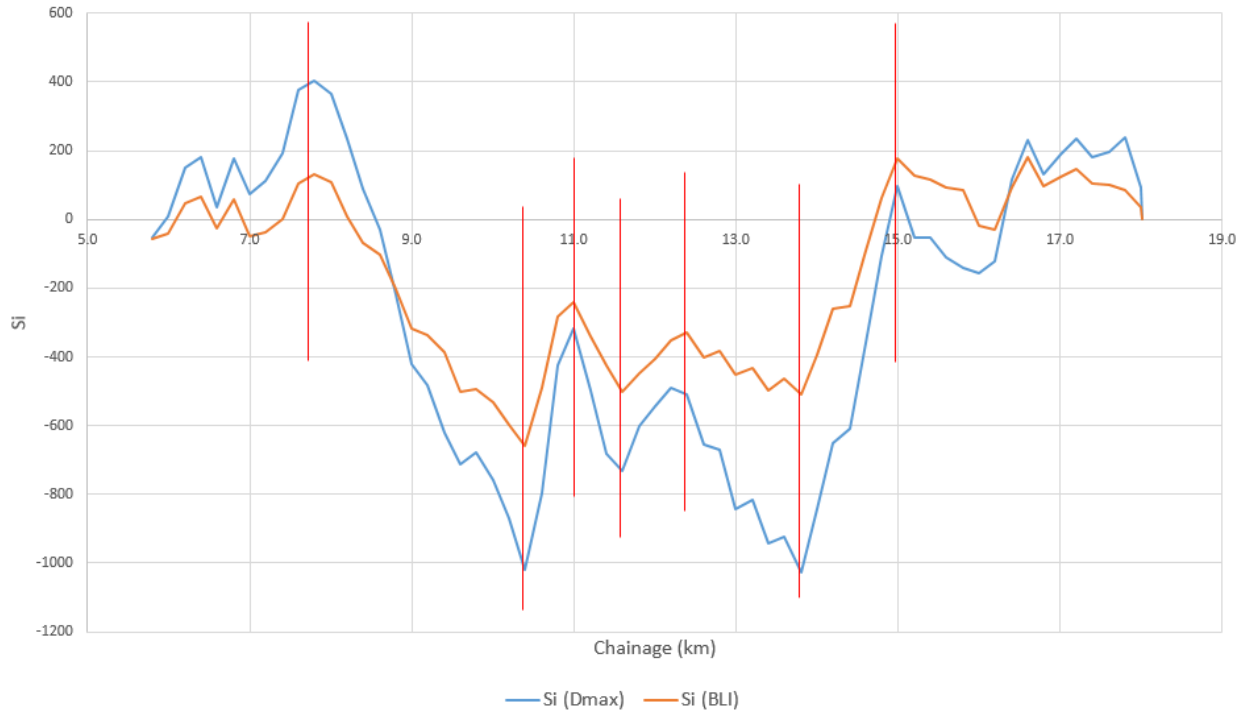

Figure 4.13: N7 Southbound cumulative sum for uniform sections

Table 4.2: N7 uniform sections

Section	Start Chainage (km)	End Chainage (km)	Length (m)	Relative condition
Northbound				
1	5.8	11.2	5400	Poor
2	11.2	13.6	2400	Fair
3	13.6	18.0	4400	Fair
Southbound				
1	5.8	7.6	1800	Poor
2	7.6	10.4	2800	Poor
3	10.4	11.0	600	Poor
4	11.0	11.6	600	Good
5	11.6	12.4	800	Fair
6	12.4	13.8	1400	Fair
7	13.8	15.0	1200	Poor
8	15.0	18.0	3000	Fair

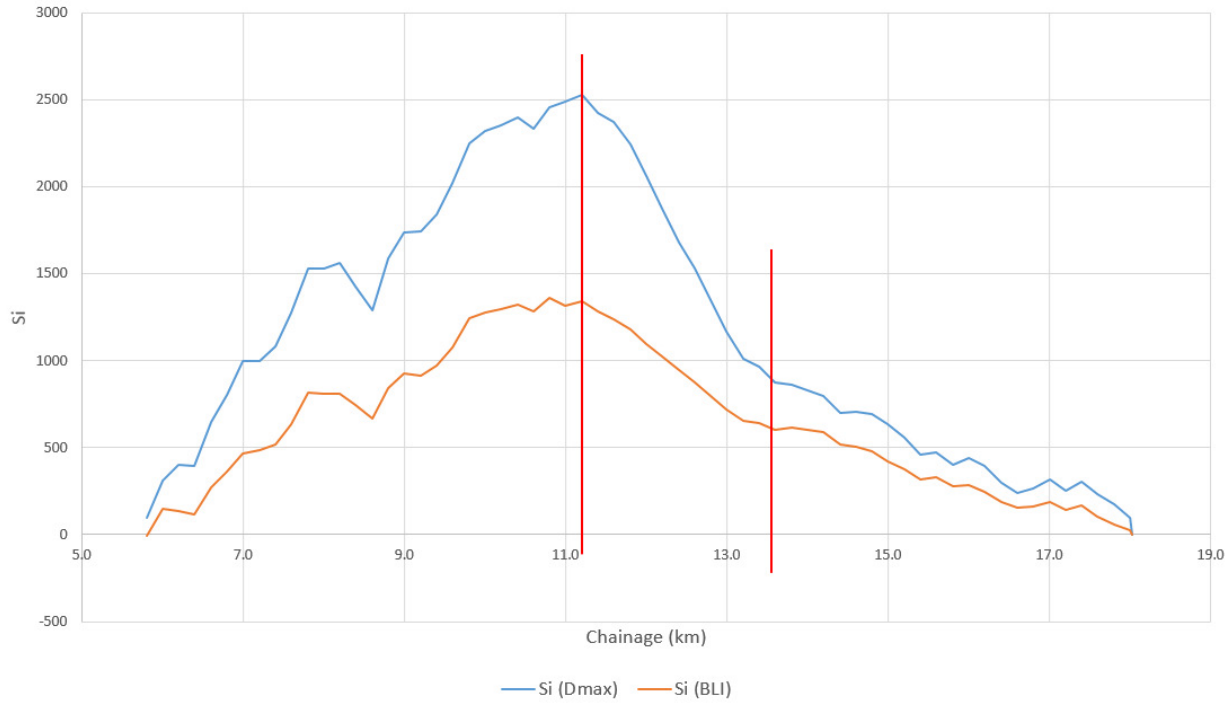

Figure 4.14: N7 Nouthbound cumulative sum for uniform sections

Figure D.8 in Appendix D illustrates the BLI for the Southbound carriageway of the N7 over the length of the road. This figure shows the 90th percentile, average and 10th percentile BLI for each of the uniform sections. The trends and magnitude of the BLI reflect the trends observed for the maximum deflection measurements. Therefore, uniform sections based on the maximum deflection would be similar to those based on the BLI.

By investigating the maximum deflection measurements and the BLI for the Southbound carriageway, an indication of the pavement performance and condition can be obtained. The 10th percentile of the uniform sections identified on the Southbound carriageway show a stiff to very stiff response.. Only in uniform sections 3 and 7 can the 90th percentile deflection measurement be classified as flexible. The difference between the 90th percentile and 10th percentile values also reflects the variance in a uniform section. Uniform sections 4, 5 and 6 show little variance, but this is due to the relatively small size of the section.

Similar to the Southbound carriageway, the Northbound carriageway was divided into uniform sections by using the cumulative sum method. Figure 4.14 shows the cumulative sum plot of the BLI and D_{max} for the Northbound carriageway of the N7. The Northbound section was analysed as one section to be divided into uniform sections. The Northbound carriageway was divided into

three uniform sections, which showed much less variance than the Southbound carriageway.

The first section division was at the end of the foam section and the start of the emulsion section. This transition occurs between km 11.2 and 11.4. From Figure 4.14 it is clear that there is a significant difference in the response between km 11.2 and km 13.6. The second division was at km 13.6 in the emulsion section. The older foam section on the Northbound carriageway showed more variance than the emulsion sections and did not provide a smooth cumulative sum plot. The emulsion section (from km 11.6 to km 18.0) was divided into two distinct uniform sections.

Figure 4.16 shows the maximum deflection measurements for each uniform section identified on the N7 Northbound carriageway. The figure illustrates the 10th percentile, average and 90th percentile maximum deflection values. In the first uniform section, the deflection measurements suggest that the pavement has a very stiff response. The other two sections, which were both emulsion treated and constructed five years later, show very stiff behaviour. Almost all of the data obtained from the emulsion section shows very stiff behaviour.

The BLI of the N7 Northbound carriageway was investigated per uniform section as illustrated in Figure D.7 in Appendix D. When comparing the maximum deflection of the two emulsion sections with their corresponding BLI, similar performance can be observed. The BLI values from these two sections indicate stiff to very stiff base layers. The BLI from the foam section shows a much less stiff base layer and also a much wider range of values.

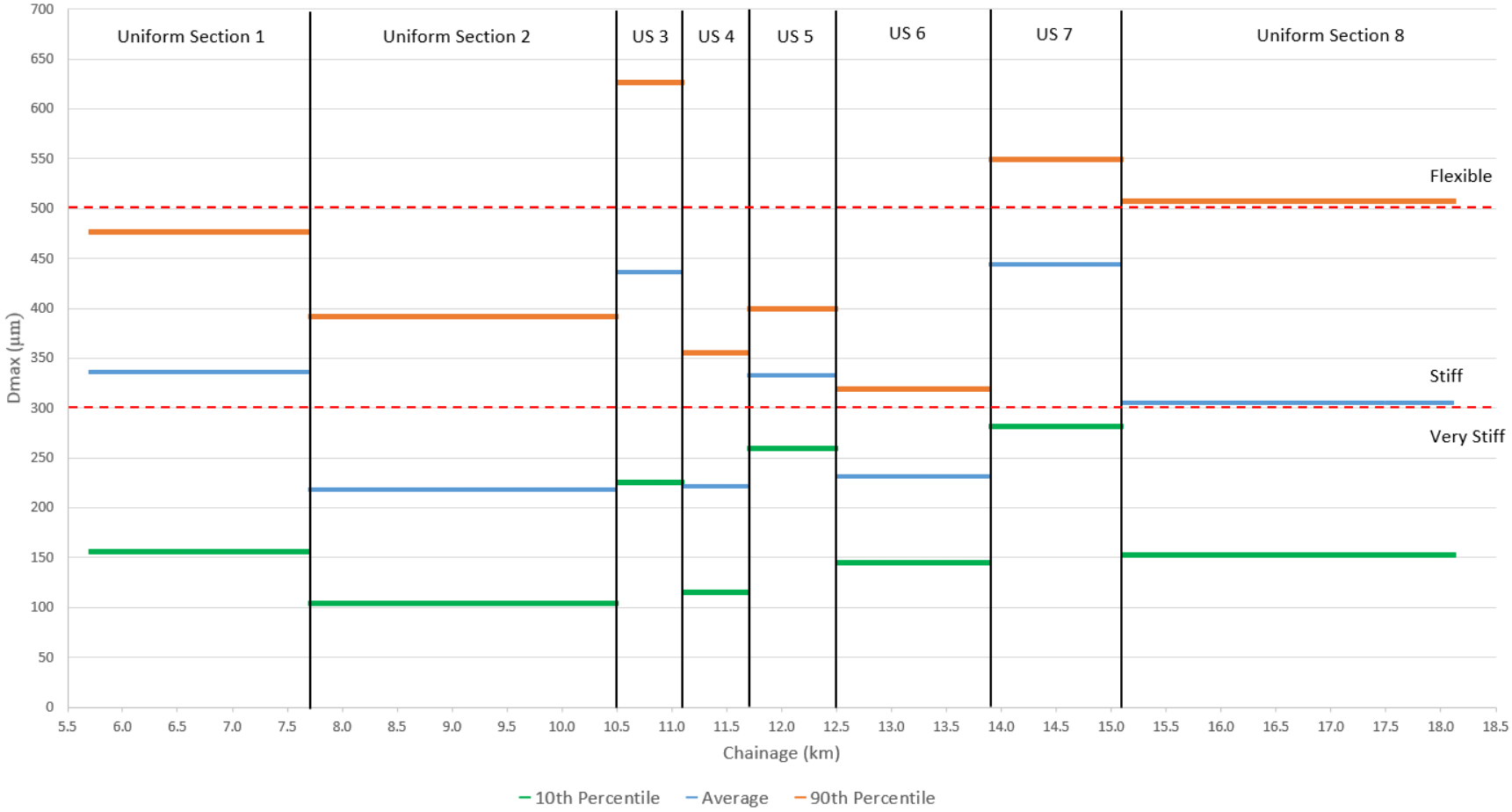

Figure 4.15: N7 Southbound maximum deflections per uniform section

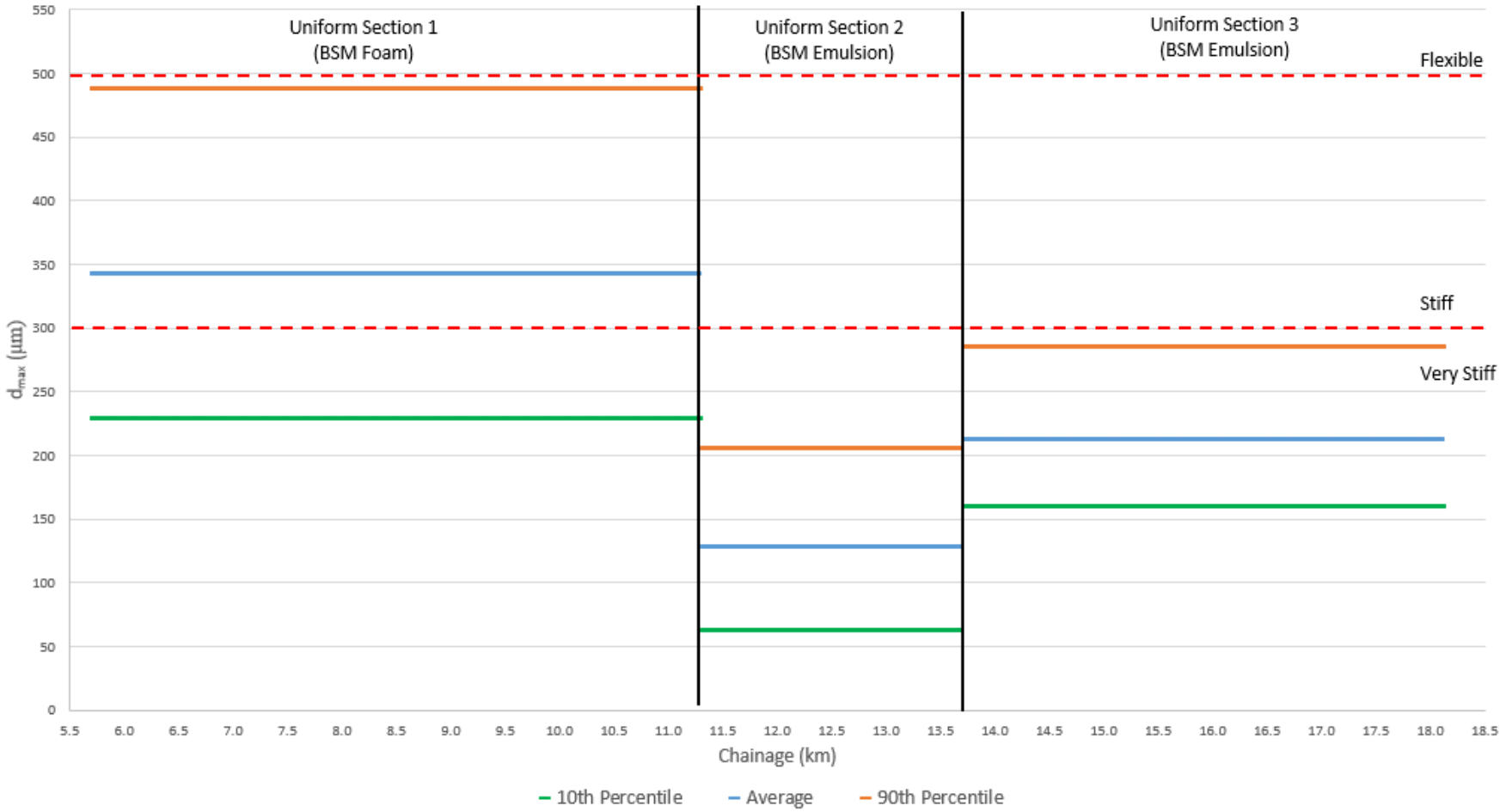

Figure 4.16: N7 Northbound maximum deflections per uniform section

4.3 Back calculation results

The FWD results obtained for the N7 highway and the LTPP pavements were analysed using the methods described in Section 3.3. The results of these analyses were discussed in Section 4.2. The analyses provided an indication of the overall condition and response of these pavements. However, further analysis was required to determine the resilient modulus response, specifically of the BSM layers. Back calculation was performed on all the available deflection data gathered for the N7 and the LTPP pavements. The process of back calculation relates the deflection response of the pavement to the resilient modulus of the individual layers. The process used during the back calculation of the N7 and LTPP deflection data is discussed in Section 3.4.

The back calculation results for the N7 and for the LTPP pavements are discussed in Section 4.3.2 and Section 4.3.1 respectively. A significant amount of deflection bowls were analysed and layer stiffness back calculation as part of this study. Therefore, only examples and summaries are provided in this report. All the deflection bowl analyses performed during this study can be found on the CD submitted as part of this report.

4.3.1 LTTP back calculation results

Data obtained from FWD tests on the LTPP pavement structures was back calculated in order to obtain resilient modulus values for the different layers in each of these pavement structures. The resilient modulus values obtained from the back calculation were used as input to determine the deviator stress ratio in the BSM layers when subjected to loading, the results of which are discussed in Section 4.5.2. The method of back calculation used for the LTPP pavements is discussed in Section 3.4.1.

The process of back calculation has four requirements: deflection measurements, weight and dimensions of the loading plate, layer thicknesses and the Poisson's ratio. This information was gathered for each of the LTPP pavements in order to perform the calculations. The layer thicknesses used for back calculation of layer stiffnesses are shown in Table 3.1 and 3.2. The deflection measurements and pressure applied by the falling load can be found on the attached CD. The Poisson's ratio was set to 0.35 for all materials.

The resilient modulus was back calculated for all the available FWD data obtained for each of the LTPP pavements. Due to the large amount of data analysed, only a summary of the results are shown in this report. Once all the back calculations were done, the average resilient modulus for each layer was determined. The average resilient modulus of each layer for each pavement

was selected as the representative value. The LTPP pavements were analysed in both directions separately where possible.

A full account of each of the deflection bowls can be found on the CD submitted as part of this research. Table 4.3 provides a summary of the average back calculated resilient modulus results for each layer of each of the LTPP pavement structures. The grey squares in this table indicate that a four layer pavement structure was used for back calculation.

Table 4.3: Summary of back calculated layer stiffnesses for the LTPP pavements

			Back calculated stiffness (MPa)				
Road	Year	Direction	Layer 1	Layer 2	Layer 3	Layer 4	Layer 5
MR 27	1998	NB	2750	794	359	291	327
MR 27	2002	NB	3000	950	408	379	352
MR 27	1998	SB	3000	700	314	315	365
MR 27	2002	SB	3000	597	283	261	303
MR 504 (A)	1997	SB	1781	665	268	193	
MR 504 (B)	1997	SB	830	431	202	246	
N1 - 1	1998	SB	2636	768	420	241	184
N1 - 13	1999	SB	1219	445	292	117	114
N1 - 13	2006	SB	844	357	257	96	179
N1 - 13	2006	NB	712	451	318	81	282
N1 - 14	1999	SB	966	345	108	56	199
N1 - 14	2006	SB	1059	356	119	58	214
N2 - 16	2006	NB	3161	800	864	430	506
N2 - 20	2001	WB	2724	768	160	83	167
N2 - 20	2005	WB	4072	895	231	117	172
N4 - 1	1999	WB	3833	940	591	293	552
N4 - 1	2005	WB	2677	905	742	186	288
N4 - 1	1999	EB	3186	833	711	209	455
N4 - 1	2005	EB	2504	770	654	144	260
N4 - 5X	2000	EB	1893	690	533	193	241
N4 -5X	2002	EB	2387	807	623	224	218
N4 -5X	2004	EB	2136	752	587	172	265
N11 - 8	2005	NB	1768	413	134	169	

Note that the N12-19(3), N12-19(4) and P243-1 are not included in Table 4.3. Deflection measurements were taken on the N12-19(3) in 2001 and 2005, but only at one location. It was therefore not deemed applicable to take one value as the average of the section. The deflection bowls for these two measurements are given in Figure G.1 for 2001 and G.2 for 2005 in Appendix G. Similarly, FWD data for the N12-19(4) was only available for two points in the BSM section. The deflection bowls for these three measurements are given in Figure G.3 and G.4 for 2001 and in Figure G.5 for 2005 in Appendix G. No FWD data for the P243-1 was available for this study,

therefore, the resilient modulus of these layers were based on other layer stiffnesses with similar material classifications. The layer stiffnesses used for further analysis as well as the DSR analysis results for all the LTPP pavements are given in Table I.2 to I.4 in Appendix I.

Figure 4.17 and Figure 4.18 graphically illustrate the resilient modulus values of the BSM base layers obtained from the resilient modulus back calculations. The red lines in these figures indicate the maximum allowed resilient modulus for BSM 1 and BSM 2 layers according to the PN design method described in the TG2 (2009). This design method is known to be conservative, therefore it is expected that the back calculated stiffnesses would exceed these limits. In addition, it should be noted that the PN design method developed purpose-derived Mr values for its system, which is not necessarily directly comparable with the Mechanistic Empirical design method.

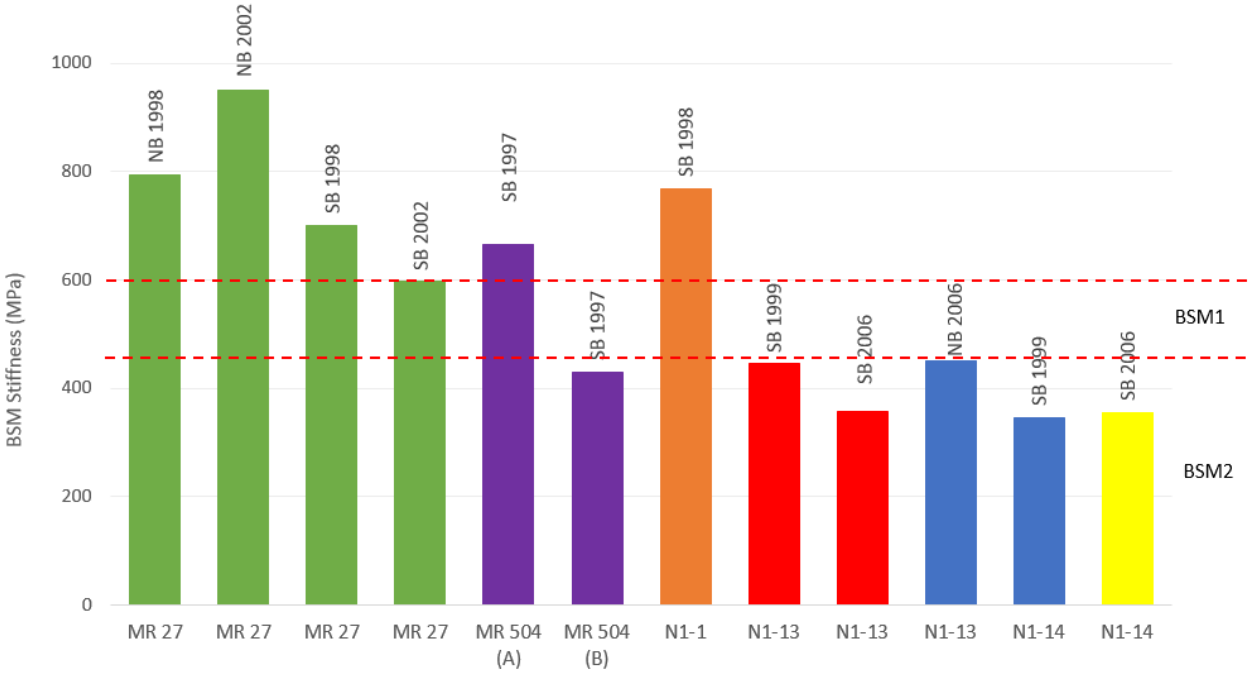

Figure 4.17: LTPP average back calculated stiffnesses for BSM base layers (1)

Figure 4.17 and Figure 4.18 shows that the resilient modulus of the BSM layer of the MR 27, MR 504 (A) and N1-1 are well above the maximum described by the TG2. The MR27 and N1-1 make use of a cement stabilised base layer and both have asphalt layers greater than 50 mm. The BSMs in these two pavements are also classified as BSM 1's, therefore, the high resilient modulus was deemed representative of the in field conditions. The stiffnesses calculated for the MR 504 (A) are significantly higher than those fore the MR 504 (B). This is supported by the BSM classes: the MR 504 (A) implements a BSM 1 base, while the MR 504 (B) uses a BSM 2 base.

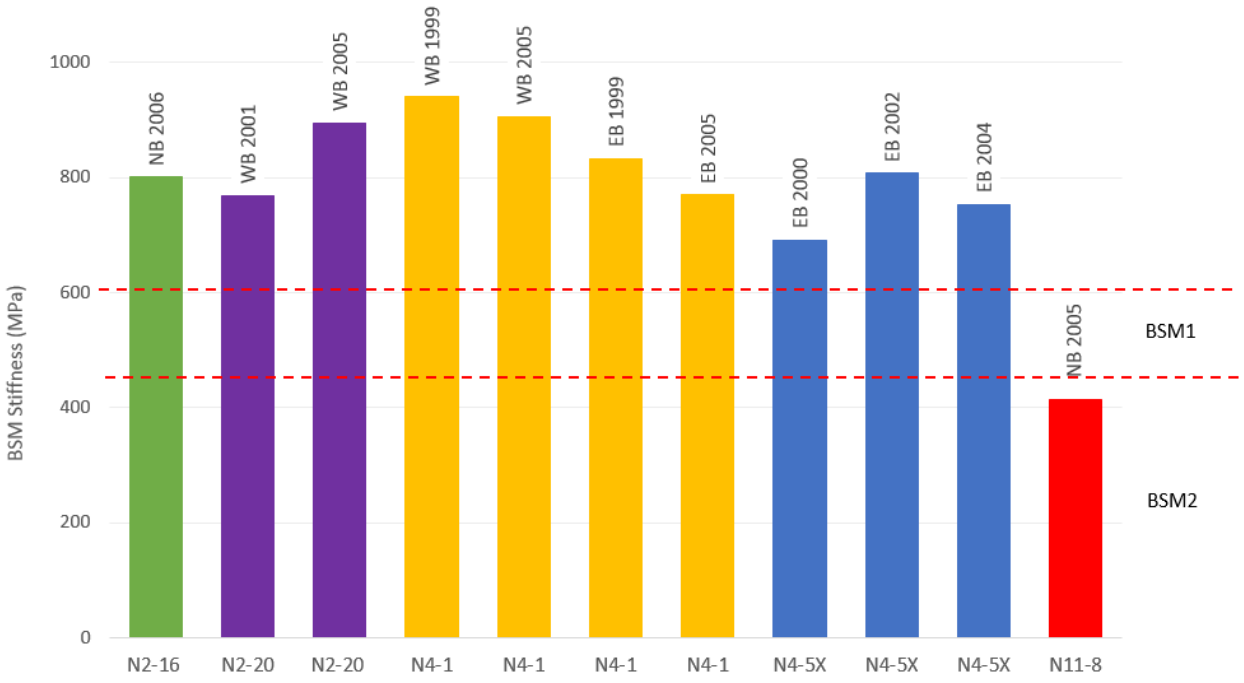

Figure 4.18: LTPP average back calculated stiffnesses for BSM base layers (2)

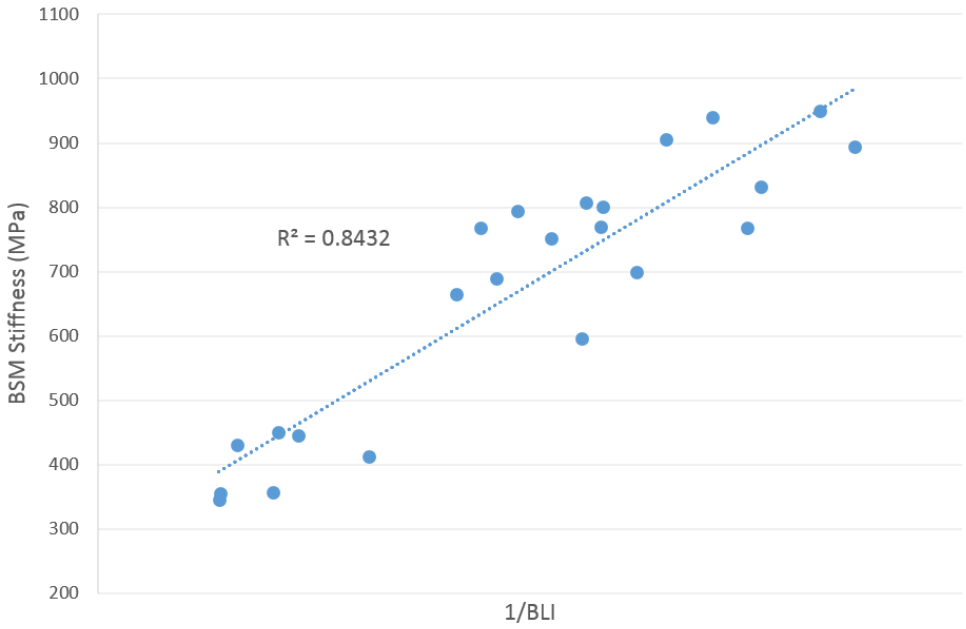

Figure 4.19: BSM resilient modulus and BLI correlation for LTPP pavements

The N1-13 showed low resilient modulus values supported by the material classification specifying the base layer as a BSM 2. The N1-14 implements a BSM 1 base with a G4 subbase, however, this pavement showed a low resilient modulus compared to the other BSM 1 results. The resilient modulus of this layer correlates well with the high value for the BLI in Figure 4.5 and D_{max} in Figure 4.3. Therefore, the low resilient modulus was deemed a result of weak support from the deeper layers.

The BSM layer stiffnesses showed in Figure 4.18 indicate that the first four of these pavements have average resilient modulus values between 600 MPa and 1000 MPa. When compared to the BLI for these pavements, in Figure 4.6, a similar situation can be observed. The BLI of these pavements show that the top section of the pavements had a stiff to very stiff response to loading. The N11-8 showed a low resilient modulus value expected for a BSM 2. This value correlates well with the BLI value obtained for the same pavement.

Figure 4.19 shows the correlation between the BLI and the back calculated stiffnesses for the LTTP pavements. The inverse of BLI was used, rather than BLI itself, for visual effect. This graph gives an indication that the back calculation data represents the measured deflection data obtained from FWD testing. As the deflection in the base decreases (1/BLI increases) the layer stiffness should increase. The correlation coefficient ($R^2 = 0.8432$) indicates that the back calculated resilient modulus values fairly represent the measured deflections and in turn the in field conditions.

4.3.2 N7 back calculation results

The N7 FWD results were used to back calculate stiffness values for the different layers in the pavement structure. The method specified in Section 3.4.2 was used during the back calculation of the N7 FWD results. These stiffness values were analysed and used to determine the stress conditions induced by loading as discussed in Section 5.1. This section discusses the results obtained from back calculating layer stiffnesses and focuses on the BSM resilient modulus development over time.

FWD test results for the N7 were available for 1994, 2000 2004 2010 and 2016. The available information for each of these points in time included the location of the test, surface temperature, air temperature, month of testing, FWD load and deflection measurements. The FWD load and pressure induced was not measured for each blow, but the load was given as 40 kN. The layer thicknesses used during back calculation of the N7 FWD results were based on observations from test pits and trenches dug on the slow lanes and are shown in Tables O.1 and O.2. The Poisson's

ratio for granular materials and BSMs was chosen as 0.35.

Each of the FWD results were analysed and layer stiffnesses were back calculated. Due to the large amount of data obtained from the back calculation, the data was summarized for this report. The results of the back calculation for each point at each of the points in time can be found on the attached CD. The average back calculated layer stiffnesses, obtained from the 2016 FWD results, for each of the uniform sections, are shown in Tables 4.4 to 4.7.

Table 4.4: Summary of back calculated layer stiffnesses for the N7 Southbound uniform sections in 2004

			Back calculated stiffness (MPa)				
Road	Year	Direction	Layer 1	Layer 2	Layer 3	Layer 4	Layer 5
US 1	2004	SB	2258	1107	490	96	270
US 2	2004	SB	3831	1316	552	128	344
US 3	2004	SB	3959	1429	313	114	250
US 4	2004	SB	2017	1243	400	92	366
US 5	2004	SB	1753	946	500	242	612
US 6	2004	SB	1248	611	481	196	471
US7	2004	SB	829	480	179	199	278
US 8	2004	SB	767	360	366	159	264

Table 4.5: Summary of back calculated layer stiffnesses for the N7 Southbound uniform sections in 2010

			Back calculated stiffness (MPa)				
Road	Year	Direction	Layer 1	Layer 2	Layer 3	Layer 4	Layer 5
US 1	2010	SB	2328	786	492	129	304
US 2	2010	SB	3724	1195	657	139	527
US 3	2010	SB	1431	575	338	105	514
US 4	2010	SB	2894	1000	413	110	260
US 5	2010	SB	1500	724	420	62	298
US 6	2010	SB	1626	756	378	65	494
US7	2010	SB	1374	557	157	117	278
US 8	2010	SB	1389	641	320	98	299

The back calculation results for the foamed BSM sections of the N7 were available for 2004, 2010 and 2016. Table 4.4 shows the back calculated layer stiffness for each of the uniform sections on the Southbound carriageway in 2004. Table 4.5 shows the stiffnesses for 2010 and Table 4.6 for 2016. Note that in some cases the resilient modulus of the subgrade (layer 5) is much higher than for a typical subgrade. This was a result of the focus placed on the base deflection bowl at depths between 0 and 300 mm.

Table 4.6: Summary of back calculated layer stiffnesses for the N7 Southbound uniform sections in 2016

			Back calculated stiffness (MPa)				
Road	Year	Direction	Layer 1	Layer 2	Layer 3	Layer 4	Layer 5
US 1	2016	SB	2317	820	254	157	297
US 2	2016	SB	3063	1387	462	222	477
US 3	2016	SB	1522	694	264	139	540
US 4	2016	SB	4172	1345	418	199	355
US 5	2016	SB	1838	664	200	167	270
US 6	2016	SB	2119	1095	280	237	610
US7	2016	SB	1413	526	164	121	364
US 8	2016	SB	1790	768	279	181	292

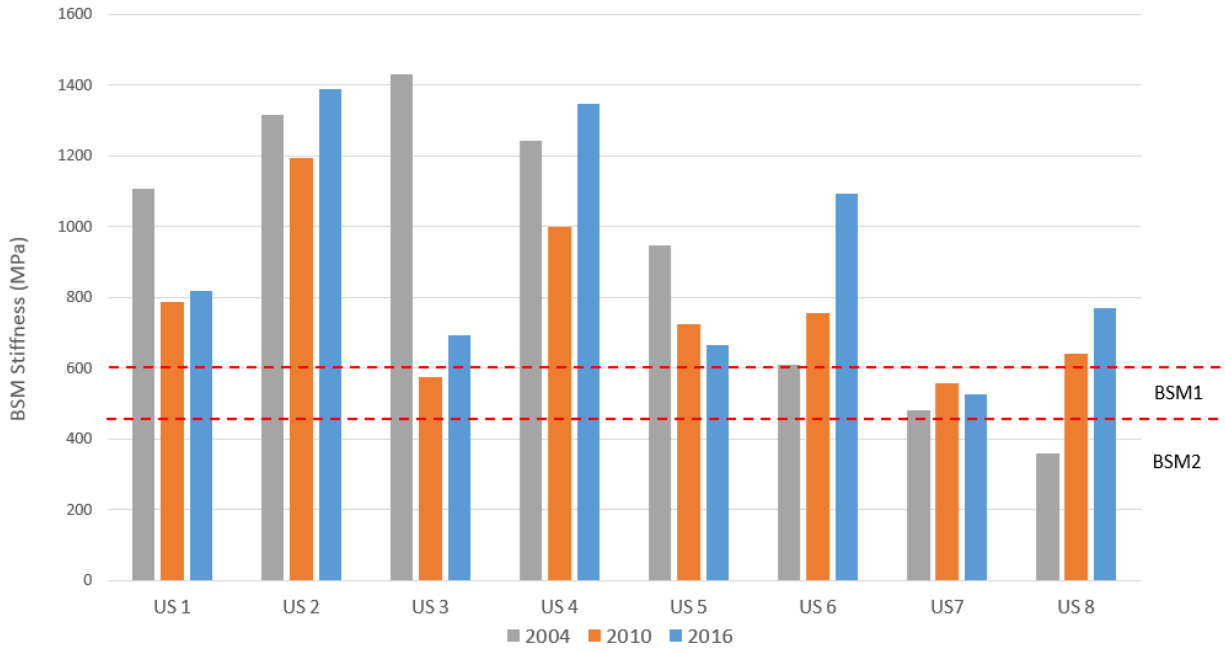

Figure 4.20: N7 Southbound back calculated resilient modulus development in BSM layers per uniform section

The back calculated stiffnesses obtained for the BSM base were further investigated. Figure 4.20 shows the average back calculated resilient modulus development over time for the each of the uniform sections identified on the N7 Southbound carriageway. This allowed investigation of the long-term stiffness behaviour of each of the sections. The back calculated stiffnesses for the three points in time were compared for and between uniform sections.

Uniform sections 1, 2, 3 and 5 show an high initial resilient modulus at two years after construction. The average resilient modulus reduced for these four sections from 2004 and 2010 . This reduction may be due to damage to the materials due to traffic. The resilient modulus was observed to

increase between 2010 to 2016, with the average resilient modulus higher in 2016 than in 2004 for some of the sections.

Uniform section 5 showed a gradual decrease in resilient modulus from 2004 to 2016. In contrast, uniform section 6 and 8 showed a significant increase in resilient modulus over the same period. The long-term resilient modulus development varies significantly between the uniform sections. With limited information available for the local conditions, explanations and conclusions based on these trends may be unreliable.

The dotted red lines in this figure indicates the maximum allowed resilient modulus limit for BSM design as per SAPEM (2014). The higher resilient modulus limit indicates the maximum resilient modulus for a BSM 1, while the lower value is the limit for a BSM 2. These limits were obtained from the PN design method and would therefore be conservative. It would therefore be expected that the resilient modulus of the BSM in the N7 would exceed these values. However, while most of the average long-term stiffnesses were found to exceed 600 MPa, the values shown in Figure 4.20 are very high.

The stiffness values were further investigated by determining the 10th and 90th percentile resilient modulus values for each section. The variation in resilient modulus for each uniform section on the Southbound carriageway is illustrated in Figure 4.21. From this figure it is clear that the back calculated stiffness values are much higher than the design values specified in the TG2. In three of the uniform sections (2, 4 and 6) very high resilient modulus values were observed. The average back calculated resilient modulus for each of these sections was in excess of 1000 MPa. The overall average resilient modulus was above 600 MPa for all but one uniform section.

These very high resilient modulus values suggest that the BSM may have been over cemented and is behaving more like a cemented material than a BSM. Field investigations confirmed this suspicion as pockets of highly cemented materials were found in the base layer. The pavement also showed cracking in some areas, which is the typical failure mechanism of cement stabilised materials. Therefore, care was taken with the N7 results as they may not be representative of a typical BSM.

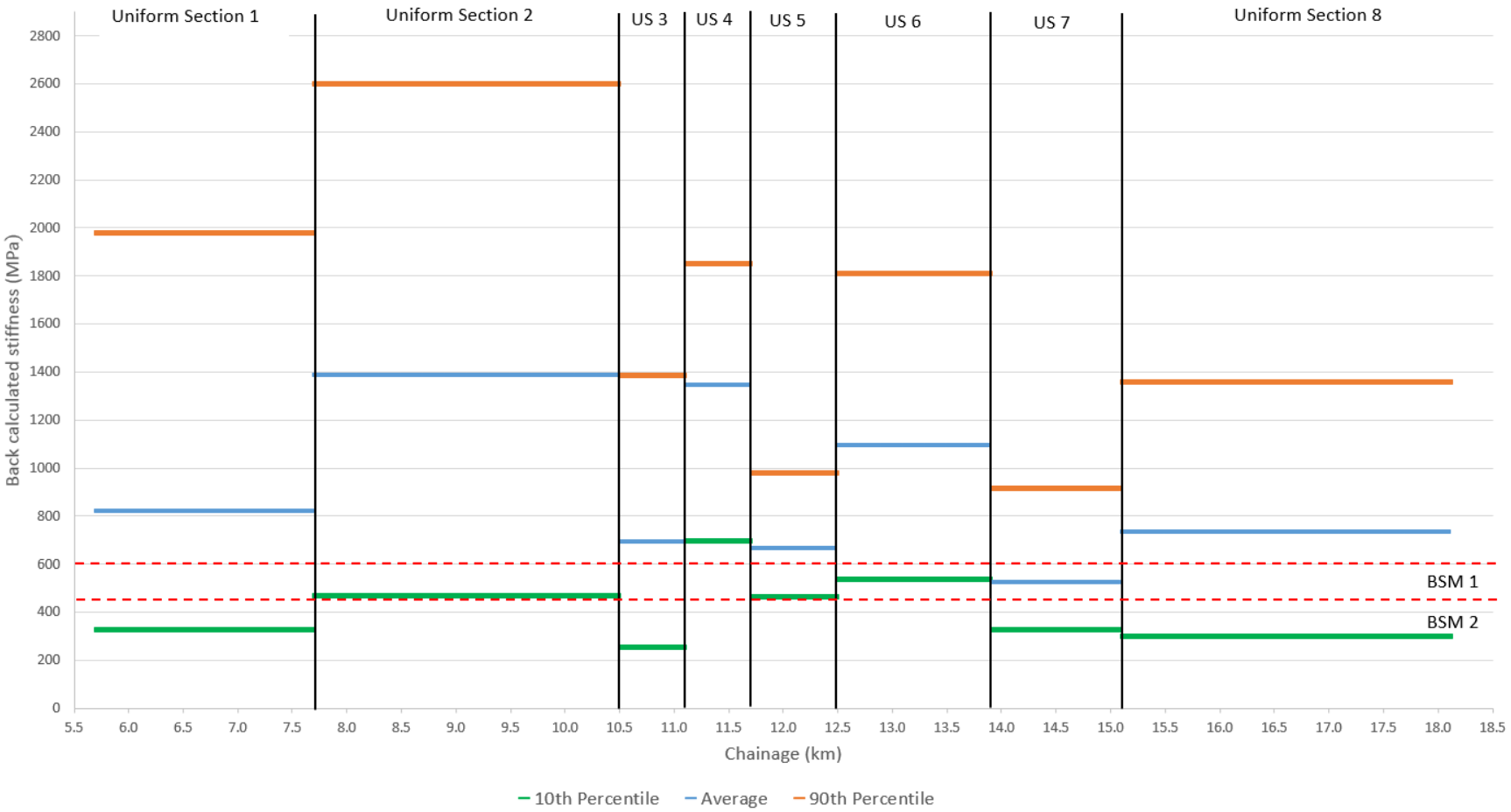

Figure 4.21: N7 Southbound back calculated resilient modulus per uniform section

The FWD data from the Northbound carriageway of the N7 highway was used to back calculate layer stiffnesses. Stiffness values were obtained for the different layers in 2004, 2010 and 2016. The average back calculated layer stiffnesses are shown in Table 4.7. Note that only uniform section 1's stiffnesses were included, as the BSM structure for uniform sections 2 and 3 were only constructed in 2007. Similar to the Southbound carriageway, resilient modulus values obtained for the selected subgrade and the subgrade were found to be unrealistic in some cases. Values representative of the type of materials were selected for these layers and used for further analysis.

Table 4.7: Summary of back calculated layer stiffnesses for the N7 Northbound uniform sections

			Back calculated stiffness (MPa)				
Section	Year	Direction	Layer 1	Layer 2	Layer 3	Layer 4	Layer 5
US 1	2016	NB	1915	775	228	141	373
US 2	2016	NB	4548	1788	722	417	570
US 3	2016	NB	2835	1349	366	180	261

			Back calculated stiffness (MPa)				
Section	Year	Direction	Layer 1	Layer 2	Layer 3	Layer 4	Layer 5
US 1	2010	NB	1567	668	475	73	396
US 2	2010	NB	2955	1152	573	181	518
US 3	2010	NB	1878	872	489	90	298

			Back calculated stiffness (MPa)				
Section	Year	Direction	Layer 1	Layer 2	Layer 3	Layer 4	Layer 5
US 1	2004	NB	3868	1214	606	196	504
US 2	2004	NB					
US 3	2004	NB					

The back calculated stiffness results obtained for the BSM base layer were further investigated. Figure 4.22 shows the average resilient modulus values back calculated for each of the three points in time per uniform section. These resilient modulus values were also found to be higher than the maximum resilient modulus specified for design purposes. As the design limits are conservatively low, the results were expected to exceed this value (600 MPa).

Uniform section 1 was selected as the whole Northbound foam section between km 5.8 and km 11.2. The trend in back calculated stiffness values indicates that the resilient modulus of the BSM was very high shortly after construction. The average stiffness value reduced from around 1200 MPa to less than 700 MPa in measurements taken between 2004 and 2010. This reduction may be due to damage accumulated due to repeated loading induced by traffic. The average back calculated resilient modulus value increased slightly between 2010 and 2016 despite the damage caused by the traffic loading.

Uniform sections 2 and 3 were part of the emulsion stabilised section which was constructed in 2007. Therefore these two sections only have two points in time where the FWD testing was conducted on the BSM. From Figure 4.22 it is clear that the BSMs in these two sections had a very stiff response. The development of resilient modulus for these two sections showed a significant increase between 2010 and 2016. The average back calculated resilient modulus values was above 1200 MPa for both of these uniform section in 2016 for both of these uniform sections. These high resilient modulus values may indicate excessive cement in the BSM. Care was taken when analysing this material as it may not be representative of a typical BSM.

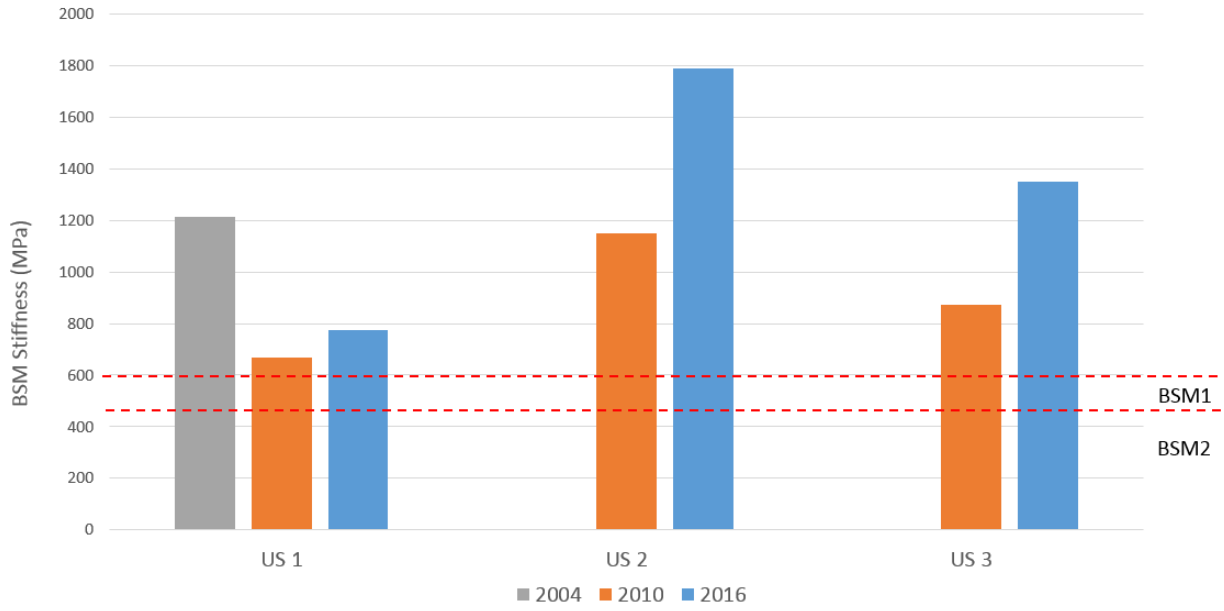

Figure 4.22: N7 Northbound back calculated resilient modulus development per uniform section

The variance of back calculated stiffness results was investigated for the Northbound carriageway. The results of the 90th and 10th percentile analysis are illustrated in Figure 4.23. The resilient modulus values used for this figure were based on the back calculation of FWD results from the 2016 tests. It can therefore be assumed that this analysis reflects the current condition of the uniform sections.

Uniform section 1 in Figure 4.23 shows resilient modulus values typical of a BSM. The average resilient modulus for this section was slightly below 800 MPa, while the stiffest values were below 1200 MPa. From this figure it is clear that the BSM in uniform section 1 has a much lower resilient modulus than the two uniform sections implementing the emulsion stabilised base. Back calculated

resilient modulus values for the Northbound carriageway did not show significant variation and were deemed to be more uniform than those of the Southbound carriageway.

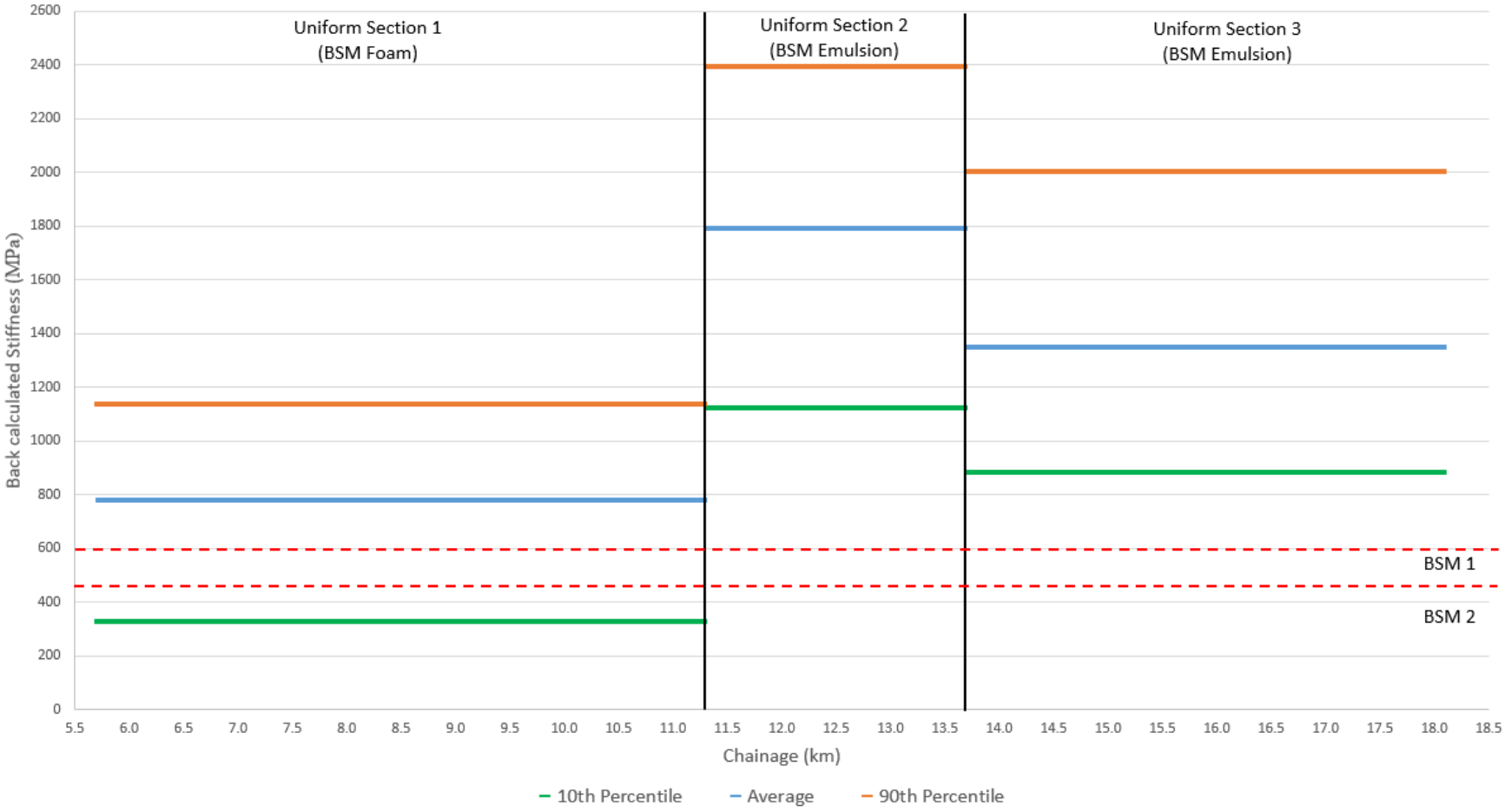

Figure 4.23: N7 Northbound back calculated resilient modulus per uniform section

4.4 Triaxial results

4.4.1 Monotonic triaxial results

Monotonic triaxial tests were performed on the cores obtained from the N7 to determine the shear properties of the BSM base layer. BSM core samples were obtained from different locations on the N7 highway. The cohesion (C) and friction angle (ϕ) were calculated for each set of core samples. A minimum of three cores were required at a specific location to obtain shear properties for the material. Most of the cores were extracted from the outer wheel path (OWP), however, some cores were drilled between the wheel paths. This allowed for a comparison between a heavily trafficked and lightly trafficked materials after fifteen years of service. The methods used for monotonic testing were discussed in Section 3.5.3.

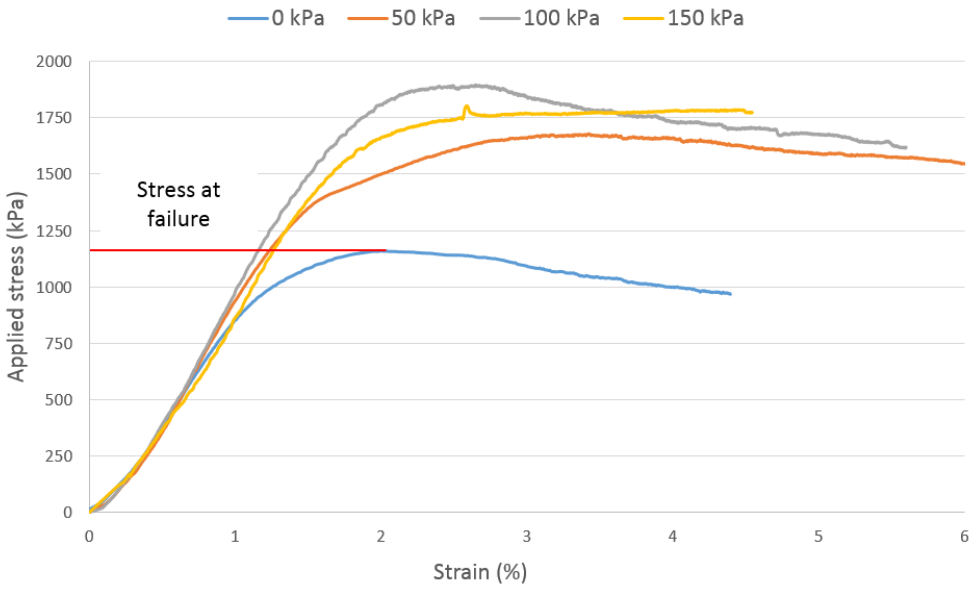

Figure 4.24: Stress-strain relationship curve for N7 NB km 10 BSM cores

Due to the limited number of cores available, tests could not be repeated at a specific confining pressure. Therefore, local effects may have a significant influence on the test results. Caution should be used when analysing the results obtained from the monotonic testing and subsequent calculations.

Each core was measured and weighed before it was tested. After testing, a representative sample from each core was dried in order to obtain the moisture content at the time of testing. Table E.2 and E.1 in Appendix E show the dimensions and the moisture contents of the core samples obtained from the N7.

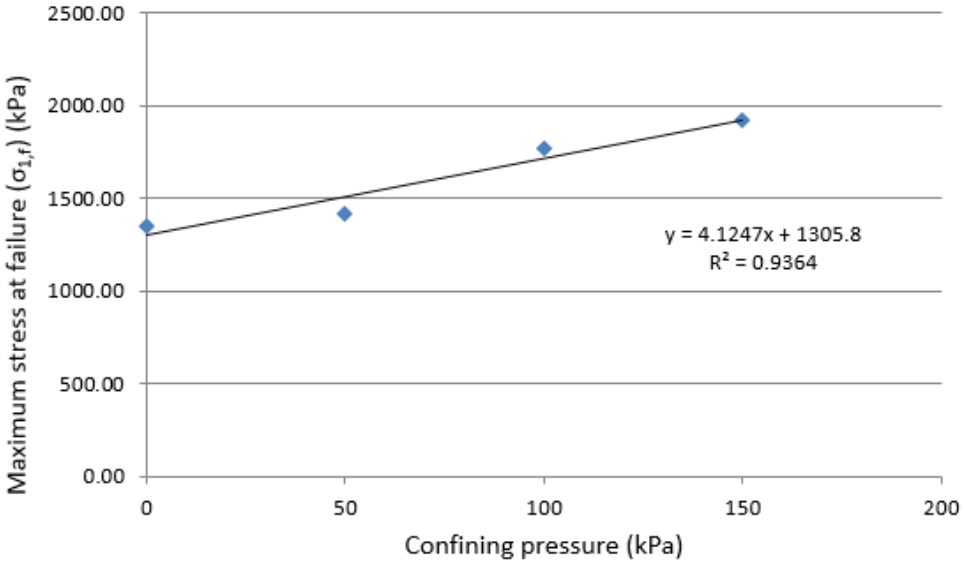

Figure 4.25: Principal stresses at failure for N7 NB km 9.2 shear properties calculation

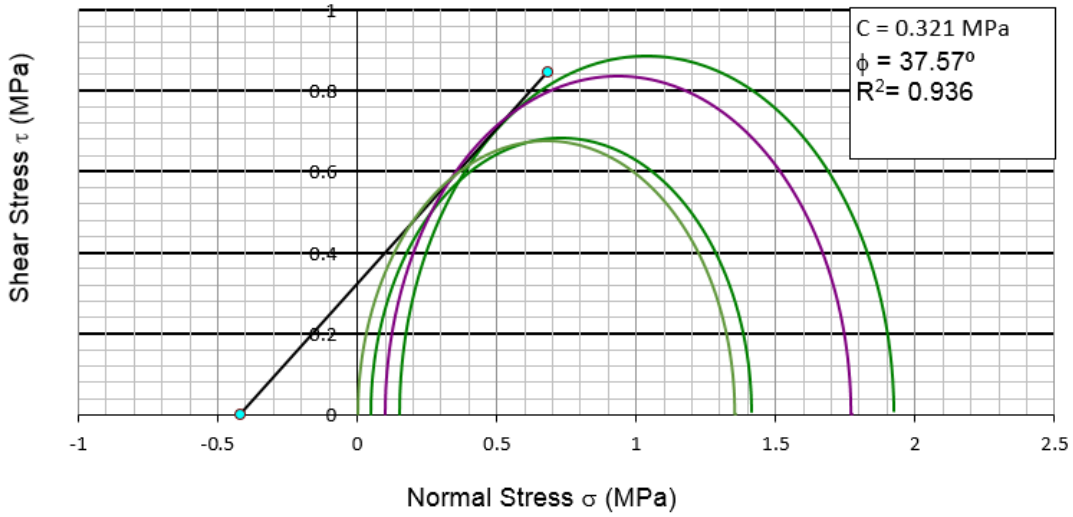

Figure 4.26: Mohr Coulomb failure circles for N7 NB km 9.2

The cores obtained from each location was tested to failure at a range of confining pressures. Figure 4.24 shows the stress strain relationship measured for the four cores obtained from km 10 on the Southbound carriageway. The maximum applied stress measured for each confining pressure was noted and used to determine the shear properties for each location. The maximum applied stress also defines the deviator stress at failure.

The deviator stress at failure was used to calculate the maximum stress at failure ($\sigma_{1,f} = \sigma_{d,f} + \sigma_3$).

The maximum stress at failure was plotted against the corresponding confining pressure as shown in Figure 4.25. The slope ($A = 4.1247$) and intersection ($B = 1305.8$) in this figure were used to calculate the cohesion and friction angle using Equations 3.8 and 3.9. This process was followed to determine the cohesion and friction angle for each of the coring locations.

Figure 4.26 shows the cohesion and friction angle for the cores obtained from km 9.2 on the Northbound carriageway. The figure shows the Mohr-Coulomb circles used to determine the cohesion and friction angle. The slope of a linear line tangent to all the circles indicates the friction angle, while the intercept of this line with the shear axis indicates the cohesion.

The monotonic triaxial results obtained from foam stabilised BSMs on the N7 are given in Table 4.8. The monotonic triaxial results obtained from the emulsion stabilised BSMs are given in Table 4.9. The minimum cohesion for the design of a BSM 1 is specified as 250 kPa. From the results it is clear that most of the cohesion values are very high. These values are much greater than typically expected for a BSM. These values cannot be taken as absolute as there were no repeated tests at the same location. Therefore, these values were interpreted with caution.

Table 4.8: Monotonic triaxial results for foam stabilised base layer

Chainage	Sample	Sigma 3 (kPa)	Failure load (kN)	Failure stress (kPa)	Sigma 1 (kPa)	R^2	A	B	ϕ (°)	C (kPa)
SB 10.5	1	0	14.96	918.65	918.65	0.97	6.69	885.08	47.7	171.1
	2	100	21.73	1353.03	1453.03					
	3	150	29.40	1805.17	1955.17					
SB 10.5 BWP	1	0	23.27	1449.04	1449.04	0.57	4.32	1662.05	38.6	399.7
	2	50	32.85	2045.62	2095.62					
	3	100	35.31	2198.61	2298.61					
	4	150	31.35	1951.95	2101.95					
SB 16	1	0	18.65	1161.19	1161.19	0.99	7.52	1180.34	49.9	215.2
	2	100	30.36	1890.18	1990.18					
	3	150	34.54	2120.65	2270.65					
NB 9.2	1	0	21.75	1354.13	1354.13	0.94	4.12	1305.85	37.6	321.5
	2	50	21.91	1364.36	1414.36					
	3	100	26.80	1668.94	1768.94					
	4	150	28.48	1773.39	1923.39					
NB 10	1	0	18.89	1159.66	1159.66	0.79	5.30	1312.32	43.0	285.0
	2	50	26.97	1679.08	1729.08					
	3	100	30.47	1896.93	1996.93					
	4	150	29.38	1803.86	1953.86					
NB 11	1	0	26.75	1665.42	1665.42	0.30	3.47	1969.95	33.5	528.7
	2	50	40.96	2550.29	2600.29					
	3	150	35.14	2188.27	2338.27					
NB 11 BWP	1	0	27.24	1696.06	1696.06	0.67	6.53	1829.06	47.2	358.0
	2	100	44.66	2780.72	2880.72					
	3	150	38.42	2392.04	2542.04					

Table 4.9: Monotonic triaxial results for emulsion stabilised base layer

Chainage	Sample	Sigma 3 (kPa)	Failure load (kN)	Failure stress (kPa)	Sigma 1 (kPa)	R^2	A	B	ϕ (°)	C (kPa)
NB 12	1	0	27.60	1718.57	1718.57	0.95	4.26	1748.18	38.3	423.6
	2	50	32.09	1970.28	2020.28					
	3	100	33.29	2044.36	2144.36					
	4	150	32.11	1999.06	2149.06					
NB 12 BWP	1	0	35.23	2163.22	2163.22	0.93	10.97	2247.83	56.4	339.3
	2	100	56.98	3498.74	3598.74					
	3	150	58.21	3574.26	3724.26					
NB 14.4	1	0	23.88	1486.97	1486.97	0.91	5.73	1403.68	44.7	293.2
	2	50	23.73	1477.30	1527.30					
	3	100	31.80	1952.83	2052.83					
	4	150	34.00	2117.02	2267.02					
NB 16	1	0	25.26	1572.96	1572.96	0.96	4.74	1515.15	40.7	348.0
	2	50	25.95	1615.45	1665.45					
	3	150	33.81	2105.11	2255.11					

At three of the coring locations, cores were drilled from the outer wheel path as well as between the wheel paths. These locations were km 10.5 on the Southbound carriageway and km 11 and 12 on the Northbound carriageway. By comparing the results obtained from cores drilled at the two positions, the heavily trafficked materials can be compared to the non trafficked (or lightly trafficked) materials. It was expected that the materials between the wheel paths would be in a much better condition as it received substantially less damage from traffic loading.

The results in Table 4.9 show that some of the samples have a very poor correlation coefficient. This is prominent at chainages 10.5 (BWP),NB 10 and NB 11 (both in the wheel path and between them). The three or four cores obtained from a specific location were less than two meters apart. This poor correlation indicates that the material varies significantly in a relatively small surface area.

The values obtained for the cohesion and friction angle were used during the validation of the transfer function (Section 5.1). The cohesion and friction angle were used to determine the shear stress ratio for each uniform section imposed by traffic loading. The shear properties were assigned to a uniform section where they were obtained from that uniform section. Uniform sections which contained more than one coring location were assigned the average of the two. In cases where no cores were taken from a uniform section, the section was assigned the average of the two nearest values. Only the shear properties for the outer wheel path were used as that is the position where the most permanent deformation occurred.

Some of these values were deemed to be non-representative of BSMs as they were much higher than that of a typical BSM. It is expected that using the values would result in very low DSR values.

The large values for cohesion and friction angle would result in small DSR values. In cases where the results were non-representative, the values were reduced or it was noted that the DSR would also be non-representative. The shear properties assigned to each uniform section of the N7 are shown in Tables O.1 and O.2 in Appendix O.

Figure 4.27: Core after triaxial testing (NB km 16 tested at 0 kPa)

Figure 4.27 shows a core from the N7 that was tested to failure. Note that the sample is upside down from the orientation in the pavement structure. The core shows cracking and breaking in

mostly the bottom half of the layer. While the top of the layer was still in relatively good, solid condition.

This difference indicates that the material behaves differently from the top to the bottom of the layer. This may be due to the compaction effort during construction, providing a density that is higher at the top of the pavement. Therefore, the top of the layer has higher confinement and is less susceptible to damage due to loading.

In addition, some of the uniform sections' base layers behaved more like a cement stabilised material than a BSM. The bound behaviour would cause tension at the bottom of the base layer resulting in microcracking. This is a possible explanation for the observed breakage of the core samples.

4.4.2 Dynamic triaxial results

Dynamic triaxial tests were performed on four core samples obtained from the N7 highway. These tests were tested at shear stress ratios calculated from the shear properties obtained from cores taken at the same locations. These triaxial tests were performed to validate the high back calculated resilient modulus results for the BSM base layer.

Figure 4.28 shows the results from the dynamic triaxial testing of the BSM core sample obtained from km 9.2 on the Northbound carriageway. The figure shows the MR at specific levels of bulk stress ($\theta = \sigma_1 + \sigma_2 + \sigma_3$). The three lines indicate the results from testing at confining pressures of 50 kPa, 100 kPa and 150 kPa. The figure shows an increase in Mr with an increase in confining pressure. This was expected as better support (in the form of confining pressure) increases the strength of the material.

The behaviour shown at 50 kPa suggests that the Mr increases with an increase in bulk stress at a specific confining pressure. This is typical of a stress dependant material. However, the trends observed at 100 kPa and 150 kPa showed the opposite behaviour. The Mr at the higher confining pressures reduced with an increase in bulk stress. This response is not what is typical of granular materials or BSMs and was counter-intuitive to what was expected.

A possible cause of this behaviour may be due to high cement content in the material. By loading the cemented material, the cement bonds may be broken and the sample damaged. The damaged sample would show a reduction in strength. The force applied to the sample (σ_1) was relatively high due to the high cohesion shown from the monotonic tests.

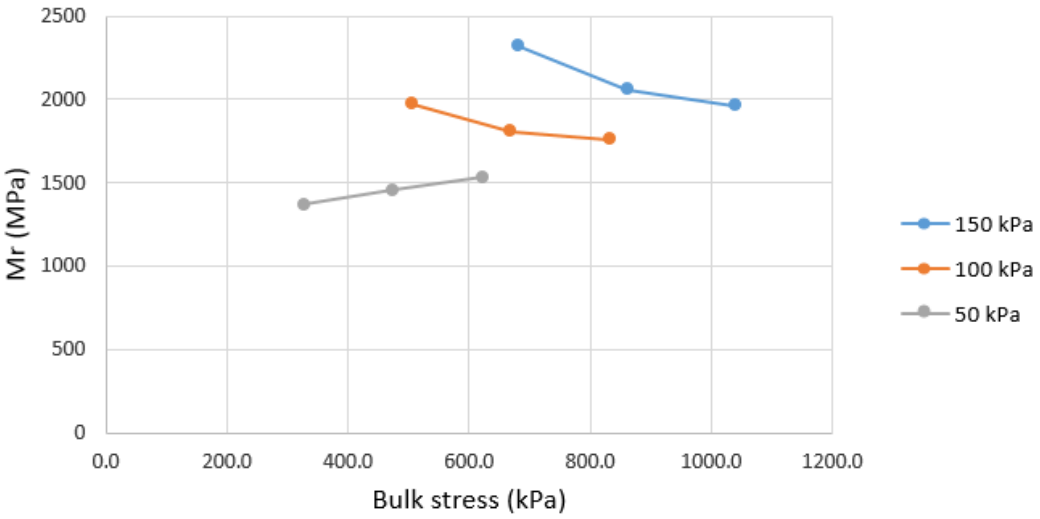

Figure 4.28: Dynamic triaxial results at km 9.2 on the Northbound carriageway

Another possible cause for the stress softening observed in the results may be due to the testing apparatus. The results indicated a high stiffness due to the low amounts of deformation measured, by the LVDTs, during repeated loading. The LVDTs may be inaccurate when measuring very small deformations resulting in unrepresentative Mr values. The sample has a reduced moisture content when compared to field condition, which may result in an increased Mr. The testing apparatus also provides significant support which may increase the resulting Mr.

The values obtained from this test were substantially higher than expected values for a BSM. The resilient modulus values ranged from 1400 MPa to 2300 MPa. These results indicate that the high back calculated resilient modulus values are representative of the in field conditions.

4.5 Transfer function calibration

4.5.1 Permanent strain development in LTPP pavements

The remaining pavement life obtained from the transfer function cannot be directly compared to field observations and traffic data. This problem is discussed in Section 3.7.1. In order to compare pavement life obtained from the new transfer function with the actual traffic data, the permanent strain development was extrapolated to reach 10% of the layer thickness. This process is explained in Section 3.7.2.

The Huurman model was used to extrapolate the permanent deformation development over repeated loading. Figure 4.29 shows the different steps in extrapolating the number of load repetitions to reach 10% deformation in the BSM for the MR 27 SB. This figure shows the

correlation coefficients (A and B), which were calculated for each pavement. The slope and R^2 values describe the regression life between N Huurman (number of axles obtained from the model) and N actual (number of axles from traffic counts). Excel solver was used to determine the value of A and B by setting the objective to maximize R^2. The slope was constrained between 0.95 and 1.05 to ensure that the results from the Huurman model reflected the actual traffic data.

The Huurman model used the permanent strain in the BSM layer (%) to calculate the number of load repetitions. Permanent strain in the BSM layer was calculated as the measured permanent strain (rutting) multiplied by the fraction allocated to the BSM layer divided by the layer thickness. This measure was then extended to reach the 10% deformation limit, allowing long-term calibration of the transfer function.

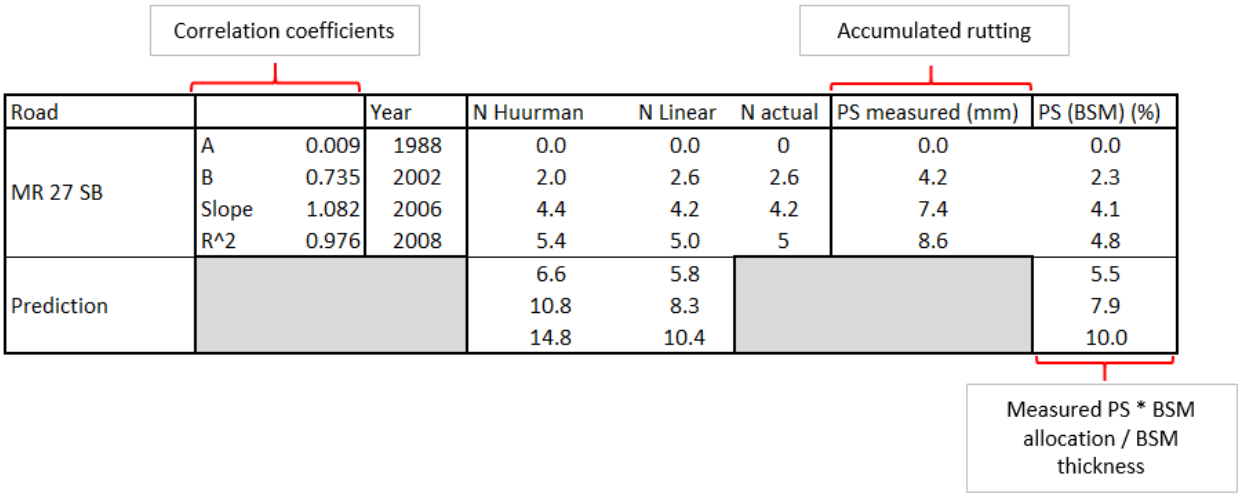

Figure 4.29: Explanation of permanent strain development prediction with Huurman model method

Tables H.1 to H.4 in Appendix H show the steps in the extrapolation process and the results thereof. The results obtained from the Huurman extrapolation compared to a linear forecast are shown in Figure 4.30 for the MR 27 and MR 504 (A). This comparison was done for all the LTPP pavements and can be found in Figures H.1 to H.5 in Appendix H.

In general the number of load repetitions obtained from the Huurman extrapolation was higher than that of a linear forecast. The larger number of load repetitions was expected as the accumulation of permanent strain in granular materials is not a linear process, but follows a logarithmic development. These results were also inspected to ensure that the difference between the linear extrapolation and the Huurman model was not of great significance as it would produce a less

conservative estimation of load repetitions. Therefore, these results were deemed realistic and used in the calibration of the transfer function. For this study it was assumed that the deformation remained in the stable state throughout its full life cycle.

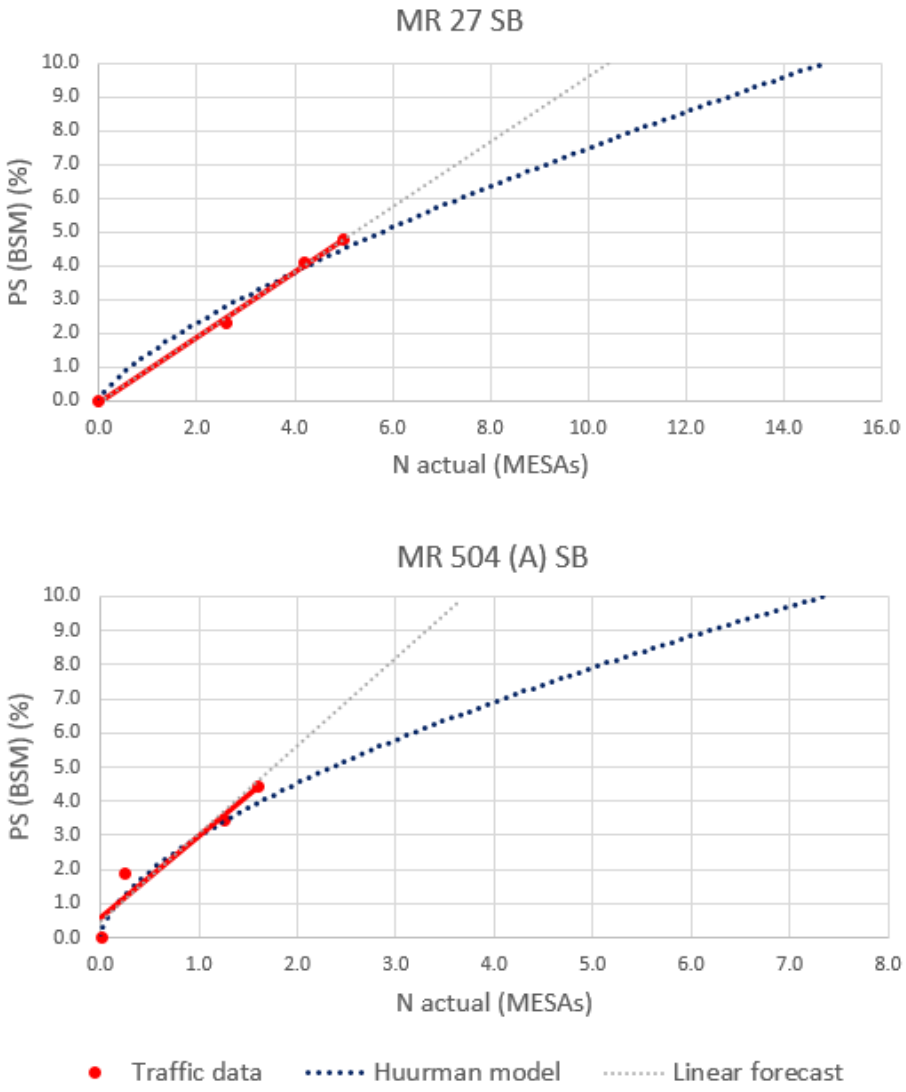

Figure 4.30: Permanent strain development prediction with Huurman model (1)

4.5.2 Deviator stress ratio

The stress conditions in a BSM layer play a significant role in the life of such a material. This variable has the largest influence on the results obtained from the transfer function as it is raised to the power three in the proposed function. Deviator stress ratio and the calculation thereof using Rubicon toolbox is discussed in Section 3.7.3.

In order to determine the DSR imposed by loading, pavement structures were modelled in Rubicon

Toolbox. Stiffness values used for the different pavement layers were obtained from FWD tests, triaxial tests and by making informed assumptions, while layer thicknesses were obtained from field investigations and as built data. The shear properties of BSMs were obtained from triaxial testing of cores from the N7 and informed assumptions were made regarding this information for the LTPP pavements as limited information was available. The results of the DSR calculations for the N7 are discussed in Section 5.1.2.

The stress ratio induced by a standard axle load was calculated for each of the LTPP pavement structures. In order to obtain the stress conditions in the BSM, the linear elastic standard axle analysis tool was used. By determining the stress conditions in the BSM layer, the deviator stress ratio induced by a standard axle could be calculated. The values obtained for the DSR from the software was checked by determining the principal stresses at the critical position and calculating the DSR manually. The critical position was defined as the position with the highest DSR. This was typically down 25 % of the layer thickness from the top of the layer.

Each of the LTPP pavements were modelled in Rubicon toolbox with layer thicknesses determined as per Section 3.2.1. This analysis requires resilient modulus values for each of the layers of the pavement structure. The resilient modulus values obtained from FWD testing were used during this analysis. Some of these values were altered to obtain a more realistic model of these pavements. These alterations were mainly for subgrade conditions, where unrealistic values were reduced.

This information was deemed to be sufficient to calculate the principal stresses and strains in each of the pavement layers. However, in order to calculate the deviator stress ratio in the BSM layer, shear properties of the material were required. The values of the shear properties were assumed based on the material reports and field conditions. The properties assigned to each of the LTPP pavements are stated in Appendix B. Each of these standard axle analyses can be found on the attached CD.

Tables I.2 to I.4 in Appendix I show the pavement structures modelled in Rubicon toolbox with layer thicknesses, stiffnesses and BSM shear properties. The DSR results for each pavement are also shown on these tables. It was assumed that the behaviour of these pavements would remain consistent throughout their design lives, therefore, the DSR was calculated for a constant layer resilient modulus for each pavement.

The results obtained from the DSR calculations show that the DSR values for these pavements are between 0.2 and 0.35. The lowest value of 0.185 was found for the subbase of the N1-13. This is a

realistic result as this layer has a significant amount of high quality cover in the form of a BSM base and asphalt surfacing. The maximum DSR was calculated for the P243-1 as 0.349. This material was classified as a BSM 2 and is predicted to carry only 2.8 MESA in its design life. The lower shear properties assigned to a BSM 2 result in a significant increase in DSR. This high value calculated for the DSR can be expected for a pavement with low shear properties and a thin surfacing layer.

Table 4.10: Summary of transfer function input values and DSR results for the LTPP pavements

Road	C (kPa)	ϕ (°)	DSR (-)	RetC (%)	P.mod (%)
MR27 SB	275	40	0.319	75	102.1
MR27 NB	275	40	0.324	75	102.1
MR504(A) SB	250	40	0.331	75	100
MR504(A) NB	250	40	0.331	75	100
MR504(B) SB	250	40	0.308	75	95
MR504(B) NB	250	40	0.308	75	95
N1-1 SB	250	40	0.305	75	101.3
N1-1 NB	250	40	0.3	75	101.3
N1-13 SB	275	40	0.301	75	100
N1-13 SB Subbase	200	35	0.203	65	97.8
N1-13 NB	275	40	0.299	75	100
N1-13 NB Subbase	200	35	0.185	65	97.8
N1-14 SB	275	40	0.303	75	100
N2-16 NB	225	40	0.339	75	100
N2-20 EB	260	40	0.309	75	100
N2-20 WB	260	40	0.309	75	100
N4-1 EB	250	40	0.306	75	101.3
N4-1 WB	250	40	0.303	75	101.3
N4-5X EB	250	40	0.316	75	100
N11-8 NB	200	35	0.333	75	100
N12-19(3) EB	265	40	0.296	75	100
N12-19(4) EB	265	40	0.285	75	100
P243-1 EB	230	40	0.349	75	100.7

Considering that the design of a pavement structure including a BSM layer is carried out based on the shear properties of the BSM measured in the mix design, it is important that LTPP data is representative of the mix design performance parameters. There is a significant data base of shear parameters from BSM mix designs that can provide a range of realistic shear parameters. Using LTPP data that is(Llwellyn, 2015) unusually high, would result in an "unconservative" design function. So, careful selection of realistic data is imperative.

Table 4.10 shows the results obtained from the DSR calculations for each of the LTPP pavements. This table also provides three of the four input parameters used in the new transfer function. These values were used with the range from 0% to 10% permanent strain as the input values for

the transfer function. The results obtained from the calibration of the transfer function using these values are discussed in Section 4.5.3.

The cohesion and friction angle values shown in Table 4.10 are very different from the N7 triaxial test results shown in Table O.1 and Table O.2. The values obtained from the N7 were not representative of a typical BSM. Therefore, the values used for the LTPP pavements was based on the specification and not the N7 results.

4.5.3 Calibration to LTPP pavements

The new transfer function for BSMs was calibrated to describe the deformation trends of in field pavement structures. Fourteen long-term pavement performance study road sections were identified and analysed. These analyses aimed to find input values for the transfer function (retained cohesion, density, stress ratio and permanent strain) and relate them to the number of standard axles the pavement had been subjected to. By comparing the development of permanent strain observed in the field with that of the new transfer function, the transfer function could be calibrated to accurately predict the number of load repetitions required to reach a certain level of permanent deformation.

Three of the four input parameters were determined for each of the LTPP pavements and are shown in Table 4.10. These three parameters were kept constant for each pavement throughout its predicted life. Although this is not the case in field, too little information was available to accurately predict the reduction or increase of these factors over time.

The final parameter used in the transfer function is permanent strain (PS). Permanent strain was set as the controlling factor for this function. PS in this function is a measure of the remaining deformation that the layer can undergo before it is classified as failed. During the calibration of the transfer function, each BSM layer was limited to a PS of 10% of the BSM layer thickness. Therefore, at the start of a pavement's life it would have accumulated zero deformation and would have 10% deformation remaining before failure. At the end of the BSM's life, it would have accumulated 10% PS and would have 0% remaining. The use of remaining PS as well as relating it to accumulated PS is discussed in Section 3.7.1 and Section 3.7.2.

4.5.3.1 Initial constant analysis

The remaining life of each pavement structure was calculated with the new transfer function for each of the pavement structures at over range of PS levels. The PS values from 10% remaining to

0% remaining to failure. This provided an initial set of results for the transfer function which could be compared to the actual deformations (extrapolated with the Huurman model) at a number of points in the life of the pavement. The values obtained from the transfer function were compared to the actual values at specific points for each pavement for the initial values of the constants:

$$\log N = A + B(DSR)^3 + C(P_{mod}.RetC) + D(PS) \tag{4.1}$$

With:

A = 1

B = -60

C = 0.001

D = 0.1

These initial values showed that the transfer function predicted the overall trend of plastic strain accumulation in BSMs. However, the function did not predict the life of the material accurately. Figure 4.31 shows the comparison between the N_{Actual} and N_{TF}, where N_{TF} was calculated using the original estimates for the four constants in the function. The regression line through the data points is described by the function $y = 2.949x + 2.2732$ with an R^2 value of 0.9165. The high coefficient of determination indicates that the form of the transfer function predicts the actual data very well. However, the slope of the regression line indicates that in all cases the transfer function overestimates the life of the pavement as can be seen by the deviation from the line of equality. This represents a transfer function with a very low level of reliability.

In Figure 4.31 a red circle indicates non representative values. These values are obtained when PS remaining is set to zero in the transfer function. Due to the logarithmic form of the transfer function and the other non zero variables, it still returns a positive N for zero PS remaining. From a practical point of view, this situation determines the number of load repetitions to failure after the layer has failed. Therefore, it does not represent a practical situation for design.

These values have an effect on the calibration of the transfer function as they raise the interception point of the trendline and in turn reducing the slope. These values do not represent a relevant situation in design, therefore, they were excluded from the calibration process with the further calibration as explained in the next section.

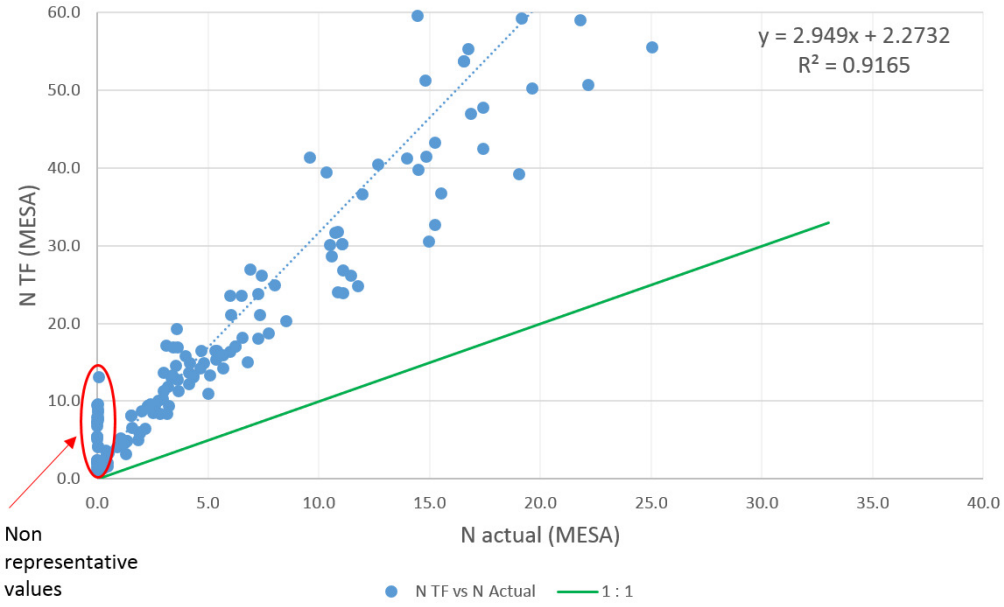

Figure 4.31: N_{TF} vs N_{Actual} using initial constant assumptions for LTPP pavements

4.5.3.2 Calibrated constants analysis

The green line in Figure 4.31 indicates a 1:1 relationship. The aim of the calibration is to change the function's constant to reach a state where N_{TF} and N_{Actual} have a 1:1 relationship. This relationship would indicate that the transfer function describes the known data and does not overestimate or underestimate it.

Excel solver was used to find values for the constants A, B, C and D in order to obtain this 1:1 relationship. The linear estimate tool was used to determine the slope, R^2 and the residual sum of squares of N_{TF} vs N_{Actual}. Solver's objective was set to find the minimum value for the residual sum of squares by changing the variables A, B, C and D. These four constants were constrained to be able to use the evolutionary solving method. The slope of the line was controlled by setting a constraint on the slope between 0.975 and 0.125.

Figure 4.32 shows N_{TF} compared to N_{Actual} calibrated to fit the 1:1 relationship indicated by the green line. The trendline plotted through the data points is described by $y = 1.0006x + 1.0572$ (the dotted line) with a correlation coefficient of $R^2 = 0.927$. The values obtained for the constants used in the transfer function using Excel solver were:

A = 1.204378

B = -57.286

C = 0.0009159

D = 0.086753

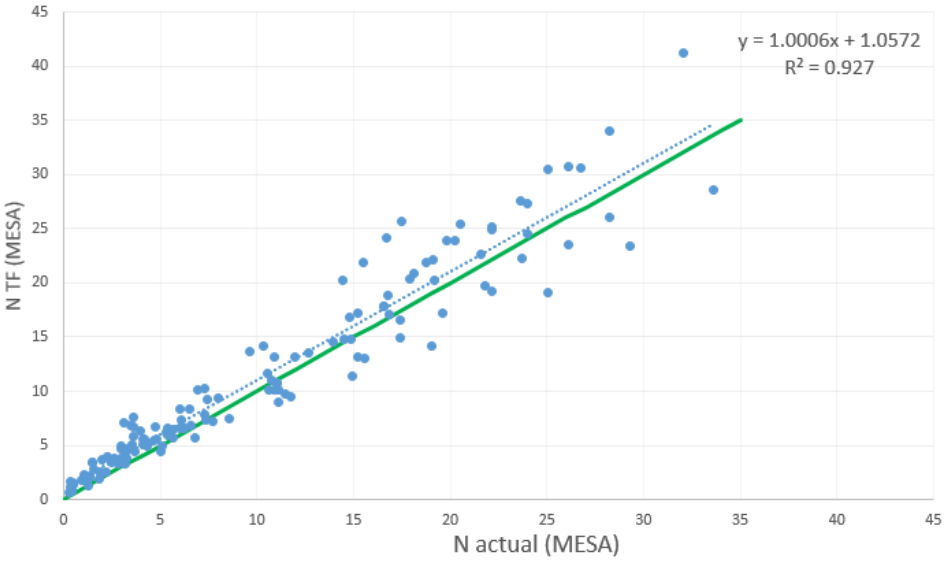

Figure 4.32: N_{TF} vs N_{Actual} calibrated to 1:1 relationship for LTPP pavements

The slope of the trendline indicates that the values obtained from the transfer function predict the actual data accurately. It was significantly reduced from the value obtained using the initial constants for the function. By adjusting the transfer function to describe the observed data with a one to one relationship, the function predicts the life of the pavement as accurately as possible. This is not applicable for design purposes as pavement design reliability levels are typically around 90%. This initial calibration only aims to describe the observed data and not produce a function to be used for designs. The function was further calibrated to meet different levels of reliability for the purpose of design, the results of which are given in Section 4.6.

The correlation coefficient obtained for the relationship in Figure 4.32 of $R^2 = 0.927$ shows a very strong relationship between the actual PS development and the new transfer function. The correlation coefficient obtained after calibration is not significantly higher than the value obtained using the initial constants. The correlation coefficient was therefore used only as an indication of the precision of the transfer function, and not its accuracy or reliability.

The intercept point shown in Figure 4.32 was also significantly reduced from the value obtained using the initial constants. The value reduced from 2.273 to 1.057, which is a significant improvement in the function's ability to describe the actual data. This reduction was in part caused by the removal of the values obtained from the function for a PS remaining value of 0%.

By inspecting the development of permanent strain using the Huurman model and the new transfer function for individual pavements, the intercept point can be explained. Figure 4.33 shows the

development of PS over number of load repetitions obtained for actual data and extrapolated using the Huurman model, compared to the new transfer function. The values obtained during the early life of the pavement (PS induced between 0% and 2%) show a significant difference between the actual data and the transfer function. This is due to the nature of the function, as it does not start at zero load repetitions for zero PS remaining. This explains why the intercept of the relationship in Figure 4.32 is not at zero but rather at 1.057.

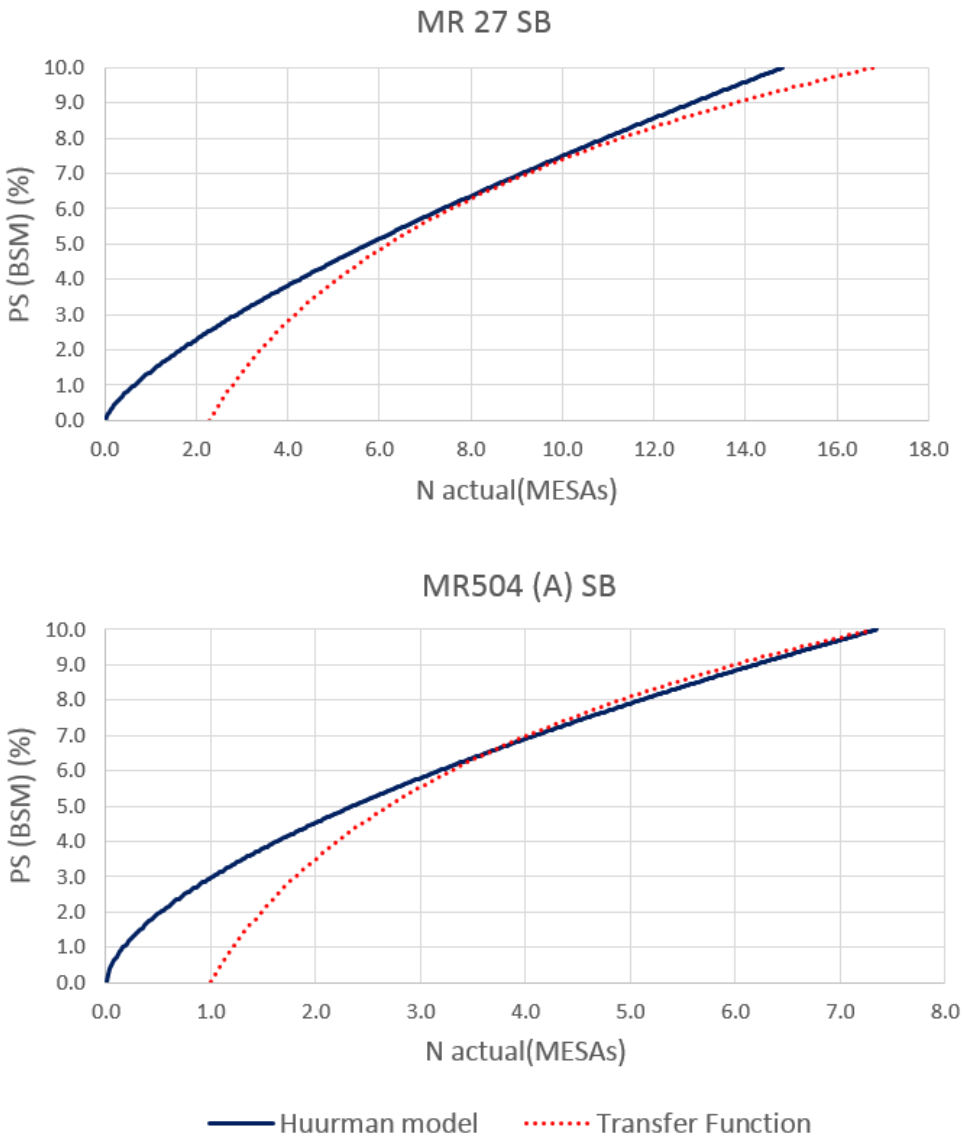

Figure 4.33: N_{TF} vs N_{Actual} for LTPP pavements (1)

Permanent strain development obtained from actual data and the Huurman model was compared to that of the transfer function for each of the LTTP pavement structures. Figure 4.33 shows this relationship for two of the pavements, while Figures J.1 to J.5 in Appendix J show this for the rest

of the LTPP pavements.

These figures, illustrating the relationship between the transfer function results and the observed data, highlight the difference in short-term results. However, the slope of transfer function's predicted life is very similar to the slope obtained from the actual data. This indicates that the transfer function predicts the long term rate of permanent strain accumulation accurately. The design function for BSM aims to provide a means of predicting the long-term in-field performance of BSMs based on material and structural properties. The function describes the long-term behaviour of BSMs and was therefore calibrated to different levels of reliability to produce a design function that accurately predicts the permanent strain accumulation rate of a BSM for specific design reliability criteria.

4.5.3.3 DSR power investigation

The effect of the power influencing the deviator stress ratio in the transfer function (Equation 4.1) was investigated. The transfer function was calibrated using the same method used previously in this section with the power influencing the DSR set to 2 and 4 and compared to the optimal results for the standard function. This was done to check if the initial assumptions to raise the significance of DSR on the function's results were correct. Figure 4.32 shows the relationship between the transfer function's prediction and the observed data for the power 3. Figure K.1 and Figure K.2 in Appendix K show the same comparison, with the power influencing DSR changed to 2 and 4 respectively.

Table 4.11 shows a summary of the linear regression information obtained during this investigation. The table shows the slope, interception point and correlation coefficient for each of the 3 powers considered. The slopes of the three sets showed a satisfactory degree of precision, with the slope for the power 4 being slightly too high. The interception point for the power 4 was very high and it showed a very poor coefficient of correlation of 0.355. By increasing this power to 4, the term reduces significantly as it is effectively timed by a fraction (usually smaller than 0.4). This causes the function to overestimate the life of the materials and reduce the effect of DSR.

By subjecting the DSR to the power 2, the function generates a large value for this term. This causes the function's intercept point to drop from 1 to -0.59. The reduction in slope indicates that the function overestimates the effect of DSR and produces a conservative function. The correlation coefficient is also significantly reduced by applying the power 2. Therefore, DSR was subjected to the power 3 for the calibration and the final transfer function for this study.

Table 4.11: DSR power investigation results

DSR power	Slope	Intercept	R^2
2	1.025	-0.5945	0.819
3	1.001	1.0572	0.927
4	1.1296	6.9172	0.355

4.5.3.4 Calibrated transfer function

The transfer function was calibrated to describe the plastic strain development observed for the LTPP pavements. Values were obtained for the four constants which control the effect the variables have on the transfer function's results. The transfer function, calibrated to predict the observed data without a reliability adjustment, is given in Equation 4.2.

$$\log N = 1.204378 - 57.286(DSR)^3 + 0.0009159(P_{mod}.RetC) + 0.086753(PS) \tag{4.2}$$

The significance of the different variables in the transfer function was investigated. The results of this investigation are given in Section 5.3.

4.6 Transfer function reliability adjustment

The new transfer function for BSMs was calibrated in Section 4.5 to best describe the observed LTPP data. By calibrating the function to fit the data the relative influence of the four variables could be determined and expressed in the constants A, B, C and D. This function only aimed to describe the observed trends and would not be applicable in design. For design purposes a function with different levels of reliability is required for different design criteria. Therefore, the transfer function was adjusted in order to describe the LTPP data at four different levels of reliability.

The calibrated transfer function was altered to describe these levels of reliability by adjusting the the first constant (A) as shown in Equation 4.3. The other three constants in the function describe the significance of the variables DSR, P_{mod}, RetC and PS. When changing the constants B, C and D the significance of the effect of the four variables on the transfer function's results would be altered. Therefore, these constants were not altered for different levels of reliability. This method has the added benefit of producing a transfer function where only the constant, A, has to be changed to select the level of reliability.

$$\log N = A - 57.286(DSR)^3 + 0.0009159(P_{mod}.RetC) + 0.086753(PS) \tag{4.3}$$

Where:

A: calibrated for 50%, 80%, 90% and 95%

Pavement design in South Africa makes use of four categories to describe the reliability of the pavement. These are Category A (95% reliability), Category B (90% reliability), Category C (80% reliability) and Category D (50%). The transfer function was altered to describe the LTPP data with these four levels of reliability. Reliability in the transfer function was measured as the percentage of data predicted by the transfer function that had a smaller value than the observed data. In other words, the function would predict the actual traffic in a conservative manner for the specific percentage of data points.

Figure 4.34 illustrates the certainty adjustments with regards to the actual traffic data. In this figure the transfer function produces values of which 90% are lower than the observed data. Therefore, the transfer function would return smaller values given the same input values when compared to the observed data. The initial function was found to describe the observed data with a 22.58% reliability. The reliability adjustments altered the function to produce lower values than the observed values at reliability levels of 50%, 80%, 90% and 95%.

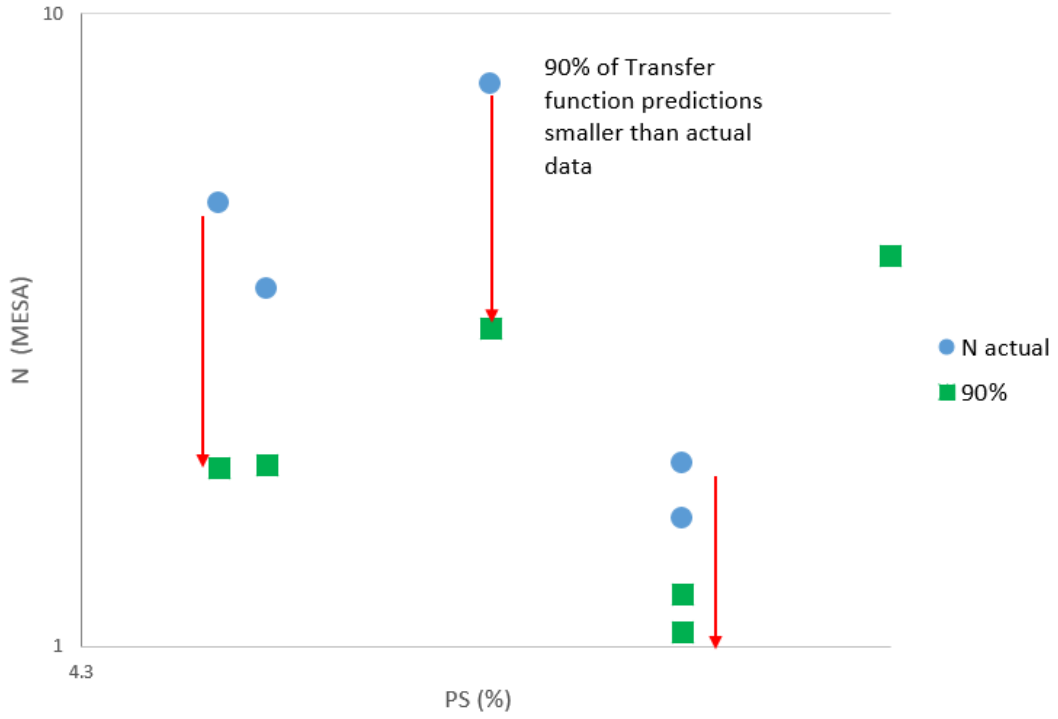

Figure 4.34: Method of transfer function value reduction for increased reliability

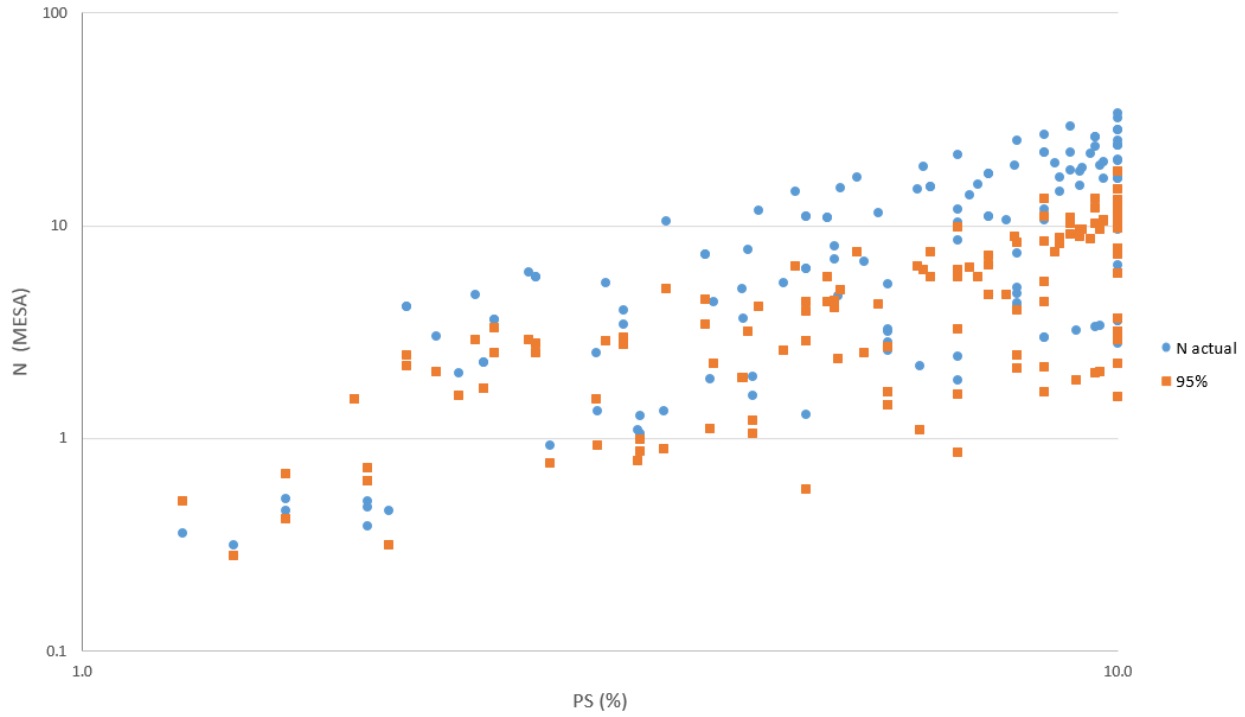

Figure 4.35: Transfer function value reduction for 95% reliability

Figure 4.35 shows the predicted values at a 90% reliability level compared to the observed data at the same level of permanent strain. Note that most the predicted points are below the observed data. The function was calibrated to predict a lower value than the observed value for 90% of the available data points. The same process was followed for 95%, 80% and 50% reliability as shown in Figure L.2 to Figure L.4 in Appendix L.

Figure 4.36 shows the relationship between the actual data and the transfer function's prediction thereof. As during the initial calibration, the slope of the original transfer function is very close to 1. This indicates that the transfer function describes the observed data and does not over or under estimate it. The original function's value for A was 1.204 and the 90% adjustment was found as $A = 0.996$.

The reduction in slope between these two lines indicates that the 90% adjustment underestimates the observed data. Table 4.12 shows a summary of the results obtained for the different reliability levels of the transfer function. The adjusted function's trend line and coefficient of variance are shown in L.1 in Appendix L for 50%, 80%, 90% and 95% reliability.

Similar adjustments were made to predict the actual data with 50% ,80% and 90% reliability. Figure

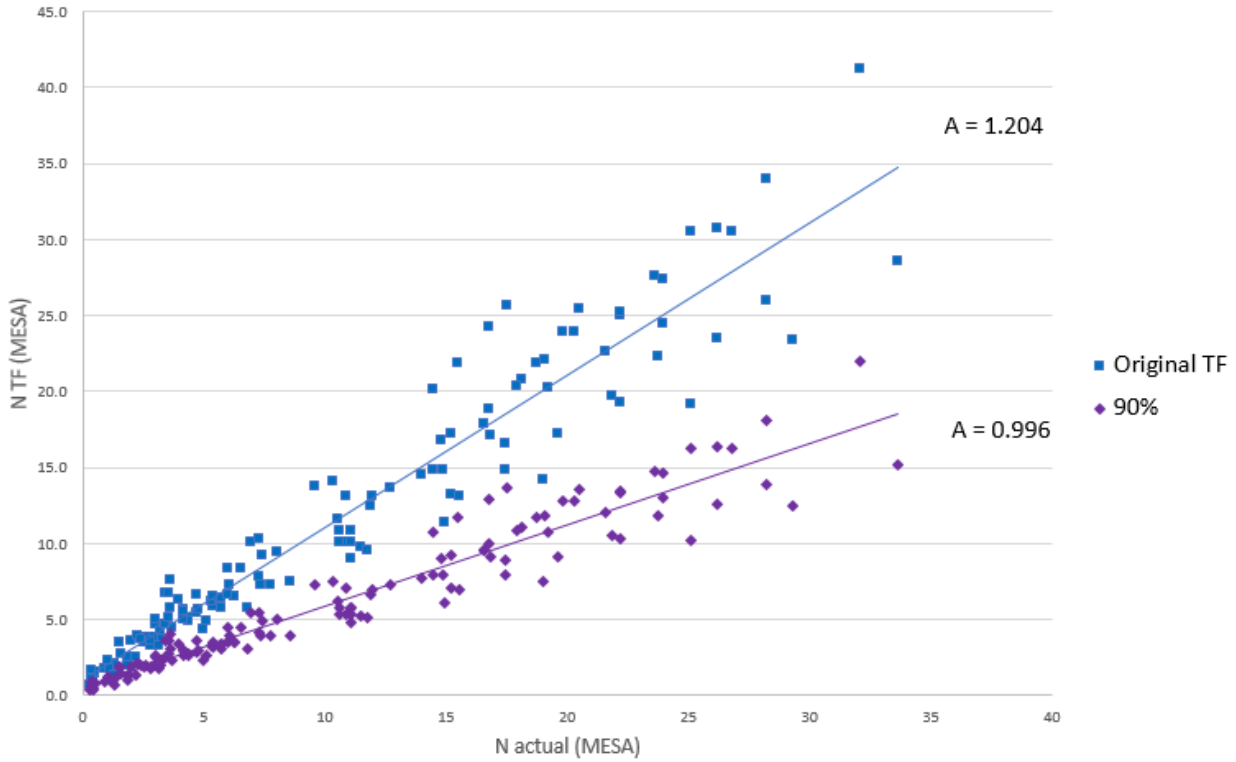

Figure 4.36: Transfer function estimates for the original function compared to 90% reliability

4.37 shows the relationship between the observed data and the transfer function's prediction at a reliability of 50% and 80%, while Figure 4.38 shows this at a reliability level of 50% compared to 95%. As is expected the values for the 80% prediction are well below that of the 50% prediction. Predictions for 95% reliability are also shown to be below those of 50%, 80% and 90%. This indicates that the transfer function underestimates the actual traffic for higher levels of reliability resulting in a more conservative function.

Table 4.12 shows the values obtained for the value of the constant A in the transfer function at different levels of reliability. The slope describes the relationship between the transfer function's output and the observed data used during calibration. A decrease in slope indicates that the function predicts that the material can sustain fewer standard axles than observed for the LTPP pavements. The intercept point of these lines reduced as the reliability increased. The lowering of the intercept point also indicates a lower result obtained from the transfer function. Due to the limited amount of data points, estimations could not be made precisely at the level of desired reliability. The table shows the actual reliability achieved for each of the desired levels.

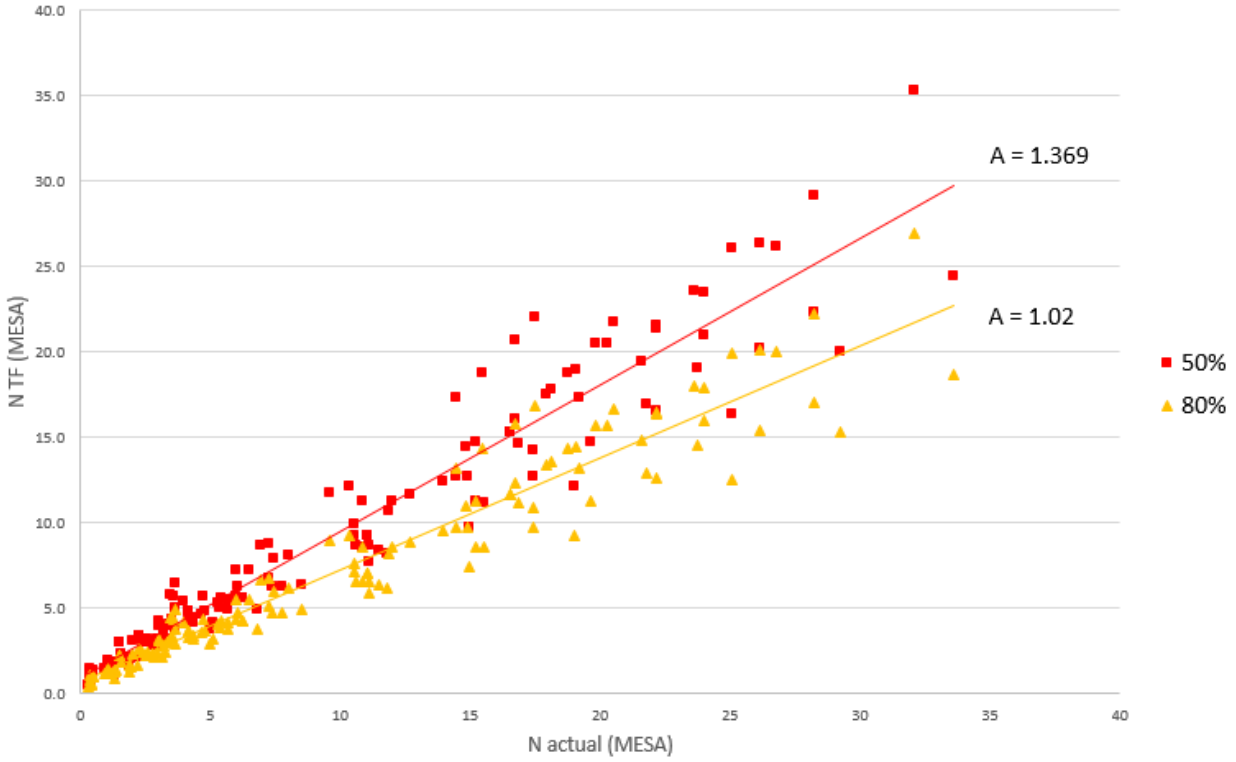

Figure 4.37: Transfer function estimates at 50% and 80% reliability

The correlation coefficient was determined for each of the levels of reliability. The results shown in Table 4.12 indicate that the correlation remains constant at all of the levels of reliability. This indicates that the function describes the significance of the material properties similarly for each of the levels of reliability.

It also indicates that the values were reduced over the whole spectrum of permanent strain values. Therefore, the certainty adjustment refines the transfer function's results equally for all stages of the material's life and it does not alter the significance of the material properties.

Table 4.12: Summary of reliability adjustments

Reliability	A	Slope	Intercept	R^2	Actual reliability (%)
Original	1.2044	1.001	1.06	0.927	21.7
50%	1.1369	0.856	0.91	0.927	50.7
80%	1.0198	0.656	0.66	0.927	81.2
90%	0.9312	0.533	0.57	0.927	90.6
95%	0.8436	0.436	0.46	0.927	96.4

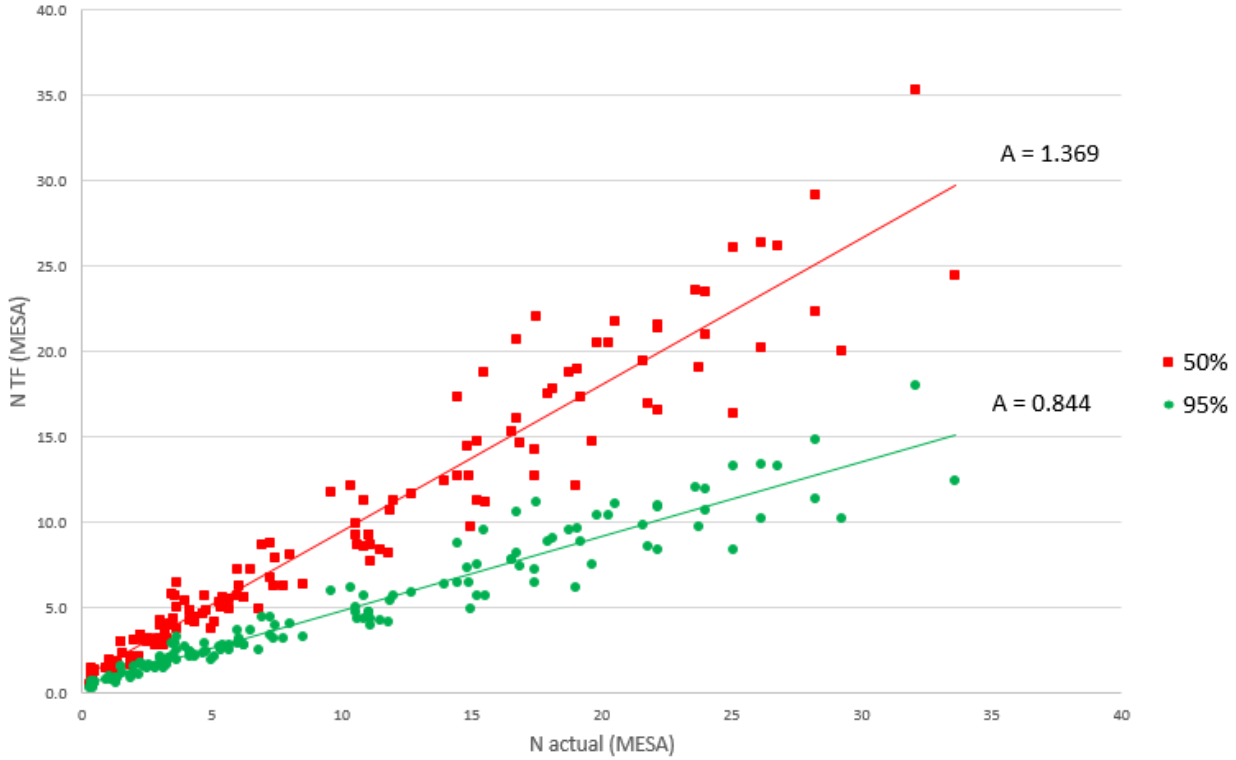

Figure 4.38: Transfer function estimates at 50% and 95% reliability

Permanent strain development predicted by the transfer function at the different levels of reliability was investigated. Figure 4.39 shows the development of the permanent strain on a log-log scale. Trendlines were drawn trough the transfer function prediction at reliability levels of 50%, 80%, 90% and 95%.

Figure 4.39 emphasizes the effect of the reliability adjustments and the constant relationship. The long-term slope of these lines show a good correlation with the observed permanent strain. This slope remains constant for all the reliability levels, indicating that there is no difference in the description of long permanent strain development in BSM. The only difference is that the values the function predicts decrease as the level of reliability increases.

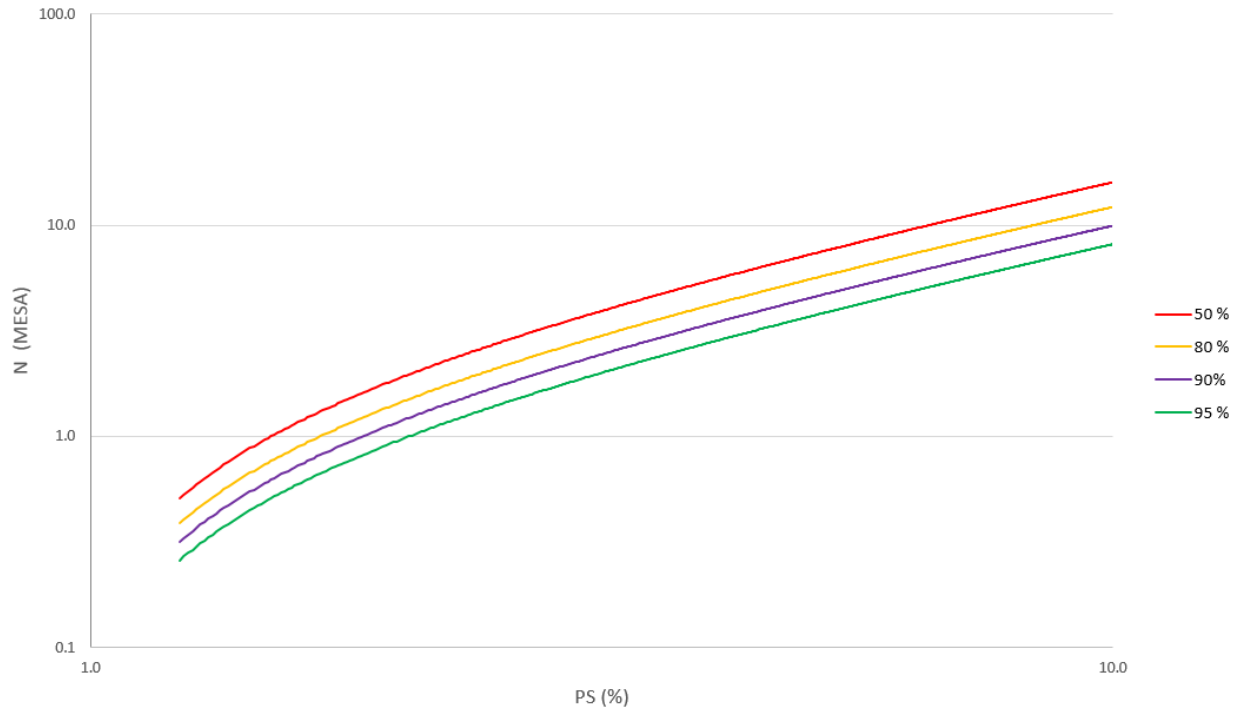

Figure 4.39: Transfer function PS development at different levels of reliability compared to N_{Actual}

4.7 Summary

Chapter 4 is summarized as follows:

1. The results and interpretation of the FWD results were given in this chapter. Focus was placed on the maximum deflection measurements and BLI. These parameters were used to divide the N7 into uniform sections using the cumulative sum method.

2. Mr values were back calculated for the N7 and LTPP pavements. Mr values were assigned for each of the uniform section identified on the N7 highway. The BSM layers on the N7 indicated a very stiff response. Stiffness values were also assigned for each layer of each LTPP pavement structure.

3. The results from the monotonic and dynamic triaxial tests were investigated. The dynamic triaxial results confirmed the stiff response from the FWD testing. The monotonic triaxial results showed cohesion and friction that were higher than expected for a BSM.

4. Each pavement was modelled in Rubicon Toolbox to determine the DSR imposed by a standard axle load. Retained cohesion values were assumed based on material classification data for the LTPP pavements. Density values and layer thicknesses were based on the available reports for the long term studies.

5. The observed deformation data was extrapolated using the Huurman model to a maximum deformation of 10% of the BSM layer thickness. The transfer function's predictions were compared to corresponding permanent strain levels. The transfer function was then calibrated to describe the observed data as accurately as possible.

6. The transfer function was adjusted to meet the design criteria regarding reliability levels.

Chapter 5

Transfer function validation

The new transfer function for BSMs was calibrated and adjusted to describe bitumen stabilised materials according to design methods' levels of reliability. This function was shown to predict the data used during the calibration with a high degree of accuracy. Validation of the new transfer function is covered in this section. Figure 5.1 shows the layout of this chapter.

In order to determine the function's ability to predict the performance of BSMs in general, the N7 highway was analysed using this transfer function. The N7 highway was not used during the calibration of the transfer function, therefore, this analysis would provide insight into the function's accuracy and precision when predicting new data. Validation of the transfer function using data obtained from the N7 highway is discussed in Section 5.1.

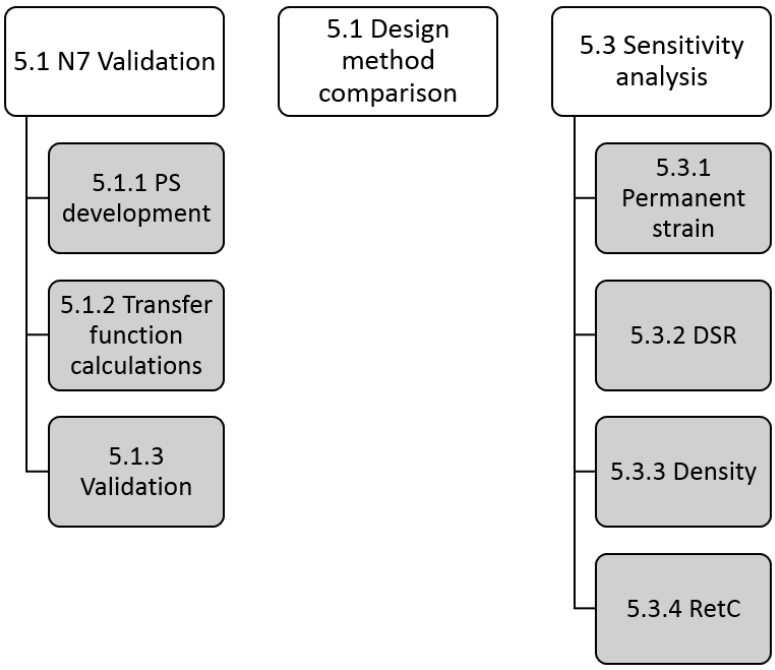

Figure 5.1: Chapter 5 layout

During calibration of the new transfer function, the significance of each of the four variables were described by three constants: B, C and D. These constants control the effect the variables have on the transfer function's results. The function's sensitivity to these variables (controlled by the constants) was investigated and is discussed in Section 5.3.

The aim of this analysis was to determine if the change of the four variables affect the transfer function in a way that reflects what is expected of BSMs. The relative effects of the variables were also investigated to ensure that they were within reason.

5.1 N7 validation

The new BSM transfer function was tested against the data obtained from the N7 highway. By comparing the permanent strain prediction to the observed behaviour of this road, the function could be validated. The transfer function was therefore tested with a data set that was not part of the calibration of the function. The transfer function was validated by using the same methods used during calibration, but not adjusting the function. The function's prediction was compared to the observed data. Where the transfer function did not predict the values accurately, the properties of the materials were investigated to determine the reason for the inaccuracy.

The N7 was chosen as the validation values for two reasons. Firstly, the information available for the N7 was more comprehensive than any of the LTPP data. A large number of FWD tests, conducted at different points in time, were available for this pavement. Test pits were also dug and accurate material classifications and layer thicknesses could be obtained. Cores were also drilled from the N7 for triaxial testing, which produced data on the shear properties and stiffness of the BSM layer. The large body of data available made it possible to investigate the cause of variable and inaccurate results obtained from the transfer function.

The high Mr values and cohesion values obtained from testing of the N7 BSM cores was suspected be a result of excess cement or poor mixing during construction. This was confirmed during investigation of the test pits using phenolphthalein to determine if active cement was present in the base layer. Figure 5.2 shows a solid BSM sample taken from the N7 and sprayed with phenolphthalein. The bright pink colour indicate a significant amount of active cement present in the BSM layer. At other locations, trenches dug across the slow lanes were also tested for active cement and no traces were found. This indicated a considerable amount of variability in the quality of construction of the BSM.

Secondly, it was known that this pavement had a very stiff response. From materials investigation and laboratory tests it was concluded that the behaviour of the base layer was not typical for a BSM. The stiffness values were much higher than expected. The shear properties obtained from the triaxial testing also showed values that were much higher than expected. The reason for this stiff behaviour could be due to excessive cement in the mix or poor mixing of the cement during construction. This would result in local areas with a very high cement content and consequently high stiffness values. The high values obtained from the FWD back calculations were confirmed with the results from the Dynamic triaxial testing.

Figure 5.2: N7 BSM sample sprayed with phenolphthalein indicating active cement

Despite the challenges with the nature of the BSMs formulation and behaviour, the N7 data was used to validate the transfer function. The locations where the BSM resilient modulus was very high or the shear properties were greater than expected were usually defined in a specific uniform section with known material properties. These cause a significantly reduced DSR imposed by traffic loading. Therefore, it was expected that the transfer function's predictions would overestimate the life of the material. This overestimation would be significant as the transfer function is weighed to the DSR by the power 3 applied to the variable.

If the transfer function's predictions were inaccurate for a material not typical for a BSM, it would indicate that it was sensitive to the material properties. This process provided valuable insight into the problems the transfer function may have and could indicate upper and lower limits for the four variables.

The aim of the validation was to compare the values obtained from the transfer function for each uniform section with the values obtained from the actual traffic and permanent strain measurements. The actual permanent strain and traffic data are discussed in Section 5.1.1. The allocation of material properties and pavement modelling to determine the deviator stress ratio are discussed in Section 5.1.2. Finally the comparison of the transfer function's prediction and the actual data are discussed in Section 5.1.3.

5.1.1 N7 Permanent strain development

The permanent strain development in the BSM was determined using the rutting data for each uniform section. It was assumed that 80% of the rutting occurred in the BSM layer. The permanent strain in the BSM layer was calculated as 80% of the rutting divided by the layer thickness and converted to a percentage value. The permanent strain was extended in the same manner as for the LTPP pavements to reach a PS value of 10% of the layer thickness. The traffic data was extended using the Huurman model fitted to the original values.

These values were extended to enable easy comparison between the results obtained from different uniform sections. The results of the traffic extrapolation are shown in Table N.1 for the three uniform sections on the Northbound carriageway. Table N.2 and Table N.3 in Appendix N show the results of the extrapolation for the eight uniform sections on the Southbound carriageway. The traffic and permanent strain values used for these results are discussed in Section 3.2.3.2.

5.1.2 N7 Transfer function prediction

In order to obtain representative results from the transfer function, values representing the different uniform sections were required. The information required was the density, retained cohesion, permanent strain and the deviator stress ratio. These variables were used to determine the life of the BSM for each uniform section at different times in its design life. Table 5.1 shows a summary of input values for the transfer function for each uniform section.

5.1.2.1 Retained cohesion

Because little information was available for the moisture susceptibility of the mix, it was assumed that the retained cohesion was 75% for all the uniform sections. By keeping these values constant, the effect of moisture susceptibility was mostly ignored. The transfer function's sensitivity was investigated in Section 5.3.4.

5.1.2.2 Permanent strain

The permanent strain used during the calculations varied from 0% to 10%. The different permanent strain values enabled a comparison between accumulated traffic and traffic estimation using the transfer function. The permanent strain values are discussed in Section 5.1.1, while the comparison between accumulated and remaining strain is explained in Section 3.7.1.

Table 5.1: Summary of transfer function input values for N7 validation

Section	C (kPa)	ϕ (°)	BSM MR (Mpa)	DSR (-)	RetC (%)	P.mod (%)
SB 1	171.14	47.71	820	0.278	75	97.5
SB 2	171.14	47.71	1387	0.287	75	98.3
SB 3	171.14	47.71	694	0.308	75	103
SB 4	171.14	47.71	1345	0.291	75	98.3
SB 5	171.14	47.71	664	0.301	75	95
SB 6	171.14	47.71	1095	0.3	75	95
SB 7	171.14	47.71	526	0.322	75	95
SB 8	171.14	47.71	768	0.285	75	98
NB 1	171.14	47.71	775	0.308	75	97.3
NB 2	347.95	40.66	1788	0.184	75	99.1
NB 3	347.95	40.66	1349	0.181	75	98

5.1.2.3 Density

The density for each uniform section was based on data obtained from test pits dug from July to August of 2017. The values assigned to each uniform section were chosen as the average of the different locations in the specific uniform section.

The density values were assumed to be constant throughout the life of the pavement structure. This assumption is not physically accurate as the permanent deformation increases the density of the material. The values assigned to each uniform section are shown in Table 5.1 as a percentage of Modified AASHTO density. Densities in most cases were reasonable, however, the values for uniform sections 5, 6 and 7 were lower than the average at 95%. The effect of these low density values were investigated in Section 5.1.3.

5.1.2.4 DSR

The final variable required for the transfer function was the deviator stress ratio. This ratio is dependent on the pavement structure, layer stiffnesses and the BSM's shear properties. Rubicon Toolbox was used to calculate the DSR for each of the uniform sections. The pavement structures

modelled in Rubicon Toolbox were similar to the structures used for back calculations in Section 3.4.2.

The layer thicknesses were based on observations made during the N7 investigations. Layer thicknesses were measured at each test pit and trench dug in the slow lane. Layer thicknesses used during the modelling in Rubicon are shown in Table O.2 for the Southbound carriageway and in Table O.1 for the Northbound carriageway (Appendix O).

Layer stiffnesses were based on back calculation of FWD tests performed in 2016. The back caculation results were discussed in Section 4.3.2. In certain cases the back calculated resilient modulus for the subgrade was unreasonably high. Therefore, the resilient modulus values for these layers were reduced based on the material classification. The average back calculated layer stiffnesses were used for each uniform section. Table O.2 and Table O.1 show the layer stiffnesses used to model the pavement structures.

Layer stiffnesses for the BSMs of each uniform section are shown in 5.1. The resilient modulus of the base layer is shown in this table as it is critical in the BSMs performance. This value was investigated with the transfer function's prediction values in Section 5.1.3.

Finally the cohesion (C) and friction angle (ϕ) values were required to determine the deviator stress ratio. The shear properties were based on the results obtained from monotonic triaxial tests conducted on the N7 cores. The results of the triaxial testing on these cores are discussed in Section 4.4. As limited cores from only a small number of locations were available, the results were not very reliable and should be interpreted with this in mind.

The monotonic triaxial results showed very high cohesion and friction angle values. These values were in most cases much higher than expected from a BSM. These large values would increase the size of the failure envelope and result in a small DSR. The small DSR value would in turn result in an overestimation from the transfer function.

The cohesion and friction angle for all foam stabilised uniform sections were selected as $C = 171.1$ kPa and $\phi = 47.7°$. These values were the results obtained from the cores drilled on the Southbound carriageway at km 10.5. It was observed that the by using the values obtained from the triaxial testing, the transfer function predicted results that were unreasonable. In an attempt to mitigate this over estimation, lower values were selected to represent a typical BSM. By assuming the low values, the effect of the other variables could also be investigated. The use of the other values was

investigated in Section 5.1.3. The cohesion is slightly lower than the design criteria for a BSM 1 and the friction angle is larger.

The shear properties used for for the two emulsion stabilised uniform sections were based on the cores tested from km 16 on the Northbound carriageway. The overall results obtained from the emulsion stabilised cores were very high and not representative of a BSM. The cohesion used for further calculation was $c = 347.95$ kPa and the $\phi = 40.66°$. The cohesion value is much larger than for a typical BSM and the resultant DSR was also very small. The shear properties used for each uniform section are shown in Table 5.1.

5.1.2.5 DSR results

Rubicon was used to calculate the DSR for each of the uniform sections. The pavement structures, layer stiffnesses and the shear properties for each section are shown in Table O.2 and Table O.1. The load was selected as a standard 80 kN dual wheel axle with a 350 mm spacing.

The DSR calculations were carried out and the results are shown in Table 5.1. The results of the foam sections were reasonable, but only due to the low values selected for the shear properties. When the actual cohesion and friction angle was used, the unreasonable results overshadowed any effect of the other variables. The DSR values obtained for the emulsion stabilised section were very low. These low values are due to the high shear properties obtained from the triaxial testing.

5.1.3 N7 Validation

The aim of the calibration was to compare the values obtained from the transfer function for each uniform section with the values obtained from the actual traffic and permanent strain measurements. The transfer function input values for each uniform section are shown in 5.1. These values were used to determine the permanent strain accumulation according to the transfer function.

The results obtained from the transfer function were compared to the actual traffic data for each of the uniform sections. The results obtained from the transfer function are shown in Tables P.1 to P.3 in Appendix P. Figures 5.4 and 5.5 graphically illustrate this comparison for the eight uniform sections on the Southbound carriageway and Figure 5.7 for the Northbound sections. The comparison between actual traffic and the transfer function's results was investigated.

5.1.3.1 Uniform Section N7 SB1

The transfer function's results for Uniform Section 1 on the Southbound are given in Table P.2 an illustrated in Figure 5.4. The figure shows that the transfer function predicts the long-term permanent deformation slope accurately. The absolute values at 10% permanent strain were 28.9 MESA from actual predictions and 34.6 MESA using the transfer function. This prediction was relatively accurate and the performance of this section was well described by the transfer function.

The shear properties and density assigned to this uniform section were reasonable and representative of a typical BSM. The resilient modulus value determined for the BSM layer was 820 MPa. This was deemed to be a reasonable resilient modulus for the BSM and realistic results from the transfer function were expected.

5.1.3.2 Uniform Section N7 SB2

Figure 5.4 shows the transfer function's prediction for Uniform Section 2 on the Southbound carriageway. From initial inspection it is clear that the transfer function underestimates the actual traffic. However, the long-term rate of permanent deformation accumulation, indicated by the slopes of the two lines, indicates a good correlation.

The maximum number of load repetitions predicted by the transfer function was 29.5 MESA, while the actual data suggests 40.9. This is a significant difference, therefore the transfer function's prediction of this section's behaviour was not as satisfactory as the previous section.

The density and shear properties used for this section were realistic and representative of a typical BSM. The resilient modulus of the BSM layer back calculated for this section was 1387 MPa. The resilient modulus value is higher than that of a typical BSM. The difference between the base layer stiffness and the resilient modulus of the subbase (462 MPa) was quite significant. The high resilient modulus of the base layer together with this difference in resilient modulus would attract more stress to the base layer. The increase in stress leads to an increase in DSR which explains the underestimation of the transfer function.

5.1.3.3 Uniform Section N7 SB3

Figure 5.4 shows the transfer function's prediction for Uniform Section 3 on the Southbound carriageway. The figure shows a very good prediction with only a relatively small underestimation of the maximum values. The resilient modulus of the BSM was back calculated as 694 MPa which is typical of a BSM. Reasonable values were used for the cohesion and friction angle as well. The

density was determined as 103% of MOD AASHTO density. This high density value might be an overestimation of the average density.

5.1.3.4 Uniform Section N7 SB4

The transfer function's prediction of Uniform Section 4 on the Southbound carriageway is shown in Figure 5.4. This figures shows a good prediction of the long-term permanent deformation accumulation rate. However, the transfer function underestimates the life of the pavement. The cohesion and friction angle used for this uniform section were the same as the previous three sections and were regarded as realistic values to represent a BSM. The DSR value calculated for this uniform section was also within reason. The density was used as 98.3% of MOD AASHTO density.

5.1.3.5 Uniform Section N7 SB5

Figure 5.5 shows the transfer function's prediction for Uniform Section 5 on the Southbound carriageway. It is immediately clear that the transfer function significantly underestimates the life of the base layer. The cohesion and friction angle used for this section were reasonable and the DSR results were also realistic. Layer stiffnesses for the pavement structure were also representative of a BSM.

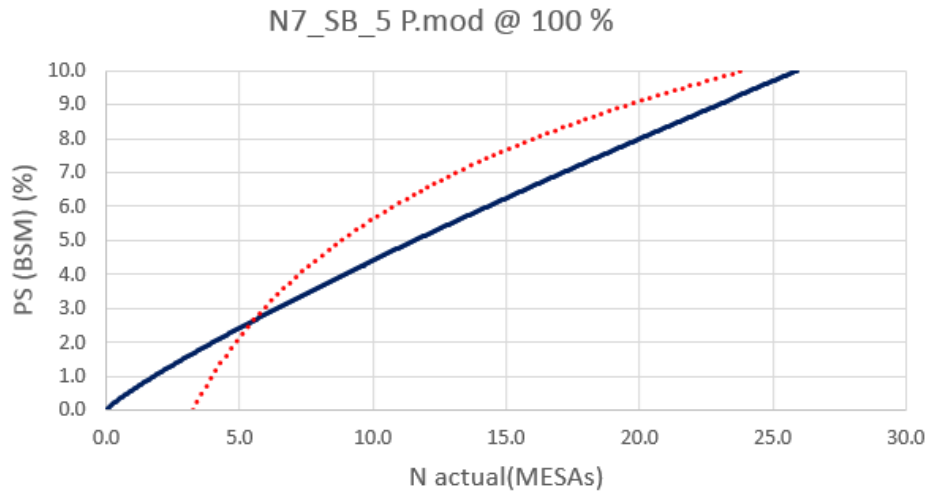

Figure 5.3: N7 Southbound Uniform Section 5 with adjusted density

The reason for the transfer function's underestimation was found to be the value for density. The value obtained from the materials testing showed that the density was 95% of MOD AASHTO density. This is a very low density for a material that has been in service for 15 years with a resilient modulus of 664 MPa. To confirm that the density was the reason for the underestimation,

the calculations were repeated at a density of 100% of MOD AASHTO density.

Figure 5.3 shows the transfer function's prediction for Uniform Section 5 with the density increased to 100% of MOD AASHTO density. This figure shows a much better prediction and indicates that the densities obtained from the materials testing may not represent the average of the uniform section.

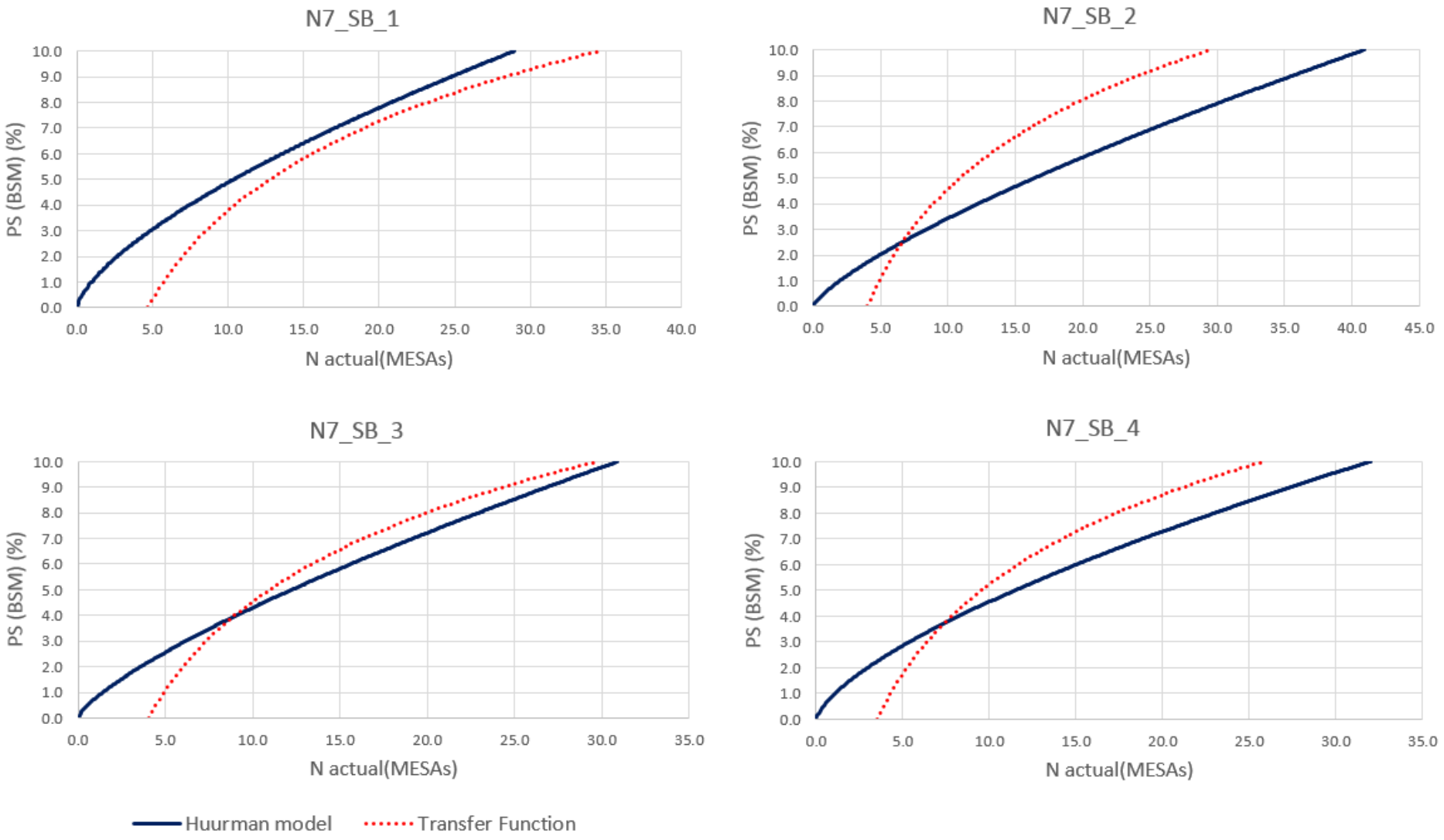

Figure 5.4: N7 Southbound: Transfer function prediction of permanent strain accumulation (1)

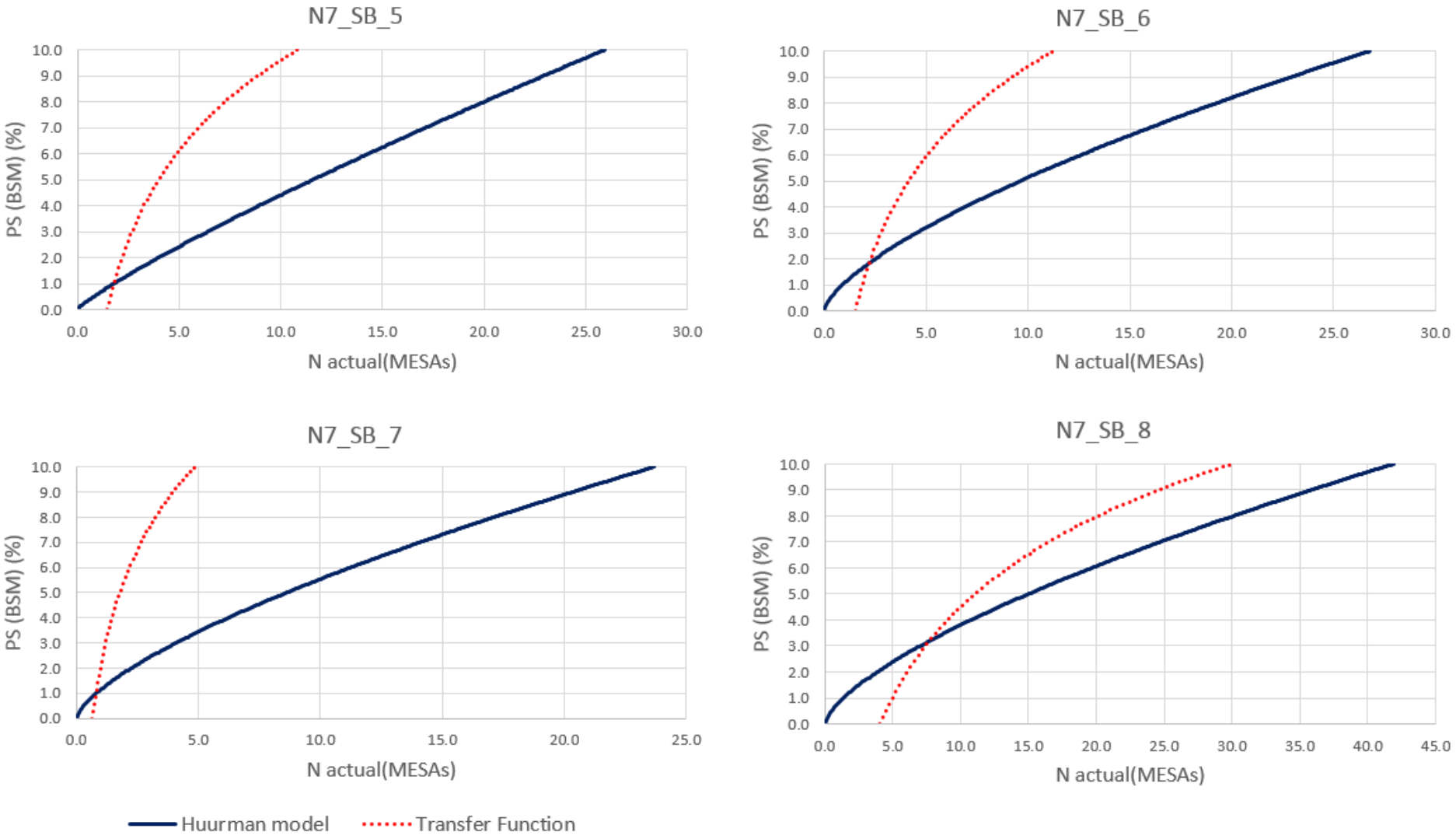

Figure 5.5: N7 Southbound: Transfer function prediction of permanent strain accumulation (2)

5.1.3.6 Uniform Section N7 SB6

Figure 5.5 shows the transfer function's prediction of the life of Uniform Section 6 on the Southbound carriageway. The results for this uniform section are very similar to those of Uniform Section 5. The cohesion, friction angle and density for Uniform Section 6 were the same as for Uniform Section 5. The significant difference between the two uniform sections was the BSM layer stiffness.

Uniform Section 6 had an average BSM resilient modulus of 1095 MPa, while Uniform Section 5 had an average resilient modulus of 664. The higher resilient modulus of Uniform Section 6 is still reasonable and can be considered representative of a stiff BSM layer. This increase in resilient modulus was observed for all layers in the pavement structure. The DSR calculated was 0.301 which did not change significantly from Uniform Section 5. The DSR did not change much due to similar ratios between layer stiffnesses.

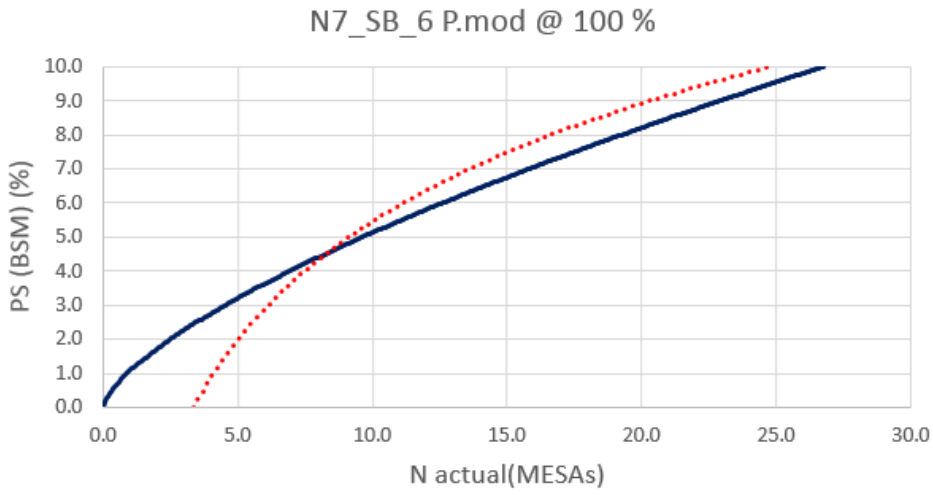

Figure 5.6: N7 Southbound Uniform Section 6 with adjusted density

The underestimation was also found to be due to the low density. The density obtained from materials investigation was found to be 95% of MOD AASHTO density. The effect of density was investigated by adjusting it to 100% of MOD AASHTO density as shown in Figure 5.6. This transfer function's prediction was very accurate after this adjustment. This may be due to an unrepresentative value for the density for a very stiff material after fifteen years of service.

5.1.3.7 Uniform Section N7 SB7

Figure 5.5 shows the transfer function's prediction for Uniform Section 7 of the Southbound carriageway. The transfer function predicts the life of the pavement as much shorter than the traffic it has already accommodated. The shear properties were similar to those of the previous sections on the Southbound carriageway. The density assigned to this uniform section was 95% of MOD AASHTO. The density was considered very low and had a significant effect on the transfer function's prediction.

Further investigation into this uniform section showed that pavement structure was much weaker than any other uniform section investigated on the N7. The lower resilient modulus may be a result of poor support conditions which were indicated by low resilient modulus values for the subbase and subgrade obtained from back calculations. The base layer, 205 mm thick, was also significantly thinner than in the other uniform sections. This uniform section was also deemed to be in a relatively poor condition compared to the other pavement structures.

The overall weaker pavement structure and relatively thin BSM layer resulted in increased stress in the base layer. The DSR for this uniform section was calculated as 0.322. The high DSR value together with the low density of the BSM layer explains the underestimation of the pavement's life. This confirms that the transfer function is sensitive to weaker pavement structures and inadequate compaction efforts.

5.1.3.8 Uniform Section N7 SB8

Figure 5.5 shows the permanent deformation predictions for Uniform Section 8 on the Southbound carriageway. The transfer function predicts the development of permanent strain of this section very well, but underestimates the maximum number of load repetitions the pavement can sustain. The cohesion and friction angle for this section were the same as the rest of the foam sections and represent a typical BSM. The layer stiffnesses were also reasonable with the resilient modulus of the base layer calculated as 769 MPa.

The deviator stress ratio in the BSM was calculated as 0.285 which indicates a good life for the base layer. The underestimation of permanent strain by the transfer function can be due to the low density. The density obtained from the materials investigation was found to be 98% of MOD AASHTO density. This value is lower than expected and a large improvement was found for the same calculations at a density of 100% of Modified AASHTO density. The transfer function's sensitivity to density is discussed in Section 5.3.3.

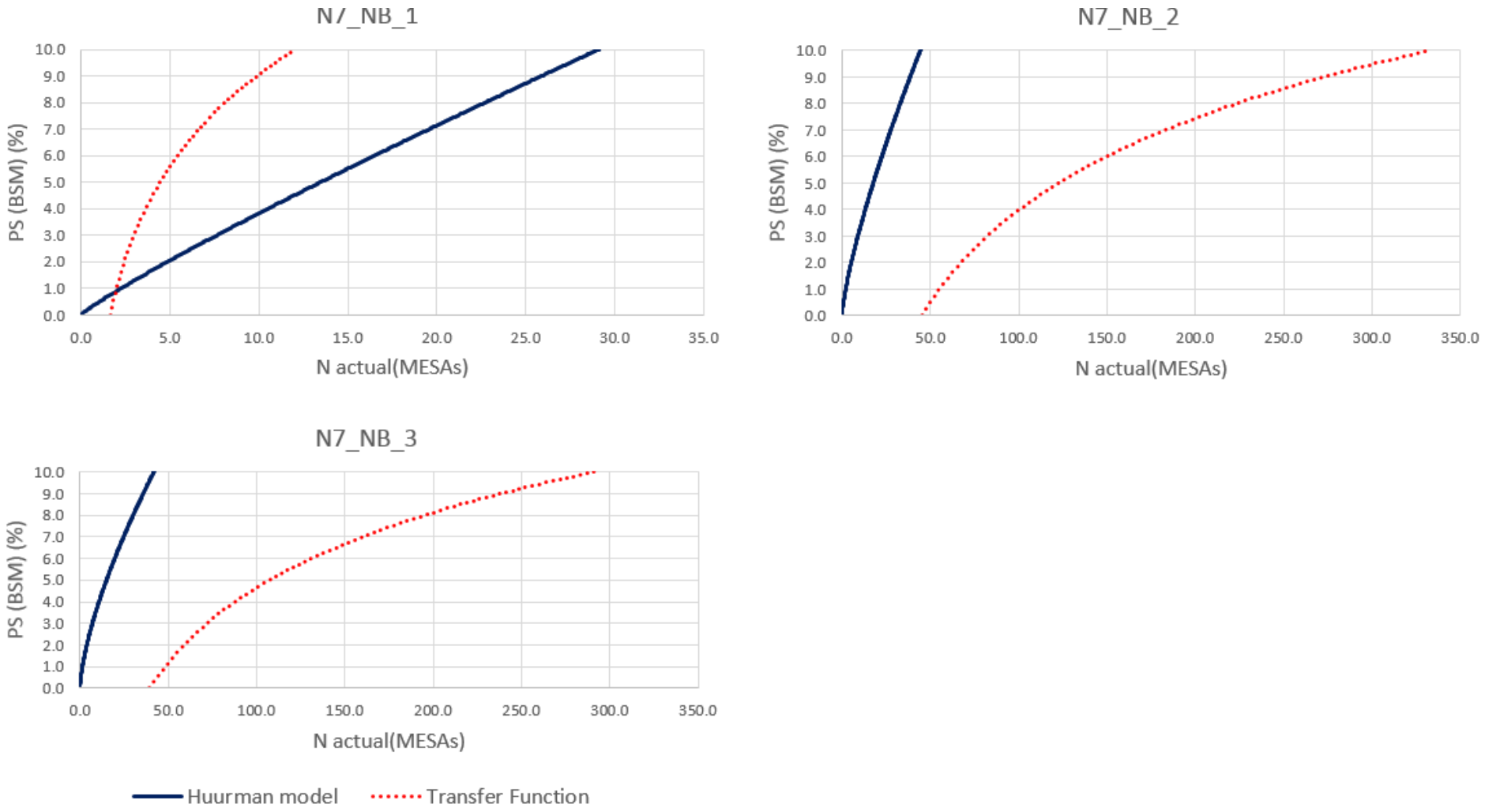

Figure 5.7: N7 Northbound: Transfer function prediction of permanent strain accumulation

5.1.3.9 Uniform Section N7 NB1

Figure 5.7 shows the permanent strain prediction for the Uniform Section 1 on the Northbound carriageway. The results obtained from the life calculations are given in Table P.1. This section utilized foam bitumen and was 5400 m in length. The shear properties selected were similar to the Southbound sections which also utilized a foam stabilised base layer.

Back calculations showed a stiff pavement structure with an average BSM thickness of 775 MPa. The pavement was modelled and the DSR calculated as 0.308. These results were reasonable and represent typical values for a BSM. The density was determined as 97.3%, which is very low for a BSM with a high resilient modulus which has been trafficked for fifteen years.

The comparison between the transfer function's prediction and the actual data shows that the transfer function underestimates the life of the BSM. This underestimation is partly due to the low density value obtained for this uniform section. Another influence on the life was the relatively weak support layers in this section.

5.1.3.10 Uniform Section N7 NB2

Figure 5.7 shows the transfer function's traffic estimations of Uniform Section 2 on the Northbound carriageway. This section was constructed in 2007 and utilizes a BSM emulsion stabilised base layer. The shear properties obtained from triaxial testing showed a friction angle that is reasonable for a BSM. However, the cohesion values obtained from these tests were very high and did not represent a BSM. Stiffness values obtained from back calculations confirmed the stiff behaviour as the BSM had a resilient modulus of 1788 MPa. It was therefore expected that the transfer function will not accurately predict the life of this material.

The cohesion and friction angle used during the calculations were selected as 347.95 kPa and 40.66° respectively. These were values were obtained from the triaxial testing of cores obtained from km 16 on the Northbound carriageway. The results obtained for the other locations showed even higher values and would result in further overestimation of the material's life. The density used for the transfer function calculations was 99.1% of MOD AASHTO density.

The high values obtained for the shear properties resulted in a very low shear stress ratio induced by a standard axle load. The DSR was calculated as 0.184. This low value resulted in very high traffic estimations from the transfer function. It is clearly overestimating the life of the pavement by a great margin. The transfer function is clearly sensitive to the type of material. The results

obtained from materials testing in this section were not representative of a BSM.

This overestimation shows that the function is very sensitive to the DSR and in turn the shear properties of the BSM. Therefore, it is suggested that a lower limit should be set for the shear properties and the DSR. Limiting these values for design would prevent unrealistic results from the transfer function. Limiting the input values for the transfer function is discussed in Section 6.5.

5.1.3.11 Uniform Section N7 NB3

Figure 5.7 shows the permanent strain development prediction for Uniform Section 3 on the Northbound carriageway. Similar to Uniform Section 2, this section makes use of a bitumen emulsion stabilised base layer. The high cohesion and friction angle assigned to this section also resulted in very poor estimations. The back calculated layer stiffnesses were also very high, with an average BSM stiffness of 1349 MPa.

The high shear properties lead to a very low DSR, calculated to be 0.181. This low value explains the degree of overestimation observed for this section. It was therefore concluded that this material is not a typical BSM. These findings made it clear that the transfer function is specific to the material properties of BSMs. This function does not provide an accurate estimation if the material properties are not typical for BSMs.

5.2 Design method comparison

The new transfer function was validated by comparing its predicted life to that of the PN design method as well as the Loudon function. Five pavement structures with different materials were chosen as shown in Table 5.2. The aim of this comparison was to validate that the transfer function produced realistic estimates and to confirm lower estimates at higher levels of reliability.

The PN design method is a very limited method with specific requirements in terms of maximum stiffnesses and layer thicknesses. This method does not use the BSM's shear properties, density or moisture susceptibility. However, these factors are taken into account when defining the material as a BSM 1 or BSM 2. There is no method to change the standard axle load from an 80 kN axle to a 100 kN. Designs using this method determine a life for the pavement as a whole and not for the BSM specifically. The PN design method should only be used for designs up to 30 MESA. It is clear that this method is very limited and comparisons between the PN design method and the new transfer function only validate that the function produces realistic values.

Table 5.2: Design method example pavements

Pavement	Pavement Layer	Material Class	Thickness	Stiffness (Mpa)	BSM Properties	
1	Surfacing	HMA	50	2500	C (kPa)	250
	Base	BSM 1	300	540	ϕ (°)	40
	Subbase	G4	250	180	PS (%)	10
	Selected Subgrade	G8	200	100	RetC (%)	75
	Subgrade	G8	N/A	100	Pmod (%)	100
2	Surfacing	HMA	50	2250	C (kPa)	200
	Base	BSM 2	150	450	ϕ (°)	35
	Subbase	C4	200	400	PS (%)	10
	Selected Subgrade	G7	300	140	RetC (%)	75
	Subgrade	G8	N/A	93	Pmod (%)	100
3	Surfacing	Surface Seals	5	800	C (kPa)	250
	Base	BSM 1	200	600	ϕ (°)	40
	Subbase	C3	250	550	PS (%)	10
	Selected Subgrade	G7	300	140	RetC (%)	75
	Subgrade	G8	N/A	97	Pmod (%)	100
4	Surfacing	HMA	50	2500	C (kPa)	250
	Base	BSM 1	300	600	ϕ (°)	40
	Subbase	C3	250	550	PS (%)	10
	Selected Subgrade	G6	300	180	RetC (%)	75
	Subgrade	G7	N/A	100	Pmod (%)	100
5	Surfacing	HMA	35	2500	C (kPa)	250
	Base	BSM 1	250	600	ϕ (°)	40
	Subbase	G5	250	252	PS (%)	10
	Selected Subgrade	G7	180	140	RetC (%)	75
	Subgrade	G8	N/A	94	Pmod (%)	100

The pavement structures shown in Table 5.2 were analysed using the PN design method for a category A road. These pavements were also modelled in Rubicon Toolbox to determine the DSR in the BSM layer. The traffic estimations according to the Loudon function was determined in Rubicon using a Relative Density (RD) of 84% and saturation of 50%. The DSR was calculated and used in the new transfer function to determine the life of the BSM.

The three design values obtained from this analysis are summarized in Table 5.3 for each of the example pavements. The pavements were analysed for a 80 kN standard axle as well as a 100 kN standard axle load. The transfer function was used at the four levels of reliability as discussed in Section 4.6.

Table 5.3: Comparison between PN method, Loudon and new Transfer Function for Road Category A to D

Pavement and load	Pavement life (MESA)					
	PN	Loudon	TF (A)	TF (B)	TF (C)	TF (D)
1 (80 kN)	30	85.06	52.13	63.79	78.22	102.43
1 (100 kN)	-	19.95	24.49	29.96	36.75	48.12
2 (80 kN)	4.31	0.027	0.06	0.08	0.10	0.12
2 (100 kN)	-	0.01	0.00	0.00	0.00	0.00
3 (80 kN)	10	13.87	19.76	24.17	29.64	38.81
3 (100 kN)	-	12.84	18.54	22.69	27.82	36.43
4 (80 kN)	30	86.78	52.13	63.79	78.22	102.43
4 (100 kN)	-	22.92	25.99	31.80	39.00	51.06
5 (80 kN)	13.80	5.35	10.43	12.76	15.64	20.49
5 (100 kN)	-	2.81	6.66	8.15	10.00	13.09

5.2.1 Example Pavement 1

Figure 5.8 shows the results for Example Pavement 1. This pavement consists of a 50 mm HMA surfacing layer and implements a 300 mm thick BSM 1 base layer. The base layer is supported by a granular subbase. The results showed that the PN design method predicted its maximum life at 30 MESA. For an 80 kN standard axle, the transfer function produced a larger number than the PN method at all levels of reliability. The values ranged from 52.13 to 102.43 MESA, which was deemed reasonable based on the material properties and thick BSM layer.

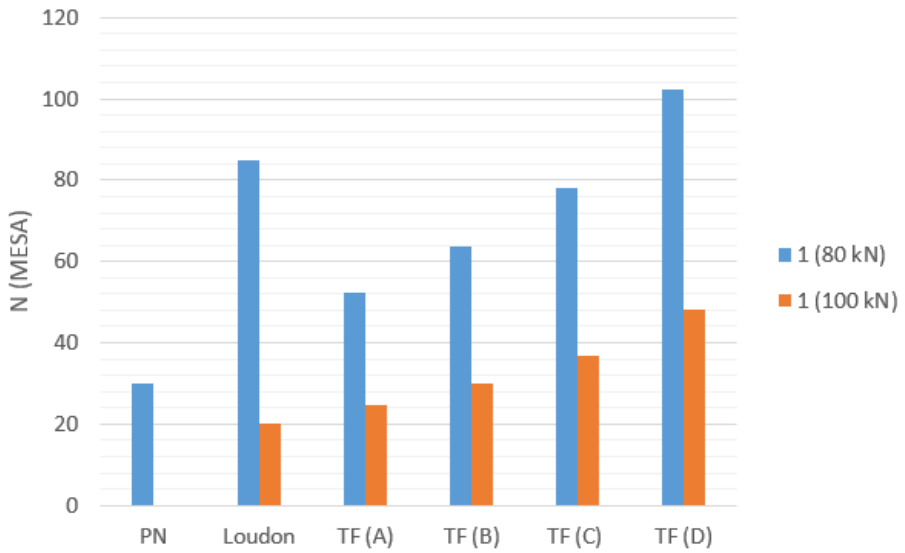

Figure 5.8: Design method comparison for Example Pavement 1

The new transfer function produced a lower estimation than the Loudon function for category A, B and C. However, for the increased load (100 kN) the transfer function produced slightly higher values. The transfer function showed a clear increase in design traffic at decreasing levels of reliability.

5.2.2 Example Pavement 2

Figure 5.9 shows the design methods' results for Example Pavement 2. This pavement consists of 50 mm HMA with a 150 mm BSM 2 base. The cohesion and friction angle for the base layer were 200 kPa and 35° respectively. The base layer was supported by a cement stabilised subbase.

The design results for this pavement show an acceptable design for low volume roads according to the PN design method. Both the Loudon transfer function and the new transfer function indicate that the BSM will fail almost immediately. This is due to the low shear properties assigned to the BSM 2 and the thin layer thickness. The thin layer and low shear properties result in a very high DSR and in turn a short life.

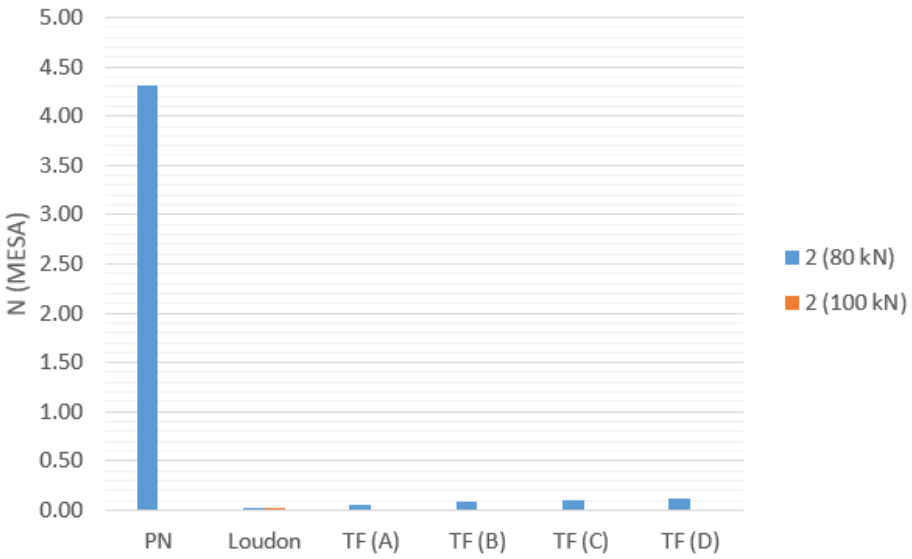

Figure 5.9: Design method comparison for Example Pavement 2

5.2.3 Example Pavement 3

Figure 5.10 shows the life predictions for Example Pavement 3. This pavement consisted of a single seal on a 200 mm BSM 1 base. The base layer was supported by a cement stabilised subbase. The PN design method predicted the life of the pavement as 10 MESA. This is a realistic value for a pavement with only a surface seal.

The Loudon transfer function predicted a life of 13.87 MESA for an 80 kN standard axle and 12.84 MESA for a 100 kN standard axle. The difference between these two values was lower than observed for the other pavement structures. This can be attributed to the good support under the BSM layer allowing sufficient load spreading through the structure.

The new transfer function predicted higher values for all levels of reliability than the PN design method as well as the Loudon function. The difference between the life for an 80 kN standard axle and a 100 kN standard axle was also very small. The values obtained from the new transfer function were regarded as realistic. The only problem with this pavement structure is that moisture can easily enter the pavement structure, reducing the life of the BSM.

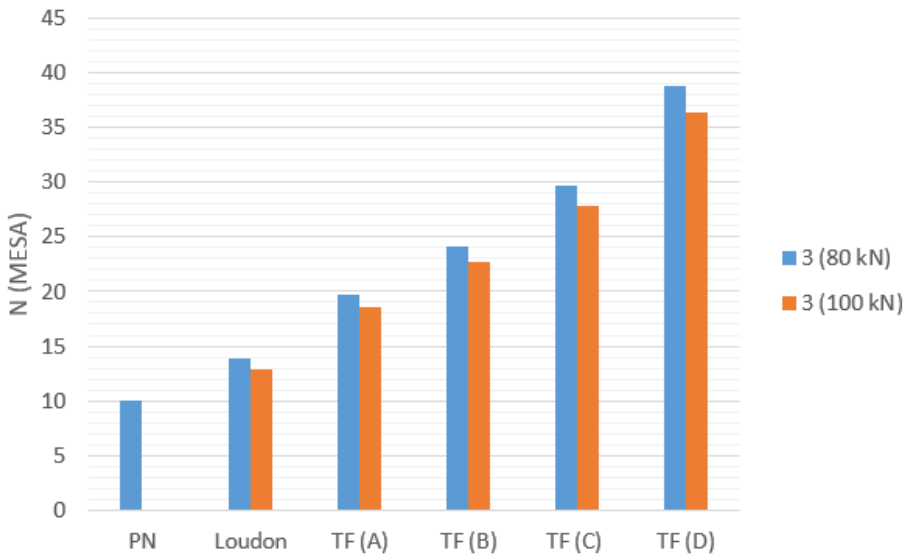

Figure 5.10: Design method comparison for Example Pavement 3

5.2.4 Example Pavement 4

Figure 5.11 shows the design method comparison for Example Pavement 4. This pavement consisted of a 50 mm asphalt layer on a 300 mm BSM 1 base layer. The base layer was supported by a 250 mm cement stabilised (C3) subbase. Due to the thick layers and high quality material, the PN design method resulted in the maximum design traffic of 30 MESA.

The Loudon transfer function showed very high results for the 80 kN standard axle at 56.78 MESA. However, this value dropped significantly when this load was increased to 100 kN. The design life for the 100 kN standard axle was calculated as 22.92 MESA. This significant difference indicates that the pavement structure is very sensitive to overloading.

The new transfer function also showed a significant sensitivity to overloading, although not to the same extent as the Loudon function. The new transfer function resulted in a design life ranging from 52.13 MESA for a Category A road to 102.43 MESA for a Category D road for an 80 kN standard axle. These values dropped to 25.99 MESA and 51.06 MESA respectively for the 100 kN standard axle.

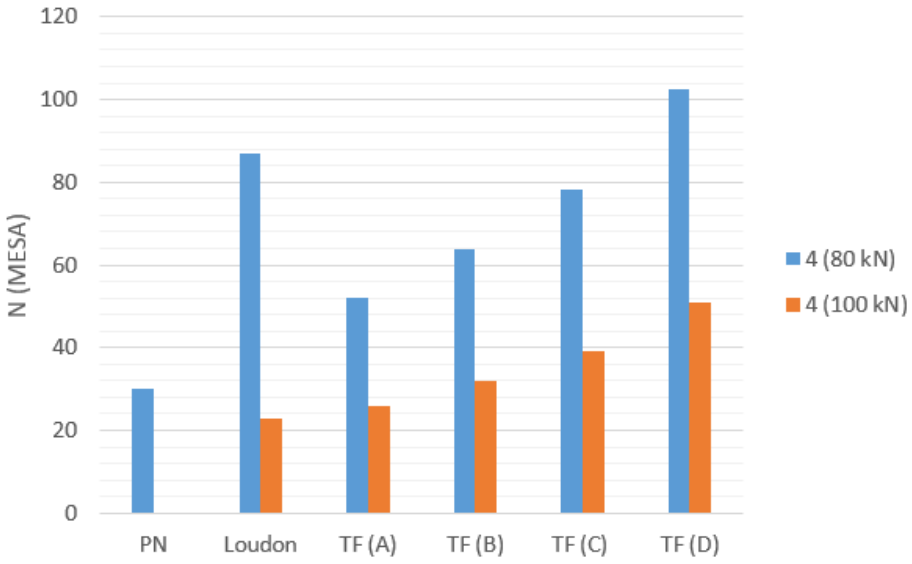

Figure 5.11: Design method comparison for Example Pavement 4

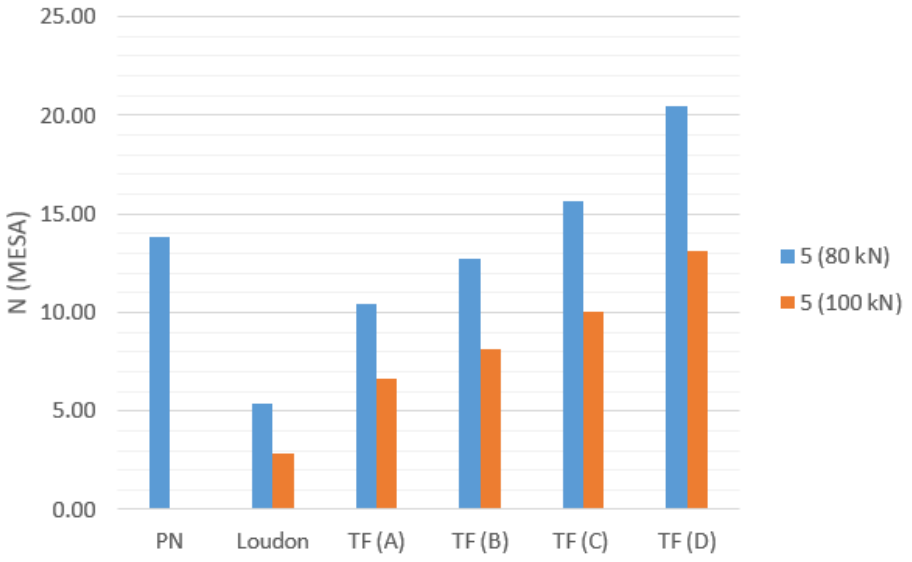

Figure 5.12: Design method comparison for Example Pavement 5

5.2.5 Example Pavement 5

Figure 5.12 shows the design life predictions for Example Pavement 5. This pavement consists of a 35 mm asphalt layer on a 250 mm BSM 1 base. The BSM layer is supported by a G5 granular subbase. This is an overall weaker structure compared to Example Pavement 4 and a lower design life was expected.

The PN design method indicated a design life of 13.8 MESA. This is typically a very conservative design method, but in this case shows higher estimates than the other two functions. This high value can be attributed to the layer thicknesses as this plays a large role in the design function. The base and subbase layers are both 250 mm thick and account for a significant amount of cover depth.

The transfer function showed realistic results for this section. The values were significantly lower than for Example Pavement 4 and can be attributed to the thinner asphalt layer, base and subbase. These thinner layer and weaker support for the base layer increase the DSR in the base layer induced by traffic loading.

5.2.6 Overall prediction

The PN design method is a conservative design method based on past experience. This method investigates the overall pavement structure and produces design traffic for the structure as a whole.

The Loudon transfer function is an unpublished, heuristically developed design model without explicit calibration references. Therefore, comparisons between the new BSM transfer function and these two methods are not accurate or representative of a good design function. These comparisons were made to get an overall impression of the function's predictions and to determine if the values were in the right order of magnitude.

From this comparison it was concluded that the transfer function produces values that are in the correct order of magnitude. The transfer function produced good design traffic estimations for most of the pavement structures. However, the transfer function predicts a very low design life for BSM 2 layers. This is due to the lower values for both cohesion and friction angle of BSMs. The minimum values for both values were used, which may be unrealistic for actual in field conditions.

5.3 New transfer function sensitivity analysis

The transfer function was calibrated using the LTPP data as described in Section 4.5. The calibrated transfer function for BSMs is given in Equation 4.2. The results obtained when using the new transfer function are dependant on four factors: density, moisture susceptibility, deviator stress ratio and permanent strain. The effect of these four factors and the function's sensitivity to these factors were investigated. The results of this investigation are discussed in this section.

5.3.1 Sensitivity to permanent strain

The transfer function's sensitivity to permanent strain was investigated and is discussed in this section. Figure 5.13 shows the number of standard axles over a range of stress ratios for PS values of 1%, 5%, 10% and 20%. These PS values represent the amount of deformation the layer can sustain before it fails. It was therefore expected that a higher amount of deformation allowed would yield higher amounts of load repetitions.

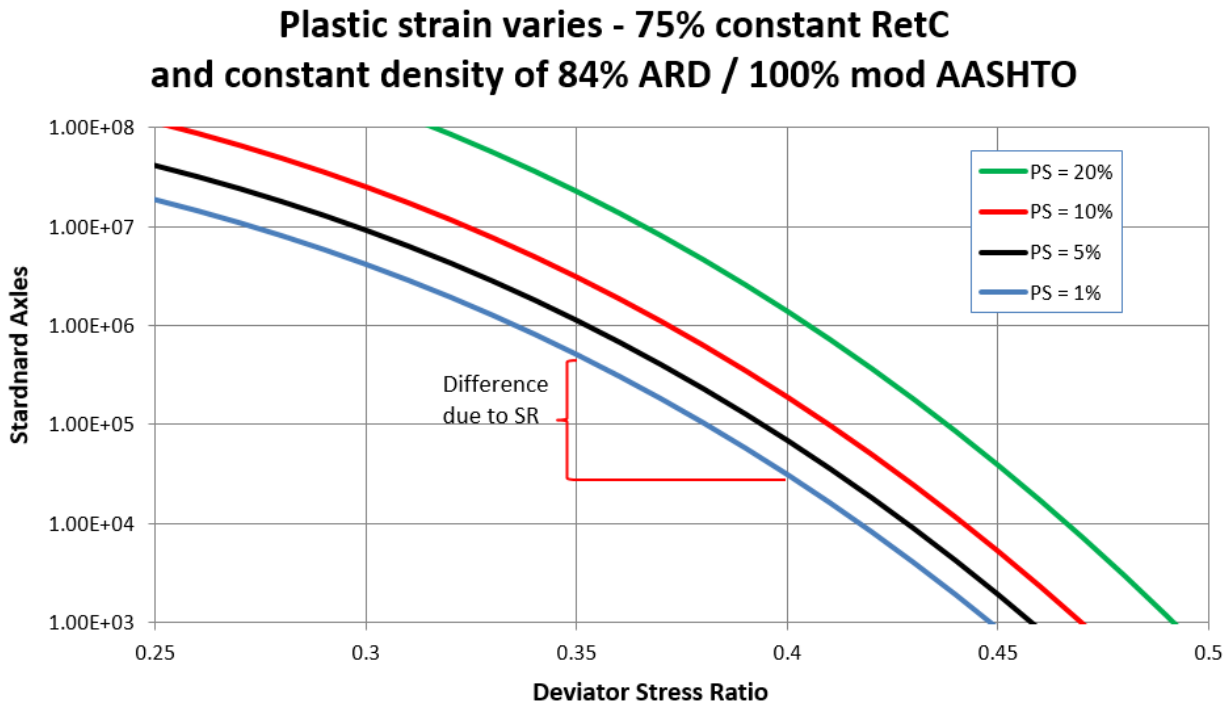

Figure 5.13: Transfer function sensitivity analysis: Permanent strain

The number of standard axles in Figures 5.13 to 5.15 is described using a logarithmic scale. Note that by illustrating the axles using a log scale, a difference in standard axles shown on the figure

between two points represents a significant difference in the absolute value. The values obtained and illustrated in Figure 5.13 were obtained by using constant values for RetC and Pmod and calculating the number of standard axles for 4 PS values over a range of stress ratios.

In Figure 5.13 the number of standard axles increases significantly with an increase in PS. The number of standard axles for an allowable deformation of 10% is much higher than for 1%. This was expected as an increase in the allowable deformation a pavement layer may sustain before failure would increase the number of standard axles the pavement can accommodate. This holds true for a constant density, retained cohesion and stress ratio. This shows that the transfer function behaves as expected with regards to the sensitivity to permanent strain.

The behaviour of the transfer function with regards to PS is as expected. However, the absolute values obtained would be different for each pavement structure and material. A good indication can be obtained by checking if the values are reasonable at a DSR of 0.3 to 0.35. The absolute values illustrated in this graph are within reason, but the function may be inaccurate when using a small amount of PS remaining. However, the long-term PS values were found to be more accurate and a good representation of the observed behaviour.

5.3.2 Sensitivity to deviator stress ratio

Figure 5.13 also shows the significant effect that the stress ratio has on the transfer function. The figure shows the difference in standard axles at 4 PS values over a range of deviator stress ratios. Considering that number of standard axles are shown on a log scale, this difference in stress ratio has a significant effect on the values obtained from the transfer function. The transfer function was developed to be sensitive to a change in DSR as a high DSR causes significant damage to the pavement structure and leads to a reduction in life. The transfer function's response to a change in DSR reflects the expected sensitivity of the material to the stress ratio.

The results obtained from the transfer function for stress ratios exceeding 0.35 show a rapid decline in life. At a stress ratio higher than 0.45 the transfer function's life prediction is very limited, in the order of 1 000 load repetitions. This response highlights the significant effect that DSR has on the material and the importance of this factor during design.

While the function declines rapidly with the increase of DSR, a reduction thereof shows a significant increase in life. At stress ratios lower than 0.25 the function returns very high values. Stress ratio is a function of the material's shear properties, the pavement structure and the load applied to the pavement. Factors like overloading or moisture penetrating the BSM can increase the DSR and in

turn reduce the life of a pavement. It is therefore important that realistic and conservative values are used for the DSR when using the new function.

5.3.3 Sensitivity to density

Figure 5.14 shows the transfer function's sensitivity to density (as a % of MOD AASHTO density). The figure shows the number of standard axles the transfer function produces for a constant PS and RetC values at four densities over a range of stress ratios. From this figure it is clear that the density of the material has an effect on the life of the pavement. The trend of this effect shows that an increase in density results in an increase in standard axles the pavement can sustain before failing. This behaviour reflects the expected and observed behaviour of BSMs, therefore, the transfer function takes the change in density into account in a predictable and realistic manner.

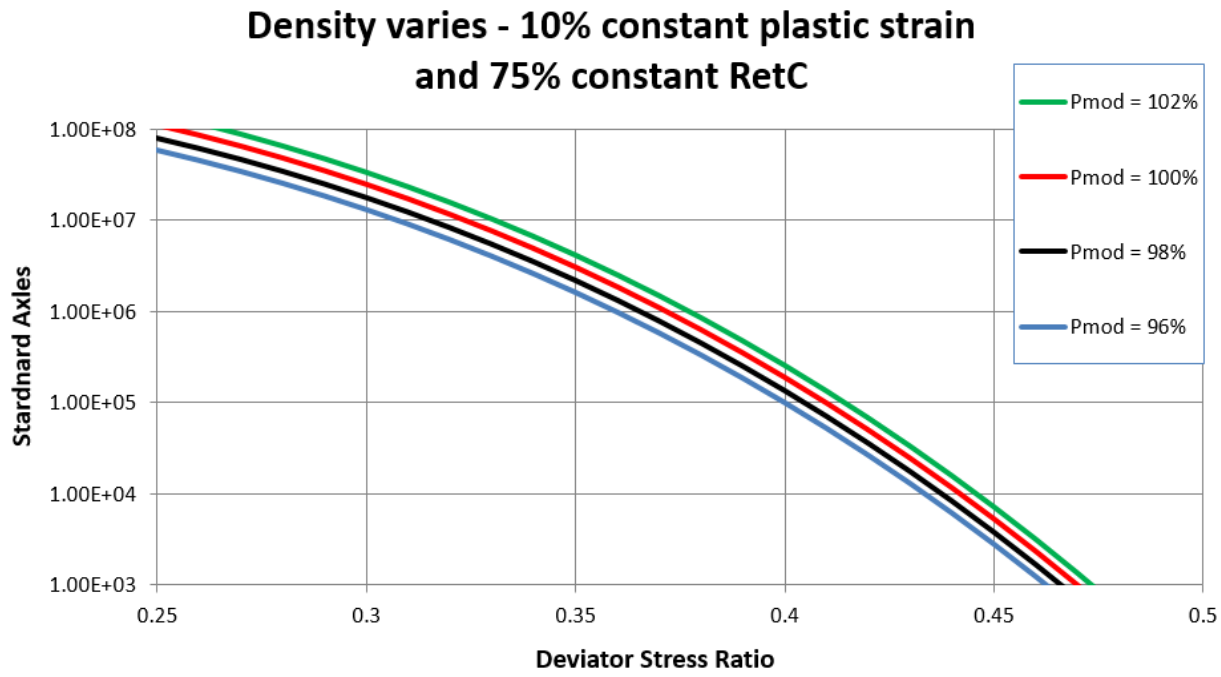

Figure 5.14: Transfer function sensitivity analysis: Density

5.3.4 Sensitivity to retained cohesion

Retained cohesion is a measure of the material's resistance to moisture damage. Therefore, an increase in a material's resistance to moisture damage (retained cohesion) should lead to an increase in the pavement's life. Figure 5.15 shows the transfer function's response to a change in retained cohesion. The figure shows that the transfer function's result does increase with an increase in

moisture damage. The transfer function therefore reflect the expected behaviour of the material regarding moisture damage.

The lines in this figure for the retained cohesion values of 100% and 85% are very high and show a significant difference in absolute values when compared to 75%. Therefore, it is suggested that the values used for retained cohesion be limited to a maximum of 75% when using this function. By implying an upper limit to the retained cohesion, the function would produce a realistic value representing a BSM.

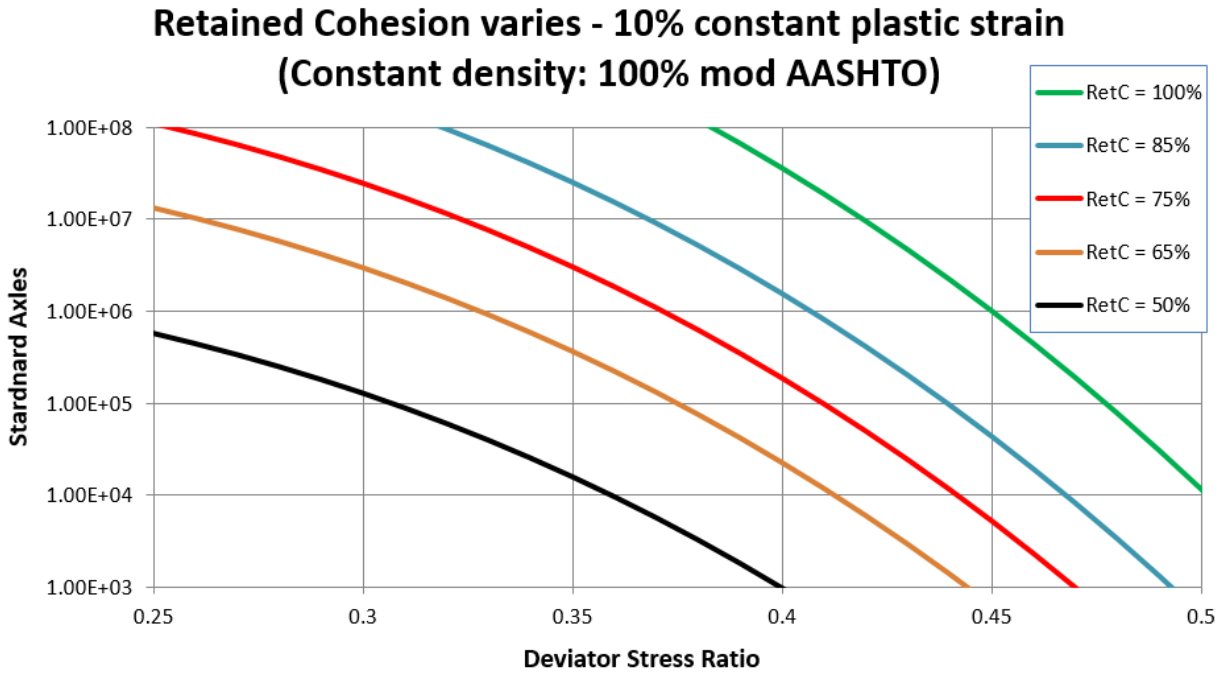

Figure 5.15: Transfer function sensitivity analysis: Retained cohesion

5.4 Summary

Chapter 5 is summarized as follows:

1. The new transfer function for BSMs was validated to confirm that it produces results that are realistic. The function's response to changes in different variables was investigated to determine if it responds to these changes in the expected manner.

2. The function was validated by investigating its ability to predict data that was not part of the calibration process. Comparison with the observed data from the N7 showed that the transfer function produces realistic results.

3. The transfer function's permanent deformation prediction was compared to the observed data for each uniform section identified on the N7. This comparison highlighted the function's sensitivity to the different variables.

4. The new transfer function was compared to the PN design method as well as the Loudon transfer function. Five pavement structures were analysed with the 3 methods and it was concluded that the new transfer function produces results that are within reason.

5. The transfer function's sensitivity to the four variables was investigated. This sensitivity analysis showed that the function reacted in a realistic manner with a change in these variables. It also highlighted that limits on these factors should be put in place for design purposes.

Chapter 6

Conclusions and recommendations

This chapter provides a summary of the conclusions drawn from this study. The transfer function was calibrated, adjusted and validated in the previous two chapters. Section 6.1 presents the conclusions drawn from the data gathered for the LTPP pavements as well as the N7 highway. The conclusions drawn from the calibration process are discussed in Section 6.2. Conclusions drawn from the validation process are discussed in Section 6.3. Finally, recommendations were made for further study and improvement of the transfer function in Section 6.4.

6.1 Conclusions from data gathering phase

Data was gathered from fourteen long term pavement performance studies as well as the N7 highway near Cape Town. Conclusions drawn from this phase of the study are outlined here:

- Information was available for the pavement structures at various points of their design life. This information was used to determine a range of factors over time which made it possible to calibrate the new transfer function.
- Traffic counts were performed at different locations on the BSM section of the N7. These counts showed a significant reduction the further the counting stations were from Cape Town. The traffic counts confirmed that the pavement had accommodated between 6 MESA and 19 MESA by 2016.
- The maximum deflection measurements from the foam sections indicated that the pavement was in a better condition in 2004, two years after construction than in 2010. The pavement conditions remained similar between 2010 and 2016, but in some cases the maximum deflection decreased. This indicates a stable resilient modulus response over time.
- The emulsion stabilised section, constructed in 2007, showed a decrease in maximum deflection and BLI from 2010 to 2016. The lower deflections indicate a stiff response of the pavement

structure. The increase in resilient modulus may be attributed to residual compaction, but it is likely due to curing of the BSM layer.

- The back calculated layer stiffnesses for the some of the uniform sections showed very high stiffnesses. These high stiffnesses were comparable to those of cement stabilised layers. It was concluded that in certain cases this material was not representative of BSMs.
- From test pits dug on the N7, material properties and layer thicknesses were obtained. These investigations showed significant variation in layer thicknesses.
- It was concluded that the cement distribution in the N7 BSM layer was poor. The clumps of cement found confirms the high stiffness values and would be prone to cracking.
- Monotonic triaxial testing indicated high shear properties for the N7 BSMs which was considered representative of the in-field conditions. The high values obtained for the shear properties were not representative of a BSM.

6.2 Conclusions from transfer function calibration

The new transfer function for BSMs was calibrated to predict the data obtained from the fourteen LTPP pavements at different levels of reliability. Conclusions drawn from the calibration are outlined here:

- Similar to granular materials, BSMs fail in permanent deformation. Therefore, the new transfer function for BSMs determines the number of standard axles the pavement can sustain, before reaching a limiting value of permanent strain. The new transfer function for BSMs was based on the design function for waterbound macadam.
- The factors influencing the life of a BSM were determined and used in the transfer function:
    1. Deviator stress ratio (DSR)
    2. Density (P_{mod})
    3. Retained cohesion (RetC)
    4. Permanent strain (PS)
- The term for DSR was raised to the power 3 and confirmed during calibration.
- The Huurman model was fitted to the observed data for each of the pavement structures individually to extrapolate traffic and permanent deformation. This extrapolation was deemed appropriate and was used during the calibration of the transfer function.

- The transfer function was found to predict significant amounts of traffic even if the remaining plastic strain was zero. This situation was regarded as unrealistic as it determined the remaining life of the materials after it had failed and was excluded for the calibration process.
- The transfer function was calibrated to best describe the observed data by changing the significance of the four variables effecting the function's results. This function was calibrated further to describe the data at different levels of reliability. The final calibrated transfer function is presented in Equation 6.1. The values for the constant A, for different levels of reliability, are given in Table 6.1.

$$\log N = A - 57.286(DSR)^3 + 0.0009159(P_{mod}.RetC) + 0.086753(PS) \tag{6.1}$$

Table 6.1: Transfer function reliability factors

Reliability	A
50%	1.1369
80%	1.0198
90%	0.9312
95%	0.8436

6.3 Conclusions from transfer function validation

The new transfer function was validated to determine if the results and behaviour were realistic and representative of the in-field behaviour. Conclusions drawn from the validation are outlined here:

- The construction and materials issues of the N7 showed that the BSMs did not behave like typical BSMs. However, distinctions could be made from those that were not representative. This allowed for prediction and evaluation of the transfer function's response to the high resilient modulus values and shear properties. It also highlighted that the function is specifically for BSMs which fail in permanent deformation.
- The uniform sections with BSM resilient modulus values that were representative of a typical BSM yielded a good correlation. The transfer function was able to predict the long-term accumulation of permanent deformation accurately.
- The effect of low density values was highlighted during this investigation. The uniform sections with low densities (95% of MOD AASHTO density) resulted in an underestimation of the pavement's life.

- Uniform sections with a stiff BSM layer and weak support layer showed higher DSR values in the BSM. The increase in DSR significantly decreases the life of the BSM. Therefore, by correctly determining the DSR, the transfer function has an indirect sensitivity to the modular ratio.

- The function was found to be very sensitive to a change in the deviator stress ratio. This confirmed the significance assigned to the variable by the power 3. It was also shown that the transfer function produced unrealistic results if the shear properties were in excess of those typical for BSMs.

- A single term was used to describe the effect of density and retained cohesion in the transfer function. From the sensitivity analysis it was shown that the large variance in retained cohesion has a significant effect on the results of the transfer function. The variance in density was much smaller and therefore had a smaller effect on the function.

- It was found that remaining permanent strain values below 3% result in unrepresentative prediction from the transfer function.

- The transfer function was found to be sensitive to a change in the four variables to a realistic degree which is representative of the in-field conditions.

- The transfer function showed realistic increase in design traffic for lower levels of reliability, which was comparable to other design methods. The function also showed the expected decrease in life for a heavier standard axle.

6.4 Recommendations

The transfer function was successfully calibrated for BSMs at different levels of reliability. However, ample room for improvement remains for both the function and the methods of calibration. This section covers the suggestions for further studies and possible improvements to the transfer function:

- It is recommended that more information regarding the long-term performance of BSMs should be gathered and included in the calibration of the transfer function. If the transfer function is based on greater amounts of data, the affect of local variability will be reduced.

- Limited information was available regarding the cohesion, friction angle, in-field densities and retained cohesion for the pavements used during calibration. Therefore, it is recommended that detailed information is gathered for these variables from different pavement structures.

- The measurement of deformation specifically in the base layer is not practical or economical. In most cases it would require destructive investigations like test pits. It is recommended that improved means of deformation measurement and allocation to BSM layer be used for future calibration.
- Retained cohesion values for most of the pavements used during calibration were unavailable. Variance in moisture resistance was therefore not fully utilized during the calibration process. Further studies on the effect of retained cohesion on the life of BSMs should be done and used to improve the transfer function.
- The effect of retained cohesion and density are termed together, therefore, their effect on the function is combined. It is therefore recommended that further investigation into possible variations of this term be considered.

6.5 Transfer function limits

The sensitivity analysis and validation of the transfer function showed that the function behaves as expected to adjustments in the different variables. It also indicated that by exceeding certain values, the transfer function showed unrealistic results. Therefore, limits on the values for the different variables are recommended for design purposes:

- Shear properties: It is recommended to limit the maximum cohesion to 350 kPa and the friction angle to 45°. This limit should be considered with the limits for the DSR.
- DSR: It is recommended that values for the DSR do not fall below 0.2 for BSM base layers. Low values for the DSR produce very high design traffic values that may be unrealistic.
- PS: It is recommended that only PS values exceeding 3% be used during design.
- Retained cohesion: Values for retained cohesion used in the transfer function should be between 70% and 80%. This ensures that the transfer function does not produce unrealistic results.
- Density: Density values ranging between 95% and 103% of MOD AASHTO density are recommended for the transfer function. Higher values might not be consistently achievable, while lower values do not represent the long-term in-field conditions.

Bibliography

Allen, J. J. and Thompson, M. R. (1974), 'Resilient response of granular materials subjected to time-dependent lateral stresses', *Transportation Research Record* **1**, 510.

Asphalt Academy (2009), 'Technical Guideline: Bitumen Stabilised Materials', **2**.

Asphalt Institute (2008), *Basic Asphalt Emulsion Manual*, fourth edn, Asphalt Institute, Inc.

Barksdale, R. D. (1972), LABORATORY EVALUATION OF RUTTING IN BASE COURSE MATERIALS, London, England.

Boyce, J. R. (1976), The behaviour of a granular material under repeated loading, Phd thesis, University of Nottingham.

Bredenhann, S. J. and Jenkins, K. J. (2015), Bitumen Stabilised Materials : Real Performance Models for BSM-foam Bases, *in* 'CAPSA'.

Brown, S. and Hyde, A. (1975), 'Significance of cyclic confining stress in repeated-load triaxial testing of granular material', *Transportation Research Record* .

Collings, D. and Jenkins, K. (2011), 'THE LONG-TERM BEHAVIOUR OF BITUMEN STABILISED MATERIALS', *10th Conference on Asphalt Pavements for Southern Africa* .

Dal Ben, M. (2014), RESILIENT RESPONSE AND PERFORMANCE OF BITUMEN STABILIZED MATERIALS WITH FOAM INCORPORATING RECLAIMED ASPHALT, Phd thesis, Stellenbosc University.

Dawson, A. and Kolisoja, P. (2006), 'MANAGING RUTTING IN LOW VOLUME'.

Dawson, A. R. (1990), Introduction to soils and granular materials, PhD thesis, University of Nottingham.

Ebels, L.-j. (2008), CHARACTERISATION OF MATERIAL PROPERTIES AND BEHAVIOUR OF COLD BITUMINOUS MIXTURES FOR ROAD PAVEMENTS, PhD thesis, Stellenbosch University.

Ebels, L.-j., Jenkins, K. J. and Collings, D. (2005), Cold Mix Technology in Southern Africa into the 21st Century, *in* 'International Symposium on Pavement Recycling', Sao Paulo, Brazil.

Hicks, R. G. and Monismith, C. L. (1971), 'FACTORS INFLUENCING THE RESILIENT RESPONSE OF GRANULAR MATERIALS', *Highway Research Record* (345).

Hunter, R. N., Self, A. and Read, J. (2015), *The Shell Bitumen Handbook*, 6 edn.

Huurman, M. (1997), Permanent deformation in concrete block pavements, PhD thesis, TU Delft.

Jenkins, K. J. (2000*a*), 'Mix design considerations for cold and half-warm bituminous mixes with emphasis of foamed bitumen'.

Jenkins, K. J. (2000*b*), MIX DESIGN CONSIDERATIONS FOR COLD AND HALF-WARM BITUMINOUS MIXES WITH EMPHASIS ON FOAMED BITUMEN, Phd thesis, University of Stellenbosch.

Jenkins, K. J., Molenaar and Groot, D. (2002), 'Performance prediction of cold foamed bitumen mixes', *9th International Conference on Asphalt Pavements,* .

Kancherla, A. (2004), RESILIENT MODULUS AND PERMANENT DEFORMATION TESTING OF UNBOUND GRANULAR MATERIALS, PhD thesis, Texas A&M University.

Kolisoja, P. (1998), Resilient deformation characteristics of granular materials, PhD thesis, Tampere University of Technology.

Kotze, N. (2014), Toets van Granulere Materiale, PhD thesis, Stellenbosch University.

Lashine, A., Brown, S. and Pell, P. (1971), 'Dynamic properties of soils', *Department of Civil Engineering, University of Nottingham* .

Lekarp, F., Isacsson, U. and Dawson, A. (2000), 'State of the Art . II : Permanent Strain Response of Unbound Aggregates', *Journal of Transportation Engineering* **January**.

Llwellyn, G. (2015), Flexibility Behaviour of BSM, Masters thesis, University of Stellenbosch.

Loizos, A. and Papavasiliou, V. (2007), Evaluation of Foamed Asphalt Cold In-Place Pavement Recycling using Non-destructive Techniques, *in* 'International Conference on Advanced Characterisation of Pavement and Soil Engineering Materials ICAPSEM', Athens, Grrece.

Long, F. and Jooste, F. (2007), Summary of LTTP Emulsion and Foamed Bitumen Treated Sections Technical Memorandum, Technical report.

Long, F. M., Theyse, H. L. and Ventura, D. F. C. (2004), 'CHARACTERISATION OF FOAMED BITUMEN TREATED MATERIALS FROM HVS TEST SECTIONS'.

Lynch, A. G. (2013), TRENDS IN BACK-CALCULATED STIFFNESS OF IN- SITU RECYCLED AND STABILISED ROAD ROAD PAVEMENT MATERIALS, Masters thesis, Stellenbosch University.

Lynch, A. G. and Jenkins, K. (2013), MATERIALS RECYCLED USING FOAMED BITUMEN STABILISATION : WHAT IS THEIR LONG TERM LOAD SPREADING CAPACITY, *in* '15th AAPA INTERNATIONAL FLEXIBLE PAVEMENT CONFERENCE', Brisbane, Australia.

Mathaniya, T. E. (2010), Influence of Durability Properties on Performance of Bitumen Stabilized Materials, Ph.d thesis, Stellenbosch University.

Moloto, P. K. (2010), ACCELERATED CURING PROTOCOL FOR BITUMEN STABILIZED MATERIALS, Masters thesis, University of Stellenbosch.

Morgan, J. R. (1966), 'THE RESPONSE OF GRANULAR MATERIALS TO REPEATED LOADING', *Australian Road Research Board* .

Mulusa, W. K. (2009), Development of a simple triaxial test for characterising bitumen stabilised materials, Masters thesis.

Pappin, J. W. (1979), Characteristics of a granular material for pavement analysis, Phd thesis, University of Nottingham, Nottingham, England.

SANRAL (2011), *Revision of the South African Pavement Design Method (SAPDM) - Proposed Protocol for Resilient Modulus and Permanent Deformation Characteristics of Unbound and Bound Granular Materials*, Pretoria, South Africa.

SAPEM (2014), *SOUTH AFRICAN PAVEMENT ENGINEERING MANUAL*, second edn, South African Nation Roads Agency SOC Ltd., South Africa.

ScanRoad (1983), ScanRoad, Technical Bulletin 2 - Bitumen Emulsions, Technical report.

Serfass, J.-P., Carbonneau, X., Delfossie, F., Triguigneaux, J.-P. and Verhee, F. (2008), Mix design method and field performance of emulsion cold mixes, *in* 'Eurasphalt & Eurobitumen - 4th Congress', Copenhagen.

Theyse, H. L., Sadzik, E. and Notnagel, J. P. (2000), A DESIGN MODEL FOR WATERBOUND MACADAM BASED ON HEAVY VEHICLE SIMULATOR AND LABORATORY TEST RESULTS, Technical report.

Thom, N. and Brown, S. F. (1988), Design of road foundations, Phd thesis, Nottingham University.

Van den Berg, J. E. (2014), The influence of filler content on the performance of unbound granular materials in pavement layers, Master's thesis, Stellenbosch University.

Van Niekerk, A. A. (2002), Mechanical Behavior and Performance of Granular Bases and Sub-bases in Pavements, PhD thesis, Technical University Delft, Delft.

Werkmeister, S. (2003), Permanent Deformation Behaviour of Unbound Granular Materials in Pavement Constructions, PhD thesis, Technischen Universitat Dresden.

Wirtgen Group (2012), *Cold RecyclingWirtgen Cold Recycling Technology*, 1st edn, Windhagen, Germany.

Appendix A

Catalogue design method

	Pavement Class and Design Bearing Capacity		Foundation (CBR)
Road Category	ES0.3 ≤ 300 000	ES1 300 000 to 1 000 000	
B (95% Reliability)		S 125 BSM2	> 15
		S 125 BSM2 150 G6	7 to 15
		S 125 BSM2 150 G5 150 G7 150 G9 40 AC 300 BSM2	3 to 7
C (80 % Reliability)	S 100 BSM3 125 G6 S 125 BSM3	S 125 BSM3 150 G6 S 150 BSM3	> 15
	S 125 BSM3 125 G6 125 G7 S 300 BSM3	S 125 BSM3 150 G5 150 G7 40 AC 200 BSM3	7 to 15
	S 100 BSM3 125 G6 125 G7 125 G9 40 AC 200 BSM3	S 150 BSM3 150 G5 150 G7 150 G9 40 AC 200 BSM3	3 to 7
D (50% Reliability)	S 100 BSM3	S 100 BSM3	> 15
	S 100 BSM3 125 G6 S 250 BSM3	S 100 BSM3 125 G6 30 AC 150 BSM3	7 to 15
	S 125 BSM3 125 G6 S 300 BSM3	S 125 BSM3 150 G6 30 AC 175 BSM3	3 to 7

Figure A.1: Catalogue design method for low volume roads (Asphalt Academy, 2009)

Appendix B

LTPP pavement sections

1. MR27: The MR27 is situated between Somerset West and Stellenbosch in the Western Cape. The slow lanes in both directions of the 200 m long dual carriageway were considered. The pavement was rehabilitated with BSM emulsion layer in 1988 and had accommodated traffic over a period of 20 years to 2008. In 2002 the pavement received maintenance in the form of a double seal. It was concluded that the road was still in a good condition in 2006. This conclusion was based on low roughness, rutting and deflection levels as well as visual assessments. The tests performed, material properties and assumptions for this pavement are as follows:

    - FWD data: FWD tests were performed on the Northbound and Southbound carriageway in 1998 and 2002.
    - Rut depth measurements were taken on the NB and SB carriageway in 1998, 2001, 2002 and 2006.
    - BSM base was classified as a BSM1.
    - The average BSM base layer in Situ Density was found to be 102.1% of Mod AASHTO density (1997).
    - The cohesion and friction angle were assumed to be 275 kPa and 40°. The cohesion was assumed at 275 kPa due to the low amount of water damage.
    - The retained cohesion of the material was assumed to be 75%.

2. MR504 (A): The MR504 (A) is situated near Key Ridge and Shongweni in Kwazulu-Natal. The lanes in both directions of the 200 m long test section were considered using BSM foam. The pavement was constructed in 1995 and had accommodated traffic over a period of nine years to the last investigation in 2004. In 1998 the pavement received maintenance in the form of a single seal. It was concluded that the road was in a warning condition by 2006. This conclusion was based on observed edge breaks and isolated failures. The tests performed, material properties and assumptions for this pavement are as follows:

- FWD data: FWD tests were performed on the Northbound and Southbound carriageway in 1996, 1997 and 2004.
- Rut depth measurements were taken on the NB and SB carriageway in 1997 and 2004.
- BSM base was classified as a BSM1.
- The average field density of the base layer was above 100% of Mod. AASHTO density.
- The cohesion and friction angle were assumed to be 250 kPa and 40°.
- Retained cohesion was assumed to be 75%.

3. MR504 (B): The MR504 (B) is situated near Key Ridge and Shongweni in Kwazulu-Natal. Lanes in both directions of the 400 m long test section were considered. The pavement was constructed in 1995 with foamed bitumen and had accommodated traffic over a period of 11 years to the last investigation in 2006. In 1998 the pavement received maintenance in the form of a 20 mm asphalt overlay. For the first three years of after construction the base was only covered with a fog seal. It was concluded that the road was in a severe condition by 2006. This conclusion was based on observed edge breaks and isolated failures. The tests performed, material properties and assumptions for this pavement are as follows:

   - FWD data: FWD tests were performed on the Northbound and Southbound carriageway in 1996, 1997 and 2004.
   - Rut depth measurements were taken on the NB and SB carriageway in 1997 and 2004.
   - BSM base was classified as a BSM1.
   - The average field density of the base layer was above 95% of Mod. AASHTO density.
   - The cohesion and friction angle was assumed to be 250 kPa and 40°.
   - Retained cohesion was assumed to be 75%.

4. N1-1: The N1-1 is situated near Kraaifontein in the Western Cape. A 200m section of the Northbound carriageway and a 300m section of the Southbound carriageway were considered. The pavement was rehabilitated with BSM emulsion in 1984 and had accommodated traffic over a period of 22 years by the end of 2006. In 1995 the asphalt was milled off due to rutting of the surface layer. A new continuously graded asphalt surfacing with rolled in chips was constructed on the BSM base layer. It was concluded that the road was still in a sound condition in 2006. The tests performed, material properties and assumptions for this pavement are as follows:

   - FWD data: FWD tests were performed on the Northbound and Southbound carriageway in 1998, 1999 and 2005.

- Rut depth measurements were taken on the NB and SB carriageway in 1995, 1996, 1999, 2000, 2001 and 2002.
- BSM base was classified as a BSM1.
- The average field density of the base layer was 104.2% of Mod. AASHTO density. This value seemed very high for field compaction, therefore, during calculations 101.3% was used.
- The cohesion and friction angle were assumed to be 250 kPa and 40°.
- Retained cohesion was assumed to be 75%.

5. N1-13: The N1-13 is situated between Springfontein and Trompsburg in the Free State province. A 3.16 km section of the Northbound and Southbound carriageways was considered. The pavement was constructed between 1978 and 1980 and had accommodated traffic over a period of 26 years by the end of 2006. In 1991 the road received a diluted emulsion after 11 years of service. In 1996 20% of the project length was patched and the section received 13.2 mm bitumen rubber surfacing. It was concluded that the road reached a warning condition by 2006. This condition was based on deflection measurements of which the median was above 600 microns.

   This pavement incorporates a 150 mm BSM base layer as well as a 100 mm BSM subbase layer. Both of these layers were analysed during this study.The tests performed, material properties and assumptions for this pavement are as follows:

   - FWD data: FWD tests were performed on the Northbound and Southbound carriageway in 1999 and 2006.
   - Rut depth measurements were taken on the NB and SB carriageway in 1999, 2000, 2001 and 2002.
   - BSM base was classified as a BSM1, while the BSM subbase was classified as a BSM2.
   - The average field density of the base layer and the subbase layer was 90.1% and 97.8% of Modified AASHTO density respectively. This value for the base layer seemed very low for field compaction, therefore, during calculations 100.0% was used.
   - The cohesion and friction angle were assumed to be 275 kPa and 40° for the base layer. The cohesion and friction angle for the subbase were assumed as 200 kPa and 35°.
   - Retained cohesion was assumed to be 75% for the base layer and 65% for the subbase.

6. N1-14: The N1-14 is situated between Springfontein and Trompsburg. A 13 km section of the Southbound carriageway was considered for this study. The pavement was constructed between 1978 and 1980 and had accommodated traffic over a period of 26 years by the end of 2006. In 1991 the road received a diluted emulsion and in 1996 20% of the project length was patched and the section received 13.2 mm bitumen rubber surfacing. It was concluded that the road has reached a warning condition by 2006. The conclusion was based on deflection data, of which the median in 2006 was above 800 microns. The tests performed, material properties and assumptions for this pavement are as follows:

    - FWD data: FWD tests were performed on the Southbound carriageway in 1999 and 2006.
    - Rut depth measurements were taken on the SB carriageway in 1995, 1996, 1999, 2000, 2001 and 2002.
    - BSM base was classified as a BSM1.
    - The average field density of the base layer was 90% of Mod. AASHTO density. This value seemed very low for field compaction, therefore, during calculations 100.0% was used as the density of the surrounding materials was much higher.
    - The cohesion and friction angle were assumed to be 275 kPa and 40°.
    - Retained cohesion was assumed to be 75%.
    - By 2006 the pavement was estimated to have accommodated between 9.5 and 15.5 MESA.

7. N2-16: The N2-16 is situated near East London in the Eastern Cape. The report focuses on two 200 m sections on the single Northbound lane. The pavement was rehabilitated between 1979 and 1981 with bitumen emulsion and had accommodated traffic over a period of 25 years by the end of 2006. The pavement received a bitumen rubber seal in 1990 and a single seal in 2005. It was concluded that the pavement was in a sound condition in 2006. The tests performed, material properties and assumptions for this pavement are as follows:

    - FWD data: FWD tests were performed in 1999, 2005 and 2006.
    - Rut depth measurements were taken in 1995, 1996, 1999, 2000, 2001 and 2002.
    - BSM base was classified as a BSM2.
    - The average field density of the base layer was 87.9% of Mod. AASHTO density. This value seemed very low for field compaction, therefore, during calculations 100.0% was used as the support was of sound condition.

- The cohesion and friction angle were assumed to be 225 kPa and 40°.
- Retained cohesion was assumed to be 75%.
- By 2006 the pavement was estimated to have accommodated between 2.3 and 3.7 MESA.

8. N2-20: The N2-20 is situated in the Eastern Cape and connects Mount Frere and Mount Ayliff. The report focuses on the East and Westbound carriageways of a 6.4 km section. The pavement was constructed in 1960 and was widened in 1979. Major rehabilitation took place in 1999 to 2000, where the BSM layer was constructed utilizing bitumen emulsion. The pavement had therefore accommodated traffic over a period of six years by the time of the assessment in 2006. No maintenance or rehabilitation has been performed at the time of the analysis. It was concluded that the pavement was in a sound condition in 2006 based on visual assessments and low levels of rutting. The tests performed, material properties and assumptions for this pavement are as follows:

   - FWD data: FWD tests were performed in 2001 and 2005.
   - Rut depth measurements were taken in 2001 and 2005.
   - BSM base was classified as a BSM1.
   - The average field density of the base layer was 100% of Mod. AASHTO density.
   - The cohesion and friction angle were assumed to be 260 kPa and 40°.
   - Retained cohesion was assumed to be 75%.
   - By 2006 the pavement was estimated to have accommodated between 1.3 and 2 MESA.

9. N4-1: The N4-1 connects Witbank with Pretoria. The report focuses on the slow lanes of both East and Westbound carriageways. The section under consideration is 6.3 km in length. The pavement was constructed in 1969 and rehabilitated with emulsion in 1997. The pavement had therefore accommodated traffic over a period of 9 years by the time of the assessment in 2006. No maintenance or rehabilitation has been performed at the time of the analysis. It was concluded that the pavement was in a good condition in 2006 based on visual assessments, roughness riding quality and deflections. The tests performed, material properties and assumptions for this pavement are as follows:

   - FWD data: FWD tests were performed in 1999 and 2005 on both carriageways.
   - Rut depth measurements were taken in 1999, 2000, 2001 and 2002 on both carriageways.
   - BSM base was classified as a BSM1.

- The average field density of the base layer was 87.9% of Mod. AASHTO density. This density is very low and is deemed to be inaccurate. For analysis of the pavements, the density was assumed to be 101.3%.
- The cohesion and friction angle were assumed to be 250 kPa and 40°.
- Retained cohesion was assumed to be 75%.
- By 2006 the pavement was estimated to have accommodated between 3.2 and 5.3 MESA.

10. N4-5X: The N4-5X is between Pretoria and Nelspruit in Mpumulanga. The report focuses on a 5 km section of the the Eastbound carriageway. The pavement was constructed in 1996 with bitumen emulsion and had accommodated traffic over a period of 10 years at the time of the assessment in 2006. No maintenance or rehabilitation has been performed by the time of the analysis. It was concluded that the pavement was in a good condition in 2006 based on acceptable levels of roughness, rutting and deflection. The tests performed, material properties and assumptions for this pavement are as follows:

    - FWD data: FWD tests were performed in 2000, 2002 and 2004.
    - Rut depth measurements were taken in 1999, 2000, 2001, 2002 and 2004.
    - BSM base was classified as a BSM1.
    - The average field density of the base layer was 89.8% of Mod. AASHTO density. This density is very low and is deemed to be inaccurate. For analysis of the pavements, the density was assumed to be 100%.
    - The cohesion and friction angle were assumed to be 250 kPa and 40°.
    - Retained cohesion was assumed to be 75%.
    - By 2006 the pavement was estimated to have accommodated between 4.3 and 6.5 MESA.

11. N11-8: The N11-8 is situated in Mpumulanga between Hendrina and Ermelo. The report focuses on a 1.5 km section of the the Northbound carriageway. The pavement was constructed in 1969 and was rehabilitated in 2003/4 using foam and emulsion. The pavement had therefore only accommodated traffic over a period of 3 years by the time of the assessment in 2006. No maintenance or rehabilitation has been performed at the time of the analysis. It was concluded that the pavement was in a good condition in 2008. The tests performed, material properties and assumptions for this pavement are as follows:

    - FWD data: FWD tests were performed in 2005.

- No rutting data was available for this section. However, it was noted from an informal visual inspection that ruts were beginning to form.
- BSM base was classified as a BSM2.
- The average field density of the base layer was 100% of Mod. AASHTO density.
- The cohesion and friction angle were assumed to be 235 kPa and 35°.
- Retained cohesion was assumed to be 75%.
- By 2006 the pavement was estimated to have accommodated between 0.8 and 1.2 MESA.

12. N12-19(3): The N12-19(3) is located in the Gauteng Province between the Gillooly's interchange and the Pansy interchange. The report focuses on a 150 m section of the the Eastbound carriageway. The pavement was constructed in 1974 and had accommodated traffic for 30 years by the time of the assessment in 2004. The pavement received a fog spray in 1991 and surface patching in 2001. There were also reports of a seal in 1984. It was concluded that the pavement was in a warning condition by 2006. At that stage the pavement had been in service for 32 years with estimated traffic between 10 and 25 MESA. The tests performed, material properties and assumptions for this pavement are as follows:

    - Limited FWD results are available for 2001 and 2005.
    - Rutting was measured in 1995, 1996, 1999, 2000, 2001 and 2002.
    - BSM base was classified as a BSM1.
    - The density of the BSM was not available, but assumed as 100% of MOD AASHTO density for further calculations.
    - The cohesion and friction angle were assumed to be 265 kPa and 40°.
    - Retained cohesion was assumed to be 75%.

13. N12-13(4): The N12-19(4) is located in the Gauteng Province between the Gillooly's interchange and the Pansy interchange. The report focuses on a 150 m section of this pavement. The pavement was constructed in 1974 and had accommodated traffic for 32 years by the time of the assessment in 2006. The pavement received a fog spray in 1991. There were also reports of a seal in 1984. The report concluded that the pavement had reached a warning condition by 2006. The tests performed, material properties and assumptions for this pavement are as follows:

    - Limited FWD results are available for 2001 and 2005.

- Rutting was measured in 1995, 1996, 1999, 2000, 2001 and 2002.
- BSM base was classified as a BSM1.
- Limited material properties are available for the BSM layer, but the density was assumed as 100% of MOD AASHTO density for further calculations.
- The cohesion and friction angle was assumed to be 265 kPa and 40°.
- Retained cohesion were assumed to be 75%.
- It was estimated that the pavement accommodated 10 to 25 MESA during its service life.

14. P243-1: The road P243/1 is located near Vereeniging and the Vaal Dam in the Gauteng Province. The report focuses both the East and Westbound carriageways. A 6.5 km section of this pavement was analysed for this report. The pavement was constructed in 1988 and rehabilitated with foamed bitumen in 2000. The report concluded that the pavement was still in a good condition 6 years after construction based on low levels of rutting, roughness and good visual conditions. The tests performed, material properties and assumptions for this pavement are as follows:

    - No FWD deflection data was available for this pavement.
    - Rutting was measured in 2005.
    - BSM base was classified as a BSM 2.
    - The density of the BSM base was found to be 100.7% of MOD AASHTO density.
    - The cohesion and friction angle were assumed to be 230 kPa and 40°.
    - Retained cohesion was assumed to be 75%.
    - It was estimated that the pavement accommodated 0.2 to 0.6 MESA during its service life.

Appendix C

Rubicon back-calculation import template

Station	Air Temp.	Surf Temp.	Time	Drop	Pressure	D0	D200	D300	D450	D600	D900	D1200	D1500	D1800
200415.8	20	23	534	3	566	490	324	214	0	102	64	44	32	0
200414.2	20	23	534	3	566	472	306	198	0	98	62	40	28	0
200413.8	20	23	534	3	566	510	344	240	0	104	56	30	22	0
200416.4	20	23	534	3	566	384	228	152	0	72	46	32	26	0
200417.6	20	23	534	3	566	434	300	202	0	112	80	62	50	0
200416.2	20	23	534	3	566	450	308	222	0	120	84	56	40	0

Figure C.1: Rubicon back-calculation import template

Station	Thick1	Thick2	Thick3
200416	58	250	75
200414	58	250	75
200414	58	250	75
200416	58	250	75
200418	58	250	75
200416	58	250	75

Figure C.2: Rubicon back-calculation thickness import template

Appendix D

N7 deflection measurements analysis

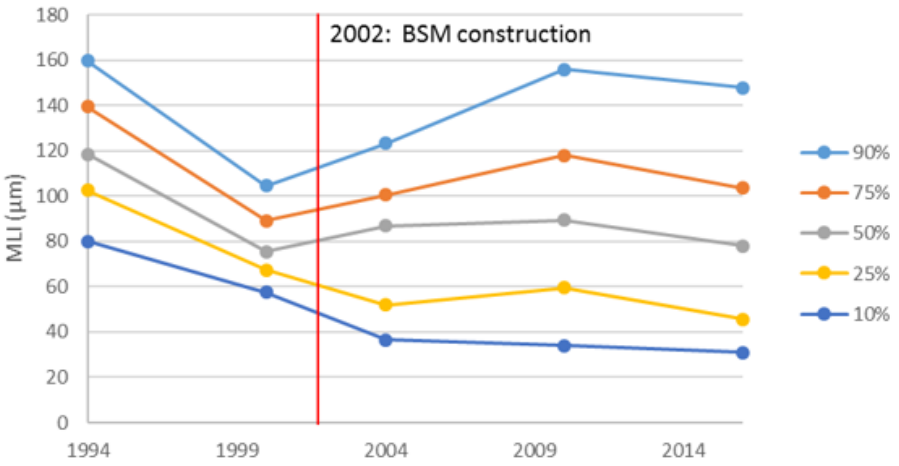

Figure D.1: MLI development for different levels of reliability for the N7 Southbound foam section

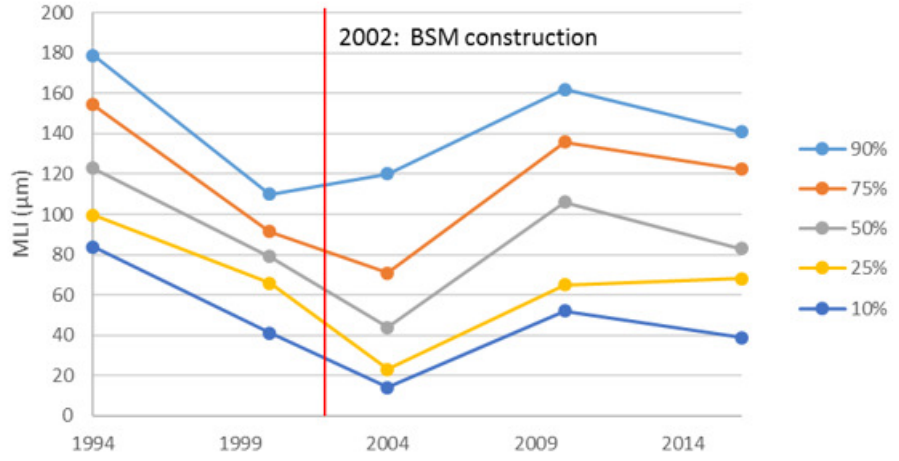

Figure D.2: MLI development for different levels of reliability for the N7 Northbound foam section

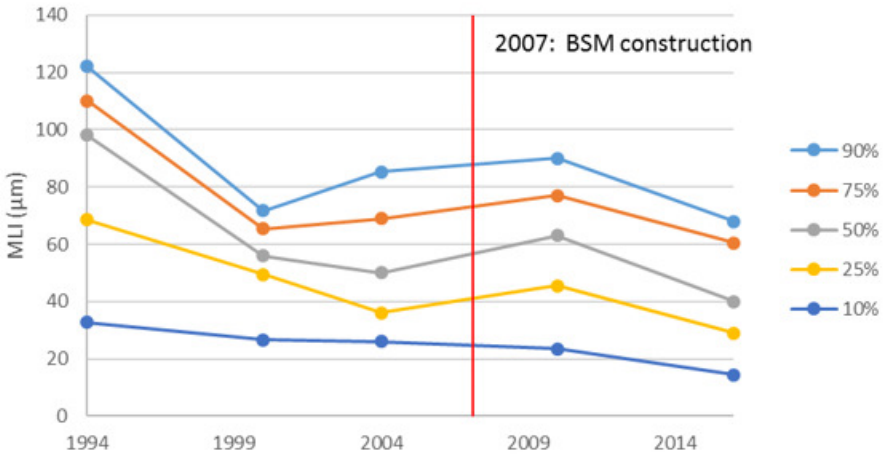

Figure D.3: MLI development for different levels of reliability for the N7 Northbound emulsion section

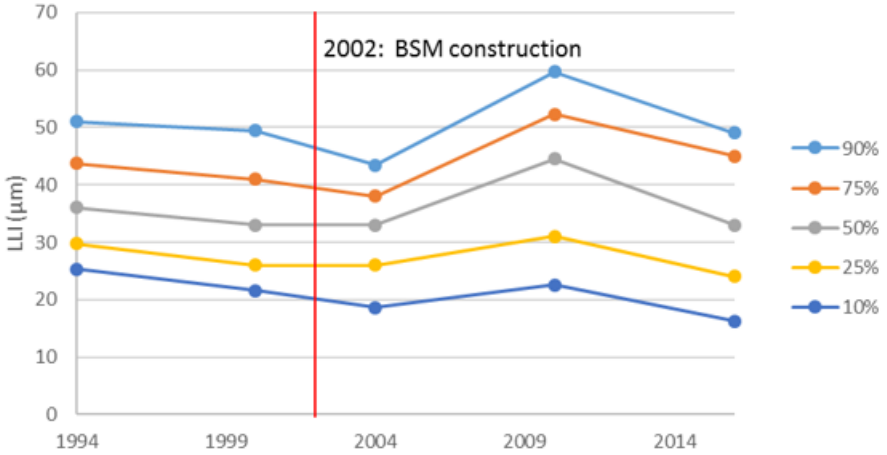

Figure D.4: LLI development for different levels of reliability for the N7 Southbound foam section

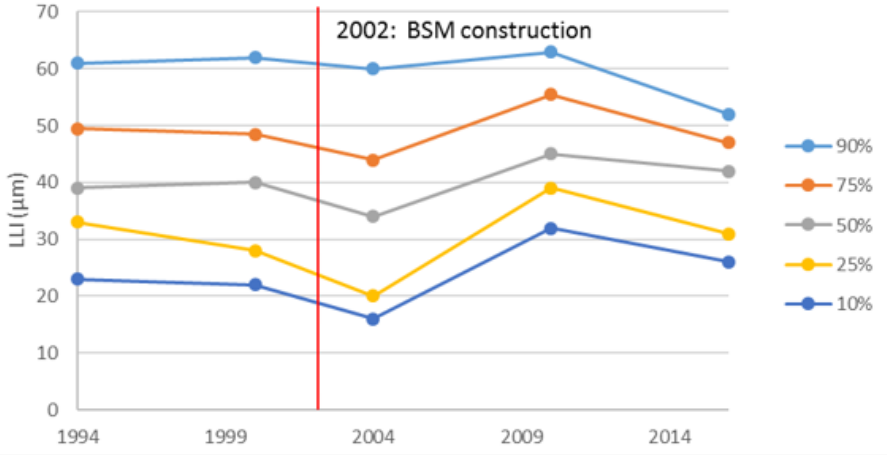

Figure D.5: LLI development for different levels of reliability for the N7 Northbound foam section

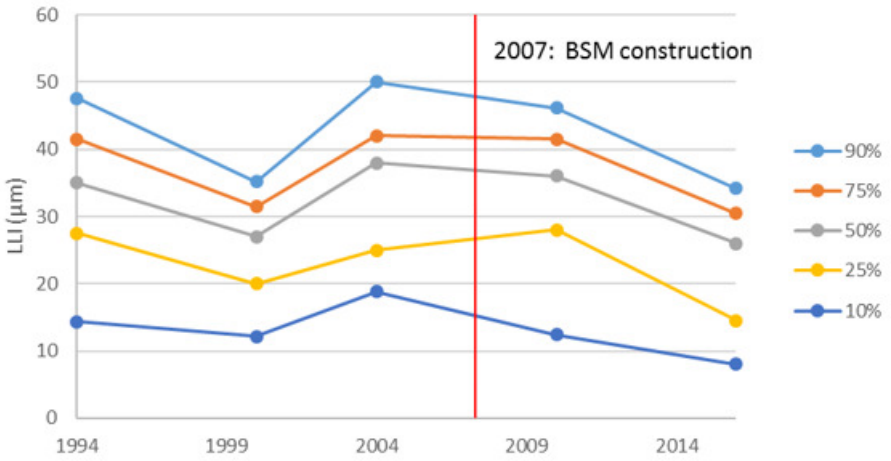

Figure D.6: LLI development for different levels of reliability for the N7 Northbound emulsion section

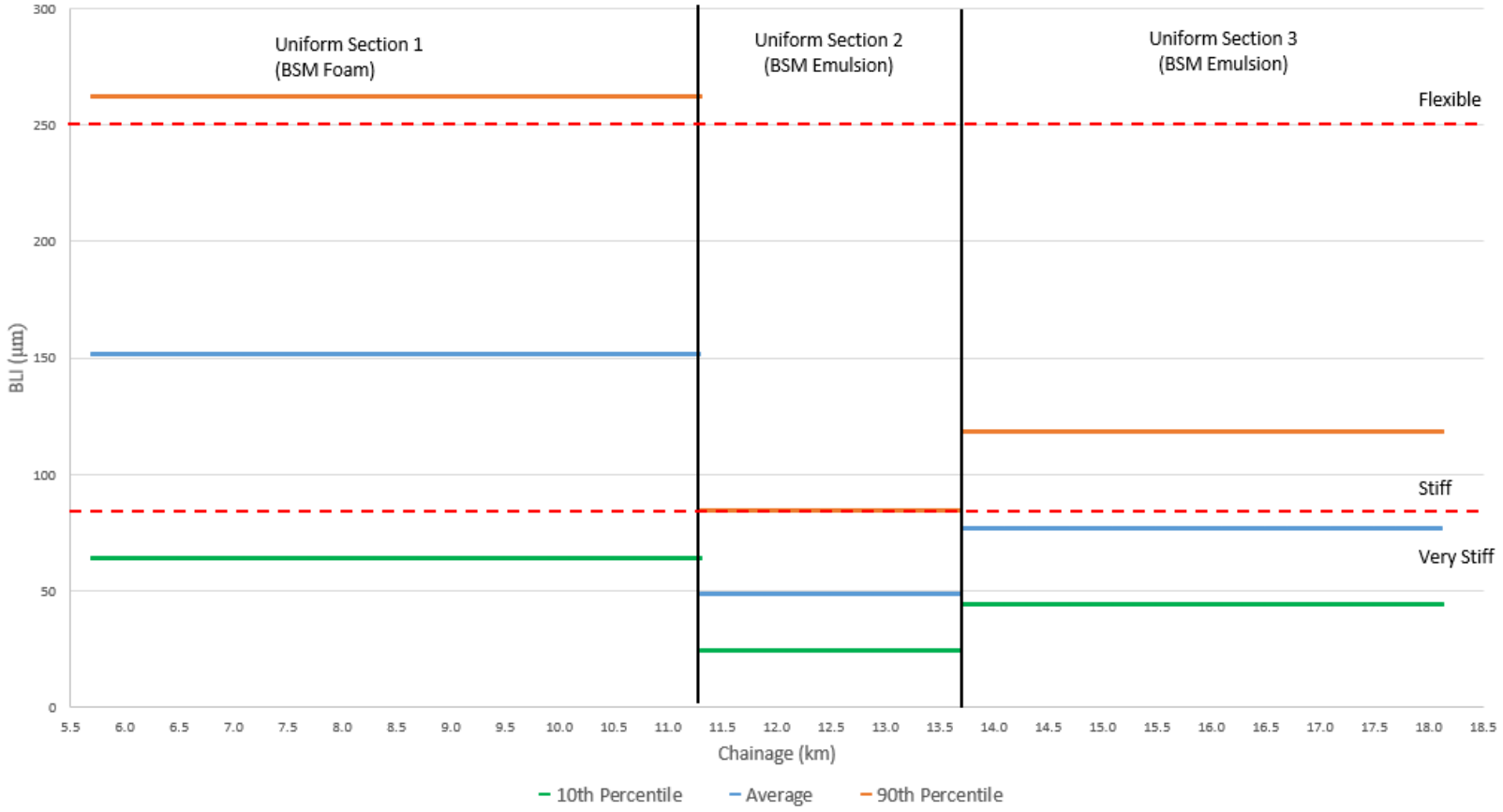

Figure D.7: N7 Northbound BLI per uniform section

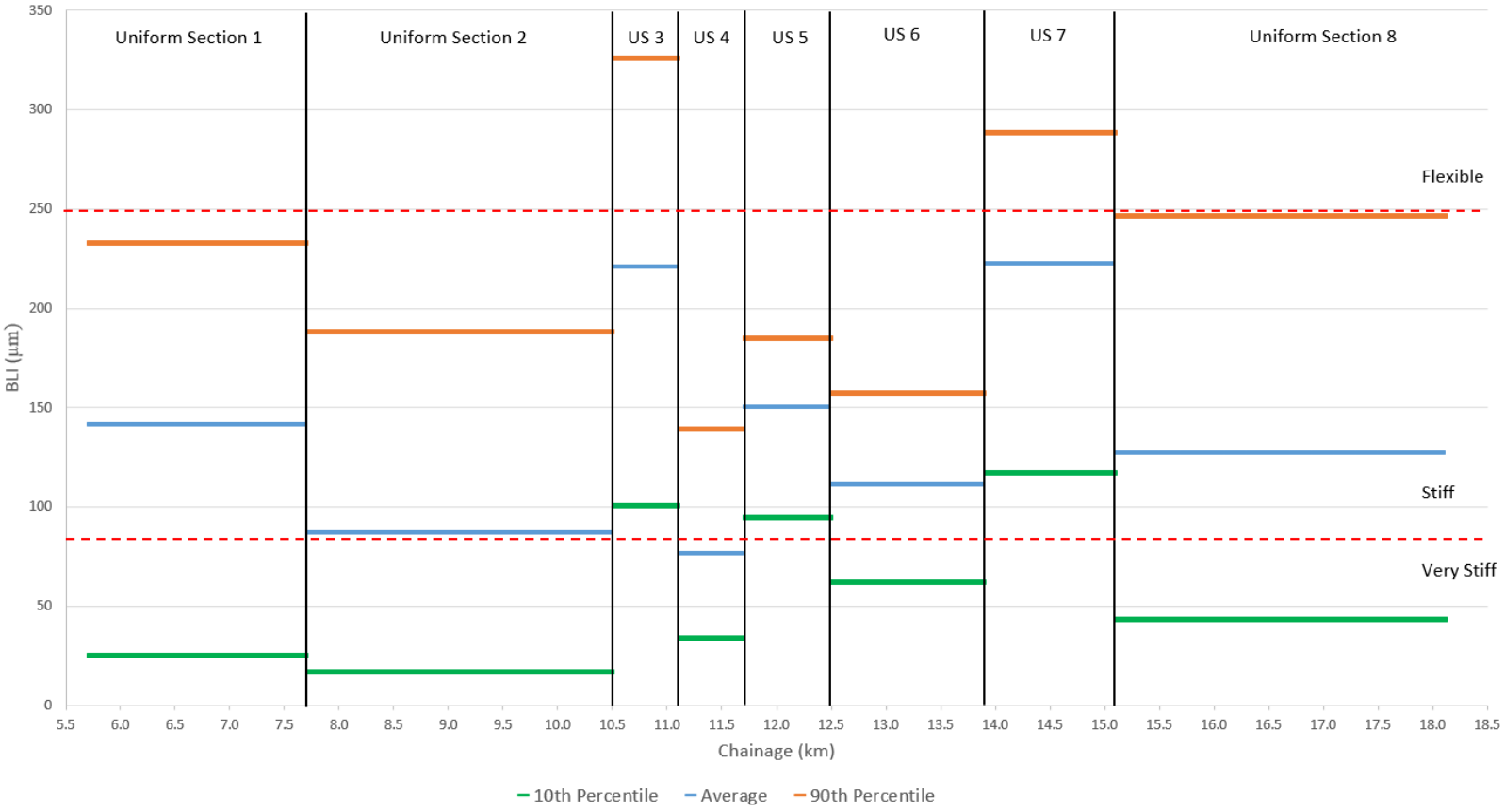

Figure D.8: N7 Southbound BLI per uniform section

Appendix E

N7 monotonic core properties

Table E.1: N7 Southbound core properties

Chainage	Sample	Diameter (mm)	Height (mm)	Mass (g)	Moisture content (%)	Dry density (kg/m³)
10.5	1	144	213	7804	4.19%	2159
	2	143	218	7772.8	3.73%	2140
	3	144	220	7953	4.15%	2131
10.5 BWP	1	143	219	7963	4.21%	2173
	2	143	242	8908.8	3.91%	2206
	3	143	221	8012	4.25%	2165
	4	143	245	8842	3.74%	2166
16	1	143	227	8699	3.90%	2297
	2	143.5	225	8526.9	3.53%	2263
	3	144	223	8501	3.51%	2261

Table E.2: N7 Northbound core properties

Chainage	Sample	Diameter (mm)	Height (mm)	Mass (g)	Moisture content (%)	Dry density (kg/m³)
9.2	1	143	227	7883	4.70%	2065
	2	143	234	8401	4.84%	2132
	3	143	219	8108	4.02%	2216
	4	143	236	8446	5.11%	2120
10	1	144	246	8958	3.13%	2168
	2	143	238	8708	3.41%	2203
	3	143	259	9376	3.80%	2171
	4	144	264	9676	4.25%	2159
11	1	145	255	9337	3.41%	2144
	2	143	228	8341.8	2.80%	2216
	3	143	231	8609	2.80%	2257
11 BWP	1	143	215	8054	4.20%	2238
	2	143	215	7955.9	1.61%	2267
	3	143	270	10138	2.66%	2277
12	1	143	241	8894	2.42%	2244
	2	144	224	7968	2.21%	2137
	3	144	231	8609	2.17%	2240
	4	143	260	9444	2.53%	2206
12 BWP	1	144	263	9772.8	2.69%	2222
	2	144	258	9571.6	2.66%	2219
	3	144	262	9749.5	3.06%	2217
14.4	1	143	247	9340	1.26%	2325
	2	143	212	7756	1.46%	2245
	3	144	251	9445	1.16%	2284
	4	143	249	9466	1.94%	2322
16	1	143	231	8983	2.78%	2356
	2	143	240	8470	2.26%	2149
	3	143	245	9180	2.07%	2286

Appendix F

LTPP pavements layer indices

The layer indices were determined for the various LTPP pavement structures based on FWD deflection measurements. The layer indices are graphically represented in the following figures:

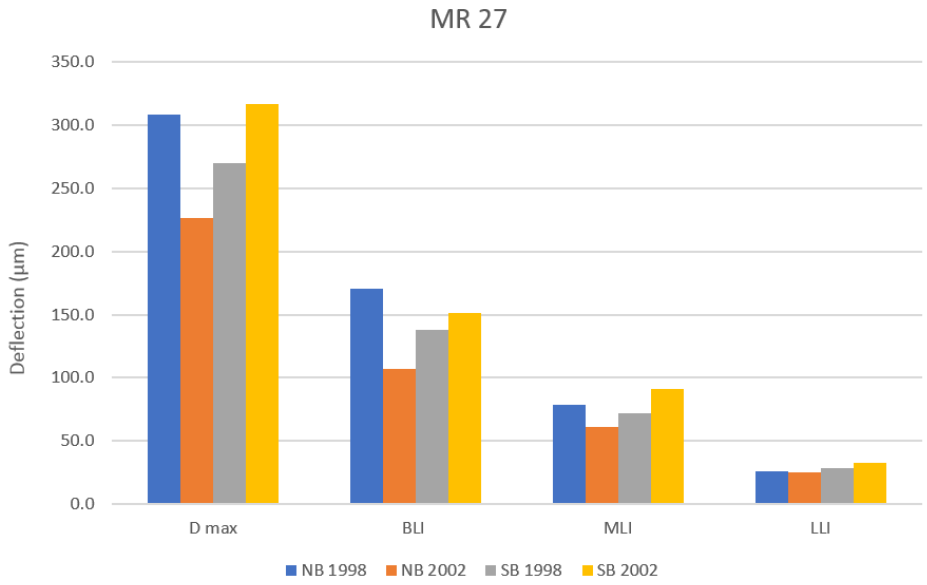

Figure F.1: MR27 layer indices

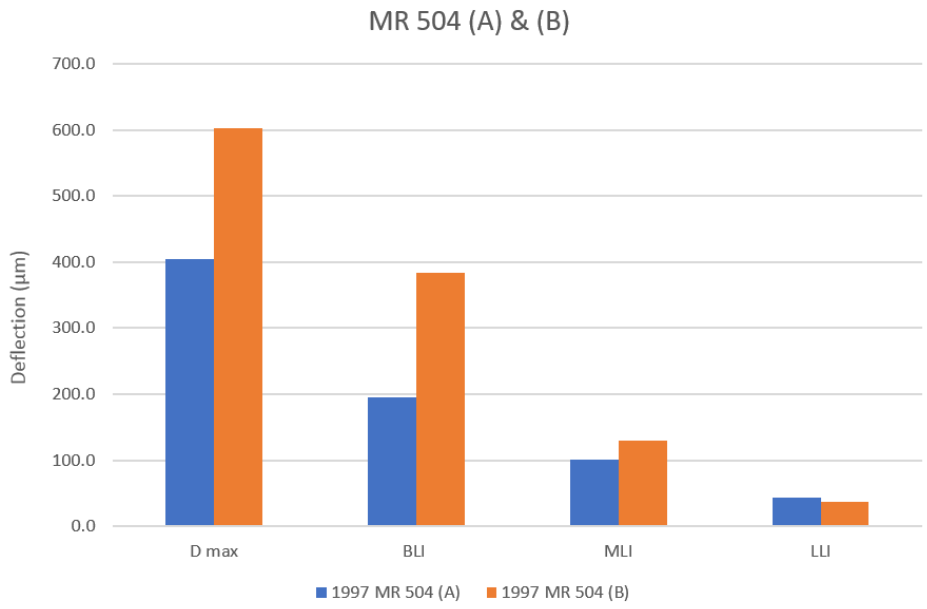

Figure F.2: MR504 (A and B) layer indices

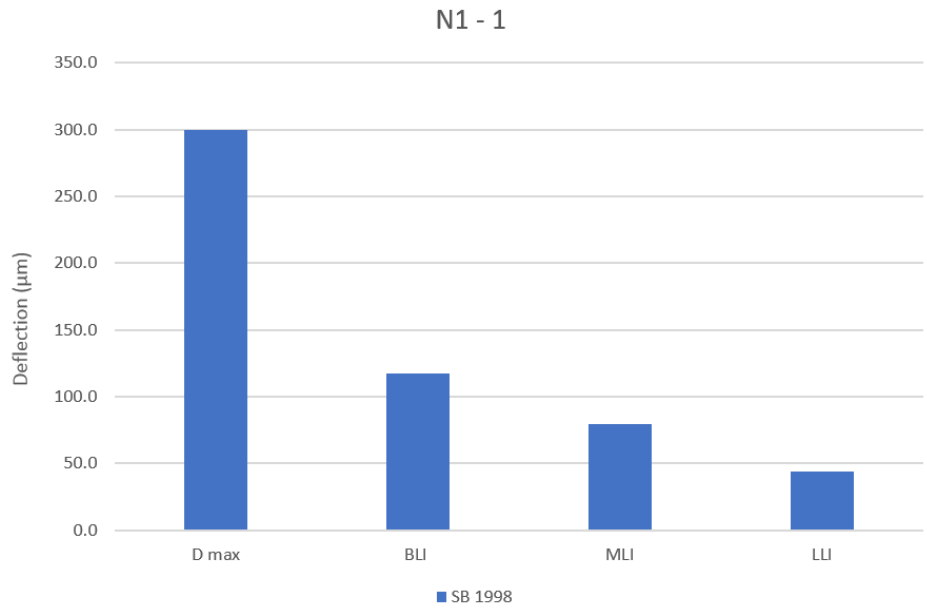

Figure F.3: N1 - 1 layer indices

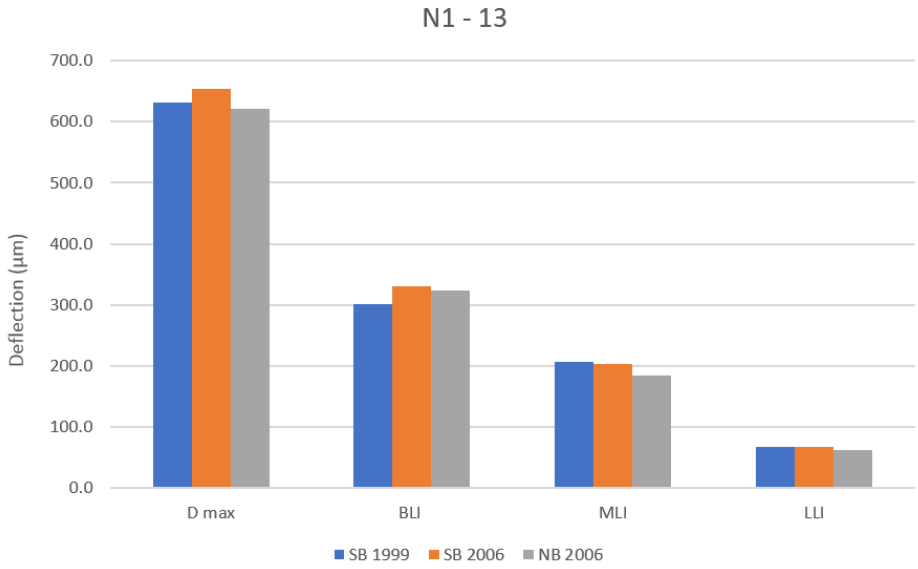

Figure F.4: N1 - 13 layer indices

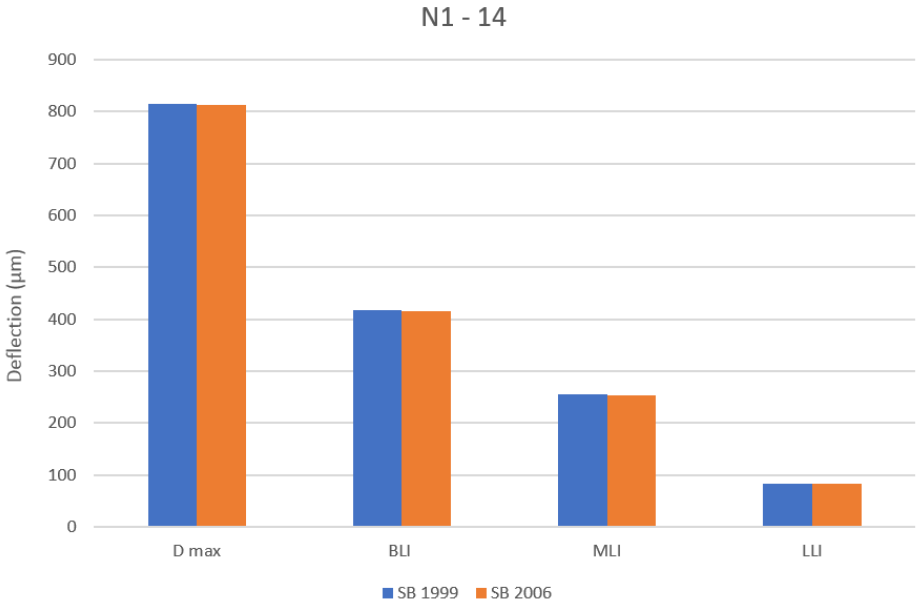

Figure F.5: N1 - 14 layer indices

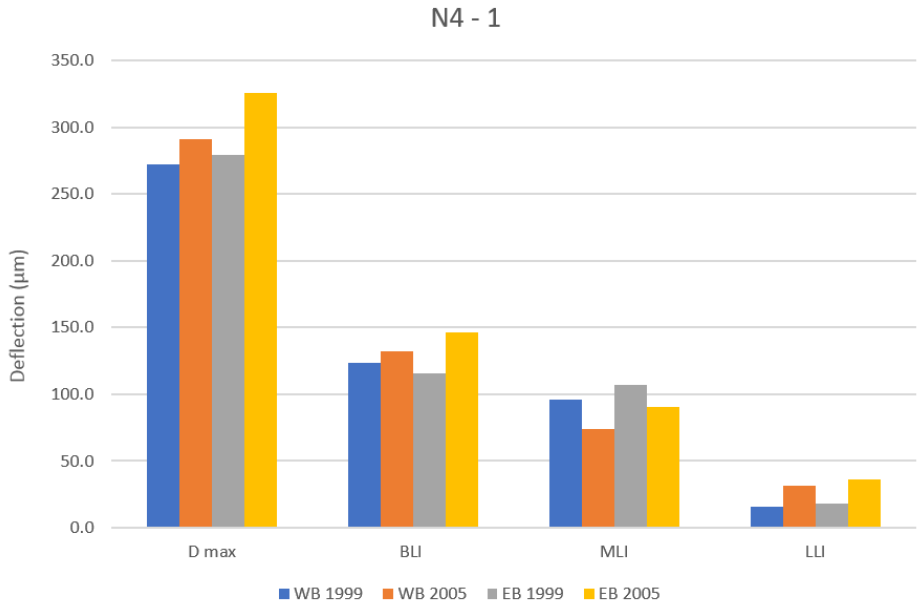

Figure F.6: N4 - 1 layer indices

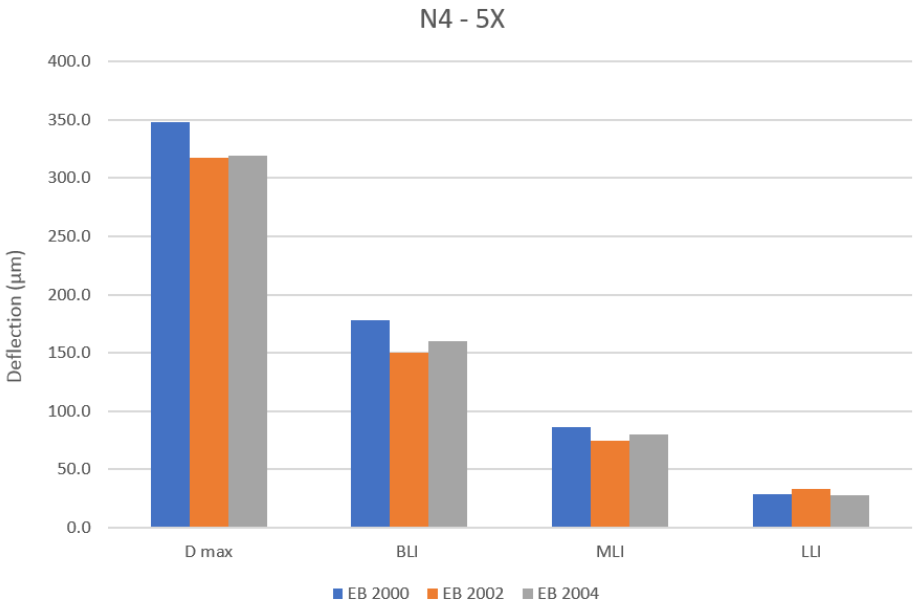

Figure F.7: N4 - 5X layer indices

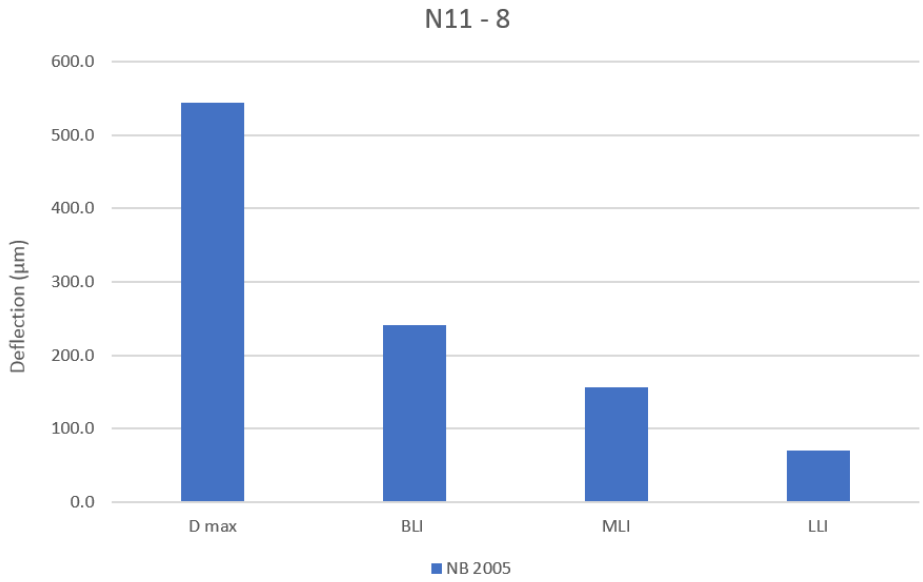

Figure F.8: N11 - 8 layer indices

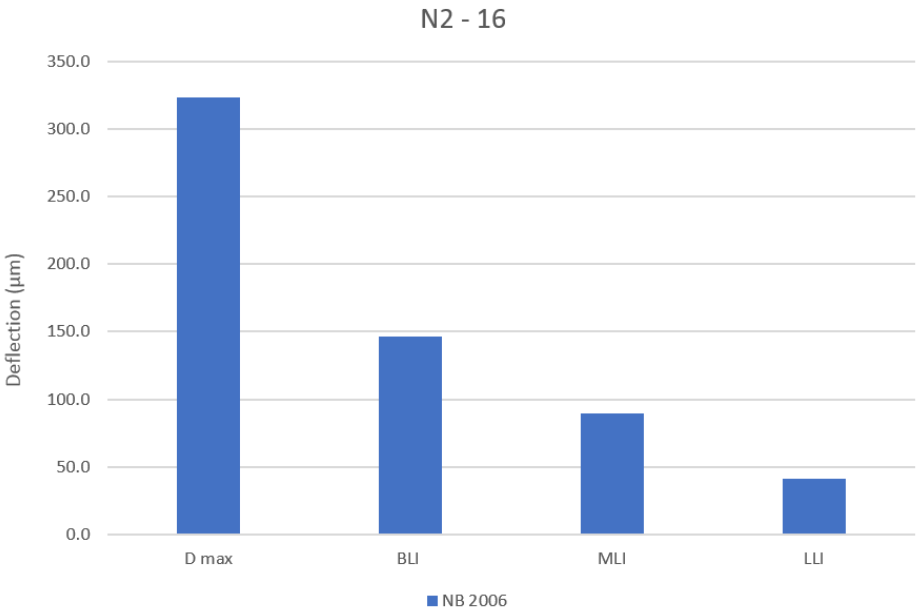

Figure F.9: N2 - 16 layer indices

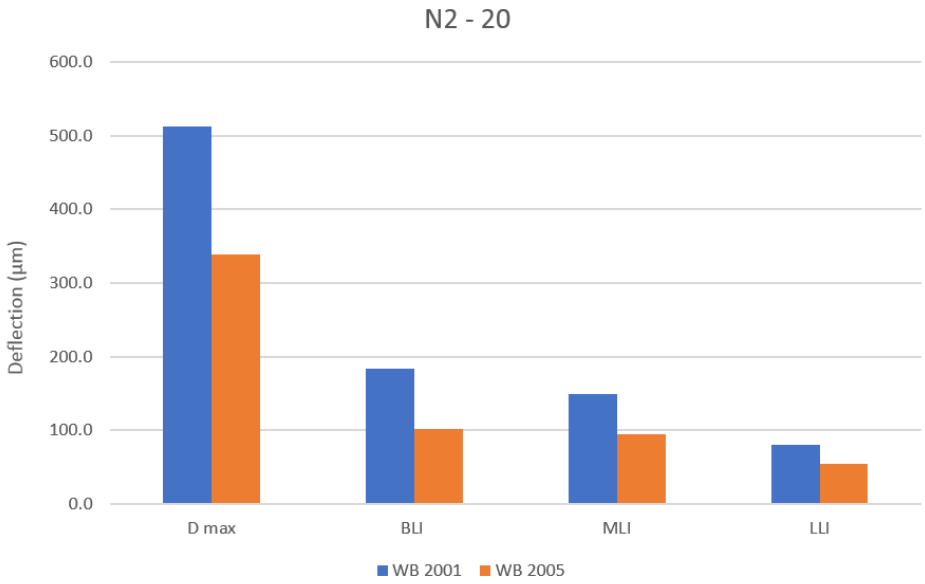

Figure F.10: N2 - 20 layer indices

Appendix G

LTPP back calculations

Deflection Bowl Report At Station 200127.4

Layer Thickness = 55 Millimetres
Layer Stiffness = 1062 MPa
Poisson's Ratio = 0.35

Layer Thickness = 120 Millimetres
Layer Stiffness = 1000 MPa
Poisson's Ratio = 0.35

Layer Thickness = 120 Millimetres
Layer Stiffness = 425 MPa
Poisson's Ratio = 0.35

Upper Subgrade:
Layer Thickness = 80 Millimetres
Layer Stiffness = 250 MPa
Poisson's Ratio = 0.35

Lower Subgrade or Substratum is Semi-Infinite, with Stiffness = 390 MPa

FWD Load applied Pressure = 583 kPa; Load Radius = 150 Millimetres;

Deflections:

Offsets (Millimetres):	0	200	300	450	600	900	1200	1500	1800
Measured (Microns):	263	168	110	67.2	45.1	26.9	18.3	15.4	12.5
Calculated (Microns):	261	147	106	70.7	51.4	32.8	24.4	19.5	16.3
Error at Sensor (%)	0	9.36	0	0	0	0	0	0	0

Average Error Per Sensor: 1.04 % **Sum of Errors: 9.36 %**

Note: Errors were adjusted for precision. Errors less than 10 micron are shown as zero.

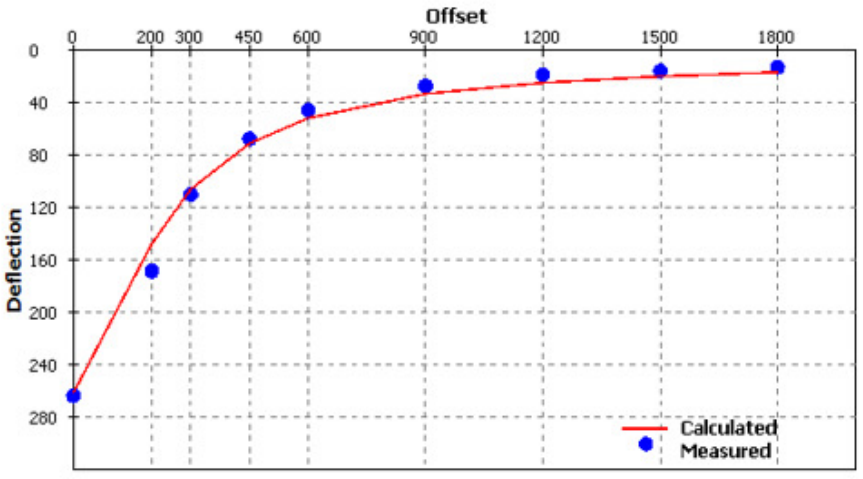

Figure G.1: N12-19 (3) deflection bowl 2001

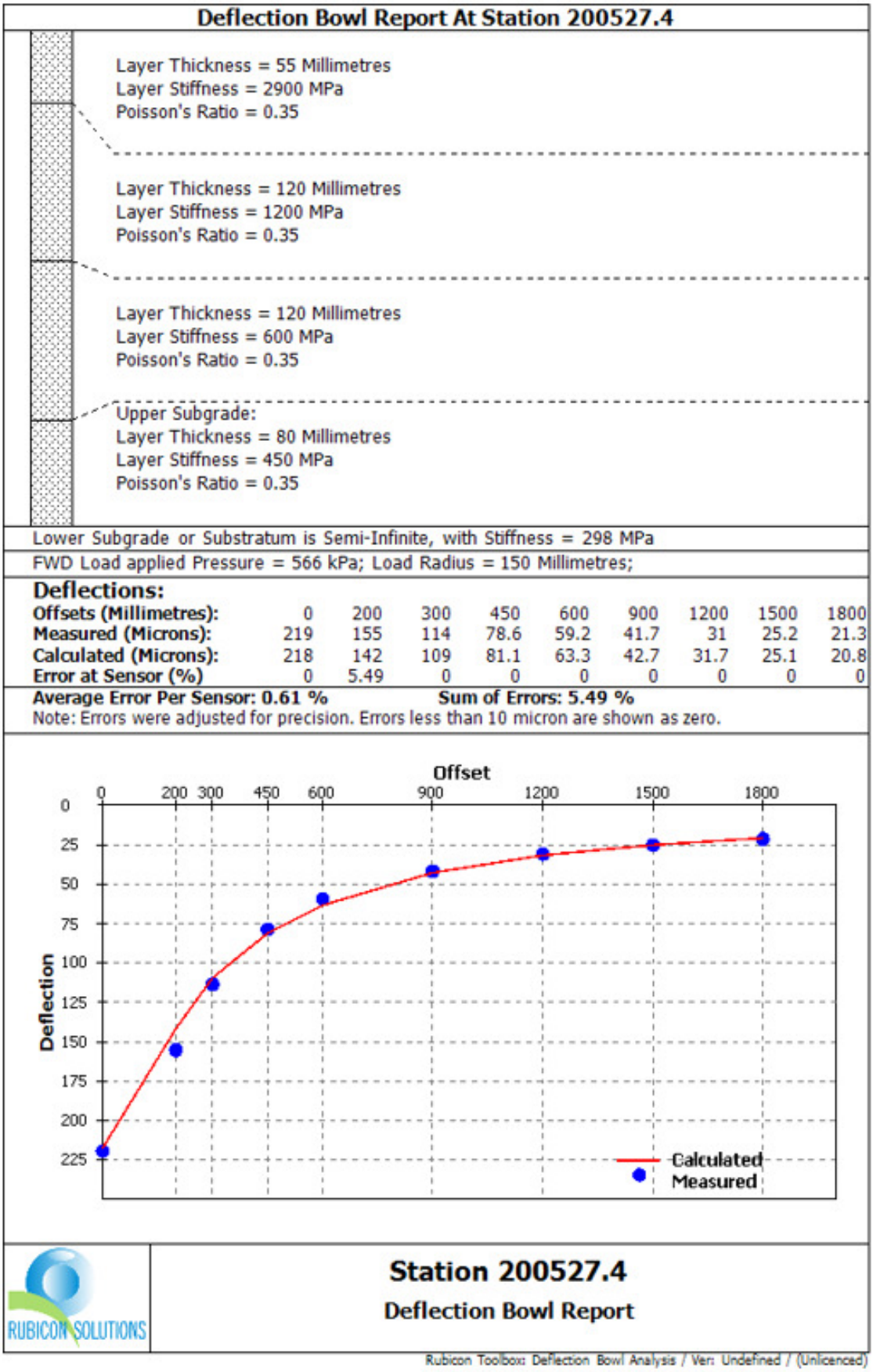

Figure G.2: N12-19 (3) deflection bowl 2005

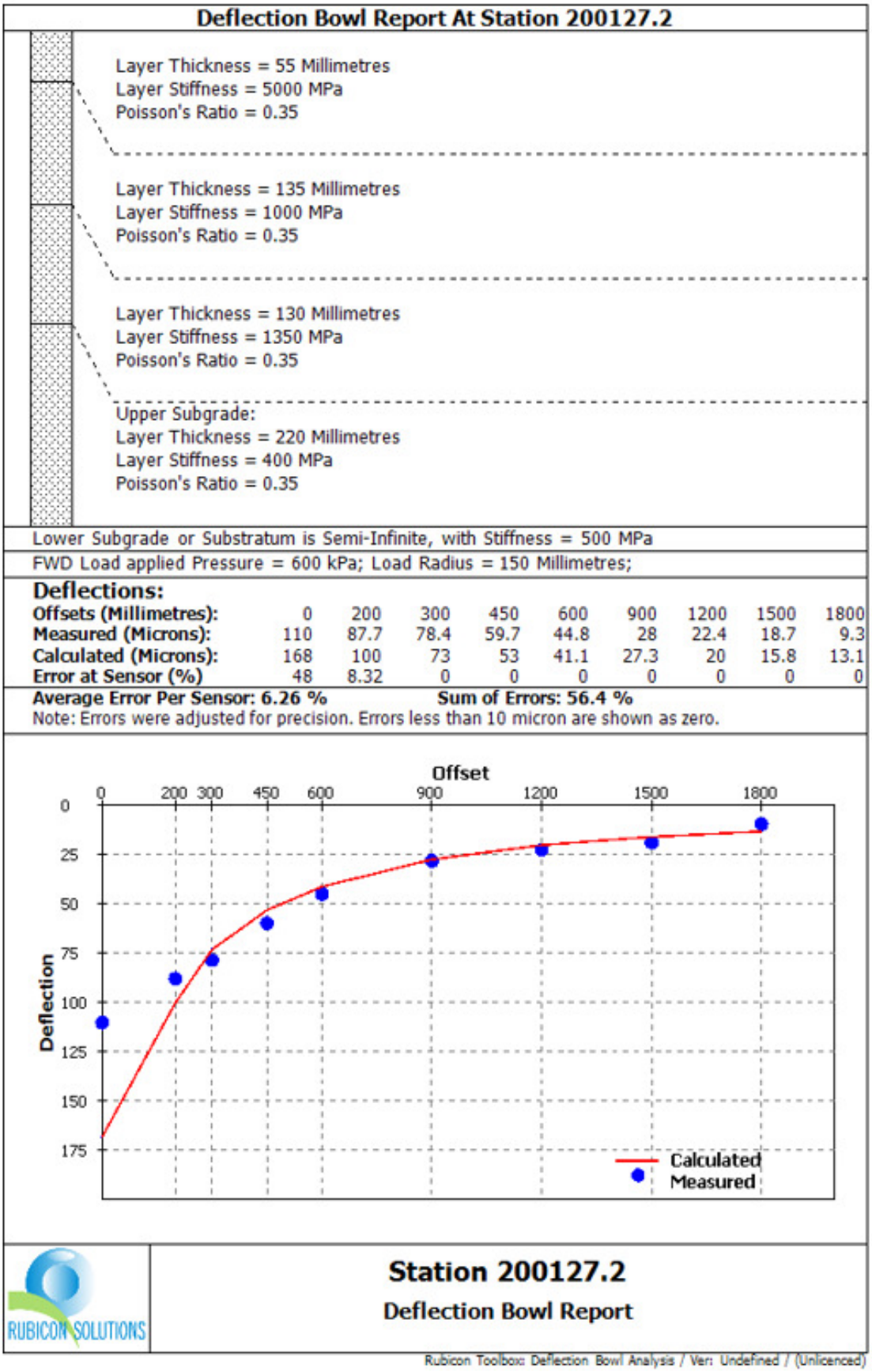

Figure G.3: N12-19 (4) deflection bowl 2001

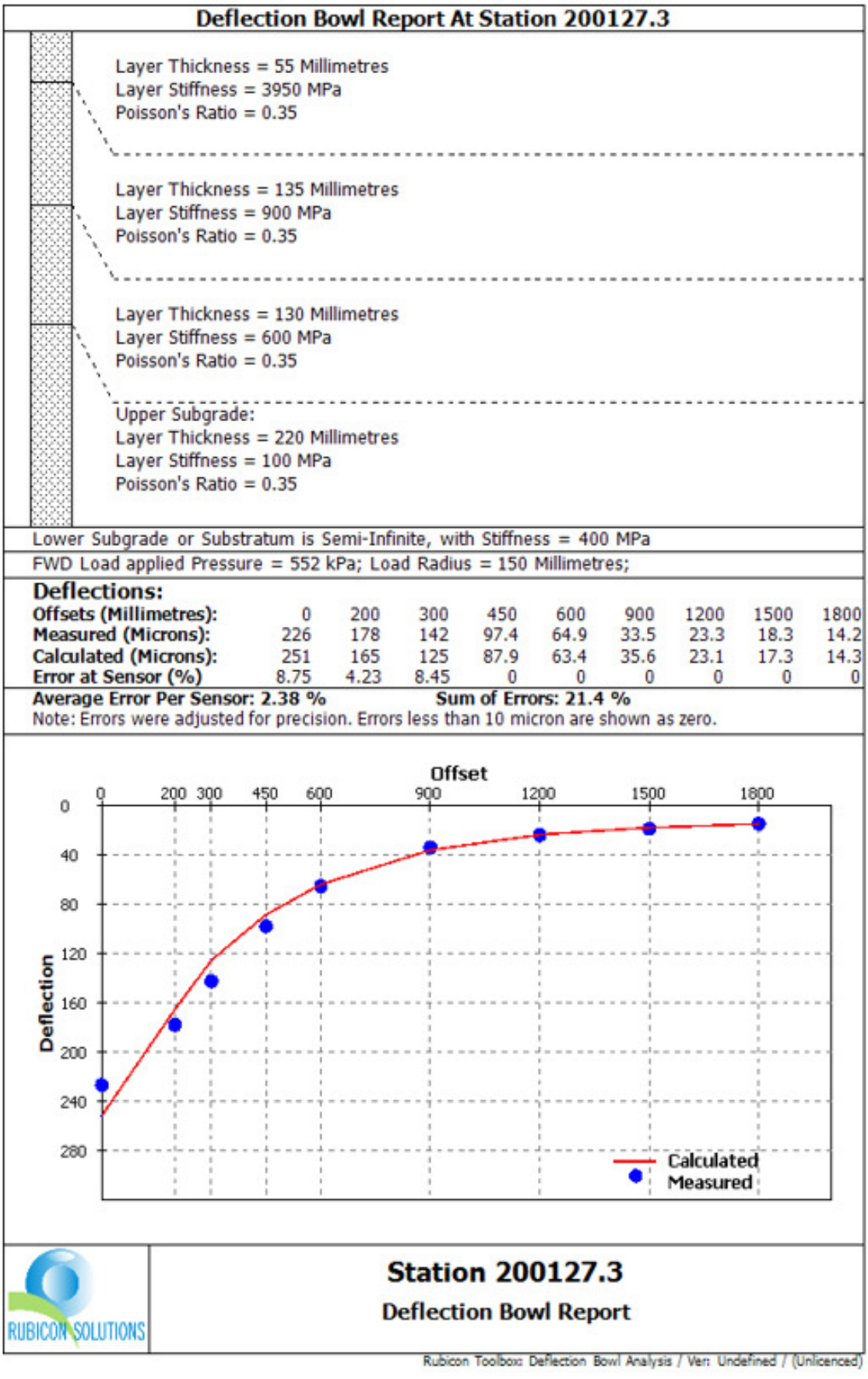

Figure G.4: N12-19 (4) deflection bowl 2001

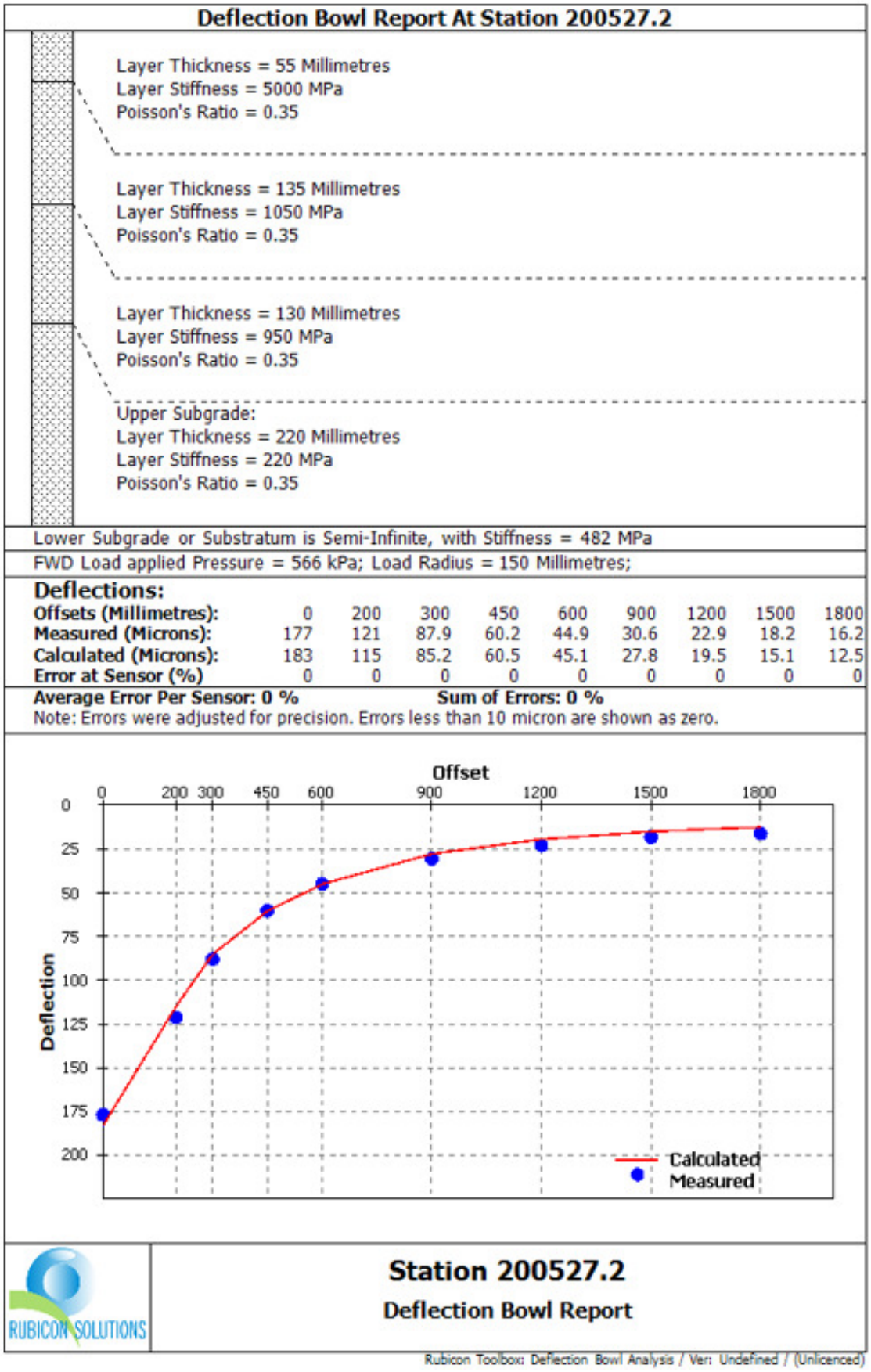

Figure G.5: N12-19 (4) deflection bowl 2005

Appendix H

LTTP permanent strain development comparison

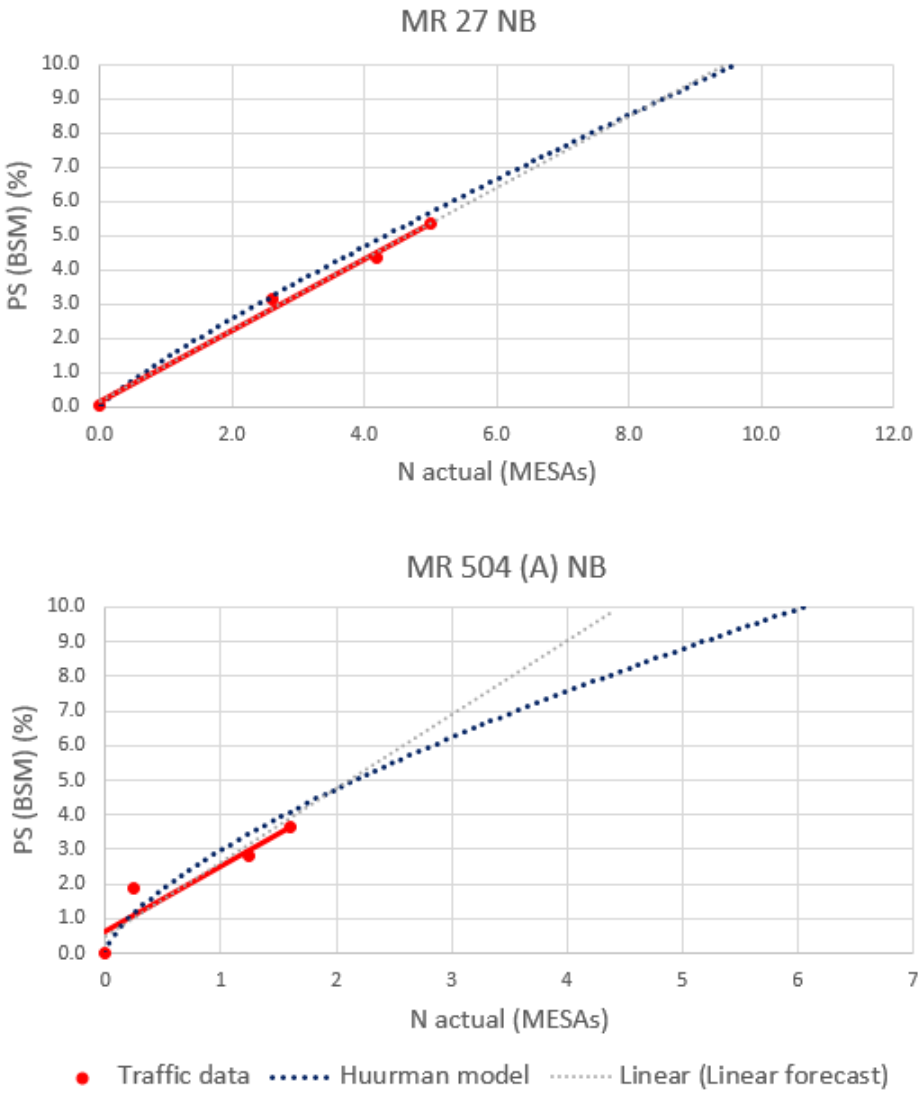

Figure H.1: Permanent strain development prediction with Huurman model (2)

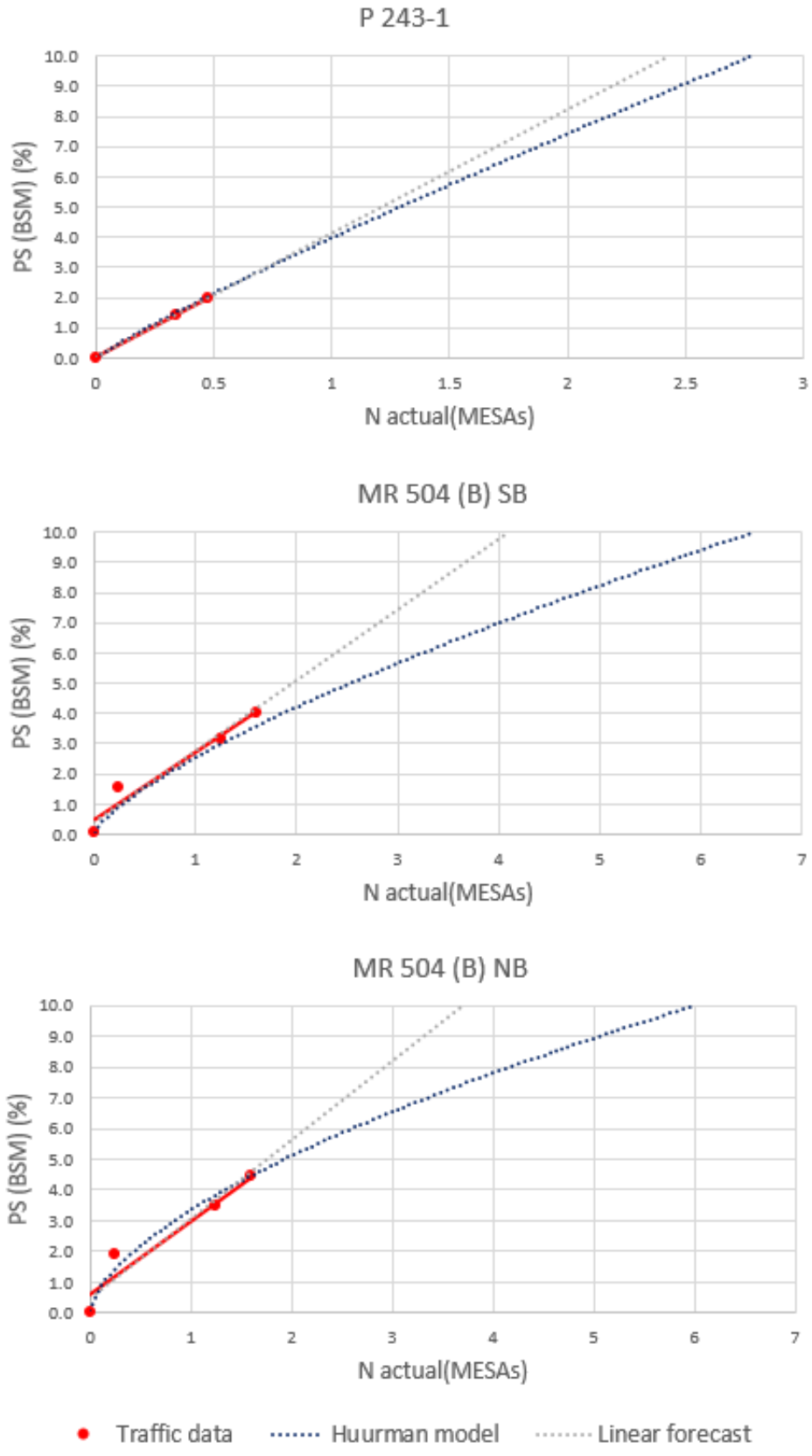

Figure H.2: Permanent strain development prediction with Huurman model (3)

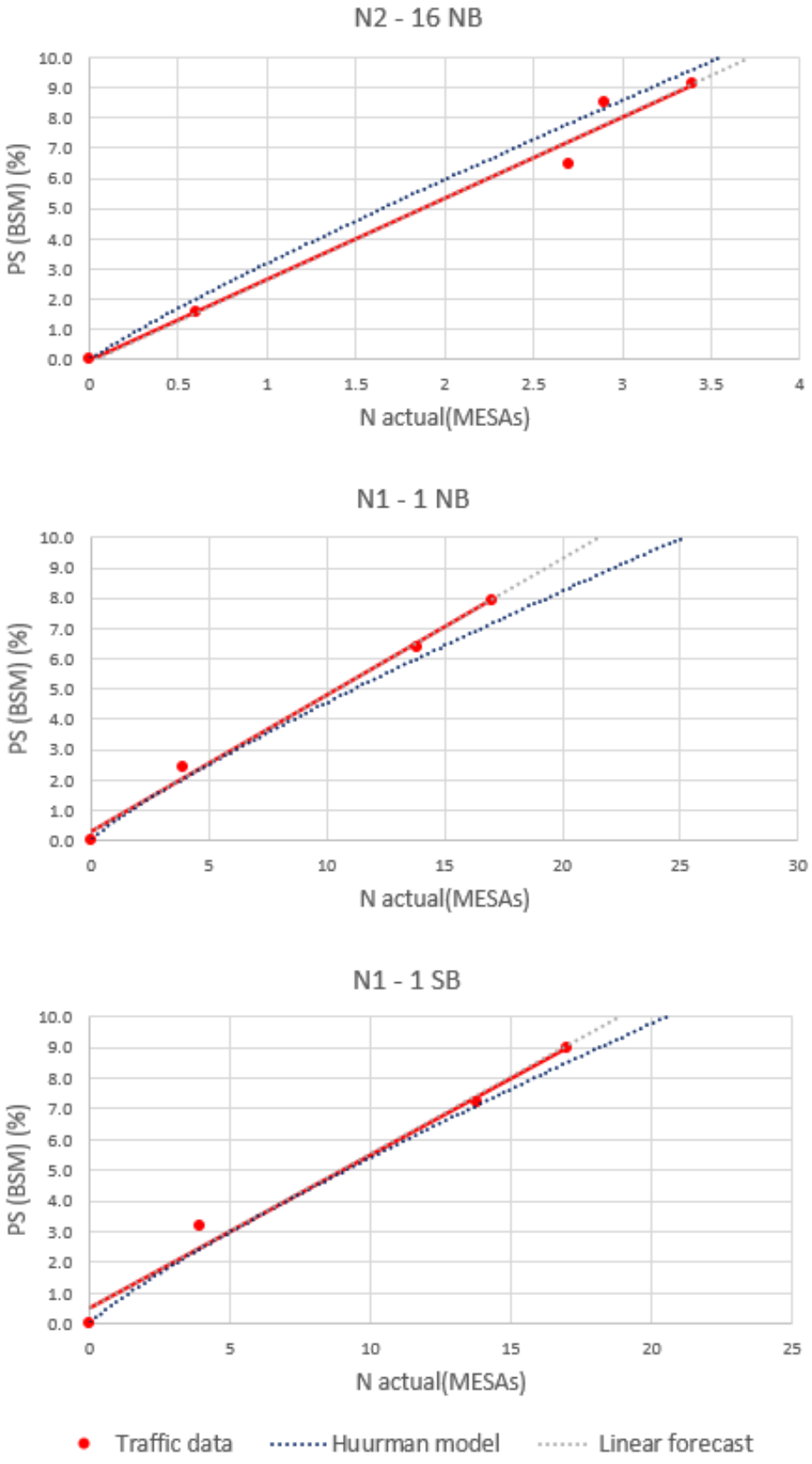

Figure H.3: Permanent strain development prediction with Huurman model (4)

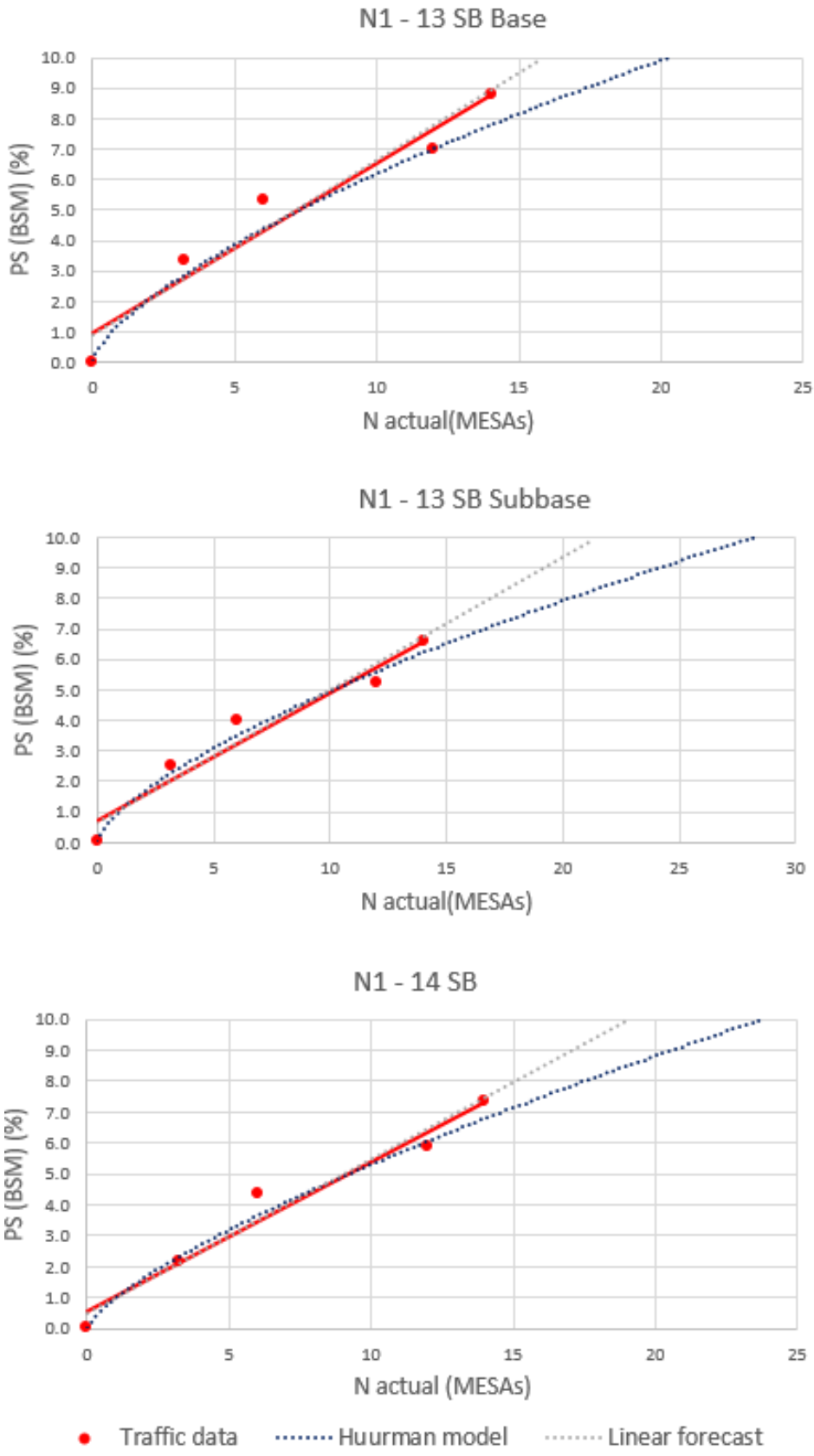

Figure H.4: Permanent strain development prediction with Huurman model (5)

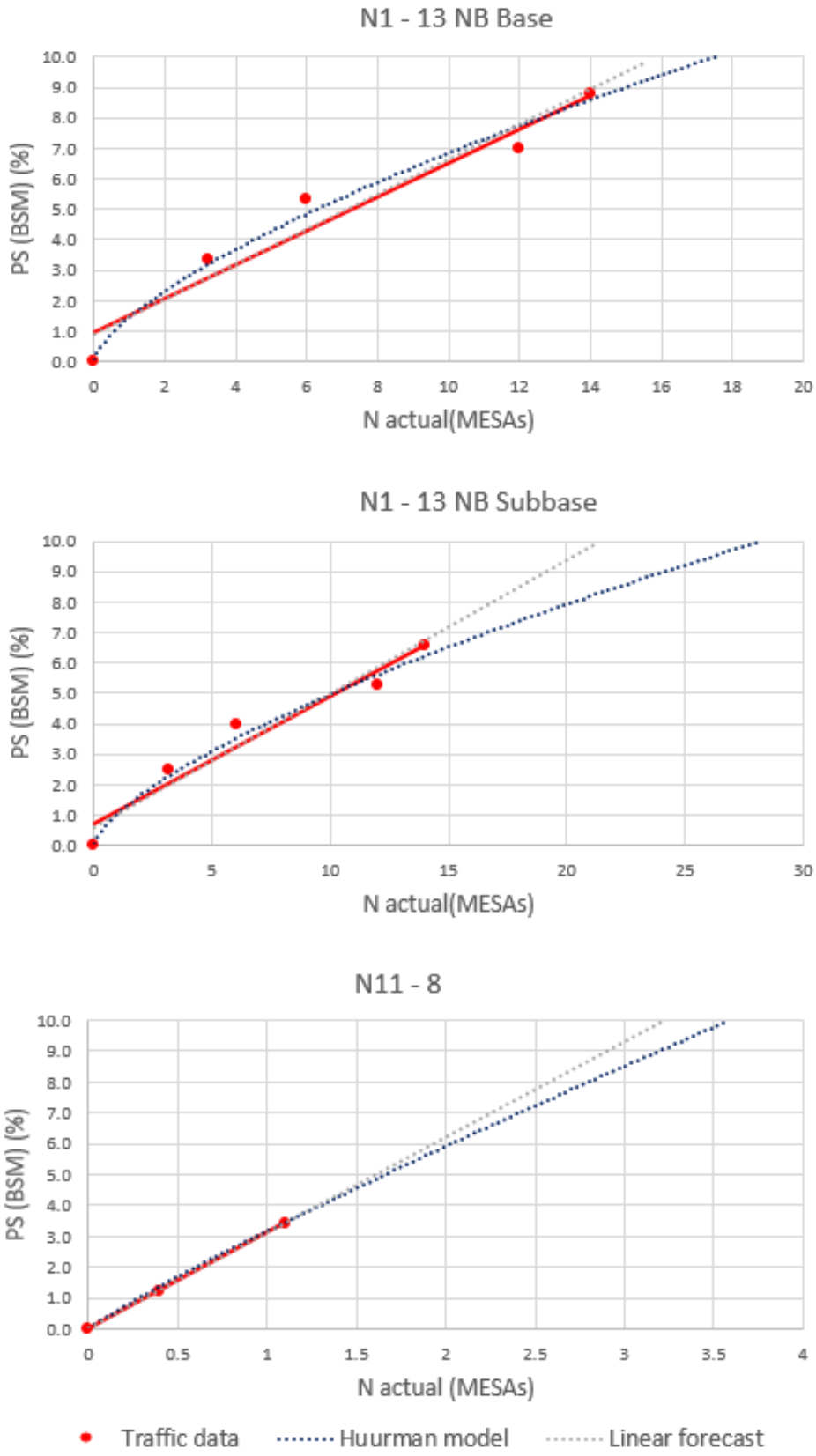

Figure H.5: Permanent strain development prediction with Huurman model (6)

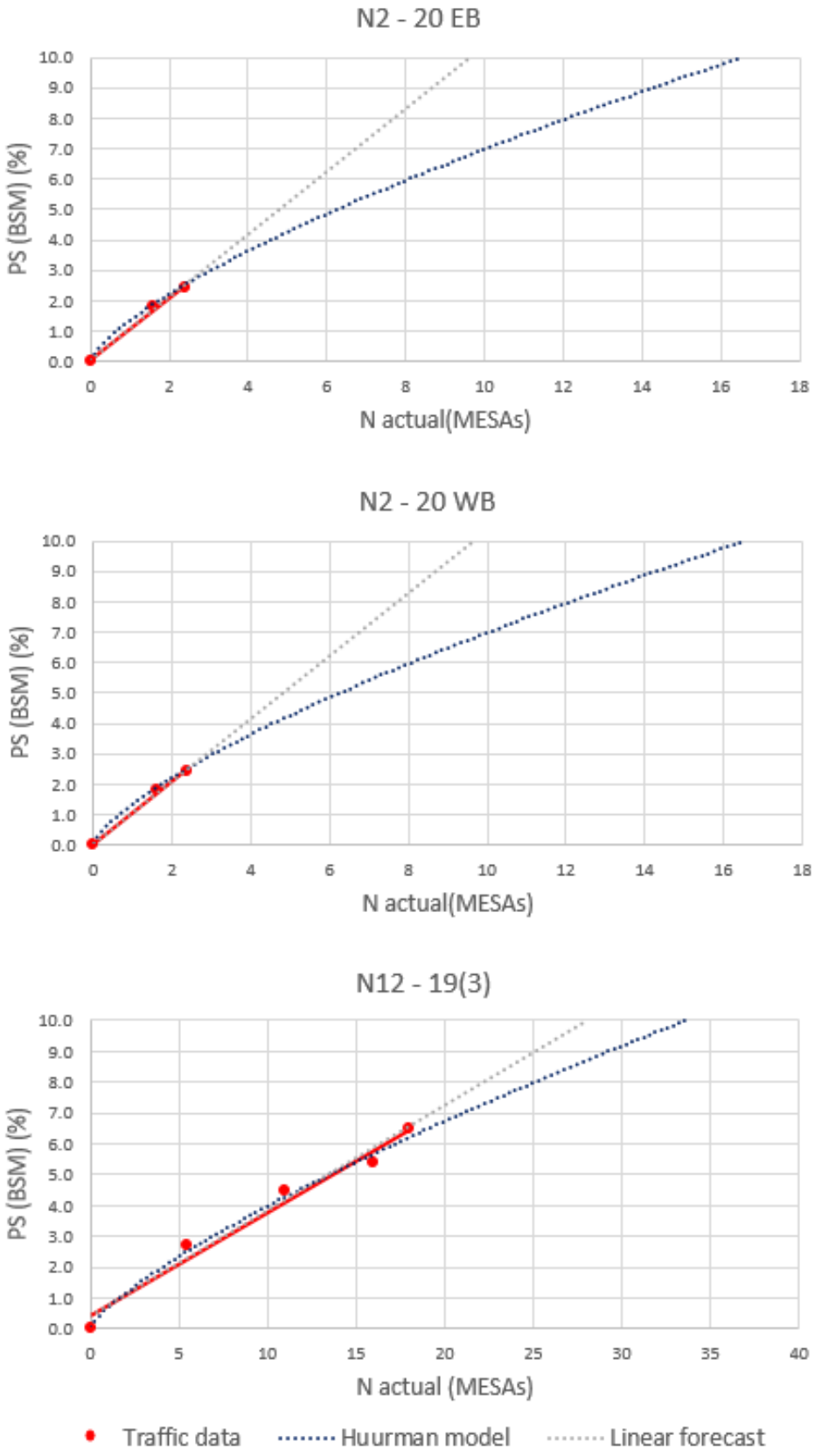

Figure H.6: Permanent strain development prediction with Huurman model (7)

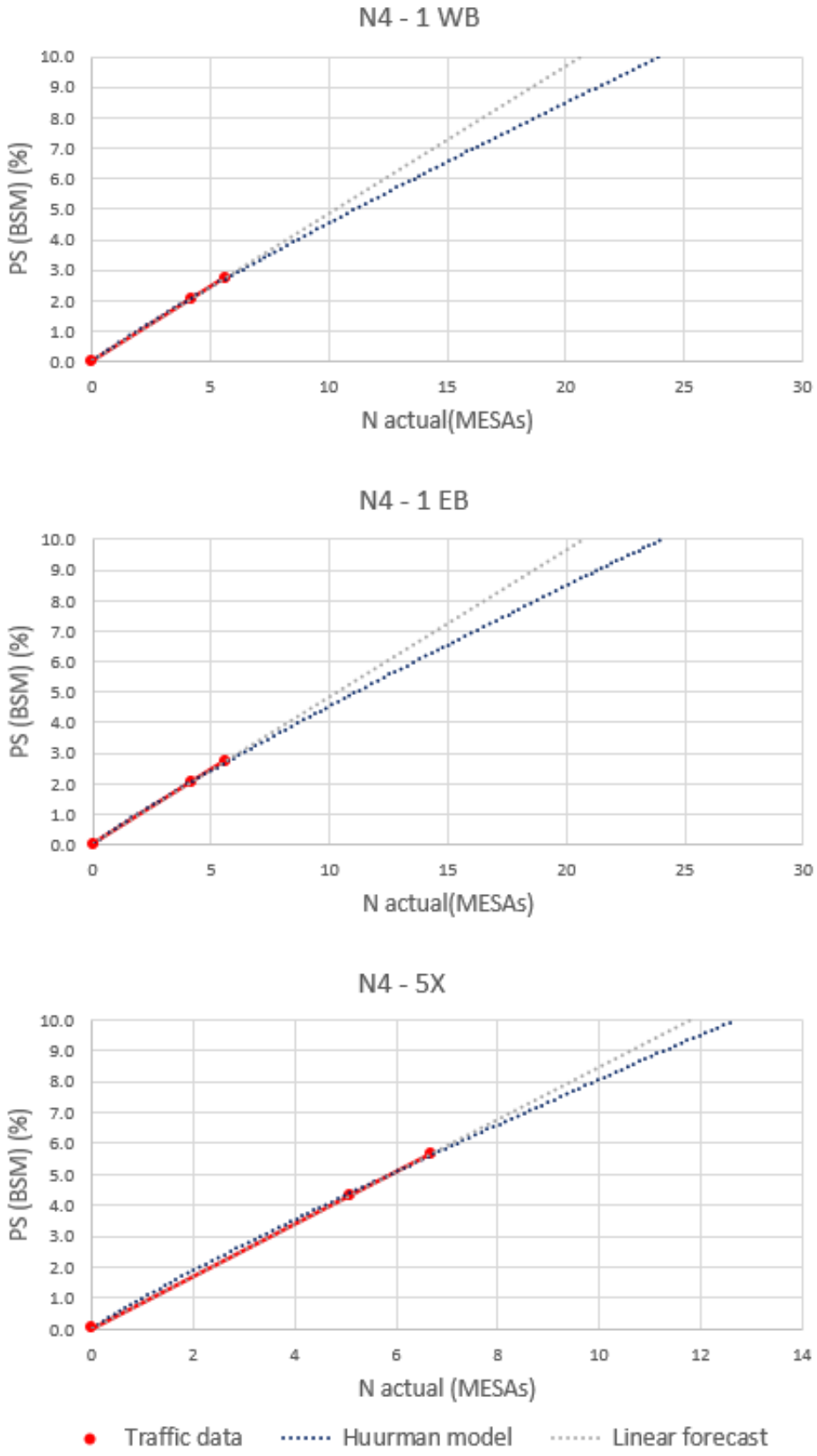

Figure H.7: Permanent strain development prediction with Huurman model (8)

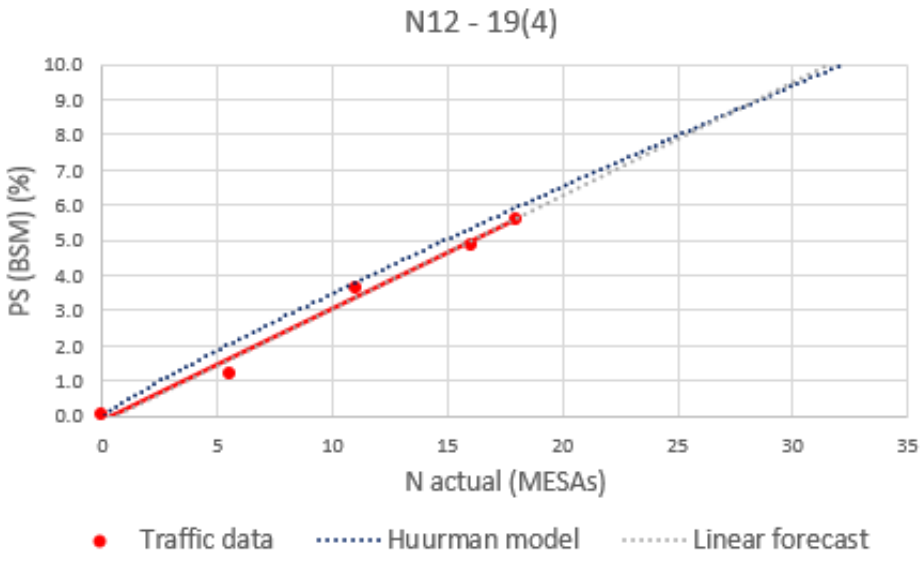

Figure H.8: Permanent strain development prediction with Huurman model (9)

Table H.1: Permanent strain prediction using linear prediction and the Huurman model(1)

Road			Year	N Huurman	N Linear	N actual	PS meusured (mm)	PS (BSM) (%)
MR 27 SB	A	0.009	1988	0.0	0.0	0	0.0	0.0
	B	0.735	2002	2.0	2.6	2.6	4.2	2.3
	Slope	1.082	2006	4.4	4.2	4.2	7.4	4.1
	R^2	0.976	2008	5.4	5.0	5	8.6	4.8
Prediction				6.6	5.8			5.5
				10.8	8.3			7.9
				14.8	10.4			10.0
MR 27 NB	A	0.004	1988	0.0	0.0	0	0.0	0.1
	B	0.865	2002	2.5	2.6	2.6	5.7	3.1
	Slope	0.906	2006	3.7	4.2	4.2	7.9	4.3
	R^2	0.995	2008	4.7	5.0	5	9.8	5.4
Prediction				5.3	5.6			6.0
				7.4	7.5			8.0
				9.6	9.4			10.0
MR504 (A) SB	A	0.045	1995	0.0	0.0	0	0.0	0.0
	B	0.608	1998	0.5	0.3	0.25	6.0	1.9
	Slope	1.100	2006	1.3	1.3	1.25	11.0	3.5
	R^2	0.973	2008	1.9	1.6	1.6	14.2	4.4
Prediction				3.2	2.1			6.0
				5.1	2.9			8.0
				7.4	3.7			10.0
MR504 (A) NB	A	0.029	1995	0.0	0.0	0	0.0	0.0
	B	0.672	1998	0.5	0.3	0.25	6.0	1.9
	Slope	0.722	2006	0.9	1.3	1.25	9.0	2.8
	R^2	0.929	2008	1.4	1.6	1.6	11.6	3.6
Prediction				2.8	2.6			6.0
				4.3	3.5			8.0
				6.1	4.4			10.0
MR504 (B) SB	A	0.016	1995	0.0	0.0	0	0.0	0.0
	B	0.732	1998	0.5	0.3	0.25	5.0	1.6
	Slope	1.078	2006	1.3	1.3	1.25	10.0	3.1
	R^2	0.977	2008	1.9	1.6	1.6	12.9	4.0
Prediction				3.2	2.4			6.0
				4.8	3.2			8.0
				6.5	4.1			10.0
MR504(B) NB	A	0.050	1995	0.0	0.0	0	0.0	0.0
	B	0.608	1998	0.4	0.3	0.25	6.0	1.9
	Slope	0.900	2006	1.0	1.3	1.25	11.0	3.5
	R^2	0.973	2008	1.6	1.6	1.6	14.2	4.4
Prediction				2.6	2.1			6.0
				4.2	2.9			8.0
				6.0	3.7			10.0

Table H.2: Permanent strain prediction using linear prediction and the Huurman model(2)

Road ID			Year	N Huurman	N Linear	N actual	PS meusured (mm)	PS (BSM) (%)
N1-1 SB	A	0.002	1984	0.0	0.0	0	0.0	0.0
	B	0.854	1995	5.4	3.9	3.9	8.0	3.2
	Slope	1.015	2006	14.0	13.8	13.8	18.0	7.2
	R^2	0.992	2008	18.1	17.0	17	22.5	9.0
Prediction				18.7	17.4			9.3
				19.8	18.3			9.7
				20.5	18.8			10.0
N1-1 NB	A	0.002	1984	0.0	0.0	0	0.0	0.0
	B	0.854	1995	4.7	3.9	3.9	6.0	2.4
	Slope	1.100	2006	14.9	13.8	13.8	16.0	6.4
	R^2	0.998	2008	19.2	17.0	17	19.9	8.0
Prediction				22.2	19.3			9.0
				23.6	20.4			9.5
				25.1	21.5			10.0
N1-13 SB Base	A	0.012	1980	0.0	0.0	0	0.0	0.0
	B	0.676	1991	4.0	3.2	3.2	10.0	3.3
	Slope	1.100	1997	8.0	6.0	6	16.0	5.3
	R^2	0.972	2006	12.0	12.0	12	21.0	7.0
			2008	16.8	14.0	14	26.4	8.8
Prediction				17.9	14.3			9.2
				19.1	15.0			9.6
				20.3	15.6			10.0
N1-13 SB Subbase	A	0.012	1980	0.0	0.0	0	0.0	0.0
	B	0.676	1991	3.4	3.2	3.2	10.0	3.0
	Slope	0.950	1997	6.9	6.0	6	16.0	4.8
	R^2	0.972	2006	10.3	12.0	12	21.0	6.3
			2008	14.5	14.0	14	26.4	7.9
Prediction				16.1	14.7			8.5
				19.0	16.6			9.5
				20.5	17.5			10.0
N1-13 NB Base	A	0.014	1980	0.0	0.0	0	0.0	0.0
	B	0.676	1991	3.4	3.2	3.2	10.0	3.3
	Slope	0.950	1997	6.9	6.0	6	16.0	5.3
	R^2	0.972	2006	10.3	12.0	12	21.0	7.0
			2008	14.5	14.0	14	26.4	8.8
Prediction				15.5	14.3			9.2
				16.7	15.1			9.7
				17.5	15.6			10.0

Table H.3: Permanent strain prediction using linear prediction and the Huurman model(3)

Road ID			Year	N Huurman	N Linear	N actual	PS meusured (mm)	PS (BSM) (%)
	A	0.012	1980	0.0	0.0	0	0.0	0.0
	B	0.676	1991	3.4	3.2	3.2	10.0	3.0
N1-13 NB Subbase	Slope	0.950	1997	6.9	6.0	6	16.0	4.8
	R^2	0.972	2006	10.3	12.0	12	21.0	6.3
			2008	14.5	14.0	14	26.4	7.9
				16.1	14.7			8.5
Prediction				19.0	16.6			9.5
				20.5	17.5			10.0
	A	0.006	1980	0.0	0.0	0	0.0	0.0
	B	0.732	1991	3.0	3.2	3.2	6.0	2.2
N1-14 SB	Slope	1.050	1997	7.7	6.0	6	12.0	4.4
	R^2	0.974	2006	11.5	12.0	12	16.0	5.9
			2008	15.5	14.0	14	20.0	7.3
				19.6	16.4			8.7
Prediction				21.8	17.8			9.4
				23.7	19.0			10.0
	A	0.006	1980	0.0	0.0	0	0.0	0.0
	B	0.900	1990	0.5	0.6	0.6	4.0	1.6
N2-16 NB	Slope	0.950	2005	2.2	2.7	2.7	16.4	6.4
	R^2	0.978	2006	3.0	2.9	2.9	21.6	8.5
			2006	3.2	3.4	3.4	23.2	9.1
				3.4	3.5			9.5
Prediction				3.4	3.6			9.6
				3.6	3.7			10.0
	A	0.010	2000	0.0	0.0	0	0.0	0.0
N2-20 EB	B	0.711	2006	1.5	1.6	1.6	6.0	1.8
	Slope	0.950	2008	2.3	2.4	2.4	8.0	2.4
	R^2	1.000		6.2	4.8			5.0
Prediction				11.0	7.2			7.5
				16.6	9.6			10.0
	A	0.010	2000	0.0	0.0	0	0.0	0.0
N2-20 WB	B	0.711	2006	1.5	1.6	1.6	6.0	1.8
	Slope	0.950	2008	2.3	2.4	2.4	8.0	2.4
	R^2	1.000		6.2	4.8			5.0
Prediction				11.0	7.2			7.5
				16.6	9.6			10.0
	A	0.001	1997	0.1	0.0	0	0.0	0.0
N4-1 EB	B	0.900	2006	4.1	4.2	4.2	5.0	2.1
	Slope	1.000	2008	5.7	5.6	5.6	6.7	2.7
	R^2	0.999		11.1	10.3			5.0
Prediction				17.4	15.5			7.5
				24.0	20.7			10.0

Table H.4: Permanent strain prediction using linear prediction and the Huurman model(4)

Road ID			Year	N Huurman	N Linear	N actual	PS meusured (mm)	PS (BSM) (%)
N4-1 WB	A	0.001	1997	0.1	0.0	0	0.0	0.0
	B	0.900	2006	4.1	4.2	4.2	5.0	2.1
	Slope	1.000	2008	5.7	5.6	5.6	6.7	2.7
Prediction	R^2	0.999		11.1	10.3			5.0
				17.4	15.5			7.5
				24.0	20.7			10.0
N4-5X EB	A	0.002	1996	0.0	0.0	0	0.0	0.0
	B	0.900	2006	5.0	5.1	5.1	10.0	4.3
	Slope	1.000	2008	6.8	6.7	6.7	13.1	5.7
Prediction	R^2	0.999		8.5	8.3			7.0
				10.6	10.0			8.5
				12.7	11.8			10.0
N11-8 NB	A	0.006	2004	0.0	0.0	0	0.0	0.0
	B	0.900	2006	0.4	0.4	0.4	5.0	1.3
	Slope	0.997	2008	1.1	1.1	1.1	13.8	3.4
Prediction	R^2	0.998		2.4	2.2			7.0
				3.0	2.7			8.5
				3.6	3.2			10.0
N12-19(3) EB	A	0.003	1974	0.0	0.0	0	0.0	0.0
	B	0.761	1991	5.7	5.5	5.5	6.0	2.4
	Slope	0.950	2000	11.2	11.0	11	10.0	4.0
	R^2	0.988	2006	14.2	16.0	16	12.0	4.8
			2008	18.1	18.0	18	14.4	5.8
Prediction				27.8	25.1			8.0
				32.5	28.4			9.0
				37.3	31.7			10.0
N12-19(4) EB	A	0.001	1974	0.1	0.0	0	0.0	0.0
	B	0.900	1991	3.1	5.5	5.5	3.0	1.3
	Slope	0.950	2000	10.5	11.0	11	9.0	4.0
	R^2	0.945	2006	14.5	16.0	16	12.0	5.3
			2008	16.9	18.0	18	13.8	6.1
Prediction				19.6	20.4			7.0
				24.3	24.7			8.5
				29.1	29.0			10.0
P243-1 EB	A	0.008	2000	0.0	0.0	0	0.0	0.0
	B	0.900	2006	0.3	0.3	0.34	5.0	1.4
	Slope	0.967	2008	0.5	0.5	0.48	7.1	2.0
Prediction	R^2	0.999		1.3	1.2			5.0
				1.9	1.7			7.0
				2.8	2.4			10.0

Appendix I

LTTP Transfer function input values

Table I.1: LTTP pavements: Allocation of plastic strain to BSM layers

Road	BSM thickness (mm)	Initial allcation	Thickness adjustment	Surfacing thickness (mm)	Surfacing adjustment	Support material class	Support adjustment	Additional adjustment	Sum of adjustments	BSM PS allocation (%)
MR27	100	50%	0%	50	-5%	C3	10%		5%	55%
MR504(A)	175	50%	7%	20	-2%	G7	0%		5%	55%
MR504(B)	175	50%	7%	30	-3%	G7	0%		4%	55%
N1-1	100	50%	0%	80	-8%	C3	10%	5%	7%	55%
N1-13	150	50%	5%	40	-4%	BSM	10%	-10%	1%	50%
N1-13 SB	100	50%	0%	40	-4%	G6	0%	-10%	-14%	35%
N1-14	150	50%	5%	10	-1%	G4	0%		4%	55%
N2-16	140	50%	4%	40	-4%	C4	10%	10%	20%	70%
N2-20	180	50%	8%	30	-3%	G6	0%		5%	55%
N4-1	170	50%	7%	30	-3%	C4	10%	5%	19%	70%
N4-5X	150	50%	5%	30	-3%	C3	10%	-5%	7%	65%
N11-8	280	50%	18%	20	-2%	G6	0%	-5%	11%	60%
N12-19(3)	100	50%	0%	55	-6%	C3	10%		5%	55%
N12-19(4)	135	50%	4%	55	-6%	C3	10%		8%	60%
P243-1	250	50%	15%	25	-3%	G8	0%	10%	23%	70%

Table I.1 summarizes the calculations to determine the plastic strain accumulation of the BSM layers of the LTPP pavements. These values are a very rough estimate and not the actual deformation in the layers. The table shows the LTPP pavements with their respective BSM layer thicknesses. Initially, 50% of all deformation (rut measurements) was allocated to the base layer.

The initial PS allocation was adjusted based on the thickness of the BSM layer. The allocation was increased by 10% of the thickness increase over 100 mm. This indicates that a thicker BSM layer can deform more than a thin BSM. The second adjustment was done based on the surfacing on the BSM. The PS allocation to the BSM was reduced by 10% of the surfacing thickness. The increase in surfacing thickness reduces the PS allocated to the BSM as some of the deformation occurs in the surfacing and the stresses are reduced in the BSM layer.

Adjustments to the PS allocation to the BSM layers were made based on the support layers under the BSMs. Cement stabilised sub-base layers increased the allocation by 10%. Cement stabilised layers provide a much stiffer support which does not tend to fail in permanent deformation. PS

allocation to BSMs with granular support layers was not adjusted.

Additional adjustments were made to the PS allocation for certain pavements based on other factors than mentioned above. Firstly, the N1-1 and the N4-1 was allocated an additional 5% due to good quality and thick support layers. The N1-13 base and sub-base was allocated a reduction in 10% of the PS allocation. This was done to achieve an overall balance in the plastic strain allocation of the pavement structure (not to exceed a 100% allocation).

The allocation of PS to the BSM of the N2-16 was increased by 10%. This increase was chosed as the material has very good support in the cement stabilised sub-base layer and a 300mm thick granular selected layer. The allocation of PS to the BSM of the P243-1 was also increased by 10%. This was chosen as the BSM base layer in this pavement is very thick compared to the other layers. Therefore, it is responsible for the majority of the observed deformation.

These adjustments were summed and rounded to the nearest five. This resulted in the total allocation of PS to the BSM layers of the LTPP pavements.

Table I.2: LTTP pavements: Analysis results and TF input values (1)

Road ID	Layer	Layer Thickness (mm)	Material Class	Back Calc Stiffness (Mpa)	BSM Properties	
MR27 SB	1	50	DS	3000	C	275
	2	100	BSM 1	650	Phi	40
	3	100	C3	300	DSR	0.319
	4	150	G7	150	RetC	75
	5	-	G9	100	P.mod	102.1
MR27 NB	1	50	DS	3000	C	275
	2	100	BSM 1	875	Phi	40
	3	100	C3	375	DSR	0.324
	4	150	G7	150	RetC	75
	5	-	G9	100	P.mod	102.1
MR504(A) SB	1	20	SS	1750	C	250
	2	175	BSM 1	650	Phi	40
	3	150	G7	150	DSR	0.331
	4	-	G10	90	RetC	75
	5				P.mod	100
MR504(A) NB	1	20	SS	1750	C	250
	2	175	BSM 1	650	Phi	40
	3	150	G7	150	DSR	0.331
	4	-	G10	90	RetC	75
	5				P.mod	100
MR504(B) SB	1	30	AC	850	C	250
	2	175	BSM 2	430	Phi	40
	3	150	G7	150	DSR	0.308
	4	-	G10	90	RetC	75
	5				P.mod	95
MR504(B) NB	1	30	AC	850	C	250
	2	175	BSM 2	430	Phi	40
	3	150	G7	150	DSR	0.308
	4	-	G10	90	RetC	75
	5				P.mod	95

Table I.3: LTTP pavements: Analysis results and TF input values (2)

Road ID	Layer	Layer Thickness (mm)	Material Class	Back Calc Stiffness (Mpa)	BSM Properties	
N1-1 SB	1	80	AC	2000	C	250
	2	100	BSM 1	750	Phi	40
	3	100	C3	420	DSR	0.305
	4	150	G5	200	RetC	75
	5	-	G8	125	P.mod	101.3
N1-1 NB	1	80	AC	1500	C	250
	2	100	BSM 1	520	Phi	40
	3	100	C3	265	DSR	0.3
	4	150	G5	200	RetC	75
	5	-	G8	125	P.mod	101.3
N1-13 SB	1	10	SS	1000	C	275
	2	30	AC	1000	Phi	40
	3	150	BSM 2	400	DSR	0.301
	4	100	BSM 2	275	RetC	75
	5	300	G6	180	P.mod	100
	6	-	G7	140		
N1-13 SB	1	10	SS	1000	C	200
	2	30	AC	1000	Phi	35
	3	150	BSM 2	400	DSR	0.203
	4	100	BSM 2	275	RetC	65
	5	300	G6	180	P.mod	97.8
	6	-	G7	140		
N1-13 NB	1	10	SS	700	C	275
	2	30	AC	700	Phi	40
	3	150	BSM 2	450	DSR	0.299
	4	100	BSM 2	300	RetC	75
	5	300	G6	180	P.mod	100
	6	-	G7	140		
N1-13 NB	1	10	SS	700	C	200
	2	30	AC	700	Phi	35
	3	150	BSM 2	450	DSR	0.185
	4	100	BSM 2	300	RetC	65
	5	300	G6	180	P.mod	97.8
	6	-	G7	140		
N1-14 SB	1	10	SS	1000	C	275
	2	30	AC	1000	Phi	40
	3	150	BSM 1	350	DSR	0.303
	4	100	G4	140	RetC	75
	5	300	G6	110	P.mod	100
	6	-	G7	100		
N2-16 NB	1	40	AC	2500	C	225
	2	140	BSM 2	650	Phi	40
	3	130	C4	550	DSR	0.339
	4	300	G7	175	RetC	75
	5	-	G9	110	P.mod	100

Table I.4: LTTP pavements: Analysis results and TF input values (3)

Road ID	Layer	Layer Thickness (mm)	Material Class	Back Calc Stiffness (Mpa)	BSM Properties	
N2-20 EB	1	30	AC	3250	C	260
	2	180	BSM 1	800	Phi	40
	3	270	G6	200	DSR	0.309
	4	150	G7	125	RetC	75
	5	-	G10	100	P.mod	100
N2-20 WB	1	30	AC	3250	C	260
	2	180	BSM 1	800	Phi	40
	3	270	G6	200	DSR	0.309
	4	150	G7	125	RetC	75
	5	-	G10	100	P.mod	100
N4-1 EB	1	30	AC	2800	C	250
	2	170	BSM 1	810	Phi	40
	3	130	C4	675	DSR	0.306
	4	300	G6	150	RetC	75
	5	-	G7	125	P.mod	101.3
N4-1 WB	1	30	AC	3000	C	250
	2	170	BSM 1	900	Phi	40
	3	130	C4	650	DSR	0.303
	4	300	G6	150	RetC	75
	5	-	G7	125	P.mod	101.3
N4-5X EB	1	30	AC	2100	C	250
	2	150	BSM 1	750	Phi	40
	3	150	C3	400	DSR	0.316
	4	150	G7	180	RetC	75
	5	-	G9	110	P.mod	100
N11-8 NB	1	20	AC	1700	C	200
	2	280	BSM 2	410	Phi	35
	3	100	G6	130	DSR	0.333
	4	-	G8	100	RetC	75
	5				P.mod	100
N12-19(3) EB	1	55	AC	2450	C	265
	2	120	BSM 1	850	Phi	40
	3	120	C3	600	DSR	0.296
	4	80	C3	320	RetC	75
	5	-	G6	150	P.mod	100
N12-19(4) EB	1	55	AC	4500	C	265
	2	135	BSM 1	975	Phi	40
	3	130	C3	600	DSR	0.285
	4	220	G5	240	RetC	75
	5	-	G6	150	P.mod	100
P243-1 EB	1	25	AC	3000	C	230
	2	250	BSM 2	450	Phi	40
	3	150	G8	100	DSR	0.349
	4	-	G9	90	RetC	75
	5				P.mod	100.7

Appendix J

N_{TF} vs N_{Actual} for LTPP pavements

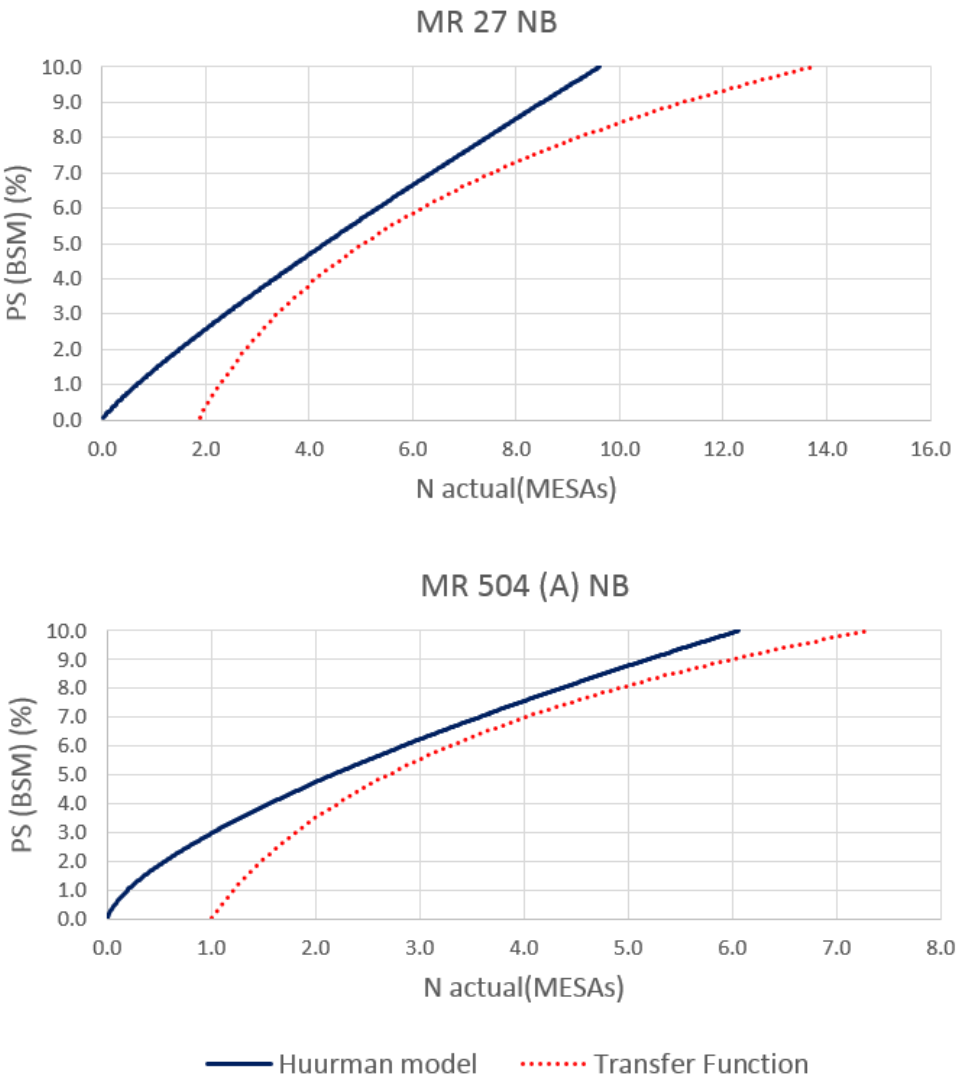

Figure J.1: N_{TF} vs N_{Actual} for LTPP pavements (2)

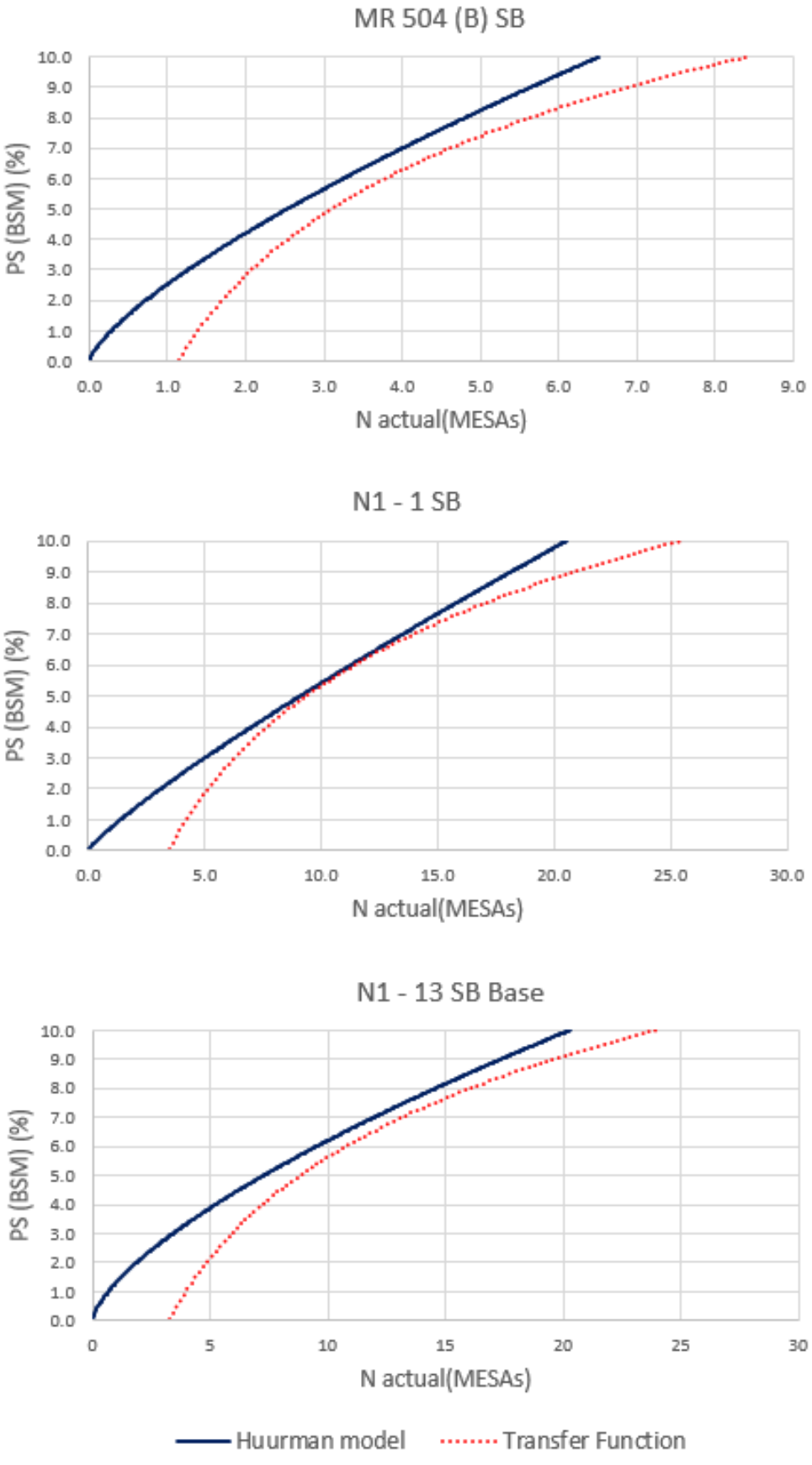

Figure J.2: N_{TF} vs N_{Actual} for LTPP pavements (3)

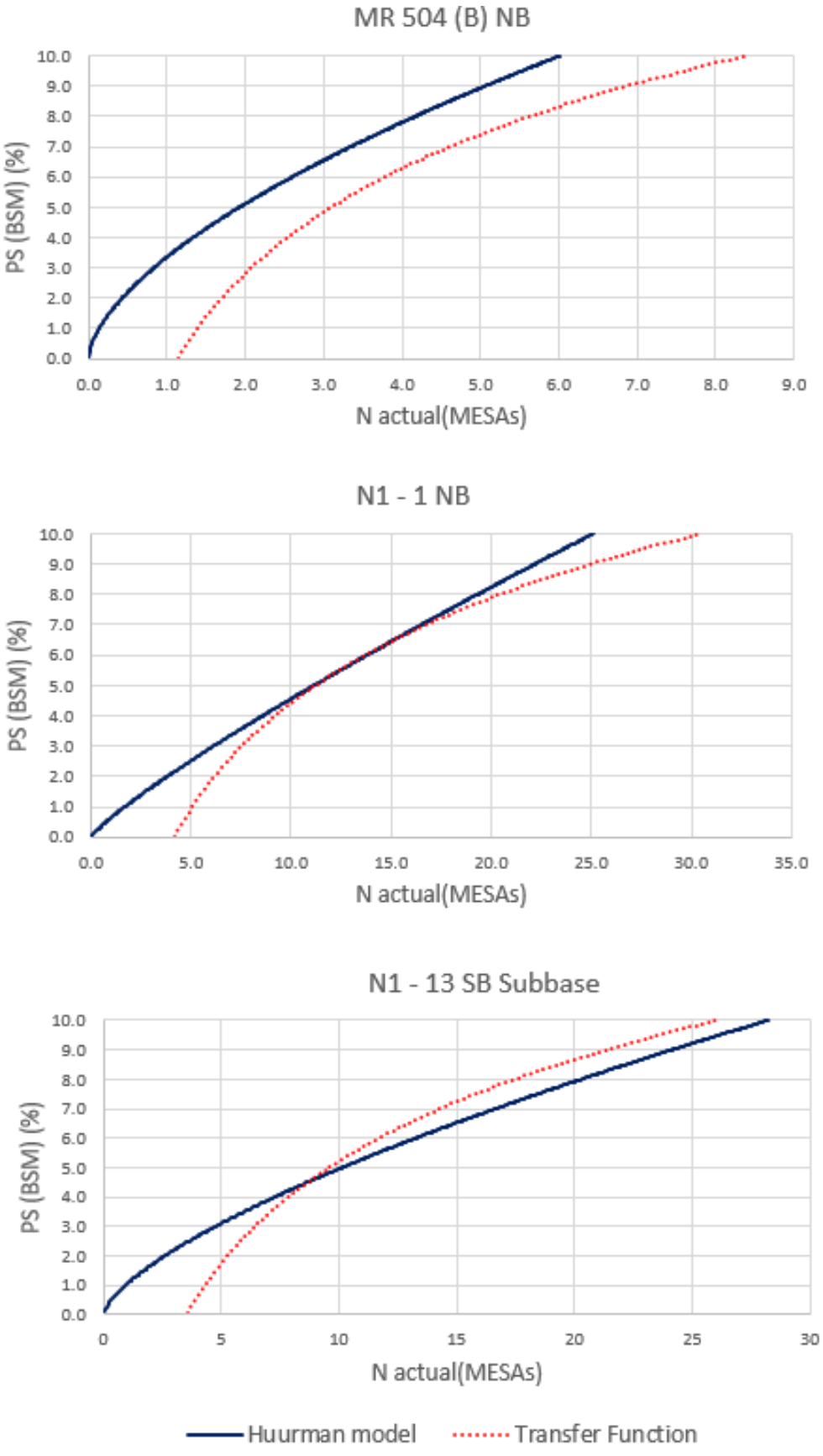

Figure J.3: N_{TF} vs N_{Actual} for LTPP pavements (4)

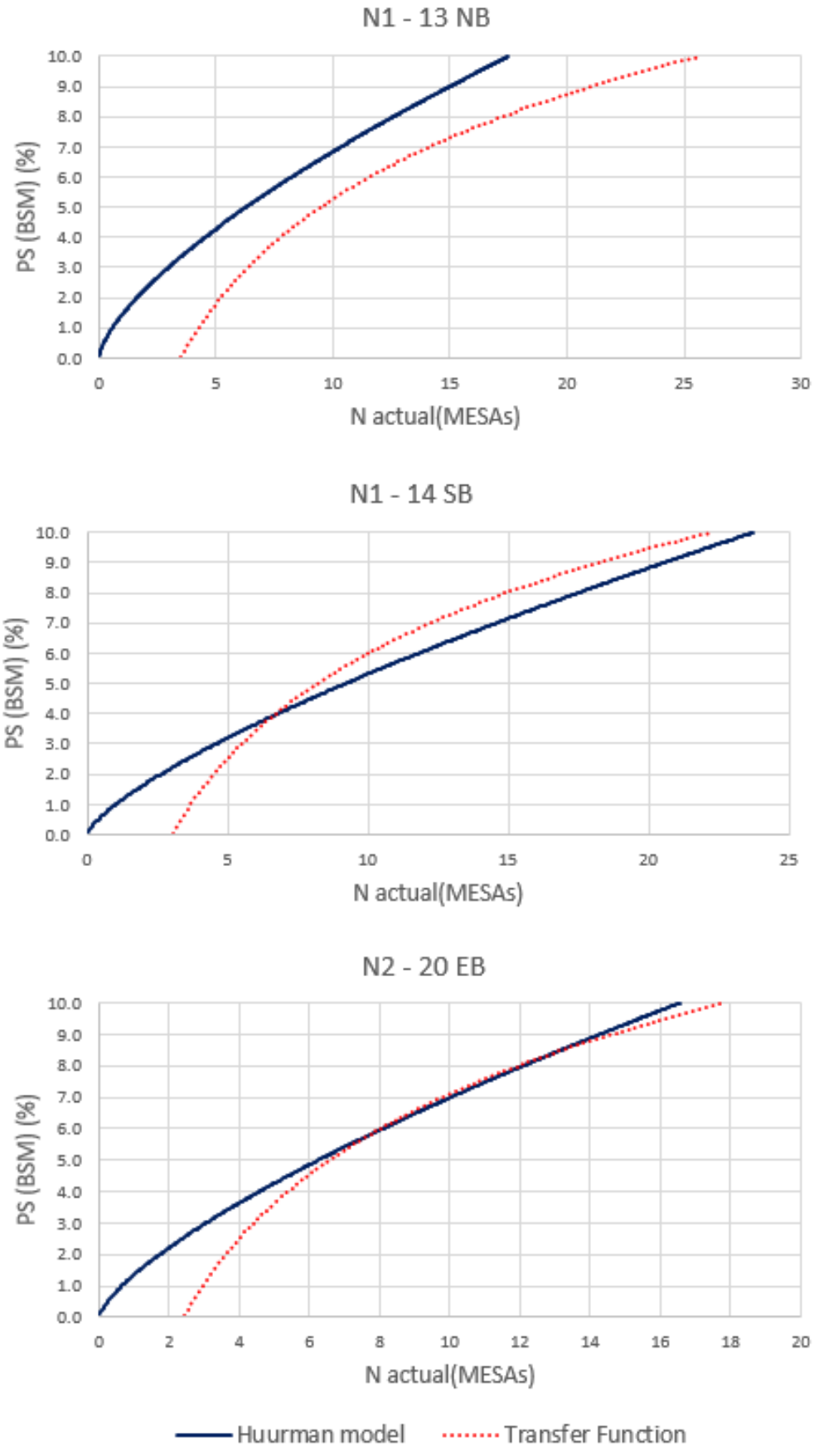

Figure J.4: N_{TF} vs N_{Actual} for LTPP pavements (5)

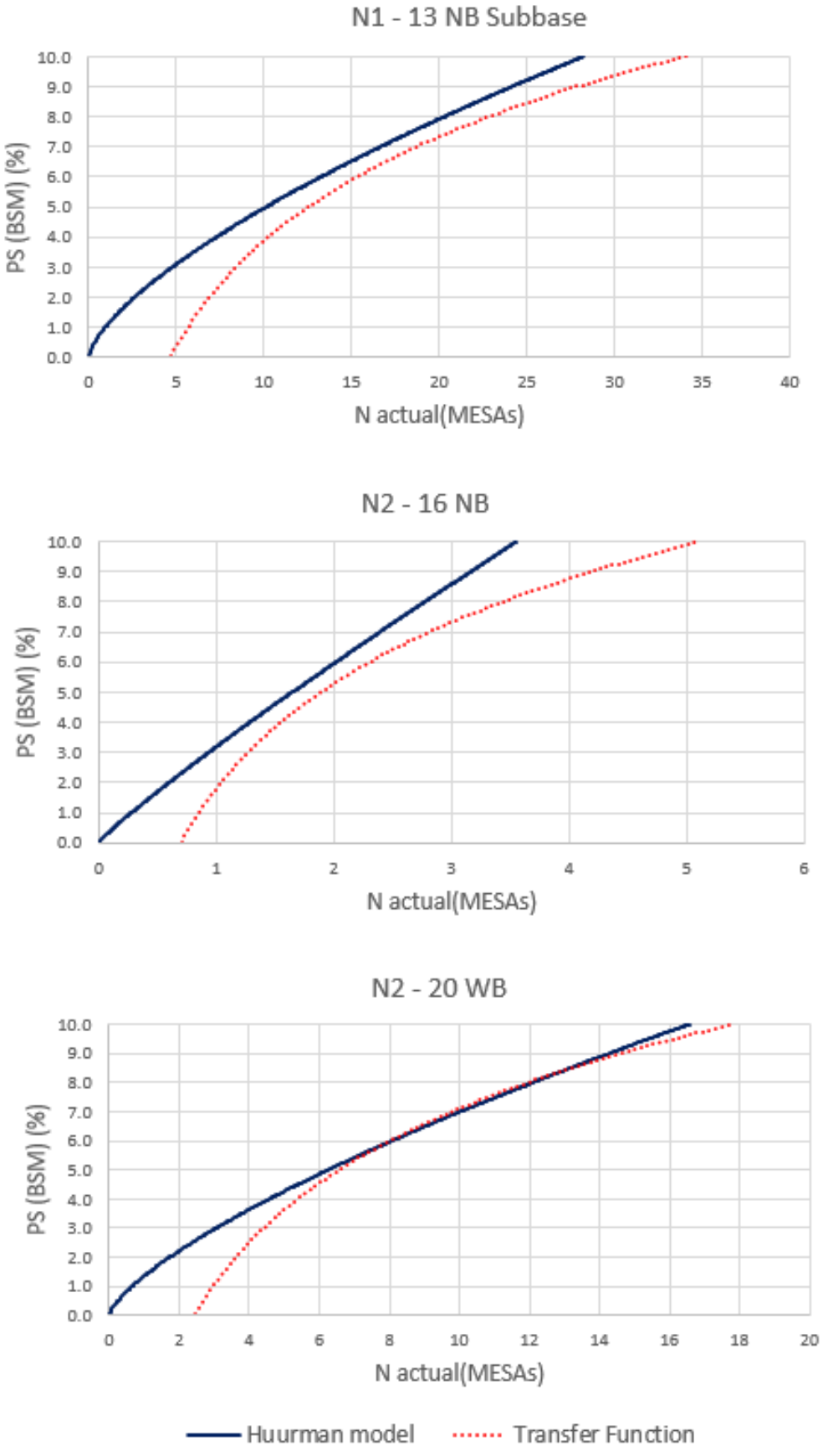

Figure J.5: N_{TF} vs N_{Actual} for LTPP pavements (6)

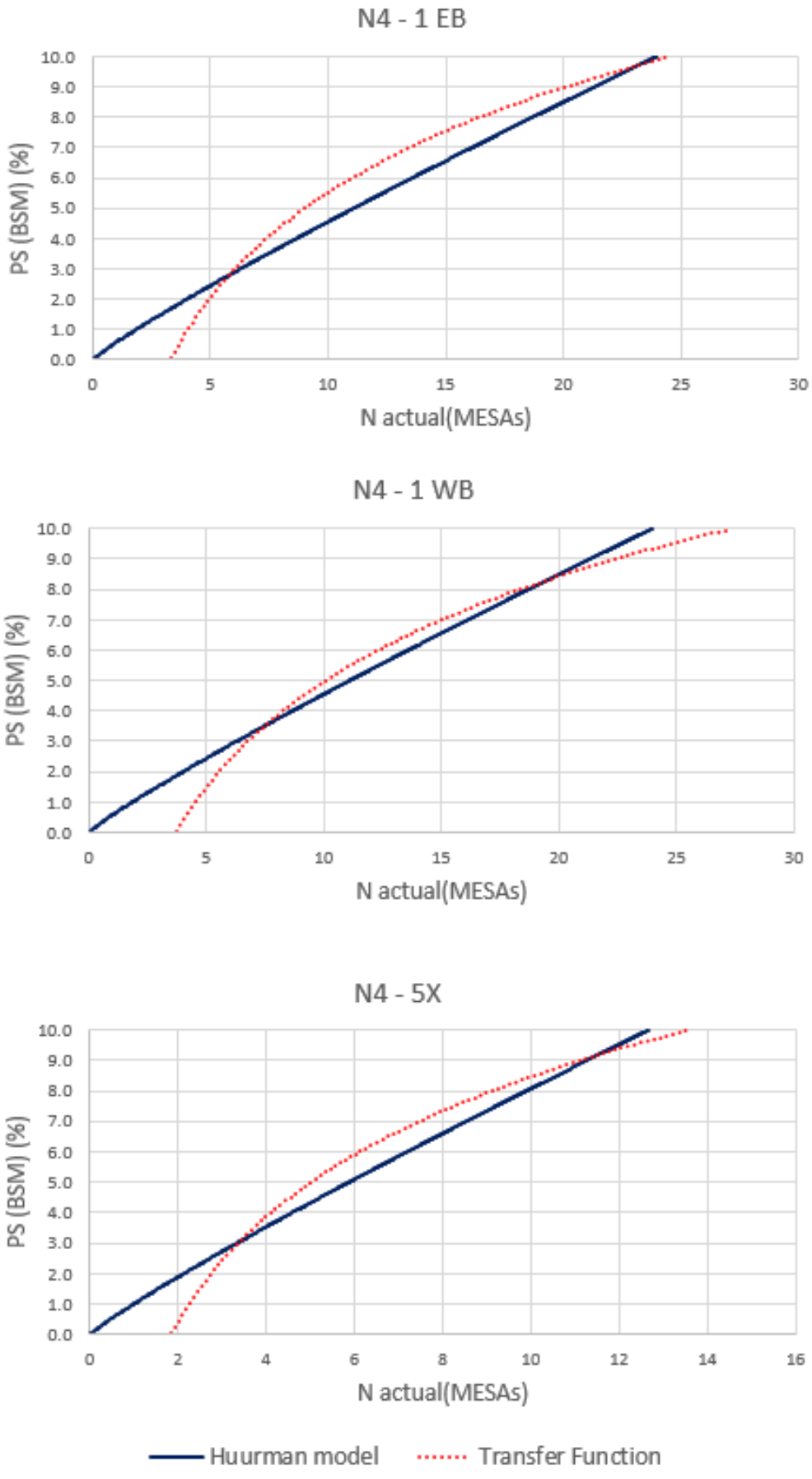

Figure J.6: N_{TF} vs N_{Actual} for LTPP pavements (7)

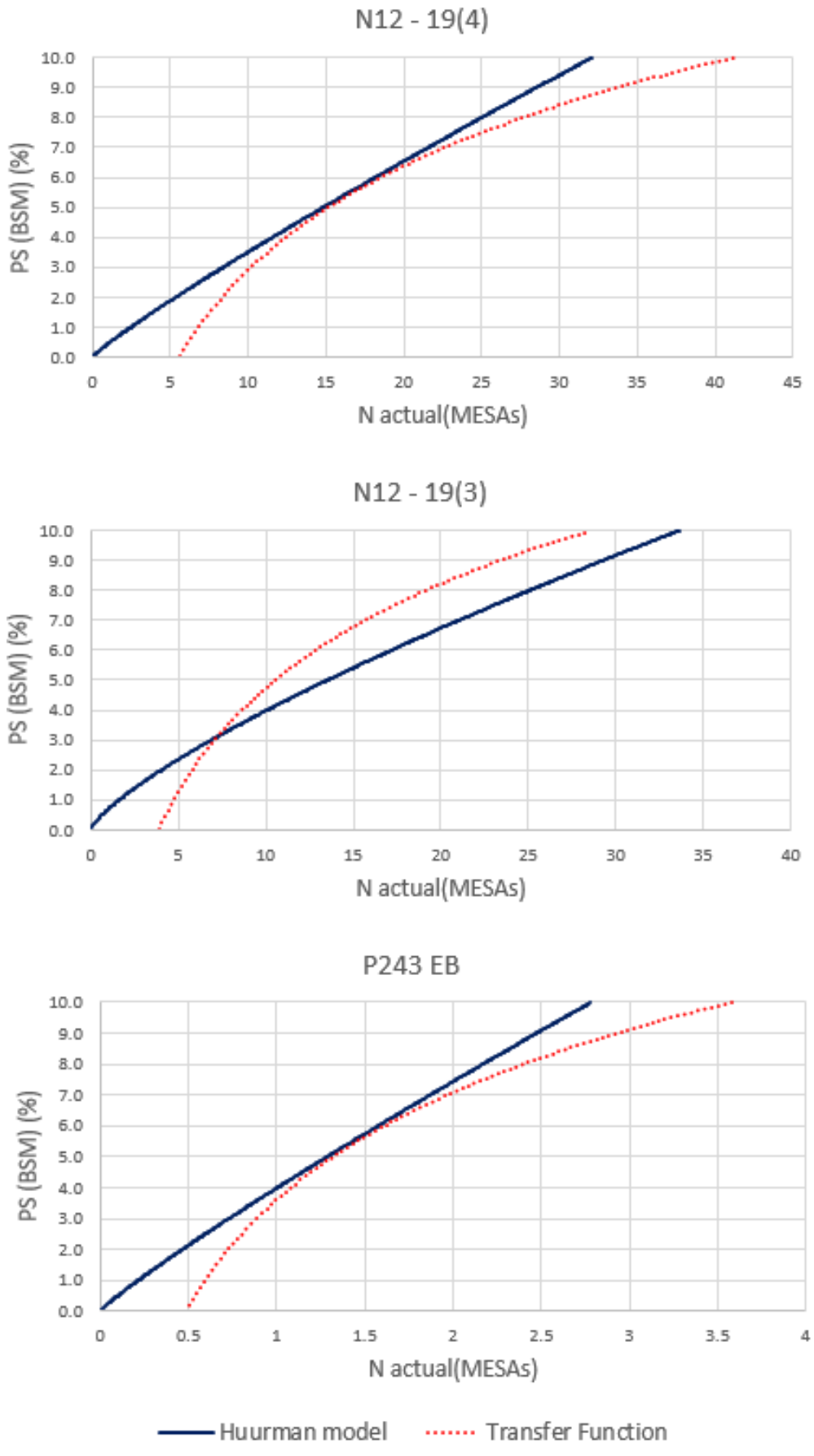

Figure J.7: N_{TF} vs N_{Actual} for LTPP pavements (8)

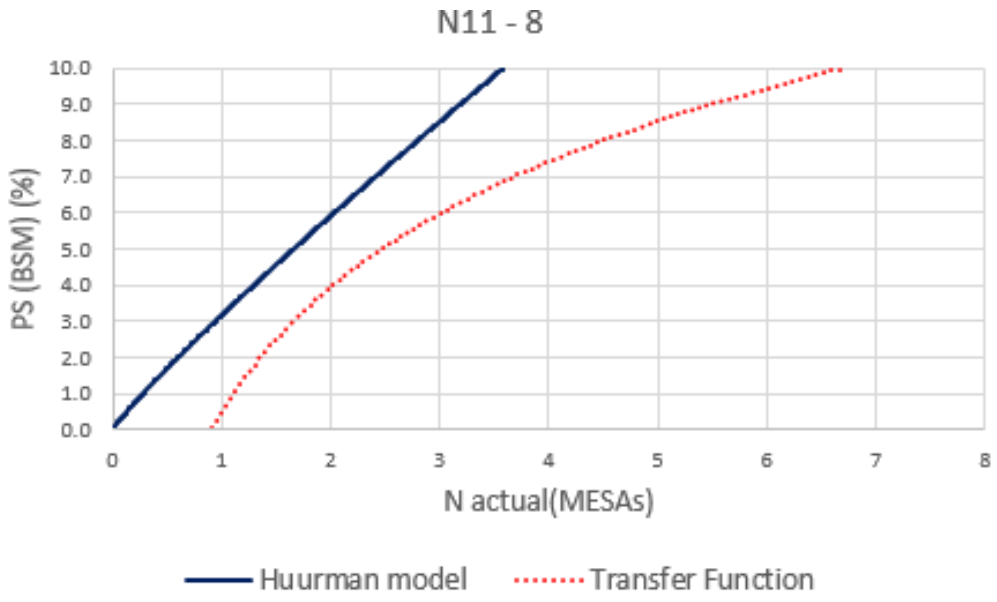

Figure J.8: N_{TF} vs N_{Actual} for LTPP pavements (9)

Appendix K

DSR power investigation

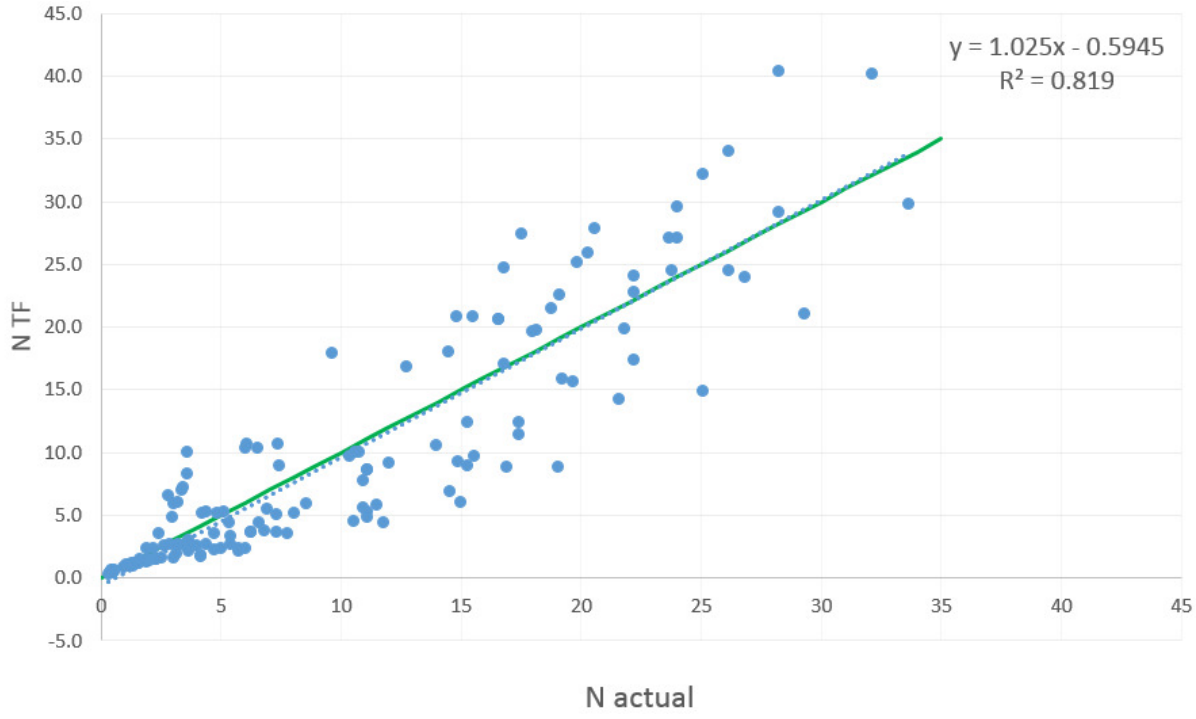

Figure K.1: N_{TF} vs N_{Actual} for LTPP pavements with DSR raised to the power 2

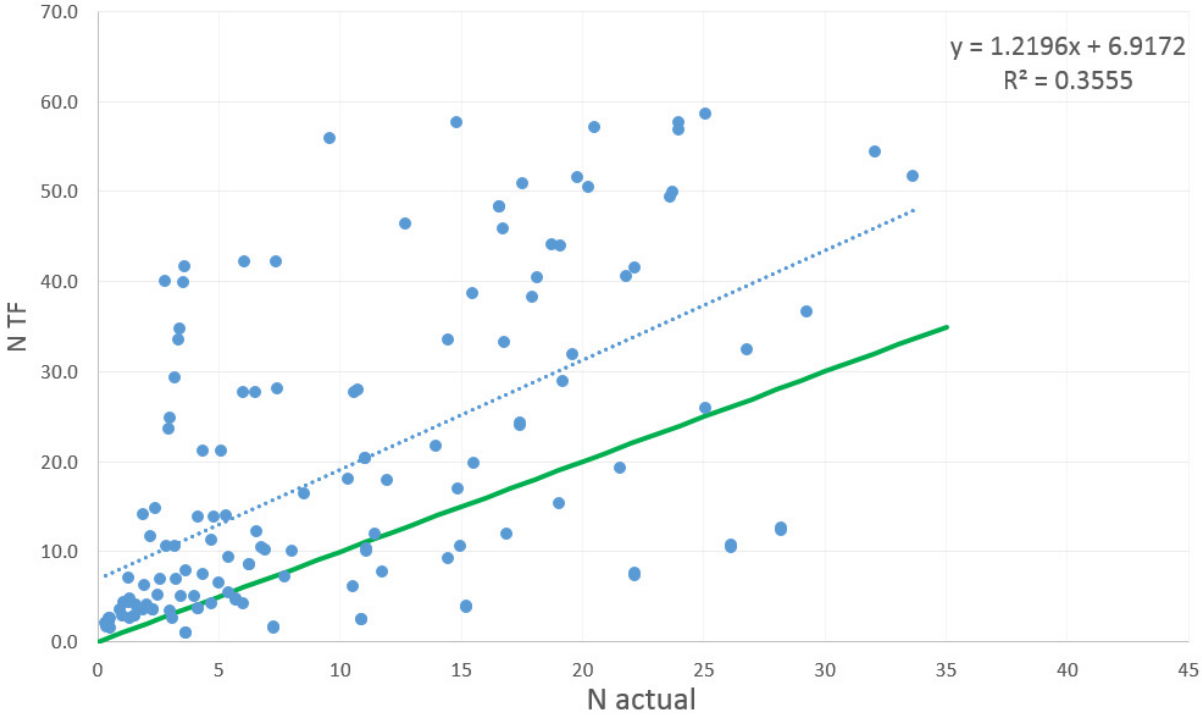

Figure K.2: N_{TF} vs N_{Actual} for LTPP pavements with DSR raised to the power 4

Appendix L

Transfer function certainty adjustments

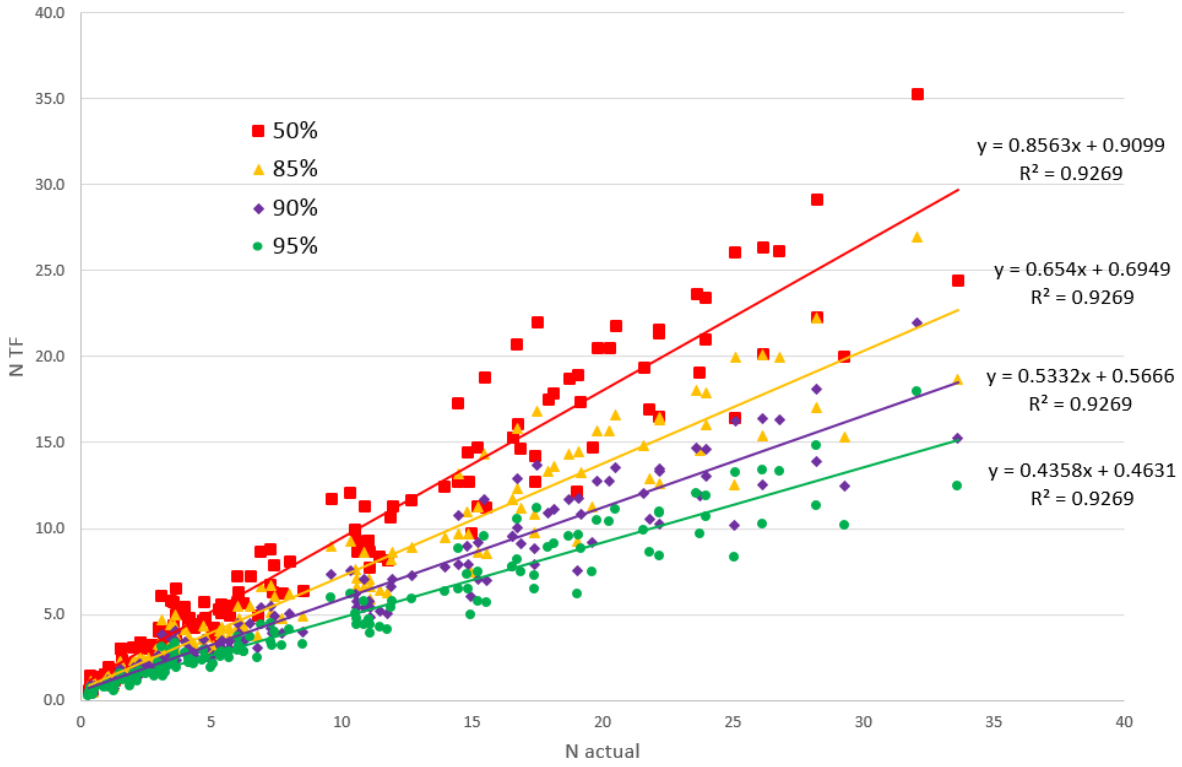

Figure L.1: Transfer function reliability adjustments

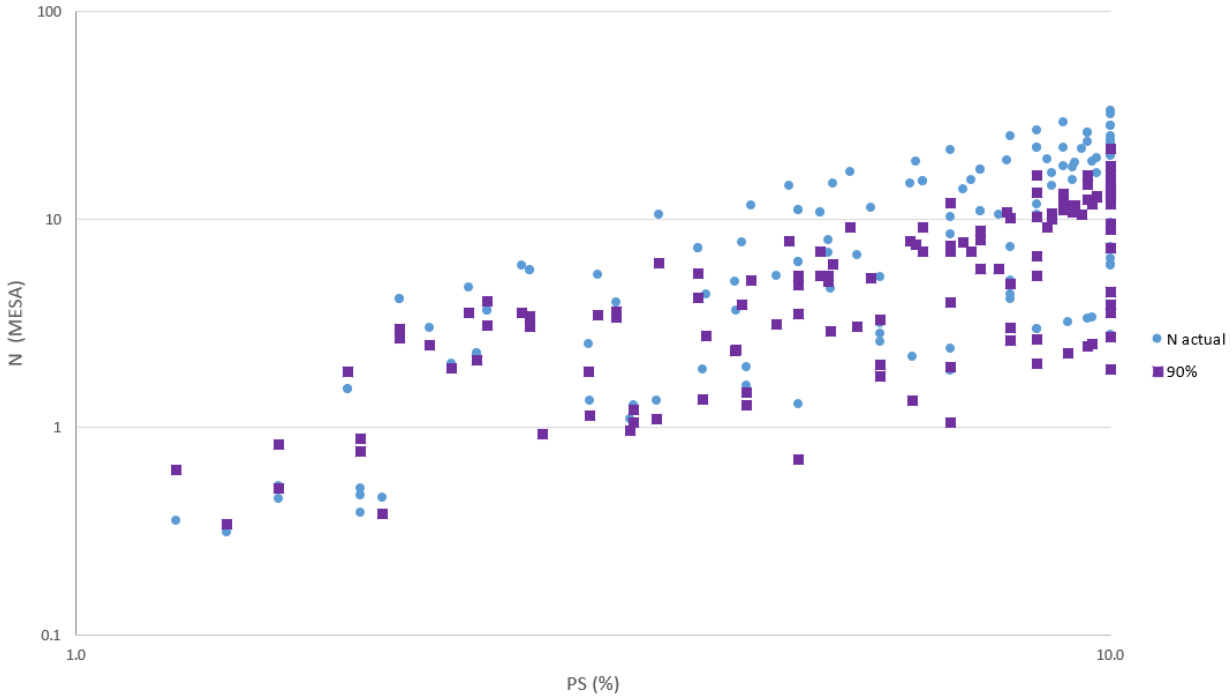

Figure L.2: Transfer function value reduction for 90% reliability

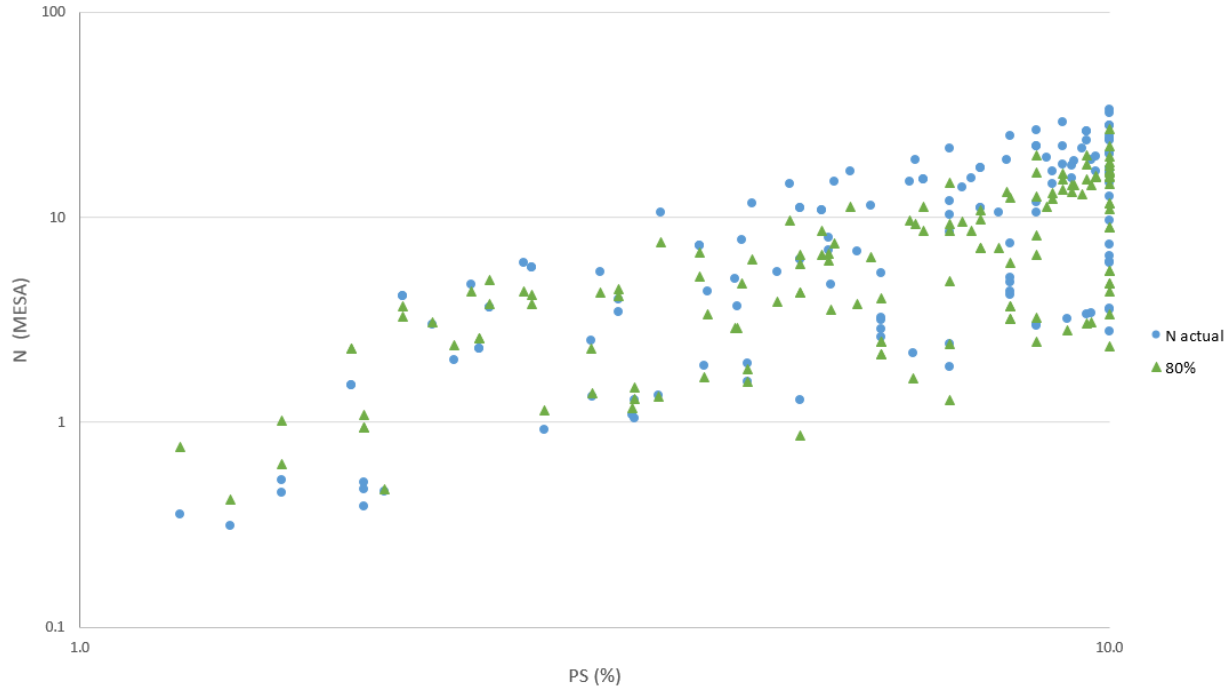

Figure L.3: Transfer function value reduction for 80% reliability

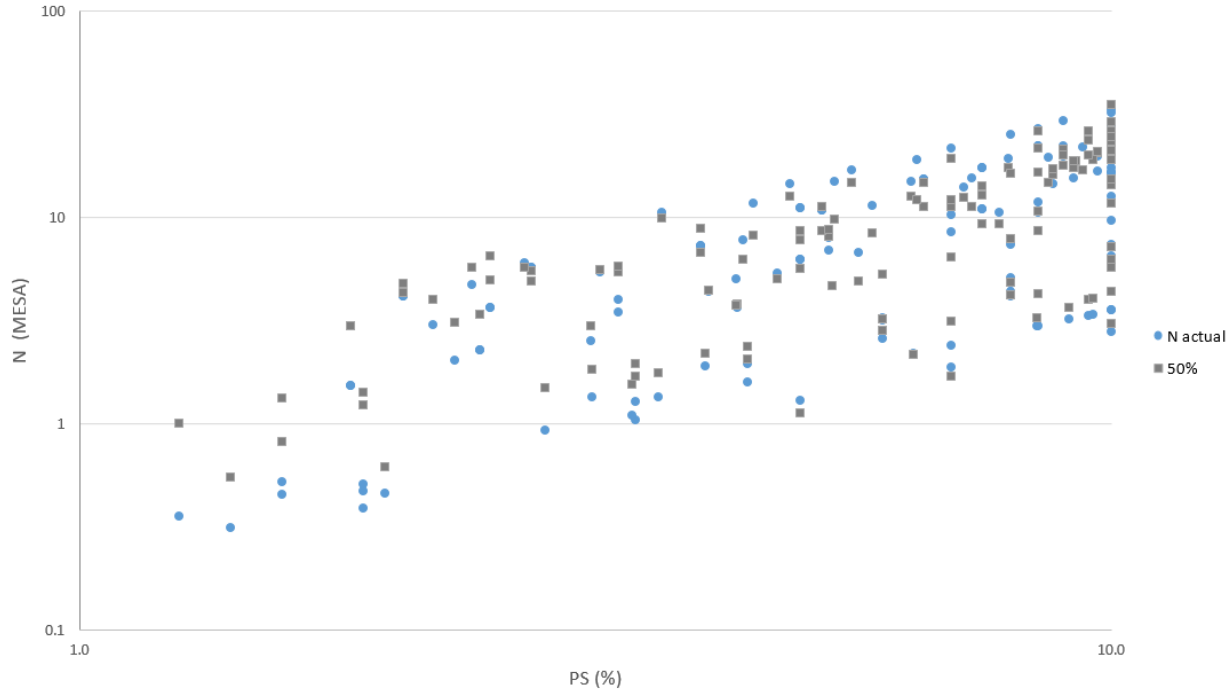

Figure L.4: Transfer function value reduction for 50% reliability

Appendix M

N7 traffic data per uniform section

Table M.1: N7 Northbound traffic data and rut depth measurements

Road	Year	Actual Traffic (MESA)	Rutting (mm)	Assigned Rutting (mm)
NB 1 (5.8 - 11.2)	-	0.00	0.0	0.0
	2004	2.06	2.3	2.7
	2006	4.15	1.9	4.6
	2008	6.26	2.6	6.6
	2010	8.40	2.9	9.0
	2012	10.57	2.9	11.3
	2014	12.77	6.3	14.7
NB 2 (11.2 - 13.6)	2007	0.00	0.0	0.0
	2008	0.79	2.1	2.1
	2010	2.37	1.8	3.5
	2012	3.96	2.2	5.2
	2014	5.55	2.3	7.0
NB 3 (13.6 - 18.02)	2007	0.00	0.0	0.0
	2008	0.65	2.7	2.7
	2010	1.94	2.5	4.5
	2012	3.24	1.5	5.6
	2014	4.53	1.8	7.0

Table M.2: N7 Southbound traffic data and rut depth measurements (1)

Section	Year	Actual Traffic (MESA)	Measured Rutting (mm)	Assigned Rutting (mm)
SB 1 (5.8 - 7.6)	-	0.00	0.0	0.0
	2002	1.14	4.8	5.3
	2004	2.28	5.0	7.7
	2006	4.53	2.5	9.1
	2008	6.77	2.4	10.9
	2010	9.00	3.2	12.9
	2012	11.21	4.3	15.6
	2014	13.42	6.8	18.1
SB 2 (7.6 - 10.4)	-	0.00	0.0	0.0
	2002	1.13	4.5	4.1
	2004	2.27	5.4	5.4
	2006	4.57	1.9	6.2
	2008	6.90	2.3	8.0
	2010	9.25	2.3	9.8
	2012	11.64	2.8	11.8
	2014	14.07	5.8	14.8
SB 3 (10.4 -11.0)	-	0.00	0.0	0.0
	2002	1.03	4.1	4.1
	2004	2.06	5.2	5.2
	2006	4.16	1.3	6.5
	2008	6.29	3.2	9.1
	2010	8.45	3.6	11.1
	2012	10.65	6.1	13.6
	2014	12.89	8.5	16.0
SB 4 (11.0 - 11.6)	-	0.00	0.0	0.0
	2002	1.03	4.0	4.0
	2004	2.06	5.2	7.2
	2006	4.16	3.5	9.4
	2008	6.29	2.4	10.9
	2010	8.45	2.4	12.6
	2012	10.65	2.8	14.9
	2014	12.89	4.1	17.5

Table M.3: N7 Southbound traffic data and rut depth measurements (2)

Section	Year	Actual Traffic (MESA)	Rutting (mm)	Assigned Rutting (mm)
SB 5 (11.6 - 12.4)	-	0.00	0.0	0.0
	2002	0.92	4.7	4.7
	2004	1.85	5.1	5.5
	2006	3.75	2.6	6.8
	2008	5.68	2.8	7.3
	2010	7.65	3.4	9.9
	2012	9.66	4.1	13.2
	2014	11.72	5.6	16.8
SB 6 (12.4 - 13.8)	-	0.00	0.0	0.0
	2002	0.77	4.3	4.3
	2004	1.54	5.1	7.3
	2006	3.06	3.0	9.3
	2008	4.58	2.8	9.1
	2010	6.10	3.6	12.0
	2012	7.61	4.2	13.7
	2014	9.12	7.3	16.2
SB 7 (13.8 - 15.0)	-	0.00	0.0	0.0
	2002	0.75	4.4	4.4
	2004	1.50	4.7	6.9
	2006	2.97	2.1	8.0
	2008	4.43	3.5	10.1
	2010	5.88	3.8	11.6
	2012	7.31	4.5	12.6
	2014	8.73	5.6	14.1
SB 8 (15.0 - 18.02)	-	0.00	0.0	0.0
	2002	0.69	4.6	4.6
	2004	1.38	3.8	4.2
	2006	2.76	2.2	5.2
	2008	4.13	3.2	6.2
	2010	5.52	3.5	8.1
	2012	6.90	4.4	9.3
	2014	8.30	5.3	10.2

Appendix N

N7 Traffic extrapolation and BSM deformation for N7 uniform sections

Table N.1: Permanent strain prediction using linear prediction and the Huurman model for N7 Northbound uniform sections

Road ID	Huurman Constants		Year	N Huurman	N	N actual	PS meusured (mm)	PS (BSM) (%)
N7_NB_1	A	0.001	2002	0.0	0.0	0.0	0.0	0.0
	B	0.900	2004	1.9	2.1	2.1	2.7	0.9
	Slope	0.950	2006	3.5	4.1	4.1	4.6	1.5
	R^2	0.989	2008	5.2	6.3	6.3	6.6	2.1
			2010	7.3	8.4	8.4	9.0	2.9
			2012	9.4	10.6	10.6	11.3	3.6
			2014	12.6	12.8	12.8	14.7	4.7
Prediction				22.7	22.6			8.0
				25.9	25.4			9.0
				29.1	28.2			10.0
N7_NB_2	A	0.003	2007	0.00	0.0	0.0	0.0	0.0
	B	0.753	2008	1.2	0.8	0.8	2.1	0.7
	Slope	1.050	2010	2.4	2.4	2.4	3.5	1.1
	R^2	0.994	2012	4.2	4.0	4.0	5.2	1.7
			2014	6.0	5.6	5.6	7.0	2.2
Prediction				33.0	20.3			8.0
				38.6	22.9			9.0
				44.4	25.5			10.0
N7_NB_3	A	0.008	2007	0.0	0.0	0.0	0.0	0.0
	B	0.675	2008	1.1	0.6	0.6	2.7	0.9
	Slope	0.950	2010	2.4	1.9	1.9	4.5	1.4
	R^2	0.985	2012	3.3	3.2	3.2	5.6	1.8
			2014	4.5	4.5	4.5	7.0	2.2
Prediction				30.1	15.9			8.0
				35.8	18.0			9.0
				41.9	20.0			10.0

Table N.2: Permanent strain prediction using linear prediction and the Huurman model for N7 Southbound (1)

Road ID	Huurman Constants		Year	N Huurman	N	N actual	PS meusured (mm)	PS (BSM) (%)
N7_SB_1	A	0.010	2002	0.0	0.0	0.0	0.0	0.0
	B	0.675	2002	2.3	1.1	1.1	5.3	1.8
	Slope	0.950	2004	4.0	2.3	2.3	7.7	2.6
	R^2	0.979	2006	5.1	4.5	4.5	9.1	3.1
			2008	6.6	6.8	6.8	10.9	3.7
			2010	8.6	9.0	9.0	12.9	4.4
			2012	11.3	11.2	11.2	15.6	5.3
			2014	14.2	13.4	13.4	18.1	6.2
Prediction				20.8	17.1			8.0
				24.8	19.5			9.0
				28.9	21.9			10.0
N7_SB_2	A	0.003	2002	0.0	0.0	0.0	0.0	0.0
	B	0.761	2002	2.8	1.1	1.1	4.1	1.3
	Slope	0.950	2004	4.1	2.3	2.3	5.4	1.7
	R^2	0.969	2006	4.9	4.6	4.6	6.2	2.0
			2008	6.8	6.9	6.9	8.0	2.6
			2010	8.9	9.3	9.3	9.8	3.1
			2012	11.3	11.6	11.6	11.8	3.8
			2014	15.3	14.1	14.1	14.8	4.7
Prediction				30.5	25.0			8.0
				35.6	28.4			9.0
				40.9	31.7			10.0
N7_SB_3	A	0.004	2002	0.0	0.0	0.0	0.0	0.0
	B	0.748	2002	2.4	1.0	1.0	4.1	1.5
	Slope	1.050	2004	3.3	2.1	2.1	5.2	1.9
	R^2	0.988	2006	4.4	4.2	4.2	6.5	2.3
			2008	6.9	6.3	6.3	9.1	3.2
			2010	8.9	8.5	8.5	11.1	3.9
			2012	11.8	10.7	10.7	13.6	4.9
			2014	14.5	12.9	12.9	16.0	5.7
Prediction				22.9	18.2			8.0
				26.9	20.7			9.0
				30.9	23.1			10.0
N7_SB_4	A	0.009	2002	0.0	0.0	0.0	0.0	0.0
	B	0.675	2002	1.6	1.0	1.0	4.0	1.3
	Slope	0.998	2004	3.8	2.1	2.1	7.2	2.4
	R^2	0.983	2006	5.5	4.2	4.2	9.4	3.1
			2008	6.9	6.3	6.3	10.9	3.6
			2010	8.6	8.5	8.5	12.6	4.1
			2012	11.0	10.7	10.7	14.9	4.9
			2014	14.0	12.9	12.9	17.5	5.7
Prediction				23.0	17.5			8.0
				27.4	19.9			9.0
				32.0	22.3			10.0

Table N.3: Permanent strain prediction using linear prediction and the Huurman model for N7 Southbound (2)

Road ID	Huurman Constants		Year	N Huurman	N	N actual	PS meusured (mm)	PS (BSM) (%)
N7_SB_5	A	0.002	2002	0.0	0.0	0.0	0.0	0.0
	B	0.859	2002	3.0	0.9	0.9	4.7	1.6
	Slope	0.950	2004	3.6	1.9	1.9	5.5	1.8
	R^2	0.941	2006	4.6	3.7	3.7	6.8	2.3
			2008	5.0	5.7	5.7	7.3	2.4
			2010	7.2	7.7	7.7	9.9	3.3
			2012	10.0	9.7	9.7	13.2	4.4
			2014	13.2	11.7	11.7	16.8	5.6
Prediction				20.0	17.8			8.0
				22.9	20.1			9.0
				25.9	22.5			10.0
N7_SB_6	A	0.010	2002	0.0	0.0	0.0	0.0	0.0
	B	0.678	2002	1.5	0.8	0.8	4.3	1.4
	Slope	1.050	2004	3.3	1.5	1.5	7.3	2.4
	R^2	0.962	2006	4.7	3.1	3.1	9.3	3.1
			2008	4.6	4.6	4.6	9.1	3.0
			2010	6.9	6.1	6.1	12.0	4.0
			2012	8.4	7.6	7.6	13.7	4.6
			2014	10.7	9.1	9.1	16.2	5.4
Prediction				19.3	13.3			8.0
				22.9	15.1			9.0
				26.8	16.9			10.0
N7_SB_7	A	0.010	2002	0.0	0.0	0.0	0.0	0.0
	B	0.686	2002	1.8	0.8	0.8	4.4	1.7
	Slope	1.050	2004	3.5	1.5	1.5	6.9	2.7
	R^2	0.972	2006	4.3	3.0	3.0	8.0	3.1
			2008	6.1	4.4	4.4	10.1	3.9
			2010	7.4	5.9	5.9	11.6	4.5
			2012	8.4	7.3	7.3	12.6	4.9
			2014	9.9	8.7	8.7	14.1	5.5
Prediction				17.1	11.7			8.0
				20.3	13.4			9.0
				23.7	15.1			10.0
N7_SB_8	A	0.008	2002	0.0	0.0	0.0	0.0	0.0
	B	0.675	2002	2.3	0.7	0.7	4.6	1.4
	Slope	0.815	2004	2.0	1.4	1.4	4.2	1.3
	R^2	0.955	2006	2.8	2.8	2.8	5.2	1.6
			2008	3.6	4.1	4.1	6.2	1.9
			2010	5.3	5.5	5.5	8.1	2.5
			2012	6.5	6.9	6.9	9.3	2.9
			2014	7.5	8.3	8.3	10.2	3.1
Prediction				30.1	21.2			8.0
				35.8	24.0			9.0
				41.9	26.9			10.0

Appendix O

N7 Pavement structure for DSR calculation

Table O.1: Pavement structure for DSR calculation (N7 Northbound)

Road ID	Layer	Layer Thickness (mm)	Material Class	Stiffness (Mpa)	BSM Properties	
N7_NB_1	1	70	AC	1915	C	171.14
	2	250	BSM 2	775	Phi	47.71
	3	185	G4	228	DSR	0.308
	4	-	G8	120	RetC	75
	5				P.mod	97.3
	6					
N7_NB_2	1	60	AC	4548	C	347.95
	2	250	BSM 2	1788	Phi	40.66
	3	360	G4	722	DSR	0.184
	4	-	G8	0	RetC	75
	5				P.mod	99.1
	6					
N7_NB_3	1	65	AC	2835	C	347.95
	2	250	BSM 1	1349	Phi	40.66
	3	360	G4	366	DSR	0.181
	4	-	G8	140	RetC	75
	5				P.mod	98
	6					

Table O.2: Pavement structure for DSR calculation (N7 Southbound)

Road ID	Layer	Layer Thickness (mm)	Material Class	Stiffness (Mpa)	BSM Properties	
N7_SB_1	1	80	AC	2317	C	171.14
	2	235	BSM1	820	Phi	47.71
	3	140	G4	254	DSR	0.278
	4	75	G5	157	RetC	75
	5	-	G8	100	P.mod	97.5
	6					
N7_SB_2	1	70	AC	3063	C	171.14
	2	250	BSM1	1387	Phi	47.71
	3	120	G6	462	DSR	0.287
	4	165	G6	222	RetC	75
	5	-	G8	120	P.mod	98.3
	6					
N7_SB_3	1	65	AC	1522	C	171.14
	2	225	BSM1	694	Phi	47.71
	3	155	G6	264	DSR	0.308
	4	260	G10	139	RetC	75
	5	-	G10	90	P.mod	103
	6					
N7_SB_4	1	70	AC	4172	C	171.14
	2	245	BSM1	1345	Phi	47.71
	3	210	G4	418	DSR	0.291
	4	-	G9	199	RetC	75
	5	0	0	100	P.mod	98.3
	6					
N7_SB_5	1	70	AC	1838	C	171.14
	2	240	BSM1	664	Phi	47.71
	3	190	G4	200	DSR	0.301
	4	-	G9	125	RetC	75
	5	0	0	0	P.mod	95
	6					
N7_SB_6	1	70	AC	2119	C	171.14
	2	240	BSM1	1095	Phi	47.71
	3	210	G4	280	DSR	0.3
	4	-	G9	140	RetC	75
	5				P.mod	95
	6					
N7_SB_7	1	70	AC	1413	C	171.14
	2	205	BSM1	526	Phi	47.71
	3	160	G6	164	DSR	0.322
	4	255	G9	121	RetC	75
	5	-	G10	90	P.mod	95
	6					
N7_SB_8	1	70	AC	1790	C	171.14
	2	260	BSM1	768	Phi	47.71
	3	155	G4	279	DSR	0.285
	4	425	G7	181	RetC	75
	5	-	G9	100	P.mod	98
	6					

Appendix P

N7 Validation resutls

Table P.1: N7 Validation results: Northbound (1)

Road ID	TF input		Year	N Huurman	N TF	PS (BSM) (%)
N7_NB_1	C	171.14	2002	0.0	1.6	0.0
	Phi	47.71	2004	1.9	2.0	0.9
	DSR	0.308	2006	3.5	2.2	1.5
	RetC	75	2008	5.2	2.5	2.1
	P.mod	97.3	2010	7.3	2.9	2.9
			2012	9.4	3.4	3.6
			2014	12.6	4.2	4.7
				22.7	8.1	8.0
Prediction				25.9	9.9	9.0
				29.1	12.1	10.0
N7_NB_2	C	347.95	2007	0.00	45.2	0.0
	Phi	40.66	2008	1.2	51.6	0.7
	DSR	0.184	2010	2.4	56.5	1.1
	RetC	75	2012	4.2	63.2	1.7
	P.mod	99.1	2014	6.0	70.5	2.2
				33.0	223.3	8.0
Prediction				38.6	272.7	9.0
				44.4	333.0	10.0
N7_NB_3	C	347.95	2007	0.00	39.5	0.0
	Phi	40.66	2008	1.1	46.9	0.9
	DSR	0.181	2010	2.4	52.6	1.4
	RetC	75	2012	3.3	56.4	1.8
	P.mod	98	2014	4.5	61.6	2.2
				30.1	195.2	8.0
Prediction				35.8	238.4	9.0
				41.9	291.1	10.0

Table P.2: N7 Validation results: Southbound (1)

Road ID	TF input		Year	N Huurman	N TF	PS (BSM) (%)
N7_SB_1	C	171.14	2002	0.0	4.7	0.0
	Phi	47.71	2002	2.3	6.7	1.8
	DSR	0.278	2004	4.0	7.9	2.6
	RetC	75	2006	5.1	8.7	3.1
	P.mod	97.5	2008	6.6	9.8	3.7
			2010	8.6	11.3	4.4
			2012	11.3	13.5	5.3
			2014	14.2	16.1	6.2
Prediction				20.8	23.2	8.0
				24.8	28.3	9.0
				28.9	34.6	10.0
N7_SB_2	C	171.14	2002	0.0	4.0	0.0
	Phi	47.71	2002	2.8	5.2	1.3
	DSR	0.287	2004	4.1	5.6	1.7
	RetC	75	2006	4.9	6.0	2.0
	P.mod	98.3	2008	6.8	6.7	2.6
			2010	8.9	7.5	3.1
			2012	11.3	8.5	3.8
			2014	15.3	10.3	4.7
Prediction				30.5	19.8	8.0
				35.6	24.2	9.0
				40.9	29.5	10.0
N7_SB_3	C	171.14	2002	0.0	4.0	0.0
	Phi	47.71	2002	2.4	5.4	1.5
	DSR	0.308	2004	3.3	5.9	1.9
	RetC	75	2006	4.4	6.4	2.3
	P.mod	103	2008	6.9	7.7	3.2
			2010	8.9	8.9	3.9
			2012	11.8	10.6	4.9
			2014	14.5	12.6	5.7
Prediction				22.9	19.9	8.0
				26.9	24.4	9.0
				30.9	29.7	10.0
N7_SB_4	C	171.14	2002	0.0	3.5	0.0
	Phi	47.71	2002	1.6	4.6	1.3
	DSR	0.301	2004	3.8	5.6	2.4
	RetC	75	2006	5.5	6.5	3.1
	P.mod	95	2008	6.9	7.1	3.6
			2010	8.6	8.0	4.1
			2012	11.0	9.3	4.9
			2014	14.0	11.0	5.7
Prediction				23.0	17.3	8.0
				27.4	21.2	9.0
				32.0	25.9	10.0

Table P.3: N7 Validation results: Southbound (2)

Road ID	TF input		Year	N Huurman	N TF	PS (BSM) (%)
N7_SB_5	C	171.14	2002	0.0	1.5	0.0
	Phi	47.71	2002	3.0	2.0	1.6
	DSR	0.287	2004	3.6	2.1	1.8
	RetC	75	2006	4.6	2.3	2.3
	P.mod	98.3	2008	5.0	2.4	2.4
			2010	7.2	2.9	3.3
			2012	10.0	3.5	4.4
			2014	13.2	4.5	5.6
Prediction				20.0	7.3	8.0
				22.9	8.9	9.0
				25.9	10.9	10.0
N7_SB_6	C	171.14	2002	0.0	1.5	0.0
	Phi	47.71	2002	1.5	2.0	1.4
	DSR	0.291	2004	3.3	2.5	2.4
	RetC	75	2006	4.7	2.8	3.1
	P.mod	98.3	2008	4.6	2.8	3.0
			2010	6.9	3.4	4.0
			2012	8.4	3.8	4.6
			2014	10.7	4.5	5.4
Prediction				19.3	7.5	8.0
				22.9	9.2	9.0
				26.8	11.2	10.0
N7_SB_7	C	171.14	2002	0.0	0.7	0.0
	Phi	47.71	2002	1.8	0.9	1.7
	DSR	0.301	2004	3.5	1.1	2.7
	RetC	75	2006	4.3	1.2	3.1
	P.mod	95	2008	6.1	1.4	3.9
			2010	7.4	1.6	4.5
			2012	8.4	1.8	4.9
			2014	9.9	2.0	5.5
Prediction				17.1	3.2	8.0
				20.3	4.0	9.0
				23.7	4.8	10.0
N7_SB_8	C	171.14	2002	0.0	4.1	0.0
	Phi	47.71	2002	2.3	5.4	1.4
	DSR	0.322	2004	2.0	5.3	1.3
	RetC	75	2006	2.8	5.6	1.6
	P.mod	95	2008	3.6	5.9	1.9
			2010	5.3	6.7	2.5
			2012	6.5	7.2	2.9
			2014	7.5	7.6	3.1
Prediction				30.1	20.1	8.0
				35.8	24.6	9.0
				41.9	30.0	10.0